

THE APPLICATION OF STATE-OF-THE-ART PETROLEUM TECHNOLOGY TO SHALE OIL REFINING.
R. E. Hildebrand and B. M. Harney. U. S. Department of Energy, ASET/FE, #20
Massachusetts Avenue, N.W., Washington, D.C. 20545

Shale oil offers one of the most promising near term options for providing transportation fuels from non-petroleum domestic resources. The unusually high nitrogen content of shale oil however, presents a significant problem in refining this synthetic fuel to specification products. Under contract to the Department of Energy, Chevron Research Company has successfully applied state-of-the-art hydroprocessing technology to shale oil refining. In addition, Chevron has estimated the economics of hydro-processing shale oil to a variety of product slates. A summary of the technical and economic results of that program will be presented. In a larger scale effort, the Department of Energy and the Department of Defense have a joint program for refining 100,000 barrels of shale oil at an existing Sohio refinery. The status and some results of this program will also be presented. The results of this on-going work indicates that refining of shale oil will be expensive. Consequently, an expanded D.O.E. shale oil refining program is being developed to assure that the cost of refining shale oil is not an impediment to commercialization of the shale resource. The goals of this program will be outlined.

Shale Oil: An Acceptable Refinery Syncrude

H. C. Stauffer & S. J. Yanik

Gulf Science and Technology Company
P. O. Drawer 2038, Pittsburgh, PA 15230

Introduction

Technology for the extraction of oil from shale has been in existence for a very long time. In a less restrictive economic and environmental climate, the production of substantial quantities of shale oil could have been realized rather quickly. It has also been well established that shale oil must be substantially upgraded before any conventional refining processes can be applied.

No refinery has the capability of effectively processing any significant volume of raw shale oil. Therefore, most upgrading studies have two objectives: 1) produce a syncrude that can be pipelined and then refined in an existing facility, or 2) upgrade and refine to a full slate of products at the retort site. In either case, the overall upgrading requirements are substantial and quite similar.

Our upgrading studies were initiated in the 1960's. As a result of our participation in the Rio Blanco Project, these have been updated during the past few years. This paper presents the results of our most recent exploratory studies made to determine 1) the effectiveness of our commercially available hydrotreating technology for upgrading shale oil to a petroleum substitute and 2) the response obtained in conventional downstream refining processes.

Upgrading Routes

In upgrading shale oil for refining purposes, there are two general approaches. In the one most often considered, Figure 1, the raw oil is fractionated to yield a residuum that may be gasified, coked or deasphalted. A heavy gas oil is obtained for hydrocracking or hydrotreating for FCC feed. The furnace oil distillate is hydrotreated to No. 2 fuel (or additional FCC feed) and a naphtha is produced for hydrotreating and catalytic reforming. The syncrude from this route is, essentially, an all-distillate stream, comprised of the reconstituted, hydrotreated fractions.

A more unconventional approach, which avoids much duplication of facilities, is shown in Figure 2. In this route, the whole shale oil is hydrotreated in a modified Gulf Residual HDS Unit. The effluent can be pipelined as syncrude or fractionated and converted to prime products via reforming, hydrocracking and/or FCC. Volumetric yields are higher, by this route, and no residual products need be produced.

Discussion

Shale Oil Quality

Although all our latest pilot plant studies were limited to a single shale oil sample, a number of different oils were examined. Assays for five of these (A thru E) are shown in Table I. These data are indicative of the variation in shale oil composition that can result from differences in retorting modes and oil shale source. Obviously, as retorting technology changes, so can the character of the oil.

Regardless of oil shale source or retorting mode, all the oils are typified by their high hetero-atom content, with nitrogen being the highest, by far. Sulfur content is relatively low in all samples and of no particular concern. As would be expected, the hetero-atom content of the particular fractions varies from sample to sample as do the yields of these fractions. In view of the present trend toward in-situ retorting, the

lower residuum and hetero-atom content of sample E is encouraging. Sample A was used exclusively for all the pilot plant studies herein reported.

Experimental

In order to meet the objectives of this study, with the amount of shale oil available, most of the data was acquired from survey-type runs, using our early exploratory studies as a basis. All the pilot plant work was done in existing facilities normally used for petroleum-based feeds.

Delayed coking runs were made in a 2 gal/hr unit, equipped for downstream fractionation and gas oil recycle.

Catalytic cracking data was obtained in a 1,500 cc/hr, automated riser unit having product fractionation and continuous catalyst regeneration facilities.

Hydrogenation and catalytic reforming runs were also made in automated units, both isothermal and adiabatic. These units are equipped for downstream product fractionation and most have gas scrubbing and recycle systems. All operations were downflow, with combined hydrogen, in catalyst beds ranging from 300 to 2,500 cc.

Only commercially available catalysts were employed, with those for hydrogenation being Gulf formulations. The riser cracking runs were made with an equilibrium catalyst of high zeolite content. A commercially available bimetallic catalyst was used in the reforming studies.

Because of the inherently poor stability characteristics of raw shale oil, it was felt that the problems this could cause during the study could be alleviated by a mild hydrogen pretreatment. Thus, the entire sample was mildly hydrotreated, with the intent of eliminating the most reactive double bonds. Although hydrogen consumption was about 150 SCF/B, except for arsenic removal, the detectable changes in product properties and composition were insignificant. It was concluded that the pretreatment would have no effect on further processing. Thus, the studies were considered to be representative of upgrading a raw shale oil sample.

Delayed Coking of Residuum

Coking of the 960 F+ fraction was done at conditions previously found suitable for shale oil residua and no unexpected problems were encountered. The conventional, relatively mild conditions, with product yields and inspections, are shown in Table II. The liquid products are typical of a coker operation and, of course, very high in nitrogen. The coke is of relatively poor quality, very high in nitrogen content, but low in sulfur and vanadium. Ash content will be a function of the carry-over from the retorting operation. It was observed that the yield structure does not fit that predicted from a petroleum-based correlation. Coke yield was higher while gas and naphtha yields were lower.

Gas Oil Hydrotreating and Catalytic Cracking

The gas oil fraction, 680-960°F, was hydrotreated in two stages to produce feedstocks for catalytic cracking. Products of 0.73 and 0.61% nitrogen were obtained at two severities in the first stage. The higher nitrogen level material served as feed to the second stage. At two severities in this stage, nitrogen content was reduced to 0.28 and 0.10%; the lower level representing 95.9% overall denitrogenation. Yields, operating conditions and product inspections are shown in Table III. For comparison, the properties of a good quality, low nitrogen, petroleum gas oil (PGO) are also shown.

Except for the unique sulfur/nitrogen ratio, the hydrotreated shale oils (HTSO) exhibit no apparent unusual characteristics. As would be expected, however, boiling range does change with denitrogenation severity.

Since the products were not stripped back to feed IBP, they contain increasing amounts of material in the furnace oil boiling range. Based on properties other than nitrogen content, the quality of these synthetic gas oils is equal to or superior than that of many petroleum based FCC feedstocks.

The response obtained in fluid catalytic cracking is shown in Table IV. The yield structure produced from the HTSO's is compared with those from the PGO and two stocks which were blends of the PGO with the raw feed to hydrotreating. The HTSO's crack very well up to a nitrogen content of at least 0.28%. Of all the stocks, maximum conversion and gasoline yield was obtained with the low nitrogen HTSO. For the hydrotreated stocks, however, response is nonlinear with nitrogen content. At the 0.61% level, conversion and gasoline yield were much poorer than those obtained with the blended feed at the same nitrogen level. This discrepancy has been attributed to the high basic nitrogen content of the HTSO.

FCC Product Quality

With one exception, adequate octane numbers were obtained with all shale oil-containing feedstocks. All research octane numbers (RON) were 91 or greater except when cracking the low nitrogen HTSO, Table V. In this case, the RON was only 89.2. This gasoline had the highest saturate content and the lowest sensitivity. It was also derived from the most paraffinic feedstock.

Gasoline aromaticity was remarkably constant for all shale oil stocks, hydrotreated or blended, but lower than obtained with the PGO. As feed nitrogen increased, saturate content decreased with a corresponding gain in olefin content. Motor octane numbers obtained from the shale oil stocks were consistently lower than from the PGO. Sensitivity increased with feed nitrogen content. The increase, however, was not as great with the HTSO's as with the blended feeds.

Relative to the gasoline from the PGO, all shale oil stocks gave gasolines of much higher nitrogen content. Of these, the HTSO's gave the lowest values at comparable feed nitrogen levels. For the cycle oils and decanted oils, however, nitrogen contents were higher from the HTSO's than the blended feeds. All available data indicate satisfactory product stability up to a feed nitrogen level of at least 0.3%.

Middle Distillate Hydrotreating

Hydrogenation of the middle distillate fraction, 375-680°F, readily yields a high quality furnace oil product. As shown in Table VI, negligible sulfur content and high cetane index is easily obtained. Compared to petroleum derived furnace oils, however, nitrogen contents are quite high. This can be reduced to a very low level; but, it should not be required except for exclusive use in combustion applications where NO_x emissions are limiting. In all other respects, the combustion characteristics of these fuels are excellent(1) and in many cases superior to No. 2 fuels from petroleum.

Naphtha Pretreating and Reforming

Unlike heavier stocks in which substantial amounts of nitrogen can be tolerated, the naphtha must be essentially nitrogen-free for satisfactory reforming response. As the inspection data show, in Table VI, the nitrogen level is many orders of magnitude greater than typical for most virgin, petroleum-based naphthas. Nitrogen at this high level totally overwhelms the difficulty associated with removal of the remaining hetero-atoms. Figure 3 shows a temperature-space velocity-pressure relationship required to produce a reformer charge of 0.5 ppm nitrogen content. These conditions far exceed typical refinery pretreating severities.

The raw naphtha has a relatively high aromatic content and is very olefinic. About 85% of the hydrogen required is consumed in saturation reactions. The total consumption, 808 SCF/B, is in excess of that required for many gas oil hydrocrackers.

As reformer feed, the treated naphtha inspections show two important points. First, the front-end volatility is very low, indicating a deficiency in C₆ and C₇ hydrocarbons. Second, the ratio of naphthenes to aromatics is exceptionally high. Consequently, the reforming results show quite low benzene and toluene yields and a high hydrogen make.

The quality of the feed, as indicated by its N+2A relationship, is significantly better than would be predicted. Although this simple relationship would indicate reforming susceptibility close to that of a Mideast naphtha, such as Kuwait, its response was actually much closer to that of a good quality domestic naphtha. This is illustrated by the yields obtained and temperature requirements shown in Figures 4, 5 and 6.

Alternate Upgrading Route

The maximum yield case is shown in the alternate approach, Figure 2. In this route, the raw, full-boiling range shale oil is charged to a modification of the Gulf HDS Process. The results shown in Table VIII are for maximizing the yield of FCC feed at the minimum denitrogenation level. The yield of 375°F+ FCC charge is approximately 85% on raw crude and contains 0.38% nitrogen with <1.0 ppm Ni equivalent. Although the 375°F+ material is relatively high in nitrogen, the naphtha is essentially nitrogen-free and can be charged directly to a catalytic reformer.

This is not a limiting case; if the furnace oil fraction is desired for other end uses, the 680°F+ can still be reduced to a satisfactory nitrogen level. The residuum, which has an API gravity higher than that of the crude, may also be more useful in other applications.

Conclusions

For satisfactory hetero-atom removal, particularly nitrogen, and for olefin saturation, hydrogen requirements are substantial. With today's commercially available catalysts, processing severities are high and costly.

With respect to FCC feed, limited quantities of raw shale oil can be tolerated in a refinery crude slate. Handling the 650°F and lighter material would require a hydrotreating capability greater than usually available.

Shale oil fractions when suitably upgraded, are quite amenable to refining in conventional processes. Product yields and quality are comparable to those obtained with a good quality petroleum crude. Upgrading the total shale oil via the modified Gulf HDS Process results in an improved yield structure and a less complex facility.

New catalyst formulations are expected to substantially reduce process severity. This will strongly affect upgrading and refining economics.

Reference

- (1) Dzuna, E. R., "Combustion Tests on Shale Oil Fuels", presented at Central States Section the Combustion Institute, April 1976.

TABLE I
ASSAYS OF RAW SHALE OILS

Sample Source Retort	A Dow Tosco	B Paraho Paraho	C Superior Tosco	D Occidental Tosco	E -- In-Situ
<u>Shale Oil</u>					
Gravity, °API	20.7	20.1	20.7	19.3	25.4
Viscosity, SUS: 130°F	85.7	121.4	105.5	92.7	42.6
Pour, °F	+75	+85	+80	+50	+80
Carbon, wt %	84.52	84.83	84.06	83.97	84.89
Hydrogen, wt %	11.14	11.51	11.27	10.72	11.82
Sulfur, wt %	0.70	0.58	0.77	0.43	0.42
Nitrogen, wt %	1.99	2.04	2.06	1.96	1.62
Oxygen, wt %	1.32	1.24	1.58	1.92	1.09
Arsenic, ppm	13.9	20.9	8.0	32.0	19.0
Ash, wt %	0.20	0.03	0.05	0.06	0.26
<u>Fractions:</u>					
<u>QP-310°F</u>					
Yield, vol %	5.20	1.17	5.08	6.30	3.58
Gravity, °API	53.3	48.0	52.2	52.4	49.6
Carbon, wt %	85.06	84.20	84.11	84.87	85.84
Hydrogen, wt %	13.35	13.03	12.87	12.37	13.02
Sulfur, wt %	0.85	0.81	1.04	0.59	0.69
Nitrogen, wt %	0.25	0.95	0.41	0.30	0.59
Oxygen, wt %	0.52	0.75	0.95	0.69	0.49
Saturates, vol %	28.0	--	26.0	27.0	--
Olefins, vol %	56.0	--	54.0	57.0	--
Aromatics, vol %	16.0	--	20.0	18.0	--
Arsenic, ppm	--	5.2	1.5	3.4	1.6
<u>310-375°F</u>					
Yield, vol %	4.54	1.13	4.58	4.53	3.39
Gravity, °API	44.8	40.7	43.6	42.8	43.0
Carbon, wt %	84.84	83.44	84.36	84.72	84.74
Hydrogen, wt %	12.97	12.68	12.80	12.71	12.67
Sulfur, wt %	0.72	0.52	0.91	0.59	0.55
Nitrogen, wt %	0.65	1.46	0.82	0.79	1.09
Oxygen, wt %	0.70	1.46	1.24	0.87	0.77
Saturates, vol %	25.0	--	25.5	23.5	--
Olefins, vol %	52.0	--	48.0	48.0	--
Aromatics, vol %	23.0	--	26.5	28.5	--
Arsenic, ppm	--	1.8	<0.2	3.9	6.0
<u>375-520°F</u>					
Yield, vol %	12.64	9.60	10.87	13.64	20.49
Gravity, °API	35.0	33.8	34.3	33.0	34.1
Carbon, wt %	84.57	84.09	83.92	84.58	84.94
Hydrogen, wt %	12.32	12.38	12.30	12.02	12.31
Sulfur, wt %	0.64	0.68	0.74	0.39	0.36
Nitrogen, wt %	1.05	1.35	1.25	1.15	1.21
Oxygen, wt %	1.24	1.53	1.70	1.38	0.85
Pour, °F	-45	-30	-35	-55	-30
Aniline Point, °F	82.0	--	73.4	80.0	93.2
Arsenic, ppm	--	24.7	1.8	9.8	1.5

TABLE I (continued)

Sample	A	B	C	D	E
Fractions: (cont'd)					
<u>375-680°F</u>					
Yield, vol %	30.85	28.92	27.37	33.07	51.33
Gravity, °API	29.3	28.4	29.7	27.0	29.5
Viscosity, SUS: 100°F	40.1	42.6	40.2	42.1	39.3
Carbon, wt %	84.56	83.90	84.09	86.00	85.29
Hydrogen, wt %	11.96	11.98	12.01	11.83	12.03
Sulfur, wt %	0.63	0.69	0.70	0.44	0.37
Nitrogen, wt %	1.47	1.60	1.62	1.56	1.47
Oxygen, wt %	1.26	1.27	1.72	1.60	0.75
Pour, °F	+15	+20	+30	+5	+20
Aniline Point, °F	87.1	--	86.0	82.4	102.2
Arsenic, ppm	8.0	23.0	3.8	20.4	5.7
<u>680-960°F</u>					
Yield, vol %	32.57	37.81	31.93	31.73	33.79
Gravity, °API	16.3	18.6	18.6	15.3	20.8
Viscosity, SUS: 210°F	66.4	57.0	56.0	91.0	50.7
Carbon, wt %	85.01	85.11	86.11	85.16	87.02
Hydrogen, wt %	10.93	11.25	11.53	10.96	11.84
Sulfur, wt %	0.60	0.53	0.65	0.36	0.24
Nitrogen, wt %	2.09	1.91	2.08	2.00	1.75
Oxygen, wt %	0.94	0.83	1.18	1.20	0.68
Pour, °F	+100	+100	+100	+85	+105
Aniline Point, °F	126.0	--	111.9	118.4	135.5
Carbon Res, wt %	0.91	0.28	0.41	0.44	0.40
Arsenic, ppm	--	12.8	15.5	29	14
Ni + V, ppm	<0.1	<0.1	0.1	<0.1	<0.1
<u>960°F+</u>					
Yield, vol %	26.84	30.97	31.04	24.37	7.91
Gravity, °API	5.9	11.8	9.2	5.3	6.8
Viscosity, SUS: 250°F	1,159	266	503	3,212	2,216
Carbon, wt %	85.14	84.61	84.81	85.20	84.85
Hydrogen, wt %	10.61	10.64	10.37	9.74	10.24
Sulfur, wt %	0.64	0.53	0.80	0.39	0.58
Nitrogen, wt %	2.84	2.60	2.78	2.95	2.26
Oxygen, wt %	1.34	0.95	1.31	1.20	2.05
Carbon Res, wt %	20.3	12.9	15.8	24.4	18.4
C ₅ Insolubles, wt %	18.1	--	15.4	20.7	18.0
Ash, wt %	0.64	0.05	0.13	0.21	2.28
Arsenic, ppm	--	26.0	7.0	59.0	67.0
Ni, ppm	15	9.2	20.8	32.0	45.6
V, ppm	1.6	0.5	1.8	0.5	22.8

TABLE III
GAS OIL HYDROTREATING

<u>Hydrotreatment</u>	<u>First Stage</u> 680°/960°F	<u>Second Stage</u>		
<u>Feed</u>	Gas Oil	First Stage Product		
<u>Operating Conditions:</u>				
Reactor Press., psig	<-----1,725----->			
Gas Circulation, SCFB	4,000	<----- 8,500 ----->		
Avg. Catalyst Temp., °F	725	720	755	
Space Velocity, vol/hr/vol	1.0	1.0	0.75	
<u>Yields, Wt % of Feed:</u>				
H ₂ (SCFB)	(1,200)	(450)	(630)	
H ₂ S	0.49	0.04	0.04	
NH ₃	2.19	0.55	0.77	
H ₂ O	0.90	-	-	
C ₁ -C ₅	4.08	0.42	1.56	
Total Liquid Product	94.21	99.75	98.70	
<u>Inspections:</u>				
	<u>Gas Oil</u>			<u>PGO</u>
Nitrogen, wt %	2.41	0.61	0.28	0.10
Gravity, °API	13.9	27.4	29.7	31.2
Hydrogen, wt %	10.85	12.56	13.00	13.18
Sulfur, wt %	0.49	<0.05	<0.05	<0.05
Oxygen, ppm	0.80	<100	<100	<100
Viscosity, SUS: 210°F	118.4	41.4	37.7	35.8
Pour Point, °F	+105	+95	+80	+85
Aniline Point, °F	101	174.6	181.9	186.1
Carbon Res., Rams.: wt %	1.34	0.12	0.07	0.05
Calc. Comp., Vol Fraction:				
Aromatics(Ca)	-	0.205	0.170	0.147
Naphthenes(Cn)	-	0.212	0.218	0.220
Paraffins(Cp)	-	0.583	0.612	0.633
Nickel, ppm	<0.1	<0.1	<0.1	<0.1
Vanadium, ppm	<0.1	<0.1	<0.1	<0.1
Distillation, Vac., °F at:				
10%	805	611	517	484
30	869	730	688	661
50	905	784	779	763
70	939	839	843	827
90	989	917	893	870

TABLE IV

CATALYTIC CRACKING AT 980°F RISER OUTLET TEMPERATURE-PRODUCT YIELDS

	PGO 0.063	<-----0.10	Hydrotreated -----0.28	>-----0.61	<-----PGO + RAW SOGO* 0.29	>-----0.61
Feed						
Nitrogen, wt %						
Product Yields:						
Vol % FF						
Total C ₁ 's	13.0	12.1	11.8	8.1	11.7	10.5
Propane	2.5	2.2	2.1	1.7	2.3	2.6
Propylene	10.5	10.0	9.7	6.4	9.4	7.9
Total C ₂ 's	20.8	20.7	19.1	10.8	18.2	13.3
Isobutane	8.3	7.8	6.2	2.1	6.0	3.4
Normal Butane	2.0	2.0	1.6	0.9	1.6	1.1
Butenes	10.5	10.9	11.2	7.8	10.6	8.8
Debutanized Gasoline:						
C ₆ -430°F TBP	60.6	62.4	60.5	41.7	58.5	50.7
Furnace Oil:						
430°-650°F TBP	11.4	11.8	13.2	19.2	13.5	16.9
Decant Oil:						
650°F+	6.1	5.0	6.2	20.9	8.3	12.7
Total C ₂ + Liquid	111.9	112.1	110.7	100.8	110.2	104.0
Product Yields:						
Wt % FF						
Hydrogen	0.09	0.05	0.09	0.15	0.11	0.13
C ₂ and Lighter	3.0	2.4	2.7	4.4	3.0	3.7
Coke	6.1	4.6	5.1	6.4	5.8	7.9
Conversion: Vol % FF	82.5	83.2	80.7	59.9	78.2	70.4

7680°/960°F shale oil/gas oil

TABLE V

CATALYTIC CRACKING AT 980°F RISER OUTLET TEMPERATURE-PRODUCT QUALITY

Feed Nitrogen, wt % Inspections	PGO 0.063	Hydro-treated		SOG0		
		<-----0.10	0.28	0.61	<---PGO + RAW 0.29	0.61
C ₅ -430°F Gasoline						
Gravity, °API	55.6	57.2	56.3	51.1	56.0	53.9
Nitrogen, ppm	14	60	130	980	163	630
Research Octane Numbers						
Clear	92.6	89.2	91.1	91.0	93.7	93.2
+3.0	99.6	99.5	98.5	97.4	99.5	97.9
Motor Octane Numbers						
Clear	81.6	79.3	80.2	78.5	79.8	80.3
+3.0	88.1	87.6	86.7	84.7	85.3	87.3
Hydrocarbon Type, vol %						
Aromatics	33.0	25.7	25.7	25.9	26.8	25.6
Olefins	20.3	23.7	33.6	51.4	36.1	44.9
Saturates	46.7	50.6	40.6	22.7	37.2	29.5
430°-650°F Furnace Oil						
Gravity, °API	14.0	17.2	18.5	24.6	19.6	23.0
Nitrogen, wt %	0.03	0.11	0.17	0.43	0.09	0.26
Pour Point, °F	-20	-40	-25	+25	-10	+10
Hydrocarbon Type, vol %						
Aromatics	83.9	73.2	66.6	45.7	64.6	49.7
Olefins	0.1	0.1	1.3	11.3	2.5	0.0
Saturates	16.0	26.7	32.1	43.0	32.9	50.3
650°F+ Decant Oil						
Gravity, °API	1.7	2.6	6.0	20.0	6.3	11.9
Nitrogen, wt %	0.12	0.20	0.33	0.37	0.21	0.37
Viscosity, SUS: 210°F	46.0	70.6	58.0	-	44.9	44.4

TABLE VI
FURNACE OIL HYDROTREATING

Operating Conditions						
Reactor Press., psig						
Gas Circulation, SCFB						
Avg. Catalyst Temp., °F						
Space Velocity, vol/hr/vol						
Yield, Vol %						
Naphtha-Free Furnace Oil						
Inspections						
Gravity, °API	29.3	99.8	99.0	100.8	99.1	
Nitrogen, wt %	1.66	39.7	38.9	37.4	39.1	
Sulfur, wt %	0.77	0.038	0.27	0.57	0.17	
Hydrogen, wt %	12.09	<0.04	<0.04	<0.04	<0.04	
Oxygen, ppm	1.20	13.80	13.54	13.45	13.66	
Flash, PM: °F	185	<100	580	1,620	320	
Pour Point, °F	+20	182	162	144	170	
Cetane Index	41	+10	+10	+20	+10	
Aromatics, vol %	-	58.0	56.0	53.5	55.5	
Distillation, D86		26.0	36.5	43.5	28.0	
°F at:						
10%	453	430	423	426	424	
30	493	468	469	475	464	
50	534	509	505	511	500	
70	574	550	550	554	540	
90	612	599	601	606	595	

TABLE VII

NAPHTHA PRETREATING AND REFORMING

Operating Conditions	Pretreating		Reforming	
Reactor Press., psig		1,400	<-----325----->	
Gas Circulation, SCFB		8,000	-	
Space Velocity, vol/hr/vol		1.0	<-----1.5----->	
H ₂ /HC, mol/mol		-	<-----7/1----->	
Avg. Catalyst Temp., °F		680	366	880
<u>Yields, wt % of Feed</u>				
H ₂ (SCFB)		(-808)	2.0	2.2
H ₂ S		0.84	-	-
NH ₃		0.69	-	-
H ₂ O		0.61	-	-
C ₁		0.20	1.2	1.4
C ₂		0.02	2.0	2.4
C ₂		0.08	3.8	4.6
C ₃		0.14	5.3	6.2
C ₄		103.0	81.9	78.8
C ₅ + Product (vol %)				
<u>Inspections</u>	<u>Feed</u>			
Gravity, °API	47.8	54.7	46.4	44.7
Nitrogen, ppm	5,700	<0.2	-	-
Sulfur, ppm	7,900	<0.5	-	-
Oxygen, ppm	5,400	<100	-	-
Hydrogen, wt %	13.28	14.77	-	-
Bromine Number	66	-	-	-
<u>Hydrocarbon Analysis,</u>				
D1319, vol %				
Saturates	38.0	-	-	-
Olefins	43.5	-	-	-
Aromatics	18.5	-	-	-
D2789, vol %				
Paraffins	-	58.8	44.0	38.7
Monocycloparaffins	-	30.6	3.2	2.7
Dicycloparaffins	-	3.9	0.1	0.1
Alkylbenzenes	-	6.1	50.7	56.7
Benzene	-	0.1	0.9	1.3
Toluene	-	0.6	6.4	7.9
C ₈	-	1.7	13.0	15.5
C ₉	-	3.7	27.8	32.0
Indanes & Tetralins	-	0.4	1.6	1.3
Naphthalenes	-	0.2	0.5	0.5
<u>Octane Numbers:</u>				
Research, Clear	-	29.0	92.9	96.7
Motor, Clear	-	-	82.9	86.0
<u>Distillation, °F at:</u>				
10%	279	262	181	178
30	300	284	-	-
50	316	304	286	282
70	334	325	-	-
90	354	349	358	358

TABLE VIII
UPGRADING FBR RAW SHALE OIL

<u>Operating Conditions</u>		
Reactor Press., psig	2,100	
Gas Circulation, SCFB	5,000	
Avg. Catalyst Temp, °F	750	
Space Velocity, vol/hr/vol	0.5	
<u>Yields, % of HDS Charge</u>		
H ₂ S, wt %	0.72	
NH ₃ , wt %	2.05	
H ₂ O, wt %	1.45	
C ₁ -C ₄ , wt %	2.09	
C ₅ + Syncrude, vol %	102.6	
Chem. H ₂ Consumption, SCFB	1,260	
<u>Inspections</u>	<u>Feed</u>	<u>Syncrude</u>
<u>Syncrude:</u>		
Gravity °API	20.7	31.5
Nitrogen, wt %	1.99	0.32
Sulfur, wt %	0.70	<0.05
Oxygen, wt %	1.32	0.03
Hydrogen, wt %	11.14	12.84
Pour Point, °F	+75	+70
<u>Fractions:</u>		
<u>Naphtha (C₆-375°F)</u>		
Yield: vol % Syncrude	16.7	
Gravity, °API	53.7	
Nitrogen, ppm	<0.5	
Sulfur, ppm	<0.5	
<u>Furnace Oil (375°-680°F)</u>		
Yield: vol % Syncrude	43.7	
Gravity, °API	36.0	
Nitrogen, wt %	0.23	
Sulfur, wt %	<0.05	
Aniline Point, °F	149	
Pour Point, °F	+10	
<u>Gas Oil (680°-960°F)</u>		
Yield: vol % Syncrude	24.3	
Gravity, °API	27.2	
Nitrogen, wt %	0.43	
Sulfur, wt %	<0.05	
Aniline Pt, °F	189	
Pour Point, °F	+95	
<u>Residuum (960°F+)</u>		
Yield: vol % Syncrude	15.3	
Gravity, °API	22.4	
Nitrogen, wt %	0.68	
Sulfur, wt %	<0.05	
Ni Equiv., ppm	<1.0	

Figure 1.
CONVENTIONAL UPGRADING ROUTE

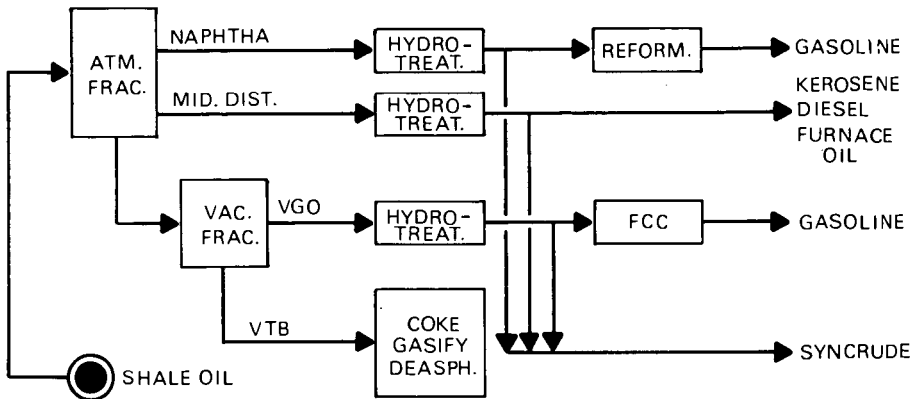


Figure 2.
ALTERNATE UPGRADING ROUTE

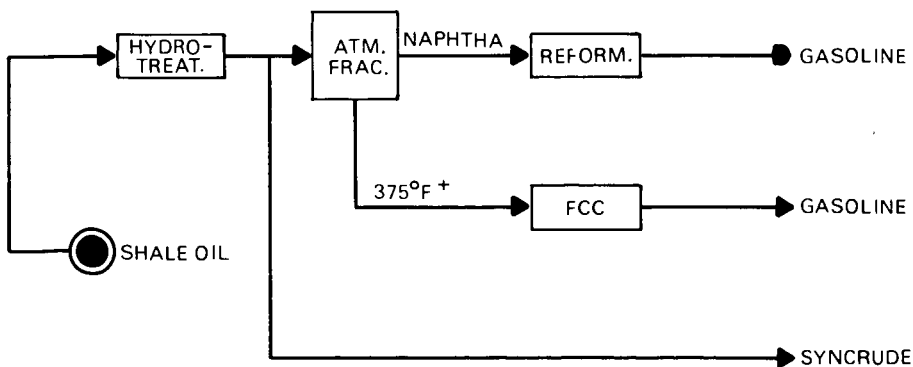


Figure 3
NAPHTHA HYDROTREATING

TEMPERATURE REQUIREMENTS FOR 0.5 ppm N

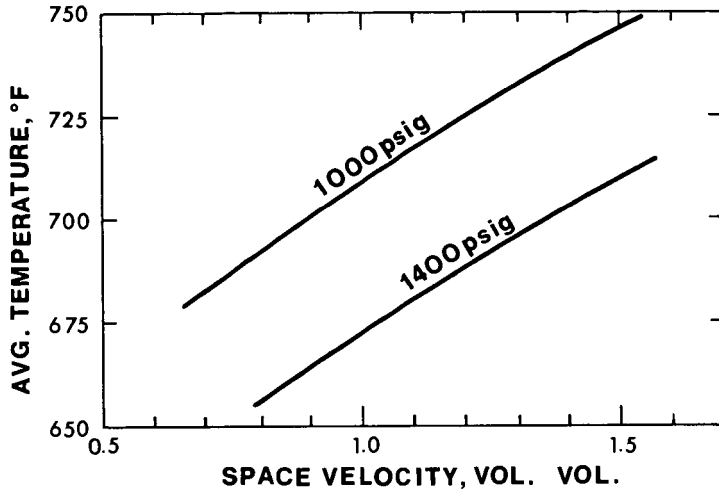


Figure 4
NAPHTHA REFORMING
C₅⁺ YIELD VS OCTANE SEVERITY

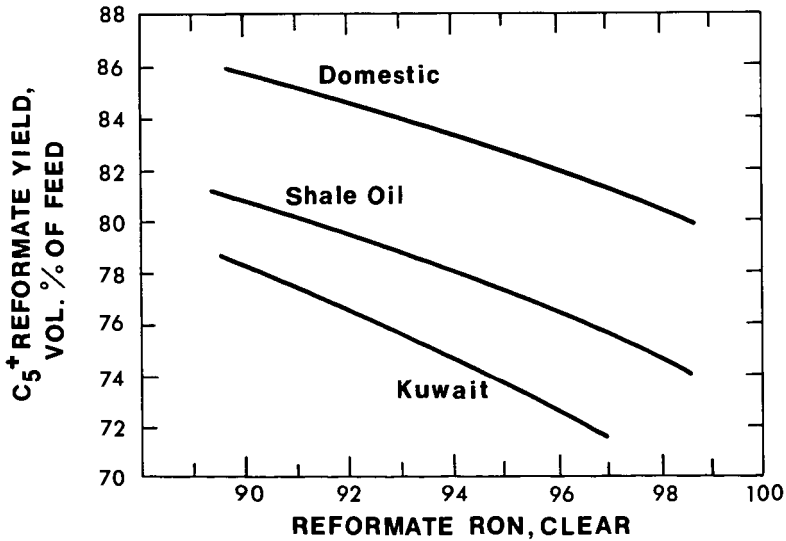


Figure 5
NAPHTHA REFORMING
H₂ PRODUCTION VS OCTANE SEVERITY

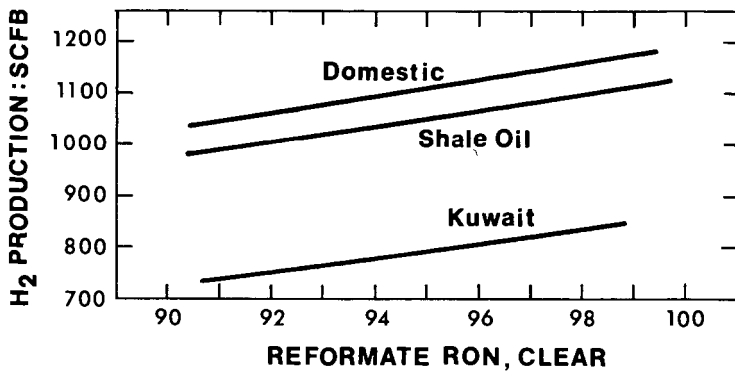
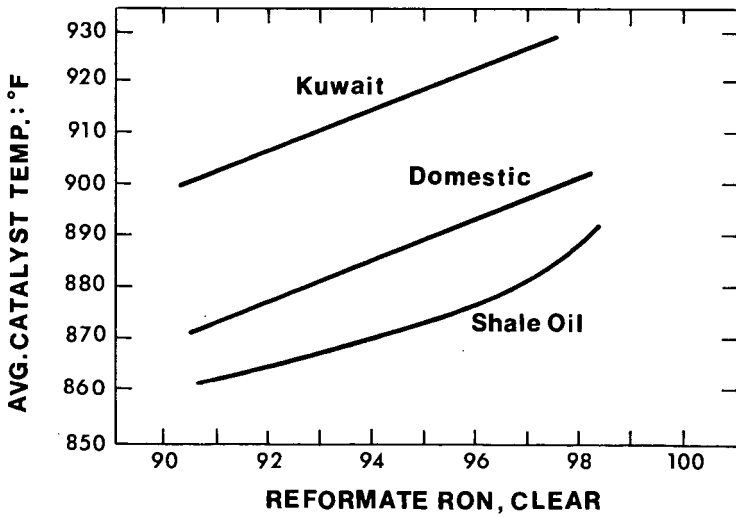


Figure 6
NAPHTHA REFORMING
AVG. CATALYST TEMP. VS OCTANE SEVERITY



ARSENIC AND NITROGEN REMOVAL DURING SHALE OIL UPGRADING

By

D. J. Curtin*, J. D. Dearth*, G. L. Everett
M. P. Grosboll, and G. A. Myers*

Atlantic Richfield Company, 400 E. Sibley Blvd., Harvey, IL 60426,
and *P. O. Box 2819, Dallas, TX 75221

Introduction

Shale oils and shale oil distillates can contain high concentrations of arsenic spread throughout their boiling ranges⁽¹⁾. Arsenic has been shown to rapidly and permanently deactivate commercial hydro-treating catalysts. Even where hydrotreating is not required, arsenic removal may be desirable.

The Nature of Arsenic in Shale Oil

Table 1 shows the arsenic distribution in a raw shale oil. The gas oil fraction contains the highest average arsenic concentration, about 52 ppm. A substantial arsenic peak occurs in the 204-260°C (400-500°F) boiling range. Following this peak, the arsenic concentration decreases. A significant arsenic level is observed in the residuum.

Table 1

Arsenic Distribution in Shale Oil

<u>Boiling Range</u>	<u>Fraction Volume Percent</u>	<u>Arsenic Content ppm</u>
IBP-204°C (IBP-400°F)	18	10
204-482°C (400-900°F)	58	52
482°C (900°F) and heavier	24	38

The distribution of the arsenic throughout the boiling range implies the presence of organic arsenic compounds. Other work reported in the literature confirms that organic arsenic compounds can be present in hydrocarbon fractions formed by the thermal decomposition of naturally occurring organic solids including European brown coal^(2,3,4,5,6,7). The pyrolysis of this coal yields a tar which has a very high arsenic content. Some of the arsenic-containing compounds have been shown to be organic in nature. We also have data which suggest that inorganic arsenic compounds are present.

Many organic arsenic compounds are known to be unstable. Thus it is possible under certain conditions that shale oil samples, including distillates, may lose a significant amount of their arsenic content. Care must be taken not only in sampling but also in storage and handling to maintain representative feedstocks. Over a long period of working with shale oil distillates in the development of the Atlantic Richfield Arsenic Removal and Hydro-treating Process, we have established many techniques necessary to ensure that the arsenic compounds remain representative of those in the commercial feedstock.

The Effect of Arsenic on Hydrotreating Catalysts

Figure 1 shows the effect of arsenic in shale oil on one commercial nickel-molybdenum hydrotreating catalyst. A shale gas oil was passed over the catalyst at 1.5 weight hourly space velocity, 2000 psig, 282°C (720°F), and 1014 m³H₂/m³ (6000 scf H₂/bbl). Initially the arsenic was totally removed from the oil by deposition on the nickel-molybdenum catalyst. When the arsenic level on the catalyst reached 7 weight percent, the arsenic level of the effluent oil increased rapidly.

The hydrodenitrogenation (HDN) activity of the nickel-molybdenum catalyst used in this test charging untreated shale gas oil is plotted in Figure 2. The HDN activity rapidly declined to a point where about 1000 grams of oil had been treated per gram of catalyst. At this point, which corresponds to the point where arsenic began to appear in the effluent oil, the rate of catalyst activity decline became less severe. Arsenic deposition appeared to be a major factor in the catalyst deactivation. This hypothesis was confirmed by an additional test of a fresh sample of nickel-molybdenum catalyst at the same conditions but charging shale gas oil with the arsenic removed. The HDN activity, also shown in Figure 2, declined much less rapidly than was the case when the arsenic-containing raw shale gas oil was treated.

Arsenic Removal from Shale Oil Distillates

Three alternatives were apparent for shale oil hydrotreating. First, one could attempt to develop a hydrotreating catalyst which would be resistant to arsenic poisoning. Our work indicated that existing catalysts with sufficient denitrogenation activity would be poisoned by arsenic due to its strong affinity for metals. A second possibility would be to remove the arsenic deposits from the catalyst during regeneration. Once again our data, later confirmed in tests by other companies, showed that standard regeneration procedures were ineffective in restoring HDN activity to an acceptable level. A third alternative would be to develop a new process to remove arsenic from the oil. In our preliminary studies, we determined that this third alternative was by far the most promising.

Many different arsenic removal process candidates were studied, and sufficient data were developed to permit us to make preliminary design and economic comparisons of the processes. The literature contains a number of patents for removal of arsenic in the parts per billion range from naphthas in order to protect very sensitive reforming catalysts. Unfortunately, such removal processes are apparently not applicable to shale oils with arsenic concentrations of 50 to 60 parts per million. As a consequence, a number of new process ideas were developed. Two processes, caustic washing and fixed-bed guard reactor, emerged from the preliminary evaluation as significantly superior to the others and were selected for further study.

A continuous bench-scale apparatus was constructed for experiments on caustic washing of shale gas oil fractions. As shown by the flow diagram in Figure 3, caustic solution and oil were pumped from storage tanks into a stirred reactor maintained at desired conditions of temperature and pressure. In the reactor a chemical

reaction occurred which resulted in the formation of arsenic compounds which were soluble in the caustic phase. The reactor effluent then flowed into a settler where the two phases were permitted to coalesce and be withdrawn through separate lines. To simulate commercial operation, a portion of the effluent caustic solution was recycled back to the feed tank. From analyses of the individual effluent phases, process conditions were evolved. This system was found to be effective for arsenic removal. Commercial design parameters were obtained from process variable studies, and economics were evaluated.

Figure 4 shows the flow diagram for the experimental guard bed apparatus. Hydrogen and oil were fed at prescribed rates into a packed reactor maintained at appropriate conditions of temperature and pressure. The hydrogen-oil mixture passed down over the catalyst bed and exited from the bottom of the reactor, at which point the gas and liquid phases were separated.

Using the data obtained from the two bench-scale units, we prepared preliminary commercial designs and calculated comparative economics for both processes. Other factors such as process operability and environmental effects were also considered. Based on our studies, the guard bed process was ultimately found to be superior to caustic washing in all three respects.

The development of the guard bed arsenic removal process was complicated by the unconventional nature of the shale oil and of the guard bed catalysts found to be most effective. For example, early catalysts tested, which were inexpensive and commercially available, performed satisfactorily in the process variable studies run to measure the effects of changing temperature and space velocity. However, in extended catalyst aging runs, problems were encountered with catalyst strength. A search for a suitable replacement catalyst was initiated, and a considerable effort was made to test commercial catalysts from a large number of different manufacturers and in several different sizes and physical configurations. Some of the candidates did exhibit performance which was superior to that for the original catalyst, but even the best catalysts did not meet our specifications. Eventually a strong, effective guard bed material was developed which was resistant to shale oil fouling and which will remove a high percentage of arsenic from shale oil distillates even at high levels of arsenic loading. The excellent effectiveness for arsenic removal provides substantial economic benefits. The use of competing materials would result in much larger and costlier processing equipment or a prohibitively high turnaround frequency to renew the guard bed material. This guard bed material, developed in a joint effort with a large catalyst manufacture using commercially projectable techniques, has been used to demonstrate this arsenic removal process for over 1000 hours charging shale gas oils at commercial process conditions. The arsenic removal dearsenation results of this demonstration run are shown in Figure 5.

This process operates over a wide range of pressures, hydrogen partial pressures and temperatures. It can process shale gas oil at high efficiency at required hydrotreating conditions for shale oil.

Pilot Plant Denitrogenation Studies

Experimental

Hydrodenitrogenation studies were performed in a bench scale continuous down-flow packed bed pilot plant unit. Over 60,000 reactor hours of shale oil processing were completed in our studies. Shale oil and hydrogen flowed through the packed bed and then through a high pressure water scrubber for removal of by-product ammonia and hydrogen sulfide gases. The latter stage avoids pilot plant operating problems due to ammonium sulfide formation. Gaseous and liquid products were then separated, metered, and analyzed to permit the determination of yields and weight balances.

Shale oil feedstocks containing both low and high arsenic levels were studied so that the effect on HDN of the arsenic removal co-process could be determined. Shale gas oil and naphtha fractions were treated separately since preliminary investigation showed this to be most economical for commercial applications. The gas oil work is discussed here.

Catalyst Screening

The denitrogenation catalyst activity and stability were shown to have a major impact on the cost effectiveness of the shale upgrading design because reactor investment is a major part of the total plant investment. To assure the selection of the best available catalyst, extensive comparison testing was done. As expected, nickel-molybdenum catalysts were better for HDN than cobalt-molybdenum catalysts. The catalyst chosen was found to have a 10-20 percent higher volume activity on shale oil than the best competitors.

Denitrogenation

An experimental program was conducted to determine the optimum range of processing conditions for achieving the desired low product nitrogen level. Process conditions studied cover a range of temperatures, 371-454°C (700-850°F), and space velocities, 0.5-2.0 (hours)⁻¹, at a reactor pressure found to provide an acceptable aging rate. A pyrolysis shale gas oil produced by a retort operation was tested along with a gas oil from the coking of the bottoms fraction of the pyrolysis oil. A pyrolysis-coker shale gas oil blend with low arsenic content was used for most of the studies, but high arsenic content pyrolysis-coker blends and coker only were also used to establish a feedstock effect.

Denitrogenation data from these tests were used to develop an HDN correlation based on first order kinetics:

$$\ln \frac{N_f}{N_p} = (K_{t,i}) \tau \cdot \alpha \quad 1)$$

where

- N_f = nitrogen content of feedstock, ppm
- N_p = nitrogen content of product, ppm
- $K_{t,i}$ = apparent rate constant at temperature t and with feed i
- τ = space time $\left(\frac{1}{\text{WHSV}}\right)$, where WHSV, the weight hourly space velocity, is defined as the weight of feed per hour per weight of catalyst.
- α = catalyst relative activity

First order kinetics gives a reasonable fit to the HDN data. This is consistent with the observation of McIlvried⁽⁸⁾ and others for the denitrogenation of various materials. Apparent rate constants calculated from equation 1) are plotted in Arrhenius form in Figure 6 showing an apparent activation energy of 26.9 Kcal/gm mole. The higher arsenic level feeds, both pyrolysis-coker blend and straight coker, showed significant HDN activity losses (5-10 percent for the blend and 35 percent for the coker alone). Figure 7 shows the actual denitrogenation data plotted in the form predicted by equation 1). Good agreement between the data and the first order kinetic form is indicated.

Hydrogen Consumption

The hydrogen consumption, calculated from material balance on hydrogen content of feed and product streams, is shown as a function of nitrogen removal in Figure 8. Feeds with higher hydrogen contents tend to consume less hydrogen by an amount approximately equal to the difference in hydrogen contents of the feeds. The range of hydrogen consumption observed for these shale oil HDN tests, 254-304 m³/m³ (1500-1800 scf/b), approach the consumptions obtained in conventional hydrocracking operations.

Aging Studies

A number of catalyst aging runs were made during the process development. One of these was a pilot plant gas oil aging run set up to simulate the production of a low nitrogen level (750 ppm) product from a feed oil containing 21,500 ppm nitrogen. Start-of-cycle process condition needed to achieve this low gas oil nitrogen level was 377°C (710°F).

During the 90-day aging run, the temperature was raised 7°C (13°F) to maintain denitrogenation. After 90 days the temperature was raised to 399°C (750°F), and operated for another 30 days. Only a 1°C temperature increase was required to maintain denitrogenation as shown in Figure 9. These results show that a 1 year cycle or greater is feasible for shale oil upgrading.

Reactor Modeling

In order to screen various reactor designs for a given application, a reactor model which simulates the important design variables was developed. Such a model must predict the required catalyst quantity, and predict yields for each reactor temperature, pressure, and hydrogen rate chosen.

For shale oil hydrotreating, the reactor model must also take into account the effect of arsenic since arsenic is a strong catalyst poison. Even with a guard bed, arsenic is deposited continually throughout the cycle and to compensate for its poisoning effect temperature must be raised to maintain HDN activity. Because of the highly exothermic reaction, many hydrogen quench points, such as shown in Figure 10, or other means of heat removal, are required to control reactor temperature. As the catalyst activity declines, both due to arsenic and time on stream, conversion in each catalyst bed changes. The lower conversion gives less heat release and, therefore, bed temperature must be increased to maintain catalyst activity. This in turn greatly changes the required hydrogen quench after each catalyst bed as the cycle progresses.

The variations are substantial, as illustrated in Figure 11. Since hydrogen quench rate varies significantly with time on stream, the quench system must be designed to handle a wide range of flows. Most conventional hydrotreaters would be unable to handle the quench rate variation along with the high heat release for shale oil processing. Flexibility must also be provided so the reactor inlet temperature can be raised. The model enables the designer to accurately take these effects into account for an optimum design.

The complexity in modeling arises when attempting to simultaneously take into account the effect on conversion of temperature, WHSV per bed and arsenic, when the amount of arsenic laydown itself is a function of WHSV and temperature. The actual system is further complicated in that the catalyst ages with time on stream as well, even if no arsenic were present.

For each catalyst bed the model does the following:

- o Calculates the severity and conversion.
- o Predicts yields including H₂ consumption needed to estimate the exothermic heat of reaction.
- o Performs heat balances to predict outlet temperature and quench rates.
- o Predicts HDS, HDN, hydrocracking, aromatic saturation, and olefin saturation.
- o Predicts catalyst activity as a function of arsenic and time on stream.

Design Studies

With such a model, the overall shale upgrading process can be optimized. Since arsenic removal and HDN are highly interdependent, the reactor design needs to be studied in order to minimize overall processing costs.

One use of the model is to determine the optimum conditions for arsenic removal since any arsenic leakage directly affects the required severity and cycle life for HDN. As the arsenic removal is increased via increased guard reactor size, capital costs increase but catalyst usage decreases. The optimum design for HDN can be found using the model. Conditions are chosen so arsenic removal and coke deposition are balanced to minimize costs.

The model has been used for two commercial designs, one for Colony Development Operation, a joint venture of which Atlantic Richfield is the operator, and another for a client of this shale oil hydro-treating technology.

Literature Cited

1. Burger, E. D., D. J. Curtin, G. A. Myers and D. K. Wunderlich, "Prerrefining of Shale Oil", Am. Chem. Soc., Div. Pet. Chem., Aug. 24-29, 1975.

2. Svajgl, O., Collection Czech Chem. Commun., 24, 3829 (1959).
3. Ibid., 28, 11 (1963).
4. Svajgl, O., Freiberger Forschung-H, A340, 89 (1964).
5. Svajgl, O., Scientific Papers of the Institute of Chemical Technology. Prague; Tech. of Fuels, 7, 187 (1965).
6. Ibid., D13, 163 (1967).
7. Svajgl, O., Sbornik praci z vyzkumu chernicke ho vyuziti, dehtu a ropy, 8, 83 (1968).
8. McIlvried, H. G., "Kinetics of the Hydrodenitrication of Pyridine", Industrial Engineering Chemistry, Process Design and Development, 10, 1, 125-130 (1971).

FIGURE 1
ARSENIC IN HYDROTREATED PRODUCT OIL

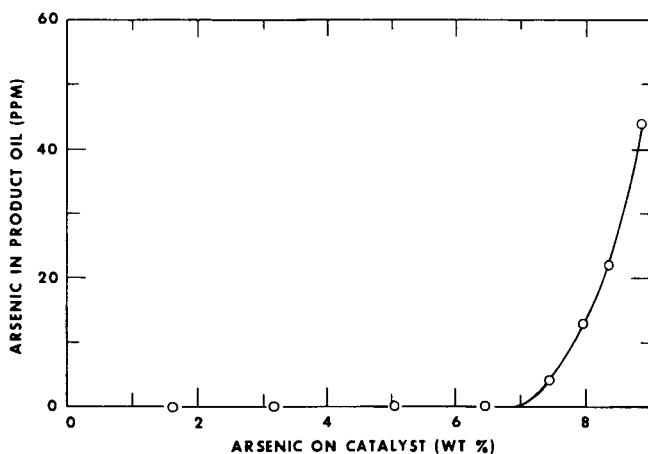


FIGURE 2
 CATALYST ACTIVITY OF A NICKEL-MOLYBDENUM
 CATALYST TREATING SHALE OIL

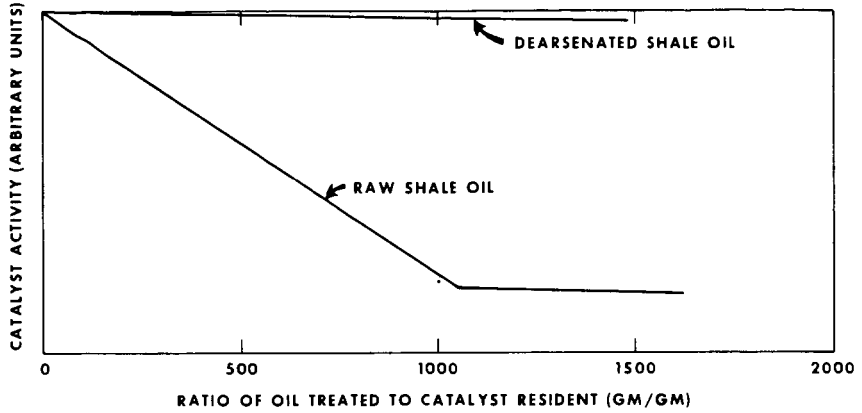


FIGURE 3
 CONTINUOUS CAUSTIC SODA WASH APPARATUS (WITH RECYCLE)

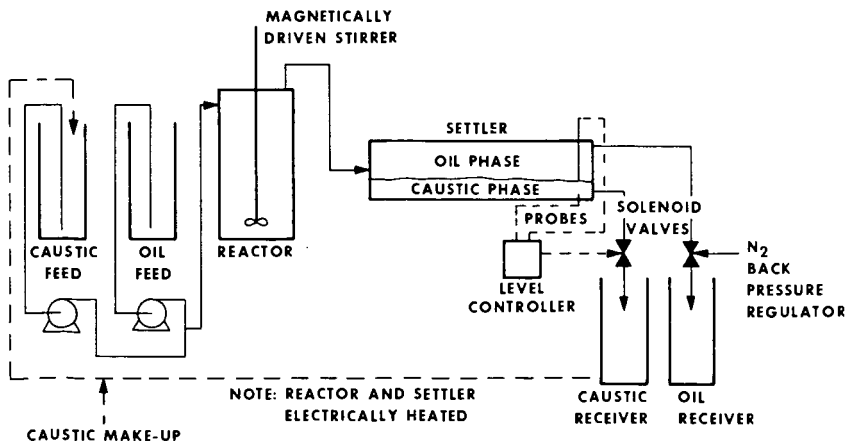


FIGURE 4
 FLOW DIAGRAM FOR EXPERIMENTAL GUARD BED SYSTEM

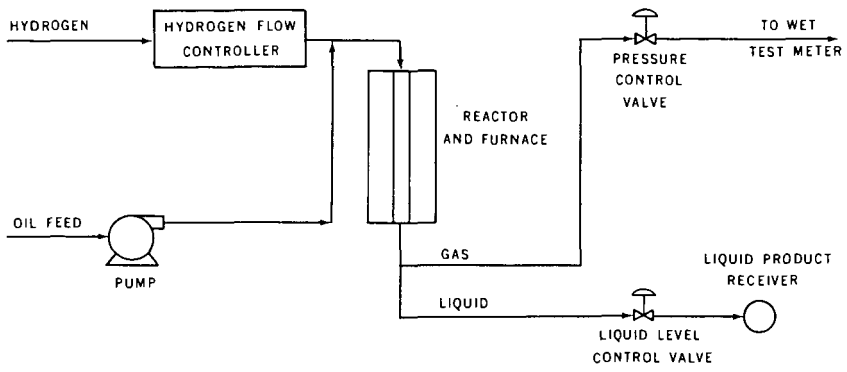


FIGURE 5
 ARSENIC REMOVAL DEMONSTRATION RUN RESULTS

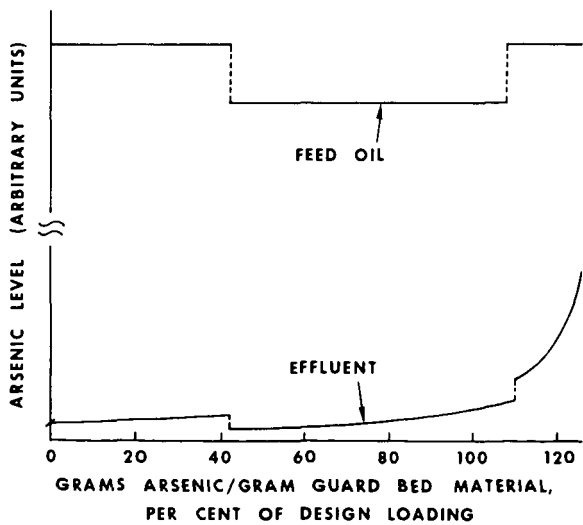


FIGURE 6
EFFECT OF FEED AND TEMPERATURE
ON DENITROGENATION RATE

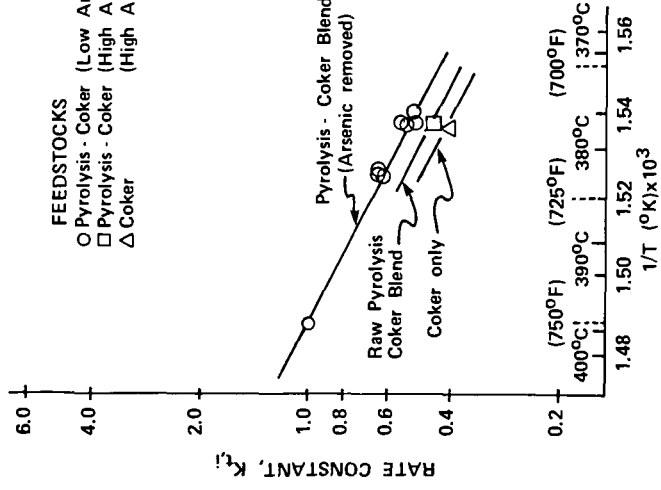


FIGURE 7
REACTOR SEVERITY vs. PERCENT DENITROGENATION

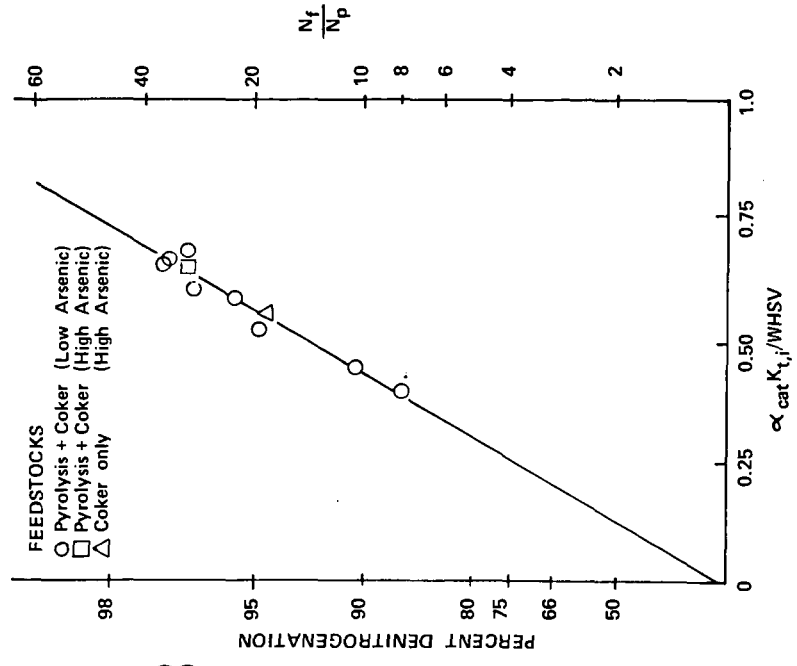


FIGURE 8

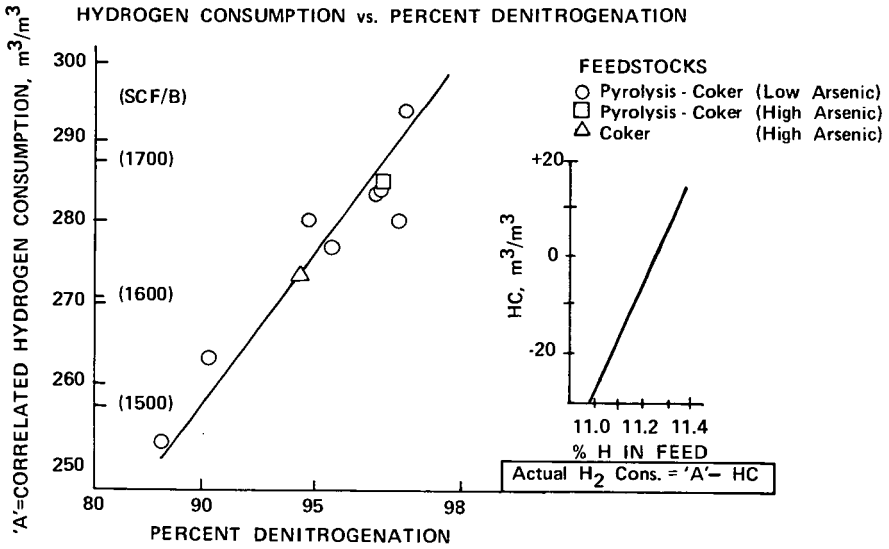


FIGURE 9
CATALYST AGING STUDY

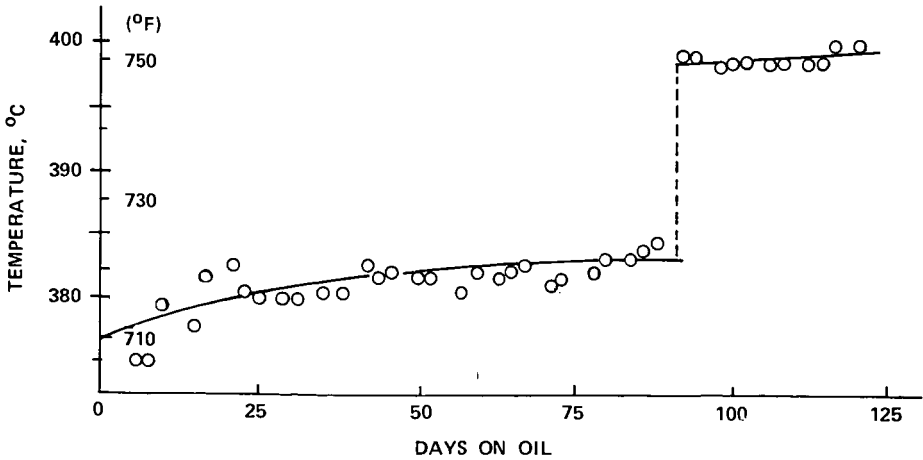


FIGURE 10
SHALE OIL UPGRADING

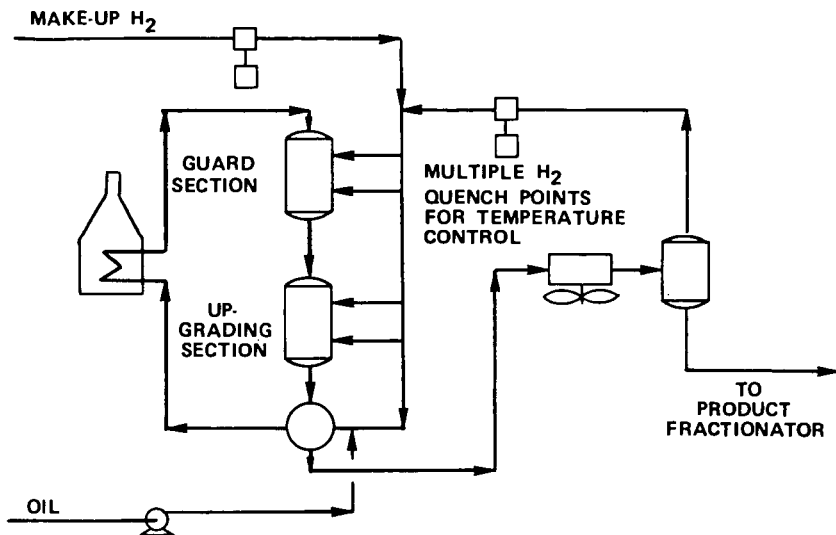
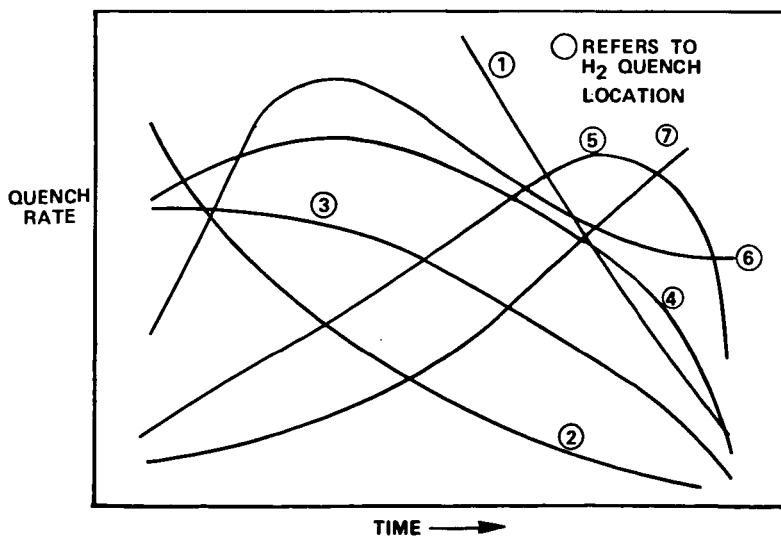


FIGURE 11
QUENCH RATE VARIABILITY



STABILIZING OF SHALE OIL-WATER EMULSIONS BY PENTANE-INSOLUBLE MATERIALS

Philip L. Cottingham, Frederic A. Birkholz, and Leo G. Nickerson

Department of Energy, Laramie Energy Research Center
P. O. Box 3395, University Station
Laramie, WY 82071

INTRODUCTION

Separation of crude shale oil from the water produced during retorting has long been a problem with some shale oils retorted from Green River Formation oil shale of the western United States. In recent work (1) it was reported that shale oil produced from the Paraho retort by the indirectly heated mode could be easily separated from retort water after being heated to 77°C (170°F) and allowed to settle at this temperature for six hours. Conversely, it has been found by the LERC authors that a sample of raw (untreated) crude shale oil produced from Site 9 of the Department of Energy (DOE) in situ retorting project near Rock Springs, Wyoming, was not separated from suspended retort water when heated in a separatory funnel to 82°C (180°F) for a period of 15 hours.

In 1949, a brief study was reported (2) on the removal of suspended solids from N-T-U shale oil by a rotary filter precoated with filter aid. Water that could not be separated from the unfiltered oil by heating was easily separated when the filtered oil was heated to 71°C (160°F) for three hours. It was not determined whether the solids removed by the filter were organic or inorganic.

The Paraho shale oil mentioned above contained only 0.17 weight-percent asphaltenes (1) insoluble in hot heptane, while the in situ shale oil contained over 3.6 percent organic material insoluble in pentane. The present study was undertaken to determine whether the portion of shale oil that is insoluble in normal pentane and other solvents may be responsible for the formation of stable shale oil/water emulsions of in situ shale oil. Greater knowledge of the cause of the emulsions may assist in developing methods of avoiding their formation during retorting or subsequent handling of the oil; it may also help in devising newer and cheaper ways of separating the oil and water phases of emulsions.

EXPERIMENTAL

General Procedure

Pentane-insoluble materials were separated from filtered, dewatered crude shale oil prepared from DOE Site 9 crude oil, and from fractions of the oil. These materials were used as additives for blending in small percentages with light gas oil, dewaxed heavy gas oil, and filtered, dewatered pentane-extracted crude shale oil.

A blend was prepared by mixing a measured weight of additive with 100 ml of oil and stirring the mixture in a beaker at room temperature for 10 minutes with an electric stirrer. Distilled water was added and the mixture was stirred for 10 minutes after which the mixture was transferred to an electrically heated separatory funnel. Amounts of additive ranged from 0.5 to 2.2 weight percent of the oil, and amounts of water ranged from 11.4 to 52.2 percent.

Mixtures in the separatory funnel were heated with an electric jacket to 77°C (170°F), and maintained at this temperature for five hours under a flowing stream of nitrogen. The water and oil phases were drained separately into graduated cylinders and were weighed. A dry ice trap connected by a flexible tube to a water-cooled reflux condenser at the top of the separatory funnel during the

heating period collected vapors leaving the funnel. Only small amounts of water and traces of hydrocarbon too small to separate from the water were collected in the trap.

Preparation of Feeds For Blending With Additives

The first of three feeds for blending with pentane insoluble material was prepared from in situ Site 9 crude by filtering the crude shale oil through 60-to-100 mesh Berkshire sand and number 40 Whatman filter paper. No measure of the solids removed was obtained. Water was eliminated by distillation to a flask temperature of 150°C (302°F) at 40 mm absolute pressure. Oil condensed with the water was separated in a separatory funnel, dried over anhydrous sodium sulfate, and combined with the cooled contents of the distillation flask.

Dried shale oil was stirred with 15 volumes of n-pentane two hours at room temperature and filtered through a medium (M) porosity fritted glass funnel. Pentane was removed from the filtrate by distillation to a flask temperature of 200°C (392°F) at 585 mm mercury absolute, and the pentane-free filtrate was used as a feed for blending with pentane-insolubles in the emulsification studies. The funnel containing pentane-insolubles was vacuum-dried (380 mm absolute) at room temperature to constant weight, and the pentane-insoluble material was used as an additive in the emulsification studies.

The second feed for the blending studies was light gas oil prepared by distillation of raw, wet, unfiltered in situ Site 9 crude shale oil to initial and final column head temperatures of 106°C (223°F) and 200°C (392°F) at 40 mm; these corresponded to 200°C (392°F) and 313°C (595°F) at 760 mm. The light gas oil contained 0.46 weight-percent insoluble in pentane at room temperature (at a pentane:oil ratio of 20:1).

Heavy gas oil, the third feed for the blending studies, was obtained by continued distillation of the crude, after removal of light gas oil, to a column temperature of 300°C (572°F) at 40 mm, corresponding to 431°C (807°F) at 760 mm. To prevent complications during mixing and measuring that would be caused by wax in the heavy gas oil, the oil was dewaxed with a 2:1 acetone-toluene mixture at 0°C. Yield of wax was 11.5 weight percent. The dewaxed oil contained 0.45 weight-percent material insoluble in pentane at room temperature (20:1 ratio).

Preparation of Pentane-Insoluble Additives Mixed Into Feeds

Four pentane-insoluble materials were used in the study. These included two different insoluble portions of the filtered, dried in situ crude oil prepared by extraction of the dried crude with different pentane:oil ratios; the pentane-insoluble portion of the vacuum distillation residuum from the raw, wet, unfiltered crude; and the pentane-insoluble portion of solids filtered from the same raw crude with a 325-mesh screen. Properties of all insoluble fractions are shown in table 1.

Preparation of the insoluble portion of the filtered, dried crude at a 15:1 pentane:oil ratio has been described. The insoluble portion amounted to 3.6 weight-percent of the dry, filtered crude. A second insoluble portion was also prepared at a 40:1 extraction ratio and was used in one emulsification experiment. It was 2.8 weight-percent of the dry crude.

Distillation residuum from the previously-discussed distillation of light and heavy gas oils from raw crude oil was extracted with pentane at a solvent:oil ratio of 20:1, yielding 24.2 weight-percent of the residuum or 3.8 percent of the dry crude as pentane-insoluble material that was used in emulsification studies. Properties of this material are also shown in table 1.

The fourth pentane-insoluble material was prepared from solids that were separated from Site 9 crude oil by screening the crude at 65°C through a 325-mesh stainless steel standard Tyler sieve. Prior to screening, the sample of raw, wet crude had been heated at 77°C (170°F) in a separatory funnel for five hours with no separation of water. The same sample was filtered through the 325-mesh screen, removing 3.5 weight-percent of the wet oil (4.9 percent, dry oil basis) as "gunk" on the screen.

Solids separated on the 325-mesh screen were extracted with pentane (15:1 weight ratio), yielding 26.5 percent material (1.3 percent of the dry crude) insoluble in pentane. When the filtered oil was replaced in the separatory funnel and heated to 77°C, water quickly separated. Water measured at the end of five hours was 29.2 weight-percent of the original wet crude. Subsequent testing for water in the dewatered oil by the ASTM distillation method (D-95) showed less than 0.05 weight-percent water in the oil.

In addition to emulsification tests made with the pentane-insoluble materials, tests for comparison purposes were made with the pentane-soluble portion of the sand-and-paper filtered dried crude and with the pentane-soluble portion of the distillation residuum (see table 2). Tests also were made with toluene-soluble and toluene-insoluble portions of pentane-insoluble material from the screen-filtered solids, and with chloroform-soluble, pentane-insoluble portion. All tests with materials separated from the wire-screen-filtered crude are shown in table 3.

Results and Discussion of Experiments

Effect of Additives From Residuum and Filtered Crude on Filtered, Pentane-Extracted Crude

Experiments A through G were made with the pentane-soluble portion of crude shale oil that had been filtered through sand and filter paper.

When distilled water alone was mixed with the pentane-soluble portion of sand and paper-filtered crude in experiment A (table 2) the oil and water phases separated in a few minutes with a clear, sharp interface. Heating was continued for the scheduled five hours, at the end of which some loss in weight of the oil was found to have occurred. Part of the loss was the result of vaporization, as shown by some condensate in the dry ice trap; part of it may have been the result of some of the oil being dissolved in the water phase.

In experiments B, C, and D, pentane-insoluble material from the vacuum distillation residuum was added to samples of the same pentane-soluble filtered crude used in experiment A. Addition of 0.5, 1.0, and 2.0 percent pentane-insoluble to the pentane-soluble-oil before mixing with water caused the oil phases to pick up increasingly larger percentages of water that did not separate from the oil phase after settling five hours at 77°C. No individual droplets of water were discernible in the oil phases. The oil phase from experiment D, in which 2.0 percent pentane-insoluble additive was used, gained 48.8 weight percent (including the 2.0 percent additive), based on the weight of the original oil.

The ash content of the pentane-insoluble material from the distillation residuum was only 1.02 percent. In a 2.0 percent blend of the pentane-insoluble material with filtered crude, the pentane-insoluble would contribute only 0.02 percent ash to the blend. It appears that the inorganic material played little part in the formation of the emulsions.

In experiments E, F, and G, 1.0 weight-percent pentane-insoluble from the sand-filtered crude was added to the pentane-soluble crude before it was mixed with water. In experiment F, the oil was heated to 100°C before the pentane-insoluble was added, and was maintained at this temperature for one hour, with stirring, after the addition to promote solution of the additive in the oil before water was added. Pentane-insoluble that was separated from the raw, filtered crude with a solvent:oil ratio of 40:1 was used in experiment G. In each of these

three experiments, a small loss in weight of the oil phase occurred, indicating no emulsion-forming tendency for the pentane-insoluble from the filtered crude under the conditions used.

Effect of Additives From Residuum and Filtered Crude on Gas Oils

When 2.2 percent of the pentane-insoluble from the filtered crude was mixed with dewaxed heavy gas oil and the mixture was heated to 320°C for one-half hour before the addition of water, the oil phase gained 8.8 percent in weight (experiment H). This contrasts with a recovery of only 98.4 weight-percent in the oil phase when the heavy gas oil alone was heated to 320°C before mixing with water (experiment Y). The results show an emulsifying effect for the pentane-insoluble from the filtered crude after it was heated. (Compare experiments E, F, and G in which it was not heated.)

Both experiments J and K of table 2 show that the pentane-soluble portion of the distillation residuum displayed little or no effect as an emulsifying agent either at room temperature or after being heated in gas oil at 320°C.

Experiments M, N, and O show that pentane-insoluble material from vacuum distillation residuum displayed very great emulsion-forming tendency when mixed in light gas oil; but pentane-soluble material from the same source displayed little or no such tendency.

Effect of Additives From Suspended Solids on Gas Oils

Data in table 3 show that the pentane-insoluble part of solids separated from the raw crude with 325-mesh screen displayed strong emulsifying power for water when mixed in light gas oil. (Compare experiment P with M in table 2).

A portion of these pentane-insoluble solids was extracted with toluene (15:1 weight ratio) to produce a toluene-soluble solid and a toluene-insoluble solid. The soluble portion did not show any emulsifying effect when mixed in light gas oil at room temperature (experiment Q) but the insoluble portion showed a strong emulsifying effect (experiment V). When the soluble portion was added to heavy gas oil and heated to 320°C for one-half hour, it showed a strong emulsifying effect (experiment R).

The pentane-insoluble, toluene-insoluble material was extracted with chloroform, also producing soluble and insoluble solids. The soluble portion did not display any emulsifying effect when mixed with light or heavy gas oils at room temperature (experiments S and T); however, when it was added to heavy gas oil and heated to 320°C for one-half hour before the addition of water, it showed strong emulsifying power (experiment U). The chloroform-insoluble portion showed strong emulsifying power when mixed in light gas oil at room temperature (experiment X).

SUMMARY AND CONCLUSIONS

Pentane-insoluble material from vacuum distillation of in situ crude shale oil, and pentane-insoluble material separated from the crude with a 325-mesh screen were found to be strong emulsifying agents for shale oil/water mixtures. The toluene-soluble and chloroform-soluble portions of pentane-insoluble material separated from the crude with the screen did not promote emulsions when mixed in gas oils at room temperature, but when heated to 320°C for one-half hour with the oil they acted as strong emulsifying agents.

The study showed that certain parts of the oil have little emulsifying power when mixtures containing them are kept at low temperatures, but display strong emulsifying power when the mixtures are heated to 320°C. This finding suggests the possibility that cooling the freshly-retorted oil as rapidly as possible after it is retorted may be a method of decreasing the formation of emulsions.

Several possibilities suggest themselves concerning why the solvent-soluble materials act as emulsifying agents after they have been heated to 320°C in gas oil, but no conclusions have been drawn. These soluble materials were all separated from the insoluble materials by filtration through a fritted-glass funnel during their preparation. This fact is further evidence that a large proportion of the emulsions in shale oil are caused by organic emulsifying agents; however, it does not entirely rule out the possibility that inorganic materials also play a part in the formation of some emulsions.

Filtering the raw, wet crude oil through a 325-mesh screen was an effective method of breaking the oil/water emulsion so the water would easily settle out with the application of moderate heat; however, the oil used was over a year old at the time of filtering. The method should be tested on several freshly-retorted crude oils to determine its effectiveness.

LITERATURE CITED

1. Sullivan, R. F., and Stangeland, B. E. Catalytic Hydroprocessing of Shale Oil to Produce Distillate Fuels. Presented before Div. of Petr. Chem., ACS, 174th National Meeting, Chicago, IL, Aug. 28-Sept. 2, 1977.
2. Secretary of the Interior. Synthetic Liquid Fuels. Annual Report for 1949, Part II. BuMines RI 4652, 70 pp.

TABLE 1. - Properties of Pentane-Insoluble Fractions From Filtered,
Dried In Situ Crude

	Source			
	Distillation Residuum	Filtered Crude	40:1	+325 Mesh From Raw Crude
Extraction ratio	20:1	15:1	40:1	10:1
Wt. % of dry crude (as pentane insoluble)	3.8	3.6	2.8	1.3
Carbon, wt. %	78.80	79.76	78.76	71.42
Hydrogen, wt. %	7.63	8.09	7.66	6.77
Nitrogen, wt. %	3.59	3.95	4.53	4.26
Sulfur, wt. %	1.42	2.78	3.18	7.15
Oxygen + mineral (by diff.)	8.56	5.42	5.87	10.40
C/H wt. ratio	10.32	9.86	10.28	10.55
Ash, wt. %	1.02	0.82	1/	1/
Mol. wt.	1000	457	1235	948

1/ Not yet available.

TABLE 2. - Emulsion-Forming Tendency of Pentane-Soluble or Insoluble Additives When Blended With Feeds Prepared From Shale Oil

Experiment Identif.	Feed for Blending	Source and Type of Additive	Percent Mixed in Oil		Oil Phase ^{1/} Wt. % of Raw Oil
			Additive, Wt. % of Oil	Water Used, Wt. % of Oil	
A	Pentane sol. from filtered crude.	None used.	0.0	11.4	97.9
B	Pentane sol. from filtered crude.	Vac. distn. res. Pentane insol.	0.5	11.4	102.6
C	Pentane sol. from filtered crude.	Vac. distn. res. Pentane insol.	1.0	33.7	113.8
D	Pentane sol. from filtered crude.	Vac. distn. res. Pentane insol.	2.0	51.2	148.8
E	Pentane sol. from filtered crude.	Filtered crude. Pentane insol. ^{2/}	1.0	33.5	97.0
F	Pentane sol. from filtered crude.	Filtered crude. Pentane insol. ^{3/}	1.0	33.4	98.5
G	Pentane sol. from filtered crude.	Filtered crude. Pentane insol. ^{3/}	1.0	33.9	97.1
H	Dewaxed heavy gas oil.	Filtered crude. Pentane insol. (Mix heated to 320°C.)	2.2	49.6	108.8
J	Dewaxed heavy gas oil.	Vac. distn. res. Pentane soluble.	2.0	49.6	100.7
K	Dewaxed heavy gas oil.	Vac. distn. res. Pentane soluble. (Mix heated to 320°C.)	2.0	49.7	101.0
L	Dewaxed heavy gas oil.	Vac. distn. res. Pentane insol.	2.0	50.6	126.9
Y	Dewaxed heavy gas oil.	None used. Heated to 320°C.	0.0	33.5	98.4
M	Light gas oil.	None used.	0.0	35.2	98.6
N	Light gas oil	Vac. distn. res. Pentane soluble	2.0	51.7	101.5
O	Light gas oil.	Vac. distn. res. Pentane insol.	2.0	52.0	140.5

36

1/ After heating 5 hours at 77°C.
 2/ Pentane-insoluble powder (15/1) stirred into oil while oil heated at 100°C.
 3/ From extraction of filtered crude at 40/1 solvent/oil ratio.

TABLE 3. - Emulsion-Forming Tendency in Shale Oil of Portions of Solids Filtered From In Situ Crude With 325-Mesh Screen

Experiment Identif.	Oil Used	Additive Mixed in Oil	Additive, Wt. % of Oil	Water Added, Wt. % of Oil	Oil Phase ^{1/} , Wt. % of Original Oil
P	LGO ^{2/}	Pentane-insoluble portion.	2.0	52.1	132.4
Q	LGO	Pentane-insoluble, toluene-soluble portion.	2.0	51.8	98.8
R	HGO ^{3/}	Pentane-insoluble, toluene-soluble; oil-additive mix heated $\frac{1}{2}$ hr. at 320°C.	2.0	49.5	138.0
S	LGO	Pentane-insoluble, toluene-insoluble, chloroform soluble.	2.0	52.0	100.5
T	HGO	Pentane-insoluble, toluene-insoluble, chloroform soluble.	2.0	50.0	100.5
U	HGO	Pentane-insoluble, toluene-insoluble, chloroform soluble. Mix heated $\frac{1}{2}$ hr. at 320°C.	2.2	49.8	136.5
V	LGO	Pentane-insoluble, toluene-insoluble portion.	2.0	52.2	121.1
W	Crude	No additive. Water only, mixed with wire-screen-filtered dewatered crude.	0.0	50.9	98.3
X	LGO	Pentane-insoluble, toluene-insoluble, chloroform insoluble portion.	2.0	52.1	120.4

^{1/} After heating 5 hours at 77°C.

^{2/} LGO is light gas oil.

^{3/} HGO is heavy gas oil.

EFFECT OF RETORTING ON WAX CRYSTALLIZATION IN UTAH SHALE OILS

P. F. Lovell

Sunoco Energy Development Co.
12700 Park Central Place, Suite 1500
Dallas, Texas 75251

and

W. H. Seitzer

Suntech, Inc.
P. O. Box 1135
Marcus Hook, Pennsylvania 19061

Introduction

The White River Shale Project (WRSP) was formed in June, 1974, by Phillips Petroleum Company, Sunoco Energy Development Co., and Sohio Petroleum Company. The purpose of the project was to develop jointly the oil shale resource on the federal lease Tracts Ua and Ub in northeastern Utah. Tract Ua is jointly owned by Phillips and Sunoco Energy Development, while Sohio holds title to Ub. This combined resource has an estimated 1.06 billion barrels of oil in place, averaging 28 gallons per ton (1).

To abide by the lease terms WRSP prepared and issued a detailed development plan (DDP) in June, 1976. This DDP included the various phases of development necessary to reach commercial production and, ultimately, abandonment of the leases. To this end, WRSP has continued evaluating the technological progress of the various retorting processes. In February, 1976, the WRSP mined several hundred tons of Uinta Basin, Utah, oil shale from an outcrop formation on patented lands about 3 miles east of the Ua-Ub federal leases in a 26 square mile area known as Hells Hole Canyon. This is shown in Figure 1.

The sample was collected in two parts: the first from an approximate 12 foot interval above the Mahogany marker, and a second sample from an approximate 20 foot interval located immediately below the Mahogany marker. The ore body was not pre-assayed at Hells Hole Canyon. Therefore, the grades of the samples were unknown until they were received and Fischer assayed by the respective toll processors, Paraho Development Corporation, Anvil Points, Colorado, and Union Oil Co., Brea, California.

Retorting

A. Paraho Direct Heated (DH) - Approximately 100 tons of 19 gpt Utah shale, sized 1/2" x 2", were processed in the 2 1/2 ft. I.D. pilot plant using the Paraho DH mode at a nominal rate of 1 ton per hour. In the DH mode the retorting heat is supplied by combustion, directly in the retort, of residual carbon by the oxygen in the gas-air mixture. Retort temperatures are controlled by adjusting the composition of the recycle gas return. Figure 2 gives a simple illustration of the process (2).

The oil yield for the Utah shale was 92.8 vol % of Fischer Assay, very similar to what has been reported for the Paraho DH mode on Colorado shale (3). The yield of product gas was about 8000 SCF/T of 66 Btu/Ft³ gross heating value material. The overall weight balance was 98.6%. Some properties of the raw and retorted shale are shown in Table I.

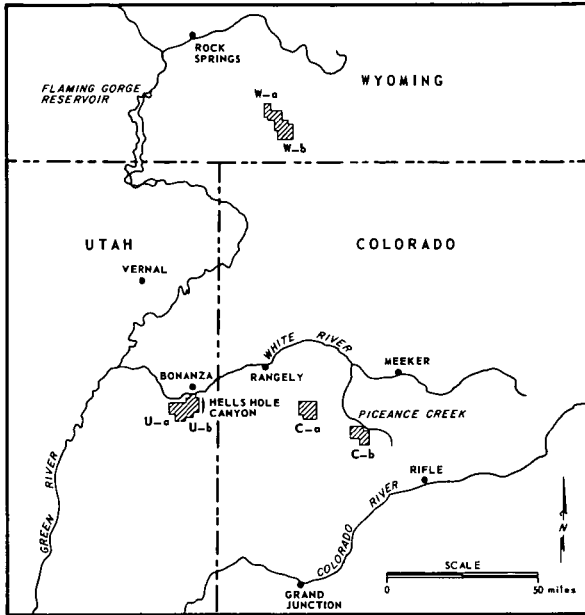


FIGURE 1. LOCATION OF U_a-U_b & HELLS HOLE CANYON

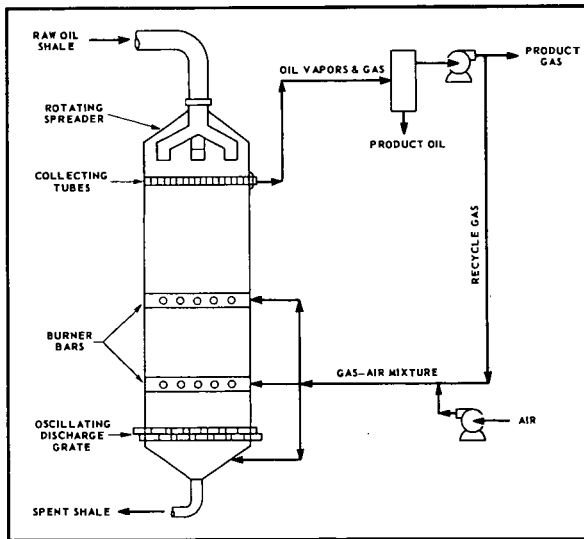


FIGURE 2. PARAHO OIL SHALE KILN

Table I
Utah Shale Properties

	Paraho DH		Union "B"	
	Raw Shale	Spent Shale	Raw Shale	Spent Shale
Fischer Assay				
Oil, gal/ton	18.61	0.69	32.20	-
Oil, Wt %	7.11	0.26	12.21	0.0
Water, gal/ton	5.85	-	2.90	2.10
Water, Wt %	2.44	0.23	1.23	0.86
Mineral CO ₂ , Wt %	19.83	13.39	18.96	21.93
Organic C, Wt %	-	1.93	13.68	2.83
Elemental Analysis				
C, Wt %	15.28	5.58	18.85	8.81
H "	1.46	0.11	2.05	0.35
N "	0.44	0.15	0.46	0.31
S "	0.35	0.31	0.53	0.41

B. Union "B" - The 100-ton sample of 32 gpt Utah shale was reduced to a consist of 1/4" x 1" and retorted in the Union "B" mode in their nominal 6 T/D pilot retort. Raw shale rate for these runs was around 3 T/D. The Union "B" process is an indirect heated mode where the retorting heat is supplied by externally heated recycle gas as opposed to direct combustion of shale inside the retort vessel. A unique aspect of the Union process is the upflow of raw shale using a reciprocating "rock pump" rather than gravity downfeed of the raw shale. A simplified diagram of the Union "B" process is illustrated in Figure 3 (4).

Oil yield was about 97 vol % of Fischer Assay (~101 vol % on a C₄+ basis) for the Union "B" processing. This yield is also similar to results on Union's Colorado shale (5,6). Retort product off-gas yield was about 725 SCF/T. This material had a calorific value of about 900 Btu/Ft³. The material balance for the Utah shale runs averaged 99+ Wt %. Properties of the Utah shale processed by Union are also given in Table I.

Analytical Results

Practically all previously reported data from these two processes have been on Colorado Piceance Basin shales. This present effort was an attempt to obtain data on Utah oil shale and determine if Utah shale oils were any different. No major differences between Utah and Colorado shale oils were found (7). Table II presents comprehensive analytical examinations of both the Paraho and Union produced whole, raw Utah shale oils. Despite the wide variation in shale grades (19 gpt vs. 32 gpt) and the known differences between both retorting processes, the raw shale oil products appeared to be quite similar both physically and chemically.

The only major difference in the two oils was in their respective pour points, 30°F for Union "B" and 75°F for Paraho DH. Known differences between the pour points of the oils produced by these processes from Colorado shale have been reported (4). The 30°F pour point for the Union "B" shale oil was lower than expected.

Transportability of raw shale oils via pipeline is a viable option for eventual marketability. Although pour point isn't the only factor determining the pumpability of oils, it is an important variable. A naturally occurring lower pour point oil could have economic advantages when compared to oils requiring additions of available, chemical pour depressants. Therefore, this observed low pour point

of 30°F for the Union "B" Utah oil is certainly an interesting and serendipitous phenomenon. On closer examination, however, it was observed that the wax in the two oils crystallized differently.

Table II
Physical and Chemical Properties of Raw Utah Shale Oils

Properties		Union "B"	Paraho DH
Gravity	°API	20.2	19.6
Carbon	Wt %	84.27	84.21
Hydrogen	"	11.68	11.82
Oxygen	"	1.23	1.89
Sulfur	"	0.55	0.50
Nitrogen Total	"	1.93	2.09
Nitrogen Basic	"	1.26	1.19
Ash	"	0.3	0.05
Conradson Carbon	"	4.3	3.1
Pour Point	°F	30	75
Viscosity @ 100°F	CS	35.3	60.9
Viscosity @ 210°F	"	4.83	5.95
Arsenic	W ppm	49	19
Chloride	"	15	6
Chemical Structure by ASTM D-2007			
Paraffins	Wt %	9	7
Naphthenes	"	10	10
Olefins	"	7	5
Aromatics	"	45	44
Polar Aromatics	"	24	29
Pentane Insols.	"	5	5
Distillation ASTM D-1160			
IBP		152	220
10		345	503
30		633	690
50		799	827
70		919	952
90		1078	-
EP		1100	1100
% Recovery		92	87

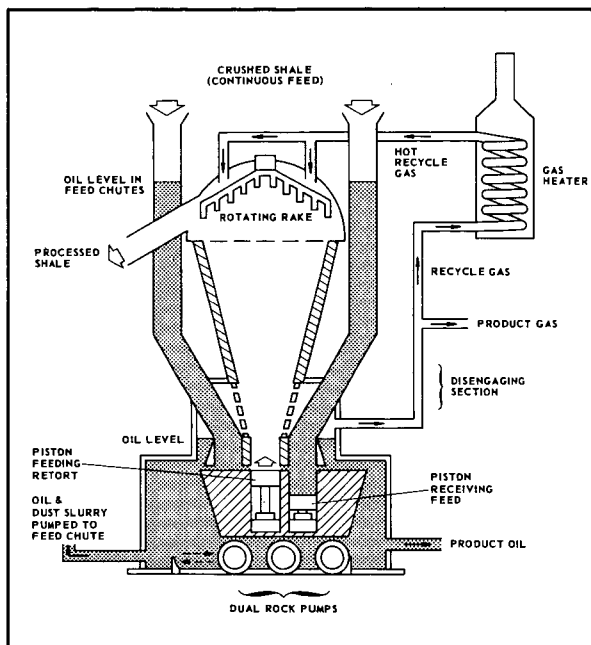


FIGURE 3. UNION "B" OIL SHALE RETORT

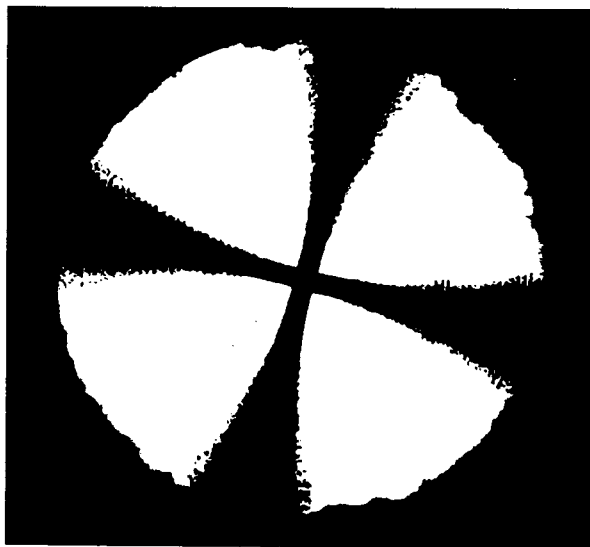


FIGURE 4. SPERRILITE OF ANISOTROPIC CRYSTALS BETWEEN CROSSED POLARS

Wax Spherulites

In the polarizing microscope at room temperature, the wax crystals in the Paraho oil appear as the expected needles and plates, but the morphology of the crystals in the Union oil is quite different. While needles are also present, most of the crystals exhibit properties characteristic (8) of spherulites of anisotropic materials. The particles are round and, between crossed polars in parallel light, display a black maltese cross which remains stationary on rotation of the stage. This is shown schematically in Figure 4 and in photomicrographs in Figure 5. X-ray examination of the oil gives only the pattern for paraffinic wax. Although pure spherulites have not yet been isolated and examined, they are believed to be formed by wax needles arranged radially. Analogous structures are seen commonly in polymers including polyethylene but, to our knowledge, this is the first time spherulites of wax have been observed.

Two questions immediately occur. Why do the spherulites form in the Union oil, and is there a connection between their formation and the lower pour point?

Cause of Spherulite Formation

Three aspects of the two oils were examined -- the wax, the mineral, and the effect of various fractions.

A. Wax - These were isolated by removing the pentane-insolubles from the 650°+ fractions, precipitating the crude waxes in methylethylketone-toluene, and deoiling these waxes in ethylene dichloride. The yields, based on total oils, were 5.0% and 4.7% from the Paraho and Union oils, respectively. Although the melting points were different (109 and 140°F), the fingerprints by gas chromatography were quite similar, so that the primary factor in formation of spherulites is not wax composition. This conclusion is further supported by the blending data reported in section C below.

B. Mineral - As could be anticipated from the larger ash content reported in Table II, many mineral particles are observed in the Union oil. These were removed by running the hot oil through a 1.5 micron filter. Removal of the mineral appeared to have no major effect on the spherulites. Heating up the mineral-containing oil on the microscope hot stage causes the spherulites to melt, leaving the mineral. Upon cooling, the wax does recrystallize around the mineral. After filtration the mineral is not present, but the recrystallization of the wax into spherulites does not seem to be appreciably slower. Thus, mineral is not the controlling factor in spherulite formation.

C. Effect of Fractions - Both oils were distilled into I-425-650-850-1050 and 1050°F+ fractions. These fractions were blended in many different ways and the blends observed with the microscope at 77°F to see if spherulites were present. It was found that:

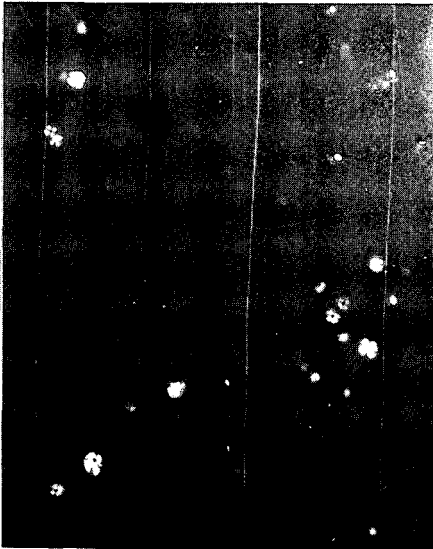
- Paraho Oil
 1. Adding or substituting Union 1050°F+ bottoms gives spherulites as shown in Figure 5D. Also, adding or substituting the pentane-insolubles from the Union bottoms yields spherulites, although perhaps not as well-formed.
 2. No other blends show spherulites.
- Union Oil
 1. Spherulites are formed if the 650-1050°F or 850-1050°F fractions from Paraho oil are substituted. Also, spherulites are present after removing the pentane-soluble bottoms.



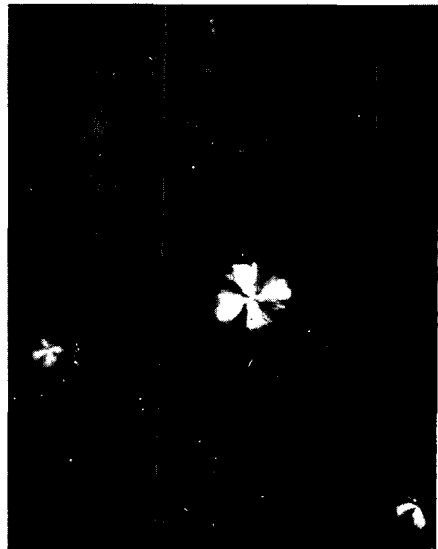
A. PARAHO SHALE OIL



B. UNION SHALE OIL



C. UNION SHALE OIL



D. PARAHO SHALE OIL SUBSTITUTE UNION
1050° F+ FRACTION

SCALE: 30μ

FIGURE 5. PHOTOMICROGRAPHS OF WAX CRYSTALS

2. Only needles are observed if either the 850-1050°F fraction or pentane-insoluble residuum is removed. Also spherulites are absent if Paraho pentane-insoluble, pentane-soluble, or whole 1050°F+ bottoms are substituted for the Union bottoms.

These facts lead to the conclusion that something in the Union 1050°F bottoms, probably in the asphaltenes, causes spherulites to form. The 850-1050°F fraction is necessary but is not unique for the Union oil.

Pour Points

Data measured on the Mectron Autopour are listed below in Table III.

Table III
Pour Points

<u>Oil</u>	<u>Crystal</u>	<u>Pour Pt., °F</u>
Whole Union	Spherulite	27
Whole Paraho	Needle	77
Union, Substitute Paraho 1050+	Needle	58
Paraho, Substitute Union 1050+	Spherulite	21
Union + 9% I-425	Spherulite	36

Substituting Paraho 1050°F+ bottoms into Union oil changes the spherulites to needles and increases the pour point from 27 to 58°F. On the other hand, changing the needles in Paraho oil to spherulites by substituting Union 1050°F+ bottoms lowers the pour point from 77°F to 21°F. Doubling the I-425°F fraction in Union oil, which should lower the viscosity, seems to increase the pour point. While a viscosity study, soon to be made, is needed for confirmation, these data indicate strongly that there is a correlation between spherulite formation and pourability of these oils. It appears in the microscope that the wax changes from a three-dimensional, irregular network of needles to spheres which have less particle-to-particle interaction. Work is continuing in an effort to achieve better understanding and control of the phenomenon.

Acknowledgements

The authors wish to thank Sunoco Energy Development Co. for supporting this work and authorizing this publication. Special credit should be given Ms. Dorothy O'Reilly, who first recognized the spherulites and who has made all of the microscopic observations; also to Suntech Analytical Department for all other analyses.

References

- (1) White River Shale Project, Detailed Development Plan, Vol. 1, June, 1976.
- (2) Jones, J. B., "Technical Evaluation of the Paraho Process," 11th Israel Conference of Mechanical Eng., Haifa, Israel, July 11, 1977.
- (3) Sladek, T. A., "Recent Trends in Oil Shale - Part 2: Mining and Shale Oil Extraction Processes," Mineral Ind. Bull., V. 18, #1, 20 p., January, 1975.
- (4) Atwood, M. T., "Above-Ground Oil Shale Retorting: The Status of Available Technology," Eng. & Mining J., V. 178, #9, Sept., 1977, pp. 148-154, 363.
- (5) Hopkins, J. M., et al, "Development of Union Oil Company Upflow Retorting Technology," 81st National Meeting, AIChE, Kansas City, MO, April 11-14, 1976.
- (6) Duir, J. H., et al, "Continuous Upflow Retort Improves Shale Processing," Hydrocarbon Processing, V. 56, #5, May, 1977, pp. 147-150.
- (7) Lovell, P. F., "Production of Utah Shale Oils by the Paraho DH and Union "B" Retorting Processes," 11th Oil Shale Symposium, Golden, CO, April 12-14, 1978.
- (8) Hartshorne, N. H. and Stuart, A., "Crystals and the Polarizing Microscope," American Elsevier Publishing Co., New York, NY, 4th Edition, 1970, p. 318.

A MARKETING PROSPECTUS FOR SHALE OIL

G. E. Ogden and R. D. Ridley

Occidental Oil Shale, Inc.
5000 Stockdale Highway
Bakersfield CA 93309

Technical developments in shale oil production achieved in the past few years signal the potential beginning of a new liquid hydrocarbon industry. Construction work has begun on commercial scale projects and coupled with the growing sense of national urgency, there is good optimism that significant shale oil production will be forthcoming. These events have generated a need to take a closer look at definition of shale oil markets.

In contrast to past efforts which have dealt hypothetically with this subject, our marketing development efforts are directed at an established objective; that is, to define the specific markets which will return an optimum price for a commercial quantity of shale oil in the mid-1980's. Consuming sectors of the petroleum market have been evaluated and compared. The transportation element has been costed for various geographic regions of interest and combined with quality differentials to identify economic alternates.

Before delving into the distribution logic, some commentary about the nature of the product is warranted. While most of the shale oil technology developed to date is derived from a variety of above ground retorting tests, oil shale projects currently underway indicate that the early production will come from a modified in situ process with later production possibly being a blend of oils from several recovery processes. Many of the early plans called for a prerefining step at the production facility to improve the oil's transportation characteristics and marketability. Strong demand projected for hydrocarbon liquids in the mid-1980's has tempered the concern over marketability of as-produced shale oil and consequently has moderated the need to upgrade at the production site. The capital intensive production operation tends to make developers favorably consider minimizing the initial investment, which can be accomplished by eliminating the oil upgrading step. Concerns over water availability and general high industrial profile in Western Colorado are also factors which will increase the probability that any processing of the oil will be accomplished downstream in existing industrial complexes. Consequently, the commodity of interest in this discussion is the as-produced shale oil from modified in situ retorting.

While shale oil will not be completely interchangeable with crude oil, its properties are sufficiently similar that it will act as a substitute in several applications. The major quality difference between shale oil and conventional crude oil is nitrogen content. Shale oil contains approximately 1.5 weight percent nitrogen compared to 0.1% for typical crude oils produced in the Rocky Mountains. Since nitrogen is an undesirable contaminant in catalytic refining processes, facilities will have to be constructed specifically for its removal. Refining technology is fully developed for this processing step and, in fact, California crudes ranging up to 0.7% nitrogen are routinely refined on the West Coast. The impact of the nitrogen can also be lessened by blending with crude oil in an existing refinery. To verify

this, a successful refinery test run was conducted on as-produced, in situ shale oil at the Chevron refinery in Salt Lake City in November, 1977.

There are also significant differences from crude in fractionation yields. These differences are explained in some detail in the refining quality discussion. A very important shale oil property is its relatively low sulfur content, 0.5-0.7 weight percent. The low sulfur content may allow the oil to be burned directly in boiler applications in its as-produced state. This factor also influences planning against incorporating an upgrading step with the production operation.

Because of its similarity to petroleum, it is expected that shale oil will compete in the same markets with crude oil or products derived from crude. The supply of crude oil to meet incremental U.S. demand is widely accepted to be foreign sourced in the 1980's and reference is made throughout the discussion to economics relative to cost of foreign crude oil.

With that overview in mind we can turn to examination of the logistic factors, the potential consuming industries, and the business and governmental influences.

Geographical orientation of the existing markets will have a strong influence on shale oil disposition, particularly in the early years. As production of shale oil expands we can expect industrial consumers to react to the supply source by locating new facilities to take advantage of logistics. However, at the outset, the processing plants that will absorb the shale oil are essentially in place. Figure 1 shows in general the concentration of the refining industry, the primary petrochemical plants and the utilities running on oil.

The refining industry is the most widespread and while large concentrations are shown in California, the Gulf Coast, the Great Lakes, and the Philadelphia area, a sufficient capacity to absorb 100-200 MB/D of shale oil exists in the Rocky Mountain/Kansas area. In perspective, the U.S. refining capacity stands at 17.6 million B/D of which 5 million B/D is located in the Rocky Mountain/Midwest area. Demand for refined products, of course, is equally widespread and should continue to grow at a moderate pace. Because of its wide geographic distribution, the refining industry has the most flexibility to modify or locate new facilities to take advantage of the logistic flow of the shale oil.

The primary petrochemical industry does not have this luxury. The great majority of the large volume petrochemical operations are centered near the U.S. Gulf Coast. There they have the necessary economic linkage with plants producing intermediates and finished products along with established outlets for by-products. If a large plant were to be constructed in the Rockies, it would have to achieve sufficient benefit to overcome the transportation penalty associated with hauling nearly all the output to the U.S. Gulf for secondary processing or by-product disposition. As traditional supply sources change, we may see evolution in this direction but it will be very slow and in small steps.

The large market for oil in direct burning applications is the utility boiler market. There is some question as to how long this outlet will

exist in light of Government policy trending against using liquids for power generation. As shown on Figure 1, oil use today is centered in three regions: California, the Great Lakes, and the Northeast. There may be a growing use in the Gulf Coast area if economics permit gas fired applications to be converted to oil, but for the very long term oil based generation is likely to be a shrinking market. As new nuclear and coal plants come onstream, they will be put in base load service and existing oil generation will be subordinated first to peak shaving and ultimately retired. With the exception of areas where very tight emission standards are required and/or nuclear and coal plants are faced with very long delays, new oil fired generation capacity is unlikely.

With the qualitative overview in mind, we can now turn to the quantitative impact of the geographical element. The table below attempts to ascribe a transportation premium or penalty for shale oil with respect to common foreign crude oil in the regions of interest. The East Coast was not included in the table since it would represent an extreme physical distribution problem for Rocky Mountain oil. The transportation costs are estimated average values for 200 MB/D and 1,000 MB/D. The estimates assume pipeline transportation to a typical destination within the area. Where existing pipelines are in place, actual tariffs are presumed. Tariffs are approximated for new pipelines using \$.20/bbl per 100 miles for 200 MB/D, and \$.10/bbl per 100 miles for 1,000 MB/D.

RELATIVE TRANSPORTATION ECONOMICS
SHALE OIL VS. FOREIGN CRUDE OIL, \$/BBL

	Shale Oil		Crude Oil	(Penalty)/Premium	
	200 MB/D	1000 MB/D		200 MB/D	1000 MB/D
Los Angeles	1.80	.90	-0-	(1.80)	(.90)
Rocky Mtn.	.60	.30	.80	.20	.50
Chicago	1.20	1.20	1.20	-0-	-0-
U.S. Gulf	2.40	1.20	-0-	(2.40)	(1.20)

The table shows the quantitative effect of transportation in 1977 dollars on a value relationship with crude oil. Location impact may result in a \$.20-\$.50/bbl premium for shale oil routed to a Rocky Mountain destination to a \$.90-\$2.40/bbl penalty for a West Coast or Gulf Coast market. The obvious conclusion is that there is a sizeable transportation advantage for shale oil if a market can be created in the Rocky Mountain/Upper Midwest area instead of a Coastal location.

Definition of quality differentials is much more difficult to accomplish with any degree of certainty. In the long term context, where the liquid demand exceeds supply, today's quality relationships are apt to be distorted. For the purpose of this discussion, however, it is assumed that foreign crude can still be purchased for incremental liquid input.

Refining value of shale oil has probably been investigated in greater detail than the other potential applications. Most of the efforts to prescribe a refining cost for shale oil, however, have viewed the problem in a very hypothetical context. Most of the data is developed for complete new facilities turning out a product slate that may or

may not relate to the actual market conditions in the environment where the oil is likely to be consumed. For the reasons discussed earlier, there is good probability that the shale oil will not be upgraded at the production facility, but rather will be integrated into existing refineries in its as-produced state.

Also, there has been no reported extensive testing on in situ shale oil which is likely to represent the quality of the majority of the early production, based on projects presently underway. Consequently, there is some divergence of opinion on the relative value of shale oil to conventional crude oil.

In our efforts to date at defining this value, we have attempted to cost the effect of integrating as-produced, in situ shale oil into typical Rocky Mountain/Upper Midwest refineries as a substitute for the crude mixes run at those locations. Figure 2 shows the various geographical areas that were analyzed in this fashion. The dollar figures superimposed are the additional refining costs resulting from substituting shale oil. While the numbers range from \$2.05 to \$3.00 per barrel in 1977 dollars, an additional refining cost of \$2.50 probably reflects a good estimate of the average additional cost. It should be noted that these cost figures include a reasonable rate of return on invested capital.

This additional refining cost appears lower than many of the recently published figures but it can be qualitatively reconciled when put in the context of the market environment in the mid-1980's. First, the existing U.S. and worldwide supplies of light crude oil are declining at a significant rate. The refining supply barrel is getting heavier, and more importantly contains a higher volume yield of residual boiling range material. We can see the impact of this phenomenon already in the U.S. noting the very depressed prices for high sulfur residual fuel which is in long supply. In situ shale oil has only 4%, 1000°F. + boiling range material compared to 20% for North Slope crude and 18% for Arabian light crude. These crudes are by no means the worst and are actually significantly better than Kuwait, Arabian Heavy and others which represent a good proportion of the unused worldwide production capacity. Upgrading crude residual material to clean transportation fuels is probably more costly than starting with shale oil.

Another factor that has historically been represented as a negative for shale oil is the very low gasoline yield. Nearly all the refining studies on shale oil have discounted its value because of the need to convert a greater proportion of the distillate to gasoline. However, the strong trend today indicates tapering gasoline growth. The major forecasters are nearly unanimous in projecting a peak in U.S. gasoline demand between 1980 and 1985. The conclusion is that the great majority of facilities to manufacture gasoline will be in place when shale oil comes on the market and the demand growth will take place in the distillate range. If this trend proves to be true, a refiner in 1985 will place a premium value on high distillate yield as opposed to high gasoline yield. The potential yield premium will act to offset the additional refining cost.

While the shale oil yields were very unbalanced with the refinery product mix outlook in 1970, those same yields will be highly attractive in 1985.

The market price for shale oil as a utility boiler fuel can be quantified in a fairly narrow range but is subject to environmental and governmental restrictions. Pricewise, where supply imbalance or regulatory effects do not create distortions in the market, 1% sulfur residual fuel sells for approximately the same price as Arab Light crude. This grade of fuel oil is currently burned in the Great Lakes area for power generation as well as industrial fuel applications. Since shale oil in an untreated form approximates the quality of 1% sulfur residual fuel, we suspect that its value in that application will approach that of Arab Light crude oil. Since we have defined refining costs for processing shale oil to transportation fuels, it is probable that its highest value will result from 1% sulfur boiler fuel.

However, the areas where 1% sulfur fuel oil can be burned are shrinking. Emission restrictions have forced many utilities to use 0.5% and lower fuels and the trend is continuing. Looking forward to the mid-1980's, there may be a market for only a small volume, say 50,000 B/D, for this application.

The potential petrochemical feedstock market has not yet been fully explored. There are some negative aspects of shale oil for petrochemicals. The existing petrochemical plants (olefins, aromatics) are tailored to the light fractions of petroleum such as LPG and naphtha. Shale oil's low yield of light hydrocarbon places it at a disadvantage with respect to crude oil. No attempt has been made to quantify a penalty for this application.

On the other hand, there is good reason for some optimism. Shale oil's very respectable hydrogen content (12%) suggests that new petrochemical technology could be tailored to this input economically. In a very forward thinking manner, members of the petrochemical industry have expressed interest in exploring new applications. However, the competing uses will likely comprise the total early market for a shale oil industry and it will only be in the long term that a petrochemical market will come into play.

The other factors that will have an influence on shale oil distribution will not be directly economic. Government policy may leverage through incentives a particular use for the long term benefit even though it may not be the most economic short term application. As an example, there may be legislation penalizing burning oil in a stationary boiler. National policy seems to be aligned in the direction of converting power plants from oil and gas to coal. For these reasons we suspect that the fuel oil application will not provide a long term market for a shale oil industry; nevertheless this outlet will be of real value for the early stages of an oil shale industry since it can utilize raw shale oil without major capital expenditure.

General business factors should be taken into account in this assessment particularly for the first 200,000 barrels per day of production. There is almost no disagreement that early production of shale oil will be a high risk, capital intensive venture. The production venturers will be inclined to limit their capital exposure to the production and look for a manufacturer to risk the upgrading capital. In this context, the fuel oil market has a strong advantage. Very little capital will need to be exposed to consume the shale oil, very little lead time

will be required and there will be a minimum risk of non-success in the application. Refining on the other hand will require substantial capital modifications, a three year minimum lead time and some risk, in the first cases.

Viewing the industry sectors in summary, a petrochemical market is the most remote. The transportation cost to reach it is high and the upgrading technology for shale oil has not yet been developed. Because it represents one of the more beneficial uses of petroleum, however, we expect that ultimately a market will develop in this sector.

Industrial and utility boiler fuel represent an attractive market for shale oil. Because of the low investment required and a geographically economic location, the first use of shale oil may be for this application in the Great Lakes area. The disadvantages of this market are its susceptibility to environmental and regulatory prohibitions and limited volume demand.

The large market for shale oil is expected to be as refinery input. Refined product growth is expected to continue and sufficient plants to absorb sizeable volumes of shale oil exist in economic proximity to the production area. Conversion of shale oil to transportation fuels is consistent with government policy on use of liquid hydrocarbons. The only deterrent to this application is the substantial capital investment for upgrading facilities. In graphical form, Figure 3 presents our projection of the time related consumption of shale oil.

FIGURE 1
POTENTIAL SHALE OIL MARKETS

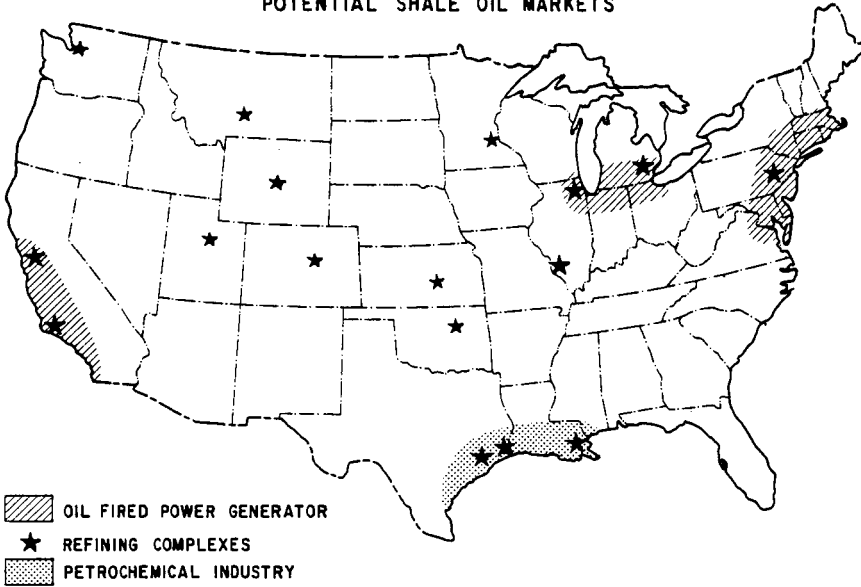
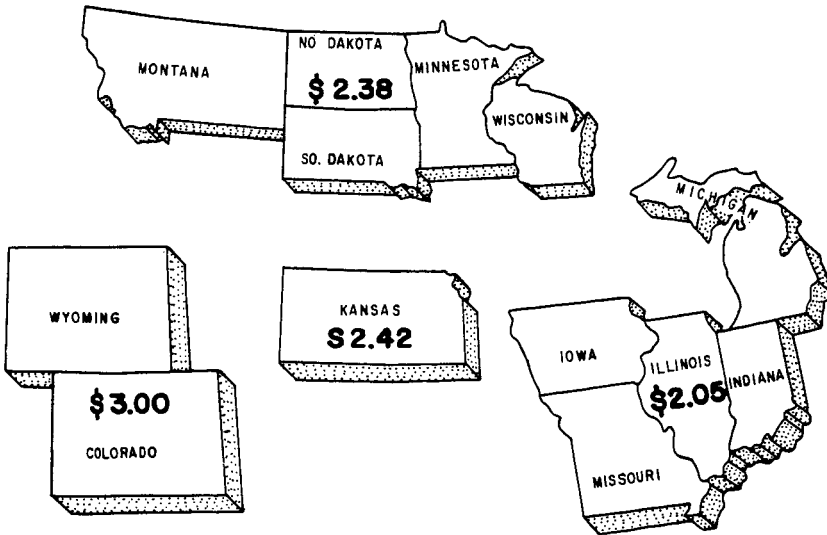
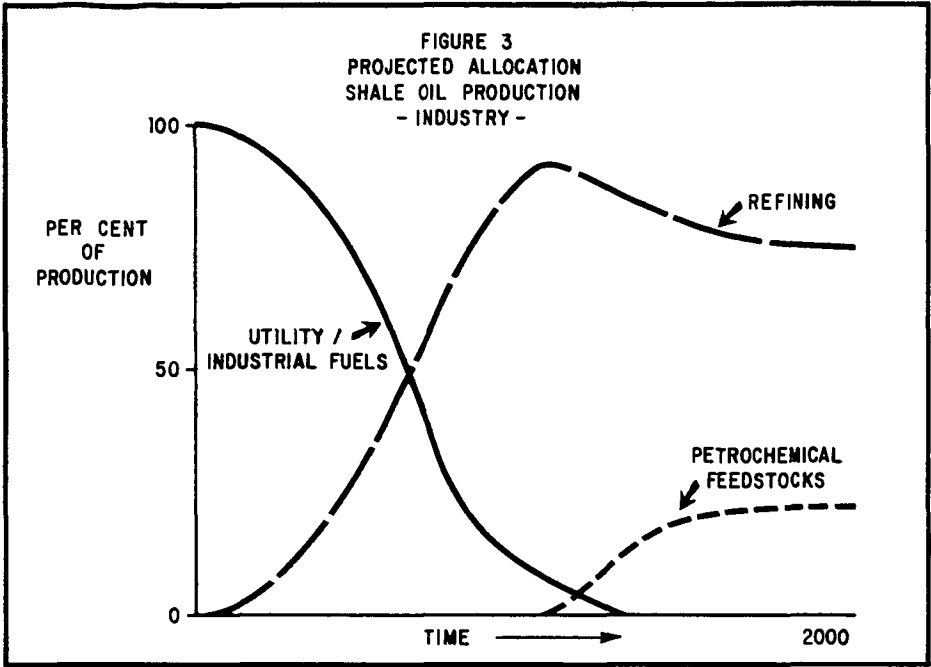


FIGURE 2
SHALE OIL REFINING - ADDITIONAL COST





BATCH EXTRACTION UNIT FOR TAR SAND PROCESSING STUDIES

E.C. Sanford and F.A. Seyer

Syncrude Canada Ltd., Research Department, P.O. Box 5790
Edmonton, Alberta, Canada T6C 4G3

INTRODUCTION

In his early studies on the hot water method of separating bitumen from Athabasca tar sand, Clark (1-4) identified two components of tar sand, the fine solids content and bivalent ion concentration, as being important variables affecting the degree of separation. He also showed that the addition of inorganic bases was generally beneficial and that the amount of mechanical energy imparted to the tar sand slurry during processing was important.

Clark's studies were carried out in a laboratory scale separation plant which took a charge of approximately 8 kg of tar sand (1). Beaker extractions, which consisted essentially of stirring 0.2 kg tar sand with hot water in a beaker, were used for demonstration purposes(5).

In a later study, Seitzer (6) described a stirred reactor (capacity 0.2 kg of tar sand) which utilized a broad U-shaped paddle for slurring and which with proper manipulation of variables could be made to simulate pilot plant extractions (7). Malmberg (8,9) used this reactor to further study the variables identified by Clark as well as others. Sepulveda utilized a commercial high shear stirred reactor for slurring and a commercial flotation cell for the separation (10). One of the main objectives of these different groups was to find a parameter or parameters which would explain differences in bitumen yield from different tar sand samples under standard conditions, in short, the factors affecting tar sand processibility. Although much useful information was generated, this objective was not fulfilled.

This paper provides details of the design and operation of a convenient laboratory batch extraction unit, which was designed specifically for studying the chemical and physical properties of tar sand as they affect processibility. The unit was used to demonstrate the importance of surfactants in the hot water extraction process and to show the interrelationship between inorganic bases used as process aids and surfactants.

Description of the Unit

The objective was to design a unit that would a) give reproducible yield data; b) be sensitive to changes so that additives could readily be evaluated; c) be versatile, so that temperature, stirring rate, etc. could easily be changed; and d) establish trends that would parallel trends in larger continuous units.

One of the problems in dealing with tar sand is the natural variability of the deposit (7). It is therefore necessary to be able to homogenize a relatively large batch and use portions of this for comparative experiments yet the sample size must not be too small, otherwise loss of bitumen on the walls, etc. of the extraction apparatus will become significant. Based on these criteria, a sample size of 0.5 kg per experiment was chosen.

Details of the unit itself are given in Figures 1 to 3. The extraction cell is jacketed to provide for constant temperature during operation; the height is sufficient to provide a quiescent zone; and the cell is square to facilitate slurring and subsequent agitation without the need for baffles. Air is added through the impeller shaft which allows good control even at low addition rates and avoids problems of plugging by fine solids experienced with other methods of addition, such as a porous plate. The air-introduction feature permits aeration of the slurry during mixing and allows one to simulate the secondary recovery step subsequent to primary recovery, practised in commercial units. After extraction is complete, tailings can easily be removed through a valve on the bottom of the cell. The valve also permits easy cleaning of the cell. The impeller speed is controlled by a variable speed fractional horsepower motor and is measured by a tachometer mounted on the impeller drive shaft. The impeller itself is easily removed so that different sizes and shapes can be used if desired.

The bitumen yield in the primary extraction step was known to be a function of stirring time and impeller speed for some types of tar sand (3,6,8). Experience with the unit has shown that for the times and speeds given in the procedure, the yield is relatively insensitive to these effects and errors resulting from small deviations are insignificant. When using a standard procedure the unit is ideally suited for studying processibility differences due to tar sand composition, the amount and type of process aid and other chemical additives.

Although a secondary recovery step similar to that practised in commercial units can readily be carried out, normally only primary bitumen recovery is used in processibility studies. The secondary recovery step is more efficient than commercial units and gives higher recoveries.

EXPERIMENTAL

Procedure I

Lab Scale Simulation of the Hot Water Extraction Process

Apparatus, Reagents, Materials:

1. Batch Extraction Unit and related components. The assembly is described in Figures 1, 2, and 3.
2. Constant Temperature Water Bath, maintained at 180°F (82°C). A pump allows water to be circulated from the bath to a jacket surrounding the stainless steel pot.
3. Timing Device, hot plate and distilled water.

Procedure:

1. Assure all air and water connections are sealed. Allow water from the bath to circulate through the surrounding jacket of the unit.
2. Heat approximately 1500 ml distilled water to 195°F (90.5°C) on a hot plate. Homogenize a quantity of the tar sand under test as outlined in Procedure II and submit three representative samples for bitumen/water/solids analysis (Procedure III). Collect 500 g of the remaining sample and weigh to the nearest 0.1 g.

3. Transfer 150 ml of the hot water to the stainless steel pot. Lower the motor and impeller assembly to its lowest possible position on the shaft rod and turn on. Allow the remaining water on the hot plate to cool to 180°F (82°C). (Impeller - ¼" from the bottom).
4. Add the 500 g tar sand sample to the pot. Within as little time as possible:
 - a) Raise and lower the motor assembly to break up tar sand lumps present and leave the assembly two notches above the lowest one. (Impeller ¾" above the bottom of the vessel).
 - b) Adjust mixer to 600 rpm.
 - c) Turn on air flow and adjust to approximately 465 cc/min on the flowmeter.
 - d) Initiate timer.Mix in this manner for 10 minutes.
5. When complete, turn the air supply off and flood the mixture with approximately 1000 ml of 180°F (82°C) water, thus bringing the froth level to the top of the pot. Mix for an additional 10 minutes at 600 rpm. (No air).
6. Cease mixing and skim as much primary froth as possible from the top of the pot with the specially designed spatula. Collect the froth in a 4 oz sample bottle and submit for bitumen/water/solids analysis. (Procedure III).
7. For recovery of secondary froth mix the remaining material for 5 minutes at 800 rpm while aerating at approximately 232 cc/min. Collect secondary froth in the same manner and submit for analysis. (Procedure III).
8. Drain the residual material from the bottom valve and wash the pot and impeller with toluene. When shut down, insure that the circulating water pump and air flow are turned off.

Comments

1. Residual material held in the stainless steel pot after recovery of the secondary froth may be differentiated as either secondary tailings or primary tailings in the following manner: Allow the mixture to settle one minute from the time mixing and aeration ceases. Decant the aqueous phase and denote as secondary tailings. The remaining heavier particles are termed primary tailings. Oil losses to the primary and secondary tailings may be obtained from bitumen/water/solids analyses of the samples.

Procedure II

Subdivision of Bulk Tar Sand Samples for Subsequent Analysis

Apparatus, Reagents, Materials:

1. Polyethylene sheet, approximately 3 feet square (1 m²).
2. Spatula, with 12 inch (30.5 cm) stainless steel blade. A handle welded in place to the center of cutting edge facilitates use.

Procedure:

1. Empty bulk sample (ideal weight = 3000 g) onto the polyethylene sheet. Remove stones greater than $\frac{1}{4}$ inch (6.5 mm) in any dimension.
2. Chop the tar sand for a period of time ensuring all particles to be less than $\frac{1}{4}$ inch (6.5 mm) diameter. Pile and quarter the mixture.
3. Combine two opposite corners.
4. Repeat the chopping, quartering, and combining procedure as outlined, twice again. Resultant particles should not exceed $\frac{1}{8}$ inch (3 mm) in any dimension.
5. Transfer approximately 50 g tar sand from the latter pile to a 4 oz sample jar and submit for analysis. Store the remaining tar sand in a tightly capped bottle at 40°F.

Procedure III

Determination of Bitumen/Water/Solids Content of Tar Sand, Froth, Middlings and Tailings Samples

Procedure:

The sample is separated into bitumen, water, and solids, by refluxing with toluene in a solids extraction apparatus (10). Condensed solvent and co-distilled water are continuously separated in a trap, the water being retained in the graduated section. The solvent recycles through the extraction thimble to further dissolve the bitumen. The bitumen/solvent and non-filterable solids fractions are subsequently separated by centrifuging. An aliquot of the resultant bitumen extract is evaporated to remove the solvent. The weight of bitumen water and solids is determined gravimetrically.

NaOH as a Process Aid

It was recognized very early in studies on the hot water extraction process that the acidity or alkalinity of the tar sand had an important effect on the efficiency of the separation (1). Strong inorganic bases, when added in small quantities, generally improved the separation efficiency. Separation efficiency was also thought to be dependent upon the concentration of certain substances which were present in the tar sand and dissolved or became suspended in the water phase during slurring (2,3). Bowman (11) isolated some of the dissolved organics by foam fractionation technique and showed that the materials were surface active. Bitumen/water, air/water and air/bitumen interfacial tensions were measured and a thorough discussion of the theoretical implications of changes in interfacial transformations was presented. A similar discussion, from a thermodynamic approach was given by Leja and Bowman (12). The batch extraction unit described here was used to study the relationship between inorganic bases and surfactants in process streams.

A typical plot (8) showing the relationship between added NaOH and bitumen recovered in the primary separation step is shown in Figure 4. As expected, there is a corresponding increase in the pH of the aqueous tailings. Less obviously, as the amount of NaOH used increases, there is also a steady decrease in the surface tension of the secondary tailings and a corresponding increase in the organic carbon content of

the samples (Figure 5). This establishes a connection between surfactants in the water and NaOH used during hot water extraction of bitumen from tar sand. Further confirmation was obtained on titrating samples of tailings. Titration curves are given in Figure 6. All tailings samples exhibited an end point characteristic of sodium oleate soap. Only at 0.056 wt% NaOH is there an end point which might be due to NaOH.

These data show that NaOH neutralizes organic bitumen acids, to give salts which are surface active in the aqueous phase. They further show that NaOH results in increasing bitumen yield. To establish that the important agent responsible for improved recovery is the surfactants produced by caustic addition, tailings samples were centrifuged to remove solids and concentrated by evaporation. The concentrate was then added to the next experiment such that the organics in total aqueous tailings from one run would be present in the slurry water of a second run. The data is given in Table I. The surfactants recovered from tailings are as effective as NaOH in improving recovery, showing that surfactants are indeed the active process aid. With repetitive recycle the effectiveness of concentrated tailings decreases, probably due to losses in handling and through the formation of salts with bi- and trivalent metals present in tailings streams. Table I also shows that commercial surfactants can be used as well although these are not economically competitive with NaOH at this time for commercial use.

TABLE I
Effect of Surfactants on Bitumen Recoveries in
the Hot Water Extraction Process

Conditions	Bitumen Recoveries Primary Froth (%)
No Additive	61
NaOH: 0.04 wt% of T.S.	88
Concentrated, centrifuged tailings	87
No Additive	71
NaOH 0.008 wt% of T.S.	81
0.024 wt% of T.S.	91
Tide 0.020 wt% of T.S.	82
0.100 wt% of T.S.	89
Na Oleate 0.020 wt% of T.S.	70
0.100 wt% of T.S.	83
Lignosulfonate nil	35
HGX 0.020 wt% of T.S.	58
0.100 wt% of T.S.	74

Conclusions

Details of the design and an operating procedure for a laboratory scale batch extraction unit have been described. Utilizing this unit, it has been shown that NaOH, when used as a process aid for tar sand processing, reacts with components of bitumen to form surfactants and that these surfactants are the primary agent responsible for improved bitumen recovery.

Acknowledgements

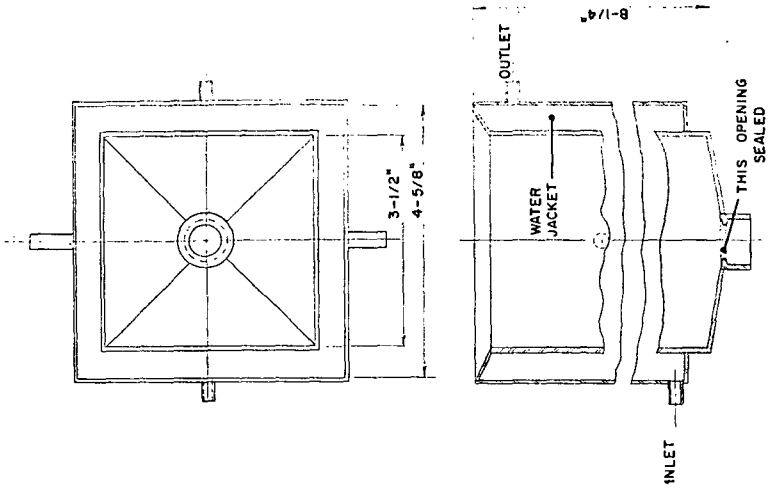
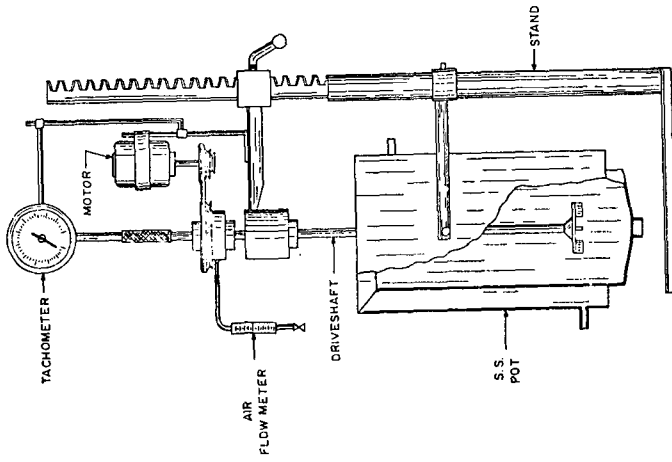
The authors wish to acknowledge the contributions of J.A. Bichard, C.W. Bowman, L.M.O. Cymbalisky, C. Guarnaschelli, and E. Nagy who, while members of or associated with Syncrude Canada Ltd. Research Department, were involved in the initial design, modification and testing of the batch extraction unit. The experiments described in this paper were carried out by M. Dmytriw and D. Famulak. The authors are grateful to Syncrude Canada Ltd. for permission to publish this paper.

References

- (1) Clark, K.A., and Pasternack, D.S., Ind. and Eng. Chem. 24(12) 1410(1932).
- (2) Clark, K.A., The Can. Inst. of Mining and Metallurgy, Transactions, XLVII 257(1944).
- (3) Clark, K.A., and Pasternack, D.S., Research Council of Alberta, Report No. 53, University of Alberta, Edmonton, Alberta (March, 1949).
- (4) Clark, K.A. Can. Oil and Gas Industries, 3(6), 46(1950).
- (5) Pasternack, D.S. Hodgson, G.W., and Clark, K.A. Proc. Ath. Oil Sands Conf. 200(1951).
- (6) Seitzer, W.H., ACS San Francisco Meeting, April 2-5, 1968, p. F19.
- (7) Innes, E.D., and Fear, J.V.D., Seventh World Petroleum Congress, Mexico City. Proceedings 3 633 (1967).
- (8) Malmberg, E., and Bean, R.M., ACS San Francisco Meeting, April 2-5, 1968, p. F25.
- (9) Malmberg, E.W., and Robinson, W.M., Ibid. p. F38.
- (10) Sepulveda, J.E., Miller, J.D., and Oblad, A.G. PREPRINTS, Div. of Petrol. Chem. ACS 21 No. 6 110 (1976).
- (11) Bowman, C.W., Proceedings of the Seventh World Petroleum Congress, 3 583 (1967).
- (12) Leja, J., and Bowman, C., Can. J. Chem. Eng., 46(12) 479(1968).

FIGURE 1

SYNCRUDE BATCH EXTRACTION UNIT



STAINLESS STEEL POT

FIGURE 2.

BICHARD, BOWMAN, CYMBALISTY, GUARNASCHELLI, NAGY

FIGURE 4 The Effect of NaOH on Bitumen Recovery in the Primary Froth and pH of Secondary Tailings

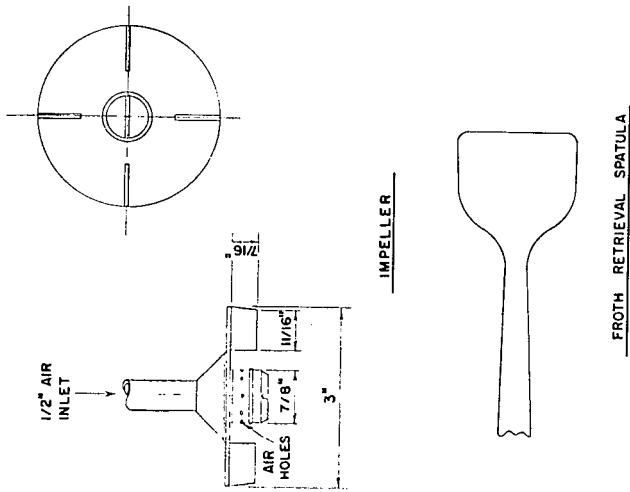
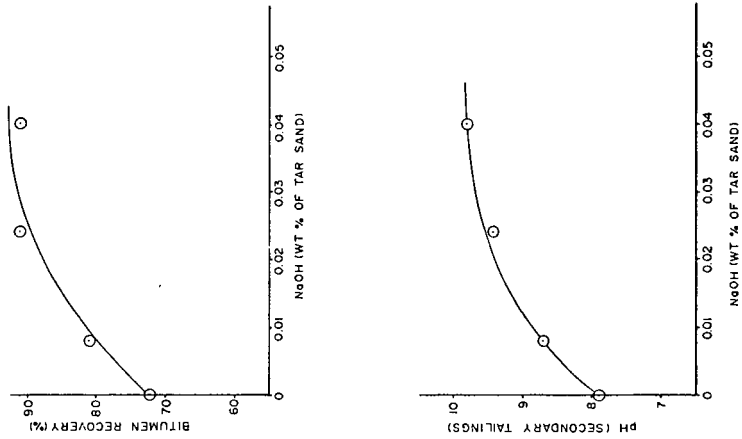


FIGURE 3.

FIGURE 5 The Effect of NaOH on Surface Tension and Total Organic Carbon Concentration of Secondary Tailings

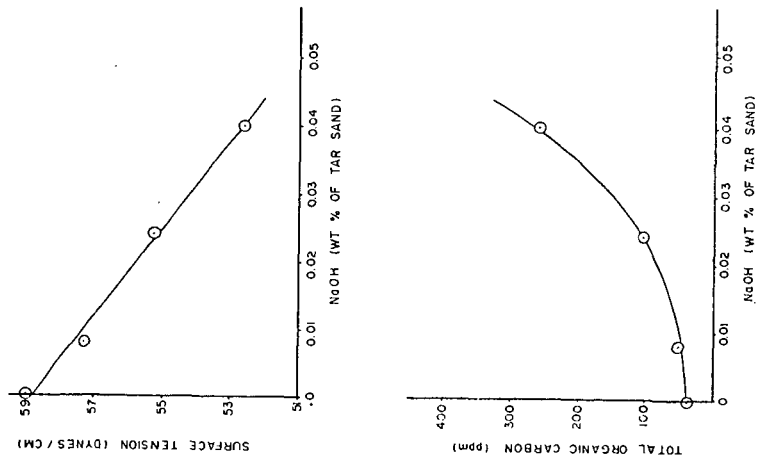
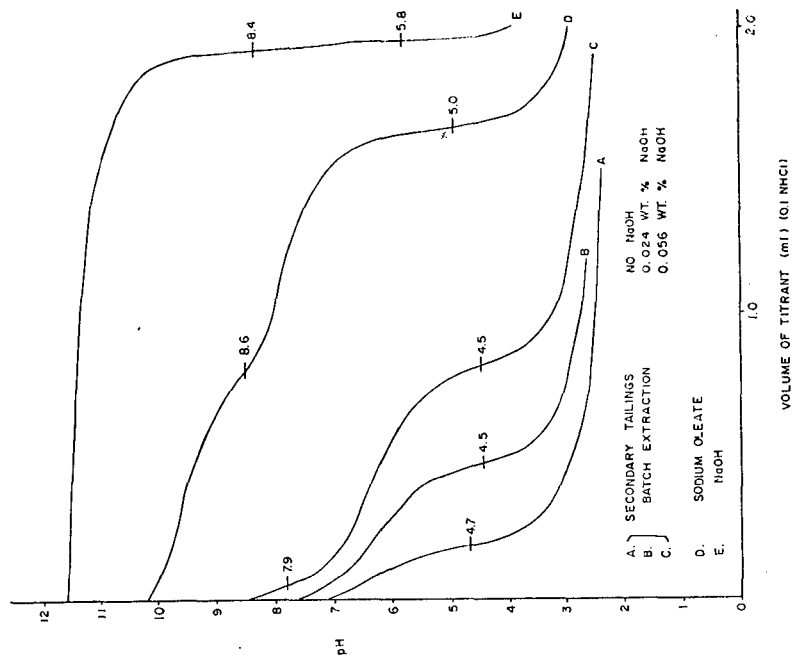


FIGURE 6 Titration Curves for NaOH, Na Oleate and Aqueous Tailings



THERMAL HYDROCRACKING OF ATHABASCA BITUMEN:
COMPARISON OF COMPUTER-SIMULATED FEED AND
PRODUCT VAPORIZATION VALUES WITH PILOT PLANT DATA

D.J. Patmore and B.B. Pruden

Energy Research Laboratories
Canada Centre for Mineral and Energy Technology
Department of Energy, Mines and Resources
555 Booth Street, Ottawa, Ontario, Canada, K1A 0G1

INTRODUCTION

The Energy Research Laboratories of the Canada Centre for Mineral and Energy Technology (CANMET) are engaged in a continuing upgrading project involving the hydrocracking of Canadian oil sand bitumen and heavy oil. Such upgrading is necessary to remove sulphur and to reduce the viscosity of the bitumen to facilitate transport by pipeline to the refinery. Currently upgrading is accomplished on a commercial scale by Great Canadian Oil Sands Limited using a coking process which converts up to 20% of the bitumen to char. One aim of the CANMET work is to develop an economical process which would convert all of the bitumen to usable products, and thus reduce the waste of a valuable resource. For this purpose a one-barrel-per-day pilot plant was built and has been operated successfully with a variety of feedstocks. This work has concentrated on both plant operability, in particular the prevention of reactor coking (1), and on the effect of operating conditions on yields and product qualities (2).

Efficient and economical scale-up of this process to a commercial-size plant requires quantitative knowledge of both the degree of vaporization of feed and product and the fraction of the reactor occupied by gas under reactor conditions. The latter, usually referred to as voidage, has already been investigated in detail (3). Such knowledge is needed to calculate hydrogen partial pressures and true liquid and vapour residence times. These in turn are necessary to accurately estimate the size of various plant components as well as to formulate a kinetic model for the thermal hydrocracking reaction.

Because it is not feasible to measure liquid and vapour compositions in the reactor directly, recourse must be made to computational methods. These involve estimating the equilibrium vaporization constant, K , for various components of the system using known or estimated values of their thermodynamic properties.

Computations for the present study were carried out using the Grayson-Streed modification of the Chao-Seader correlation employing the principle of corresponding states (4,5). A package program was employed.

Vapour-liquid equilibrium data were obtained from measurements in a hot separator downstream of the pilot plant reactor. This well-mixed separator, which was temperature controlled, was assumed to behave as a single stage contactor, and measurements of liquid and vapour flows and concentrations were taken at steady state conditions.

EXPERIMENTAL

The pilot plant is shown schematically in Fig. 1. Bitumen and hydrogen are fed at the bottom of a long unpacked heated tubular column (3.81 cm diam. x 3.95 m long). The hydrocracked products are led from the top of the reactor to a hot separator kept at a temperature below that of the reactor. The heavy oil product is withdrawn and the vapour passed into a cold receiver and condensed. The light oil product is again withdrawn and collected. The hot separator was well mixed as the reactor products entered below the liquid level, and there was a high ratio of gas to liquid. It follows that the fraction of liquid vaporized, f , was the weight of light oil product divided by the total liquid product. The hot separator was temperature controlled so that the above ratio could be obtained as a function of temperature. The gas flow was metered using the orifice, and the gas composition at the reactor inlet controlled by scrubbing. Accordingly the actual gas composition and flow in the hot separator could be computed by using these data along with dissolved gas flows and compositions, reaction hydrogen requirements and hydrocarbon gas make.

Athabasca bitumen containing 51% pitch (material boiling above 524°C equivalent atmospheric boiling temperature) was fed in all cases. Products are identified by the amount of pitch conversion based on feed. Further details are given in Reference 6.

The computer simulation was carried out for CANNET by Saturn Engineering, Calgary, Alberta, using the DISTILL program licensed by the Chem Share Corporation, Houston, Texas. Simulations were carried out for Athabasca bitumen and four typical hydrocracked products covering the range 49 to 93% pitch conversion. Input to the program consisted of liquid and gas rates, compositions and properties. The composition and properties of liquid feed and product were approximated by ten fractions with mean average boiling points ranging from 65.5°C (150°F) to 648.9°C (1200°F). These fractions were derived from Hempel distillations and gravities of each cut, using standard correlation procedures for petroleum fractions.

For each specified temperature and pressure combination the program calculated f , the weight fraction of liquid that vaporizes under the specified conditions, as a function of specified values of G/L, the ratio of gas rate at STP (in g mol/h) to liquid rate at STP (in kg/h). Gas composition was also entered and treated as a parameter.

RESULTS AND DISCUSSION

Calculated values of the degree of vaporization were plotted as functions of G/L and temperature (Figs. 2 to 5). From these graphs interpolations can be made to obtain f values at conditions other than those specified. Figures 2 and 3 illustrate the effect of G/L on f for different pressures and temperatures for bitumen and for a hydrocracked product with 93% pitch conversion. The trend is an initial rapid increase in f followed by a general flattening out of the curve, a trend which becomes more pronounced at higher temperatures and pressures. This reflects the presence of a very high boiling fraction (pitch) which is vaporized to only a small extent. A similar trend is seen when f is plotted against temperature as shown in Figs. 4 and 5 for bitumen and 3 hydrocracked products (49, 76 and 93% pitch conversion) at 10.44 MPa and various G/L values. The degree of vaporization in the high conversion case reached very high values.

The effect of pressure on f is also illustrated in Figs. 2 and 3. For typical conditions of 450°C and G/L = 40 g mol/kg, increasing pressure from 10.44 to 17.34 MPa decreases f by 50% from 0.37 to 0.185 for Athabasca bitumen, and by 20%,

from 0.86 to 0.69 for product hydrocracked to 93% conversion; while for G/L = 10, f is decreased by 54% and 44% respectively.

Another factor which influences the degree of vaporization is the gas composition; increasing the concentration of hydrogen causes a decrease in f. This is illustrated in Fig. 6 for 350°C and 13.89 MPa for a product hydrocracked to 83% conversion. In the range 50 to 90 mol % H₂, f is linearly proportional to hydrogen concentration. For all hydrocracked products, f was calculated for both 60 and 80 mol %; for most cases studied an increase of 33% from 60 to 80 mol % H₂ caused an approximate 10% decrease in f.

Average liquid residence times (t) can be calculated from these vaporization figures by taking average values for bitumen and hydrocracked product, after making allowance for the fraction of reactor volume occupied by gas (voidage), as follows:

$$t = \frac{[(\text{reactor vol}) \times (1 - \text{voidage})]}{(\text{vol of liquid fed per h}) \times (1 - \text{ave. fraction vaporized})}$$

Such calculations were carried out for a series of pilot plant runs as shown in Fig. 7, where the product of average residence time and liquid hourly space velocity (LHSV) were plotted against the temperature at which each hydrocracked product was obtained. The average fraction vaporized was taken as the average of f for bitumen and for product. As each product represented a different pitch conversion, and as the computer simulation gave vaporization values only for a limited number of products at fixed conversions, a linear interpolation was used to calculate values for these intermediate conversions. A similar interpolation was also used to correct for different hydrogen concentrations. Figure 7 shows that the calculated residence times are very sensitive to reaction temperature, and become increasingly higher than the nominal space time as temperature and space velocity increase.

Although experimental vaporization data for the reactor were not available, it was possible to test the computer simulation by comparing the calculated values of f with experimental data obtained at lower temperatures for the hot separator where vapour/liquid ratios are routinely measured. Again the f values calculated by computer were interpolated to correct for pitch conversion and hydrogen concentration for each run considered. To test the data for bitumen itself a series of runs were carried out with both reactor and hot separator at 350°C and 370°C at which temperatures hydrocracking reactions occur to only a limited extent (≈ 3% pitch conversion at 370°C). Calculated values were plotted against experimental data (Fig. 8). The best line fitted the equation:

$$F_E = (3.3 \pm 0.9) + (0.85 \pm 0.07)F_C$$

where F_E and F_C are experimental and calculated values of the per cent of liquid vaporized. The agreement is reasonable considering all the possible sources of experimental error, and in fact F_E and F_C are in close agreement above about 15%.

The results for hydrocracked products are shown in Fig. 9, in which 75 data from pilot plant runs carried out under a variety of conditions are compared with calculated values. Pressure ranged from 10.44 to 17.34 MPa, and temperature from 300 to 430°C. Although there is considerable spread in the data, the best line lies close to the diagonal and is given by the equation:

$$F_E = (1.8 \pm 1.2) + (0.95 \pm 0.04)F_C$$

It is believed that much of the spread is caused by experimental error, particularly in measurements of gas rate and composition where errors of ± 5% or

more can occur. Errors can also occur in weighing and in temperature determinations. The following Table illustrates the sensitivity of f to variations in G/L and temperature for typical values of these variables.

Sensitivity of f to Variations in G/L and Temperature

	G/L = 20 g mol/kg					G/L = 40 g mol/kg				
	400°C	δ , % ^a	450°C	δ , % ^a	Δ , % ^b	400°C	δ , % ^a	450°C	δ , % ^a	Δ , % ^b
Bitumen	0.1175	8.5	0.241	8.3	105.1	0.205	10.0	0.378	4.2	84.4
93% Prod.	0.505	4.6	0.712	3.2	29.1	0.672	4.2	0.860	1.7	28.0

^a Percentage increase in f for a 12.5% increase in T.

^b Percentage increase in f for a 12.5% increase in T.

It is seen that for a 12.5% increase, temperature has a greater effect than G/L. However, as the accuracy of temperature measurements is much greater than those of G/L determinations, the errors are probably of similar magnitude.

Errors can also be introduced by the approximations used in the interpolations for pitch conversion and hydrogen concentrations, as well from discrepancies between simulated and actual liquid and gas properties.

CONCLUSIONS

Comparison of calculated values of liquid vaporization using a computer simulation with experimental data indicated that such computational methods will give reasonably accurate values for the degree of vaporization, considering the approximation and experimental errors involved, for a very heavy oil such as tar sand bitumen and its hydrocracked products.

REFERENCES

1. Merrill, W.H., Logie, R.B. and Denis, J.M. "A pilot scale investigation of thermal hydrocracking of Athabasca bitumen"; CANMET (Canada Centre for Mineral and Energy Technology, formerly Mines Branch, Department of Energy, Mines and Resources) Research Report R-281; Dec. 1973.
2. Pruden, B.B., Logie, R.B. and Denis, J.M. "Thermal hydrocracking of Athabasca bitumen: Reduction of reactor fouling"; CANMET Report 76-33; Aug. 1976.
3. Shah, A.M., Pruden, B.B. and Denis, J.M. "Thermal hydrocracking of Athabasca bitumen: Correlation of reactor voidage in vertical two-phase flow"; CANMET Report 77-48; Dec. 1976.
4. Chao, K.C. and Seader, J.D. "A general correlation of vapour-liquid equilibria in hydrocarbon mixtures"; Am. Inst. Chem. Eng. Journ.; v. 7, no. 4, p 598; Dec. 1961.
5. Grayson, H.G. and Streed, C.W. "Vapour liquid equilibria for high temperature, high pressure hydrogen-hydrocarbon systems"; Proc. Vith World Petrol. Congr., Frankfurt/Main; Sect. VII, paper 20, P07, p 233; June 1963.
6. Pruden, B.B. and Denis, J.M. "Heat of reaction and vaporization of feed and product in the thermal hydrocracking of Athabasca bitumen"; CANMET Report 76-30; Apr. 1976.

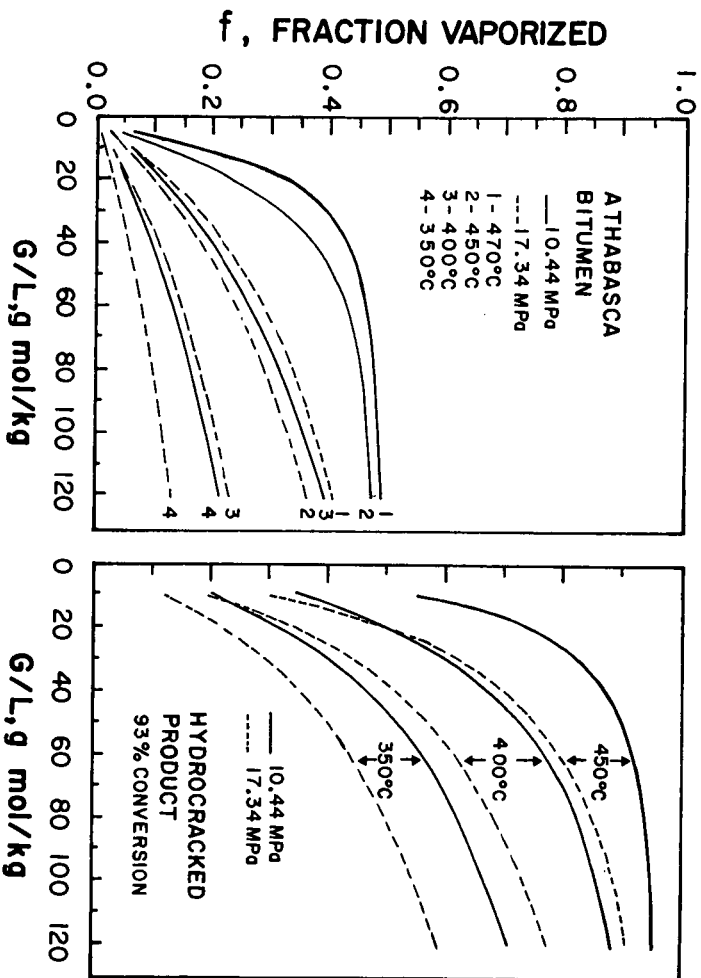


FIGURE 2 - Fraction of Liquid Vaporized, f , as a Function of Gas to Liquid Feed Rate Ratio, G/L g mol/kg, for Bitumen at 10.44 to 17.34 MPa and 350 to 470°C

FIGURE 3 - Fraction of Liquid Vaporized, f , as a Function of Gas to Liquid Feed Rate Ratio, G/L g mol/kg, for 93% hydrocracked product at 10.44 to 17.34 MPa, and 350 to 450°C

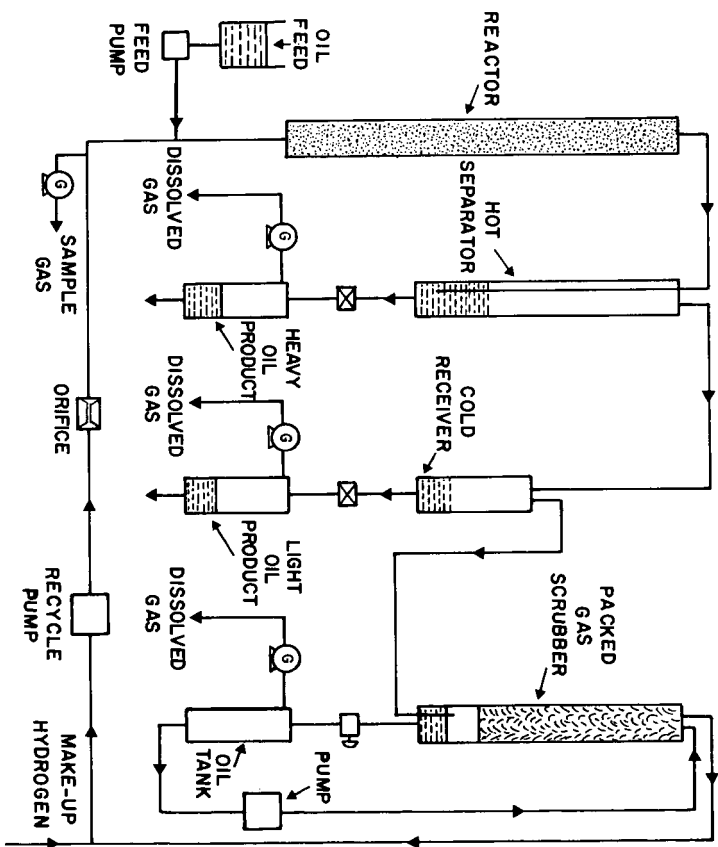


FIGURE 1 - Schematic Diagram of CANMET Hydrocracking Pilot Plant

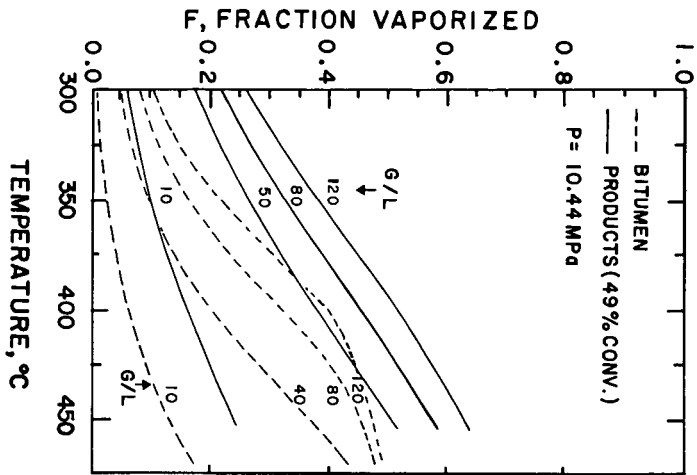


FIGURE 4 - Fraction of Liquid Vaporized, f , as a Function of Temperature for Bitumen and 49% Hydrocracked Product at 10.44 MPa and G/L Values of 10 to 120 g mol/kg

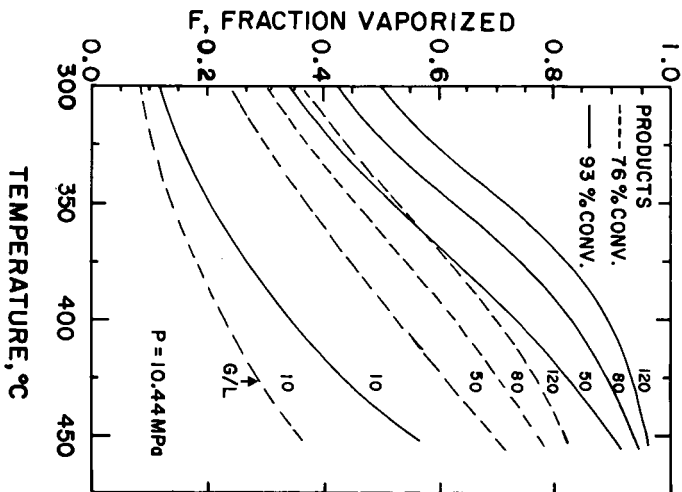


FIGURE 5 - Fraction of Liquid Vaporized, f , as a Function of Temperature for 76 and 93% Hydrocracked Products at 10.44 MPa and G/L Values of 10 to 120 g mol/kg

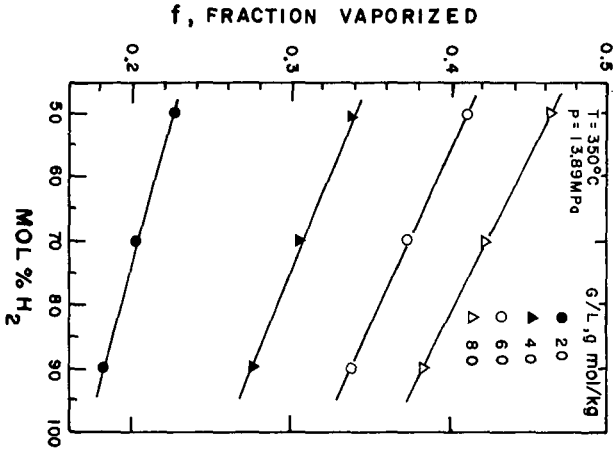


FIGURE 6 - Fraction of Liquid Vaporized, f, vs mol % H₂ for 83% Hydro-cracked product at 350°C, 13.89 MPa and G/L Values of 20 to 80 g mol/kg

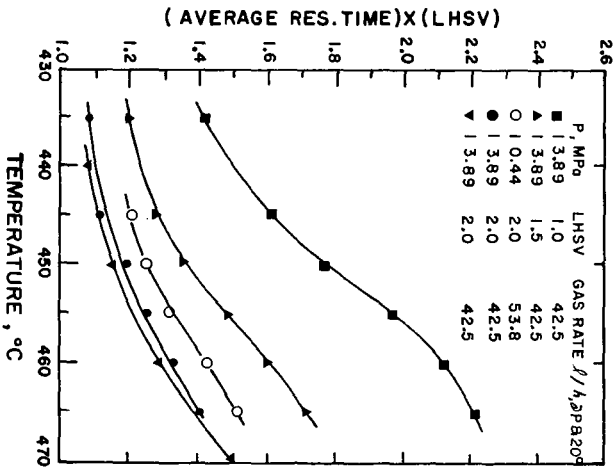


FIGURE 7 - Product of Calculated Average Liquid Residence Time and Liquid Hourly Space Velocity vs Temperature for a Series of Hydrocracked Products Obtained Under the Indicated Conditions

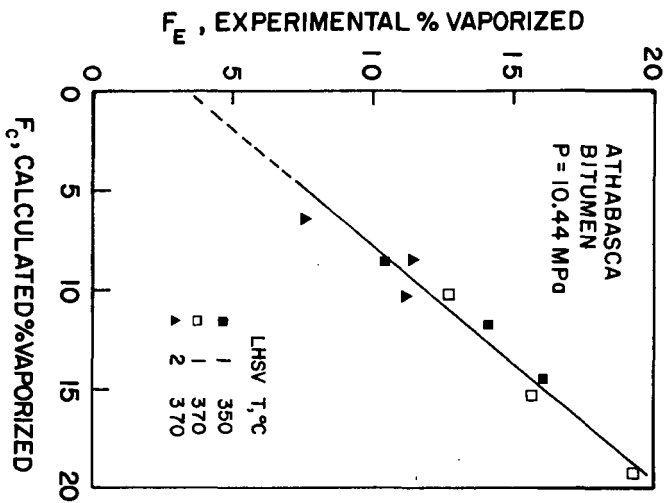


FIGURE 8 - Experimental vs Calculated Per Cent of Liquid Vaporized for Athabasca Bitumen at 10.44 MPa

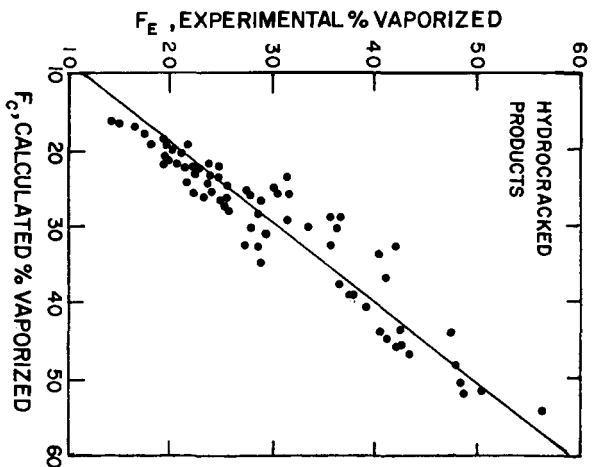


FIGURE 9 - Experimental vs Calculated Per Cent of Liquid Vaporized for 75 Hydro-cracked Products for Pressures of 10.44 to 17.34 MPa and Temperatures of 300 to 430°C.

The Effect of Tin Catalysts on Hydrorefining
of Athabasca Oil Sand Bitumen and on Coal Hydrogenolysis

J.F. Kriz, K. Belinko and B.N. Nandi

Energy Research Laboratories,
Canada Centre for Mineral and Energy Technology,
Department of Energy, Mines and Resources,
Ottawa, Canada

INTRODUCTION

The development of catalysts for up-grading of Canadian oil-sand bitumen and for conversion of coal into liquid products has been of considerable interest at the Energy Research Laboratories. The study reported below was part of an investigation of the suitability of different catalyst systems for hydrocracking heavy oils, and involved the use of tin compounds with bitumen and heavy oil feeds.

Tin compounds have generally been found to be particularly effective in coal hydrogenation processes (1-4). Recent studies have included the use of tin catalysts in hydrorefining of coal-derived feeds such as asphaltenes (3) and solvent refined coal (4). Although much attention has been given to the activity of supported and unsupported tin catalysts, little effort has been made to examine the fate of the tin during the liquefaction process.

Guided by the outcome of previously published work, a series of tin-containing catalysts was tested for bitumen and coal up-grading. Emphasis was placed on studying the changes occurring within the catalysts during these processes. Results obtained in preliminary tests stimulated further development such as the use of different methods of catalyst preparation.

EXPERIMENTAL

Feedstocks and Equipment

Athabasca bitumen was obtained from Great Canadian Oil Sands, Fort McMurray, Alberta, Canada, and some of its properties are given in Table I. Asphaltene feedstock from bitumen was obtained by precipitating the asphaltenes by addition of pentane to bitumen according to the ASTM method (7). High volatile Devco 26 coal was obtained from Cape Breton Development Corporation, Nova Scotia, Canada. The properties of this coal are given in Table II.

TABLE I

Properties of Athabasca Bitumen

Specific gravity	1.009 (15/15°C)	Benzene insolubles	0.72 wt%
Sulphur	4.48 wt%	Carbon	86.36 wt%
Ash	0.59 wt%	Hydrogen	10.52 wt%
Conradson carbon residue	13.3 wt%	Nitrogen	0.45 wt%
Pentane insolubles	15.5 wt%	Pitch (524°C+)	51.5 wt%

TABLE II

Properties of Devco 26 Coal
(High Volatile Bituminous A)

Proximate Analysis wt%		Ultimate Analysis wt%		Petrographic Analysis vol%	
Moisture	1.13	Carbon	83.97	Vitrinite	77.8
Ash	2.18	Hydrogen	5.36	Exinite	6.6
Volatile matter	31.35	Sulphur	0.62	Micrinite	3.6
Fixed carbon	65.34	Nitrogen	1.80	Semi-fusinite	8.8
		Oxygen (by dif)	4.94	Fusinite	2.6
				Pyrite	0.6

Bitumen tests were carried out in a bench-scale fixed bed reactor having a volume of 155 cm³, a length to diameter ratio of 12 and a continuous up-flow arrangement (5). Experiments were performed at a pressure of 13.9 MPa, a liquid volumetric space velocity of 0.278 ks⁻¹ (1.0 h⁻¹) based on the reactor volume and a hydrogen (electrolytic) flow rate of 37.5 cm³s⁻¹ at STP (5000 cu ft/bbl). The temperature range was 420^o-460^oC. 2000 P51
7

A batch shaker autoclave, into which about 25 g of coal was charged, was used for experiments involving coal hydrogenolysis. The runs were carried out without a vehicle oil, at an initial (cold) hydrogen pressure of 6.5 MPa and a temperature of 350^oC for 2 hours.

Optical microscopic examinations of the catalysts were made before and after use and were complemented by electron microprobe analysis.

Catalyst Description and Preparation

The catalysts tested with bitumen were alumina-supported and were prepared as described below.

Catalyst A:

Alpha alumina monohydrate (obtained from the Continental Oil Company, Peterboro, New Jersey) was gelled with slightly acidified water and made into 3.2 mm (1/8 in) extrudates. These were then dried at 110^oC for 6 hours and calcined at 500^oC for 6 hours. The calcined extrudates were impregnated with a solution of SnCl₂ in methanol, the volume of which was about one-half that of the extrudates. Methanol was subsequently purged out of the extrudates in a nitrogen flow at 150^oC. The final concentration of Sn was ca. 7 wt%.

Catalyst B:

Extrudates of Catalyst A were sulfided in a flow of a mixture of H₂S and H₂ (1:3 by vol.) at 150^oC for 5 hours at atmospheric pressure.

Catalyst C:

An aqueous solution of SnCl₂ was added to the alpha alumina monohydrate and milled in a mix-muller. The resulting paste was extruded, dried and calcined as in the case of Catalyst A. The final concentration of Sn was ca. 7 wt%.

Catalyst D:

A solution of aluminum isopropoxide and SnCl_2 in isopropanol was co-precipitated by hydrolysis using diluted ammonium hydroxide. The precipitate was extruded, dried and calcined as in the case of Catalyst A. The final concentration of Sn was ca. 15 wt%.

Separate experiments with bitumen involved testing alumina extrudates used for preparation of Catalyst A and B, and also testing a series of catalysts containing both Mo and Sn in different concentrations. The latter series was prepared by adding, successively, an aqueous solution of ammonium paramolybdate $(\text{NH}_4)_6 \text{Mo}_7 \text{O}_{24} \cdot 4\text{H}_2\text{O}$ and an aqueous solution of stannic chloride $\text{SnCl}_4 \cdot 5\text{H}_2\text{O}$ to alumina monohydrate in the mix-muller. Atomic ratios of molybdenum and tin added were, respectively, either 1:1 or 1:0. The resulting paste was extruded, dried and calcined as described above.

For experiments involving hydrogenolysis of coal and bitumen-derived asphaltenes, an aqueous slurry of pulverized feed and tin catalyst was prepared and subsequently dried under vacuum at 80°C . The catalysts tested included stannous chloride, stannous oxalate and stannous sulfide. The concentration of tin in the feed was approximately 5 wt%.

RESULTS AND DISCUSSION

Compared with pure alumina, tin compounds supported on alumina were generally found to exhibit only marginal improvements in liquid product quality in bitumen hydrotreating. The usual properties of the liquid product, such as specific gravity, sulfur and nitrogen content and percent pitch conversion, were not significantly changed when, for instance, in one series of tests the tin concentration was varied. The results are shown in Figure 1, which compares Mo/ Al_2O_3 -type catalysts both with and without a tin additive. It was found that the extent of decrease in the specific gravity of the liquid product caused by an increasing molybdenum concentration was not significantly affected by a simultaneous increase in tin loading.

The influence of the conversion of bitumen-derived asphaltenes into pentane-soluble products was also investigated. The influence of SnS on asphaltene conversion was much less apparent than on coal. The conversion of bitumen-derived asphaltenes increased from 69% with no catalyst to about 75% in the presence of SnS.

The conversion of coal into benzene-soluble products was found to increase substantially in the presence of the various tin catalysts tested. The conversion increased from 12.4% with no catalyst to an average of approximately 51% for all three tin catalysts investigated. The effectiveness of tin compared favourably with other catalysts tested, as shown in Table III.

TABLE III
Effect of Catalysts on Conversion of Coal
into Benzene-Soluble Products (350°C)

Catalyst	None	SnCl_2	SnS	$\text{Sn}(\text{COO})_2$	FeSO_4	FeCl_2	ZnCl_2
Conversion (% daf)	12.4	53.2	52.0	47.5	23.2	19.3	51.5

These results agree well with those obtained previously by Kawa *et al* (2,3) showing high activity of tin compounds for coal hydrogenolysis. Asphaltene production is probably the first step in coal liquefaction and more severe conditions are needed to increase the yield of pentane-soluble products. The conversion of asphaltenes produced from coal was not determined in the present work. However, the effect of stannous chloride on bitumen-derived asphaltenes appeared smaller than would be expected if asphaltenes produced from coal were used (2). In this respect the work with asphaltenes from solvent refined coal (4) produced more comparable results. The reason for the differences in reactivity between asphaltenes from coal and asphaltenes from bitumen feedstocks are not known and one can only speculate that they result from variations in chemical structures. A detailed analysis of bitumen-derived asphaltenes was presented by Strausz (6), and the sulfur content (about 8 wt%) is higher and oxygen content (about 1 wt%) is lower than those in asphaltenes produced from coal (2,3,4). The high sulfur content suggests that Mo/Al₂O₃ based catalysts may be the most efficient catalysts for hydrogenolysis since they seem to be the best hydrodesulfurizing agents.

Notable changes resulting from different catalyst preparation methods were observed. Table IV presents some results of analyses of liquid products from bitumen experiments for different tin-containing catalysts.

TABLE IV

Effect of Catalysts on Liquid Products from Bitumen***

Catalyst	Specific Gravity	%S Removed	%N Removed	% Pitch Converted
Al ₂ O ₃	0.951	33.3	26	62
A	0.932*	41.1*	52*	77*
	0.952**	31.0**	32**	66**
B	0.947	30.1	28	67
C	0.928	34.2	-	87
D	0.903	41.6	40.0	97

* Initial run

** Second run

*** Run at 440°C

It is noteworthy that there was a drop in the activity of Catalyst A from the initial run to the second. Presumably, the impregnated SnCl₂ initially present was not completely transferred into SnS before the first run commenced and exhibited a greater activity at that stage. Two separate batches of SnCl₂ impregnated on alumina showed such deactivation. The deactivation was not observed when pre-sulfided batches were used (Catalyst B). Liquid products of improved quality, namely lower specific gravity, were obtained when Catalysts C and D were used. A different procedure was applied to prepare these catalysts and their properties are discussed below.

The supported tin catalysts of the type A and B tested with bitumen were found to exhibit little increased activity when compared with alumina alone. Microscopic examinations of the used extrudates revealed extensive sintering of the tin component within the cracks in the alumina, (Figure 2). Identical results were obtained regardless of whether the starting material was SnCl₂ (Catalyst A) or SnS (Catalyst B). These observations suggested that very little of the tin catalyst was actually exposed to the bitumen during the process. The optical reflectance of the streaks seen in Figure 2 compared well with that of pure SnS.

In addition, electron microprobe analysis of the spent catalyst confirmed that the high reflectance streaks were composed of tin and sulfur in atomic ratios of approximately 1:1. No streaks were observed in the unused extrudates, indicating even dispersion of the tin compounds on the surface of alumina. This was confirmed by electron microprobe analysis. Microscopic examination of the benzene-insoluble residue from coal liquefaction experiments revealed a sintering effect similar to that noted with bitumen runs, irrespective of whether SnCl_2 , $\text{Sn}(\text{COO})_2$ or SnS was used as the catalyst, (Figure 3). The high reflectance streaks were again found to be composed of tin and sulfur in atomic ratios of about 1:1.

The formation of SnS from SnCl_2 is feasible under typical hydrogenation or hydrotreating conditions provided sufficient sulfur is present in the feed material. It has been suggested (1) that SnS becomes the most stable form of tin and would be formed from SnCl_2 , for example, according to:



At reaction temperatures, SnCl_2 could conceivably flow into pores and cracks of the support or coal, and subsequently be converted to the sulfide form. On the other hand, SnS melts at 880°C , which is considerably higher than the reaction temperature used. Nonetheless, sintering had occurred to the same extent when SnS was used. The migration mechanism may therefore involve an intermediate species having a low melting point, such as elemental tin. This species could then migrate into void areas of the support before being converted back to SnS . In a separate experiment the fresh SnS - and SnCl_2 -containing catalysts were subjected to reaction conditions in the absence of the feed. Spots of high reflectance indicated the possible formation of metallic tin in extrudates subjected to this type of reducing condition.

In view of the extensive sintering effect the original dispersion of the tin compound was reduced considerably and consequently the effectiveness of both high- and low-surface area supports was expected to be comparable, as reported by Kawa *et al* (3). Figures 4 and 5 show sintering of SnS in the extrudates of Catalysts C and D (Table IV). Comparison with Figure 2 indicates that a more even dispersion of tin sulfide was established in the extrudates of Catalysts C and D. The sintering still occurred but the SnS appeared to assume a larger surface area. The higher dispersion correlated well with the activity observed with bitumen tests using these catalysts. One additional observation relates to Catalyst D in Figure 5. It appears that concentration of the tin component is greater in the regions between the particles of alumina than inside the particles. One could speculate that these regions may have been more accessible to the reactant fluids than the regions within the alumina particles. This would be in agreement with the enhanced activity of Catalyst D.

In conclusion, the present findings may be summarized as follows:

Tin compounds were found relatively less effective for bitumen hydro-refining than for hydrogenolysis of high volatile bituminous coals, possibly because of the different structure of bitumen-derived asphaltenes. The original dispersion of the catalyst on the support was significantly reduced. The extent of sintering of tin catalysts under reaction conditions correlated with their activity. It may be that an improved catalytic system would require a stronger bond between the tin compound and the support to hinder surface migration.

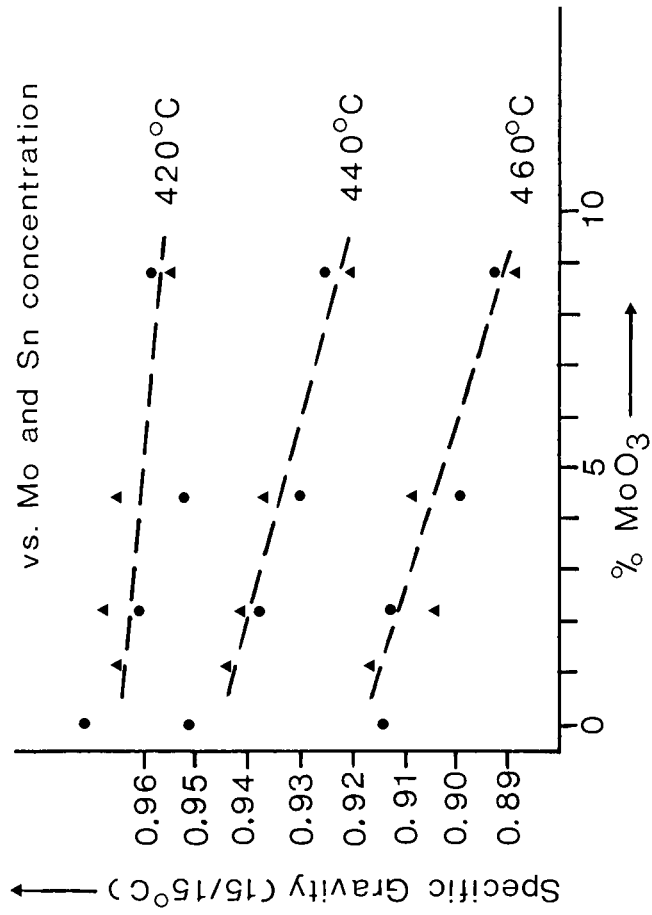
ACKNOWLEDGEMENT

The authors gratefully acknowledge the contribution of L.E. Galbraith and B.M. Moffat for their technical assistance. Thanks are also due to Dr. R.H. Packwood for carrying out the electron microprobe analyses.

REFERENCES

1. Weller, Sol and Michail G. Pelipetz. Catalysis in Liquid-Phase Coal Hydrogenation. Proc. 3rd World Petrol. Cong., Sect. IV, Subsect 1, 91 (1951).
2. Kawa, Walter, H.F. Feldmann and R.W. Hiteshue. Hydrogenation of Asphaltene from Coal Using Halide Catalysts. Amer. Chem. Soc., Div. Fuel Chem., Prepr. 1970, 14 (4) (Pt. 1), 19-26.
3. Kawa, Walter, Sam Friedman, W.R.K. Wu, L.V. Frank and P.M. Javorsky. Evaluation of Catalysts for Hydrodesulfurization and Liquefaction of Coal. Amer. Chem. Soc., Div. Fuel Chem., Prepr. 1974, 19 (1), 192-206.
4. Lovetro, David C. and Sol W. Weller. Stannous Chloride and Cobalt Molybdate-Alumina Catalysts in Hydrogenolysis of Solvent Refined Coal. Ind. Eng. Chem., Prod. Res. Dev., 1977, 16 (4), 297.
5. O'Grady, M.A. and B.I. Parsons. The Hydrogenation of Alberta Bitumen over Cobalt Molybdate Catalysts. Mines Branch Research Report R-194, Department of Energy, Mines and Resources, Ottawa, 1967.
6. Strausz, O.P. Some Aspects of the Chemistry of Alberta Oil Sand Bitumen. Amer. Chem. Soc., Div. Petro. Chem. Prepr. 1976, 21 (3), 456-481.
7. American Society for Testing and Materials, Part 15, D-2042; 1975.

Figure 1: Specific Gravity of Liquid Product



- ▲ Mo:Sn=1:1
- Mo:Sn=1:0



FIGURE 2: OPTICAL MICROGRAPH OF USED CATALYST A SHOWING HIGH REFLECTANCE STREAKS OF SINTERED TIN COMPONENT

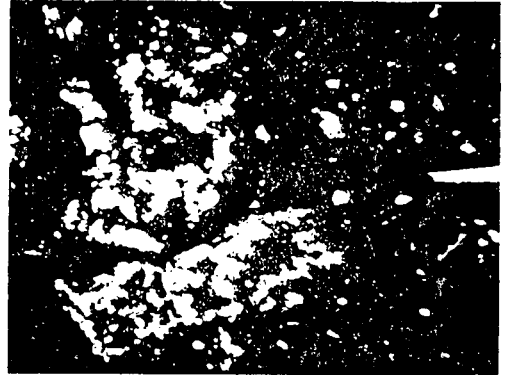


FIGURE 3: MICROGRAPH OF THE BENZENE-INSOLUBLE RESIDUE FROM COAL LIQUEFACTION EXPERIMENTS WITH STANNOUS OXALATE

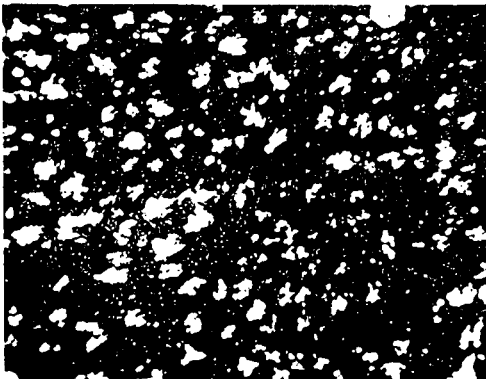


FIGURE 4: OPTICAL MICROGRAPH OF USED CATALYST C

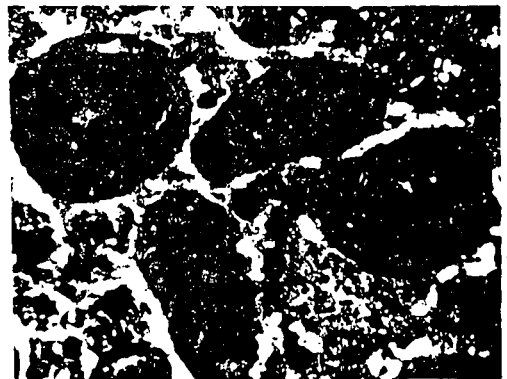


FIGURE 5: OPTICAL MICROGRAPH OF USED CATALYST D

50 μ m



FIGURE 2: OPTICAL MICROGRAPH OF USED CATALYST A SHOWING HIGH REFLECTANCE STREAKS OF SINTERED TIN COMPONENT

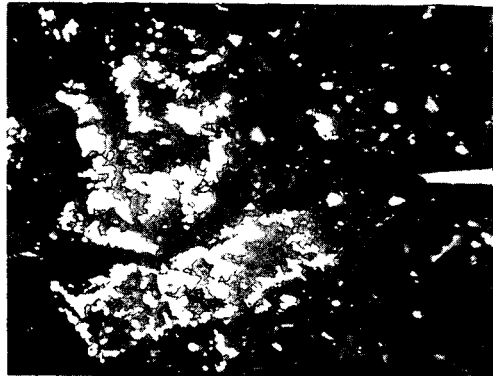


FIGURE 3: MICROGRAPH OF THE BENZENE-INSOLUBLE RESIDUE FROM COAL LIQUEFACTION EXPERIMENTS WITH STANNOUS OXALATE

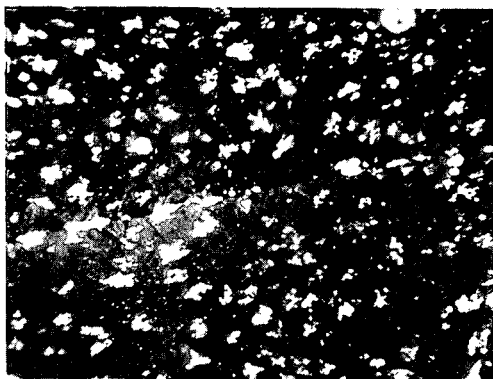


FIGURE 4: OPTICAL MICROGRAPH OF USED CATALYST C

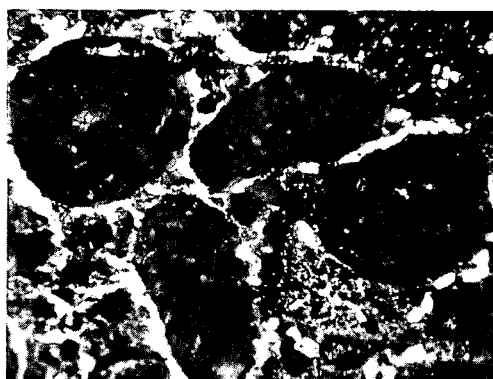


FIGURE 5: OPTICAL MICROGRAPH OF USED CATALYST D

50 μm

Behavior of Tar Sand Bitumen With Paraffinic Solvents and Its Application to Separations for Athabasca Bitumen

Edward W. Funk
Exxon Research and Engineering, Linden, N.J., 07036

The main purpose of this paper is to present the behavior of tar sand bitumen when contacted with low-molecular-weight paraffins at ambient temperatures. We have found that an understanding of this phenomenon can lead to new separation and upgrading approaches for Athabasca tar sands. Furthermore, the ideas generated by the study of tar sand bitumen may possibly also be applied to other synthetic fuels such as coal liquids and shale oil.

1. Tar Sand Bitumen Dissolution Using the Spinning Disc Method. The dissolution behavior of tar sand bitumen depends primarily on the solvent, contacting conditions, and the temperature. For studying the dissolution mechanism we have chosen the spinning disc technique as a simple, well-understood system. The spinning disc technique for examining mass transfer and dissolution phenomena is well established in electro-chemistry but can be applied to a variety of systems (1,2). The experimental procedure consists of rotating a circular disc immersed in a liquid at a constant speed. Mass transfer from the disc can be experimentally measured as a function of time and rotational speed. The principal advantage of this geometry is that the mass-transfer coefficient is the same at all points on the surface and can be expressed as

$$k = 0.62 D^{2/3} \nu^{-1/6} \omega^{1/2} \quad 1)$$

where D is the binary diffusion coefficient, ν is the kinematic viscosity and ω is the rotational speed of the disc. The dependence of k on the rotational speed allows separation of mass transfer resistances between phases from resistances within the bulk phase.

For our study, a glass disc 2.54 cm. in diameter was coated with 0.10 grams of tar sand bitumen. The concentration of bitumen in solution was measured using a Beckman DB-G spectrophotometer operating at 530 nm. Details of this analytical technique are given by Funk and Gomez (3).

Figure 1 presents the experimental data for *n*-pentane as the solvent at 25°C. The data were obtained at rotational speeds of 0, 7 and 17 RPM. Figure 1 shows that, over the range of speeds studied, the rate of bitumen dissolution is independent of the rotational speeds. Equation 1 then indicates that the principal resistance to dissolution resides in the bitumen layer and not in transport across the solvent-bitumen interface. This resistance within the bitumen layer is large enough to require several minutes (≈ 10 minutes) for all the deasphalted oil to diffuse out of the bitumen layer.

For a variety of paraffinic solvents, dissolution data were obtained at 25°C and the discs were removed and the remaining asphaltene crust was examined by microscopy. Figure 2 presents SEM photomicrographs for pentane and decane asphaltenes at a magnification of 500. The results show that the asphaltenes form a porous network similar to an alloy which has had one component leached out. For the pentane asphaltenes, the pore size is $\approx 1 \mu$; for decane-precipitated asphaltenes the pores are considerably smaller. Examination of asphaltenes from dissolution using other paraffins showed that the pore size became smaller the higher the carbon number of the paraffinic solvent.

The experimental data can be modeled using Fick's second law which is expressed as

$$\frac{\partial c}{\partial t} = D_{AB} \frac{\partial^2 c}{\partial x^2} \quad 2)$$

To describe the unsteady-state diffusion in the spinning-disc experiments, we use the boundary conditions of $c=c_0$ for $t < 0$ and $c = 0$ in the solvent for all t . Crank (4) gives the solution to Equation 2; the expression for D_{AB} , the binary diffusion coefficient expressing mutual diffusion of solvent and deasphalted oil, is particularly simple at time where one-half of the deasphalted oil has been leached out

$$D_{AB} = \frac{0.049}{(t/L^2)} \quad 3)$$

where L is the thickness of the bitumen layer on the disc. Experimental data consistent with the above model usually show a linear plot of M_t/M_∞ (the fraction of deasphalted oil leached out) versus t^2 over a considerable time range. Figure 3 presents M_t/M_∞ as a function of t^2 for dissolution using pentane, heptane and decane. Equation 3 was used to calculate effective diffusion coefficients from the experimental data. For the pentane system, D_{AB} is 1.41×10^{-7} cm²/sec at 25°C. The results with heptane give a value of D_{AB} of 1.21×10^{-7} cm²/sec and the value for the decane system is 6.50×10^{-9} cm²/sec.

2. Particle Size Analysis of Asphaltene Aggregates. To determine the particle-size distribution of asphaltene aggregates which would be breaking away from the crust, tar sand bitumen was deasphalted using pentane, hexane and heptane at room temperature. The bitumen was contacted with ten times its weight of solvent and the asphaltenes were precipitated using a laboratory centrifuge operating at 2000 RPM. The asphaltenes were washed until they were free of deasphalted oil.

The HIAC model PC-230 was used to measure the particle-size distribution. This instrument uses a light-sensitive diode to determine light attenuation due to particles flowing past the sensor. Figure 4 shows the particle-size distributions for pentane, hexane and heptane precipitated asphaltenes. The results indicate that the pentane asphaltenes are somewhat larger than the hexane asphaltenes; this trend was found consistent through heptane.

3. Structure of Athabasca Tar Sands. For the tar sand system, the bitumen is associated with the sand and water as shown schematically in Figure 5. Typically the Athabasca tar sands contain 12% bitumen, 5% water and 83% sand and other minerals. Details of characterization of tar sands are summarized by Camp(5).

4. Fluid-Bed Studies. A liquid-fluidized bed is a convenient and conventional technique for contacting solids and liquids and we have applied this technique to contact tar sands with paraffinic solvents. Experimental data on the size of asphaltene aggregates for the tar sand system were obtained by using paraffinic solvents to elutriate the asphaltenes from a well-mixed fluidized bed of tar sands. Figure 6 gives a schematic diagram of the equipment used for the elutriation studies. The tar sands were placed in the 2" I.D. glass extraction column and a set of turbine mixers operating at 200 RPM was used to assure good solids-solvent contact. For each run, solvent was passed up through the tar sand bed at a known flowrate and collected at the top of the extraction

column. The extract was then analyzed for the percentage of asphaltenes. Figure 7 presents the results of the elutriation studies at 25°C. The percentage of asphaltenes entrained is expressed relative to the total asphaltenes in the bitumen for the particular paraffinic solvent used. As an example, we expect the extract with pentane to be 20% asphaltenes if all are small enough to be entrained; if the extract is 10% asphaltenes we calculate that only 50% of the asphaltenes were entrained. We see from Figure 7 that liquid flowrates in the range of 1 cm/sec are required to entrain all the asphaltenes with the extracted oil. Consistent with the results shown in Figure 4, the pentane asphaltenes behave as larger particles than the hexane asphaltenes and this trend continues through octane. Figure 8 presents similar data as a function of temperature for heptane as the solvent. As the temperature increases, higher liquid flowrates are required to entrain the asphaltene aggregates and this indicates that the size of the aggregates is increasing. The change in solvent density and viscosity is much too small to account for the higher liquid flowrates.

Use of Stokes' law and the elutriation data shown in Figure 7 were used to calculate effective maximum diameters for the asphaltene aggregates. For heptane, the maximum aggregate diameter is 100 μ and for pentane 150 μ ; these values are somewhat higher than those found using the HIAC particle-size analysis. The difference may be due to the estimated asphaltene density used in the Stokes' law calculation.

5. Novel Approach to Bitumen Separation from Athabasca Tar Sands. We have examined the use of paraffinic solvents for separation of bitumen from tar sands in a fluid bed since this type of contacting equipment has reasonable potential to be scaled up to the very large sizes required for tar sands.

Fluidization data were measured using the equipment shown schematically in Figure 6. For the sample of tar sands used, the particle-size distribution of the inorganics is shown in Figure 9. Figure 10 presents a plot of $\ln U$ versus $\ln \epsilon$ for the tar sand system; these data are for heptane as the solvent and at ambient temperature. The bed shows some expansion at liquid velocities substantially below the minimum fluidization velocity; this is not the case for a bed of equal-sized particles; it probably occurs in the tar sand system due to some segregation of different sized particles to give a fixed-bed region and a fluidized region. The curves A and B for dry tar sands (water removed by evaporation) give an approximate minimum fluidization velocity of the inorganics equal to 1 cm/sec. Curve B simulates the bottom of a hypothetical extractor where the solvent is nearly pure heptane; curve A simulates the other end of the extractor where the solvent has a relatively high bitumen concentration (in this case, heptane/bitumen = 4). The fluidization behavior is very different for fresh water-wet tar sands. These data are shown in Figure 10 by the solid dots. The minimum fluidization velocity is much higher than for dry tar sands. This great difference can be explained by agglomeration of the inorganics in the tar sand bed. Spherical agglomerates are formed in the fluid bed because the water-wet inorganics associate to minimize surface area between water and the hydrocarbon. Details of spherical agglomeration and its application to other systems are given by Smith and Puddington (6).

The results of Figure 10 show that the tar sand inorganics behave like large particles in a fluid bed if care is taken to maintain them as

water-wet. From Figure 7, we know that the asphaltenes behave as relatively small particles. Combining the results of Figures 7 and 10 suggests the conceptual separation approach shown in Figure 11. Figure 11 shows that for a paraffinic solvents there is a range of liquid flowrates which gives carryover of asphaltenes from a fluidized-bed type contactor but does not entrain the inorganics. For example, operating at 1.0 cm/sec to entrain the asphaltenes would entrain an important fraction of the unagglomerated inorganics. Then, a further separation of bitumen from inorganics would be required. The separation shown in Figure 11 is for essentially ambient temperatures.

The results shown in Figure 11 only suggest a conceptual approach for bitumen separation from tar sands. Use of this separation approach on a commercial scale requires considerable process development to generate an integrated system including tar sands preparation, solid-liquid contacting equipment, solids handling, and economic solvent recovery from the extracted tar sands.

6. References

- (1) Levich, V. G., "Physicochemical Hydrodynamics," Prentice-Hall, Inc., Englewood Cliffs, N. J., 1962.
- (2) Chan, A. F., Evans, D. F., and Cussler, E. L., "Explaining Solubilization Kinetics," AIChE Journal 22,1006 (1976).
- (3) Funk, E.W., and Gomez, E., "Determination of Vanadium in Athabasca Bitumen and Other Heavy Hydrocarbons by Visible Spectrometry," Anal. Chem. 49,972 (1977).
- (4) Crank, J., "The Mathematics of Diffusion," Oxford University Press, Second Edition, 1975.
- (5) Camp, F. W., "The Tar Sands of Alberta, Canada," Cameron Engineers, Denver, Colorado, 1969.
- (6) Smith, H. M. and Puddington, I. E., "Spherical Agglomeration of Barium Sulfate," Can. J. Chem., 38, 1911 (1960).

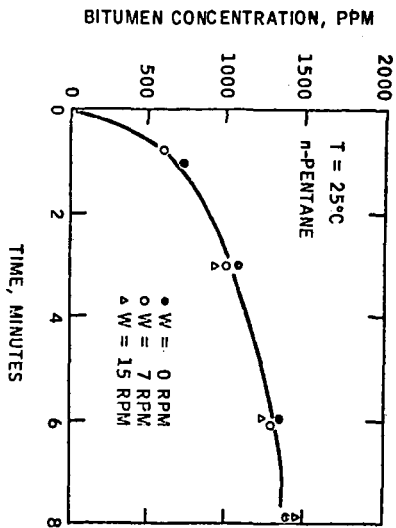
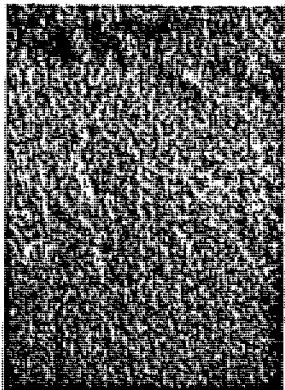


Figure 1 - Spinning Disc Experiments for Tar Sand Bitumen Dissolution in Pentane



Pentane Asphaltenes



Decane Asphaltenes

Figure 2 - Photomicrographs at 500x of Pentane and Decane Asphaltenes

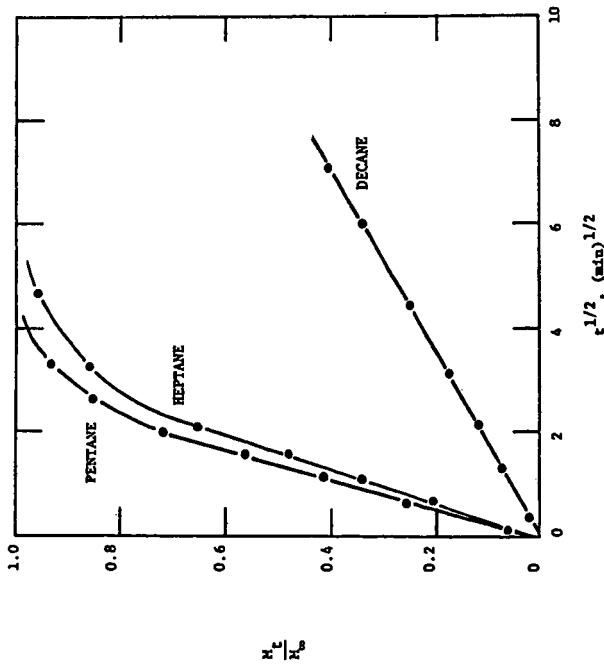


Figure 3 - Bitumen Dissolution in Normal Paraffins

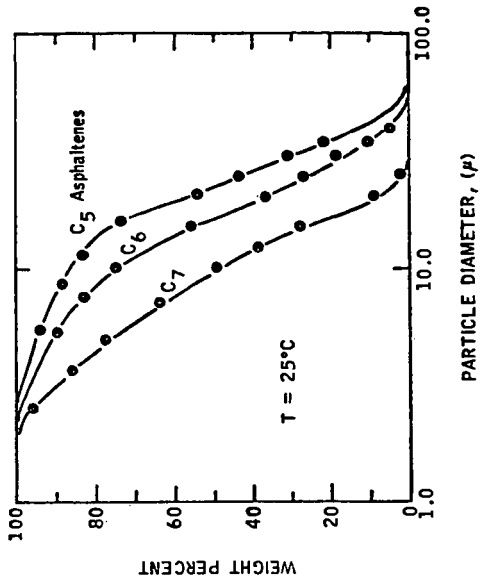


Figure 4 - Particle-Size Distribution of Asphaltene Aggregates

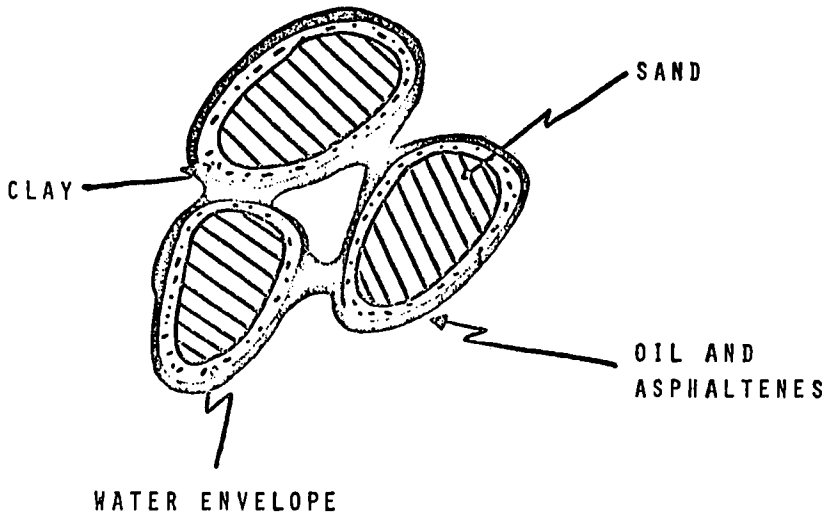


Figure 5 - Basic Model of Athabasca Tar Sands

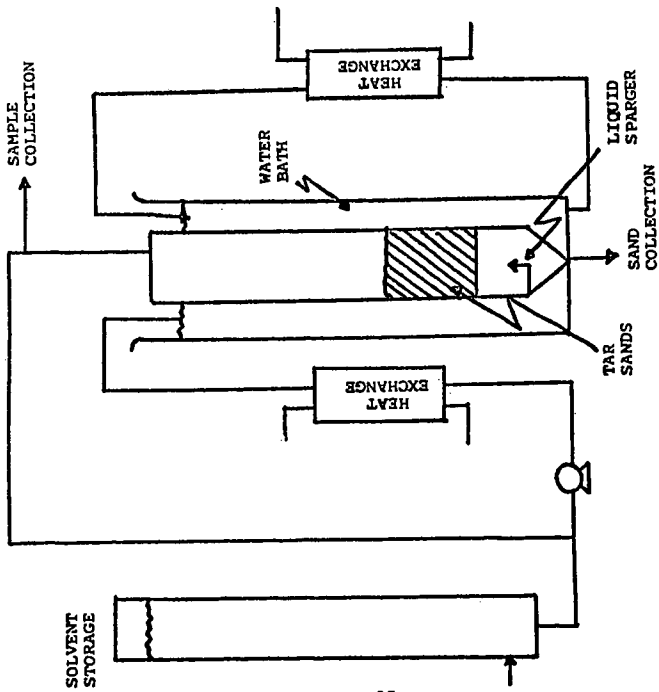


Figure 6 - Schematic Diagram of Fluid-Bed Contactor for Tar Sands

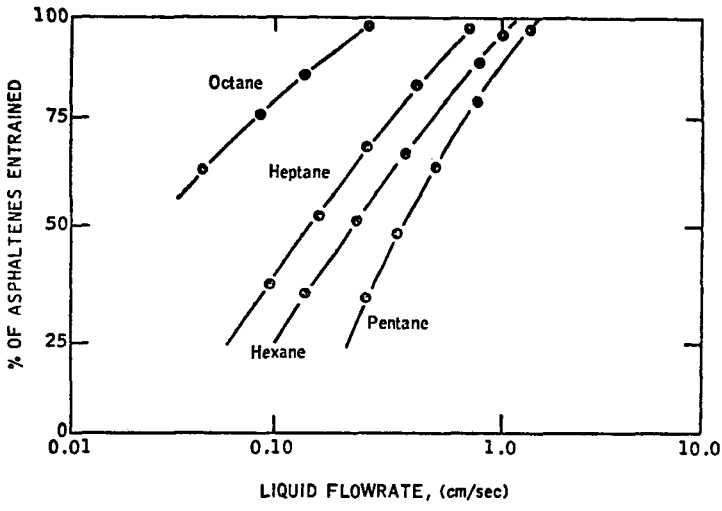


Figure 7 - Entrainment of Asphaltenes from a Tar Sand Bed as a Function of Liquid Velocity

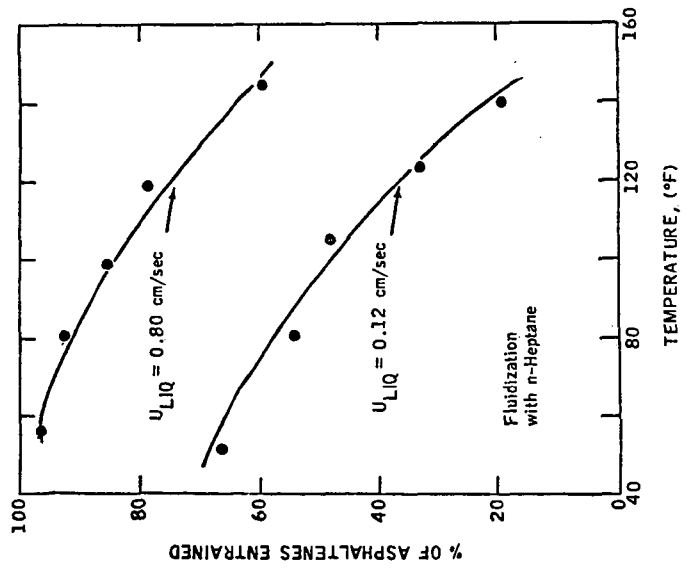


Figure 8 - Effect of Temperature on Entrainment of Asphaltenes from a Fluidized Tar Sand Bed

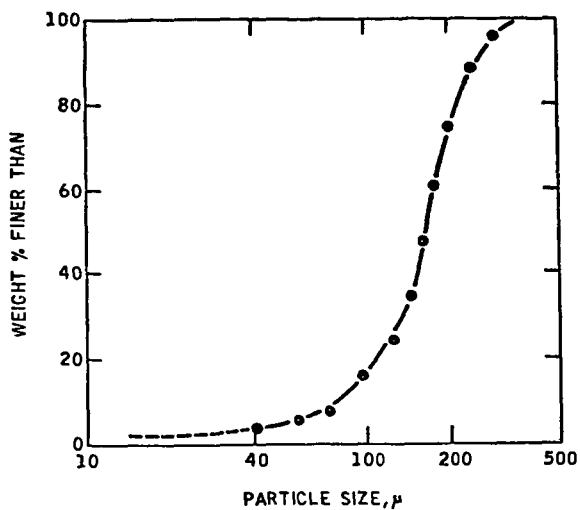


Figure 9 - Typical Particle-Size Distribution of Athabasca Tar Sand Inorganics

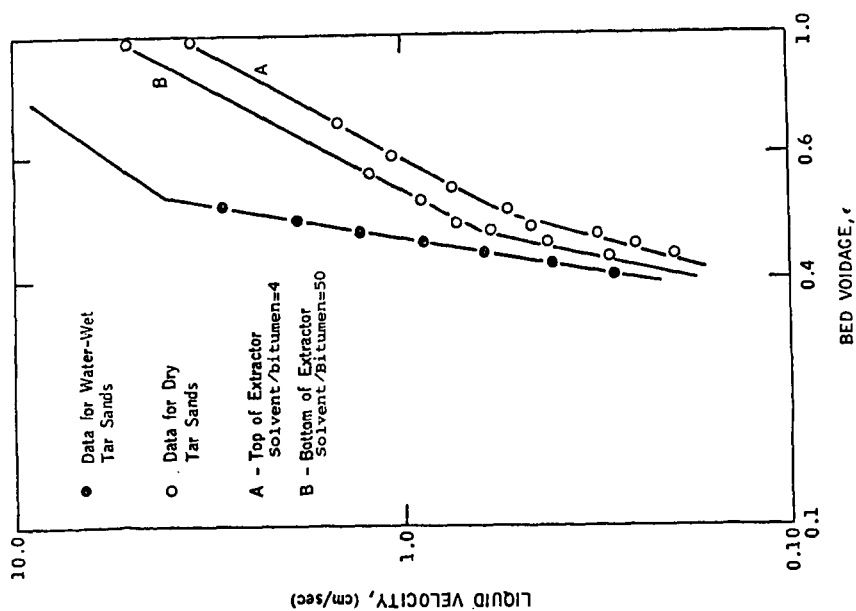


Figure 10 - Fluidization Data for Athabasca Tar Sands with n-Heptane

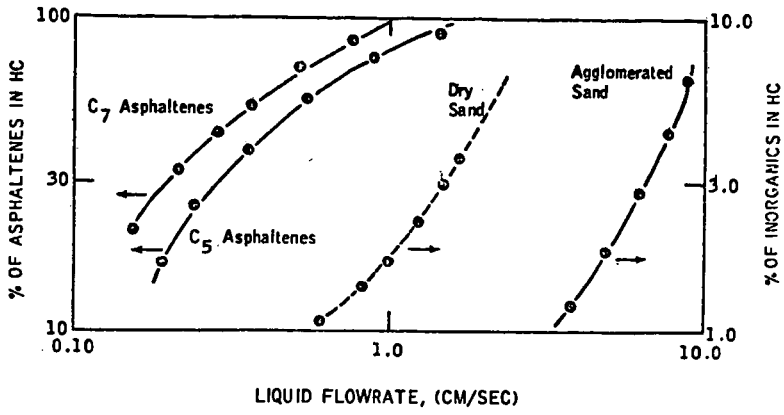


Figure 11 - Conceptual Process for Bitumen Separation from Athabasca Tar Sands

OXIDATION OF THE ATHABASCA OIL SAND AND ITS FRACTIONS

K.N. Jha, P.M. Rao and O.P. Strausz

Hydrocarbon Research Centre
Department of Chemistry, University of Alberta
Edmonton, Alberta, Canada, T6G 2G2

INTRODUCTION

The Athabasca oil sand and its fractions are known to be thermally unstable and sensitive to air (1-2). They react with molecular oxygen even at low temperatures. It has been reported that oxidation of bitumen generates high molecular weight material (3). The high susceptibility of the oil sand to aerobic oxidation could have practical relevance with regard to the surface strip mining and processability of the oil sand. Apart from its influence on the quality of the product, the phenomenon is also relevant to the origin, history, thermal and microbial maturation of the deposits and also to the *in situ* fire-flooding recovery technology of the oil sand.

Results of laboratory and field experiments on the production of crude oil by *in situ* forward and reverse combustion have been reported (4-7). However, quantitative studies of the parameters related to the chemical aspects of these processes, such as oxidation kinetics, have not been performed.

The chemical transformations in the oil sand due to oxidation reactions at low temperatures are difficult to detect by analysis of the bulk composition but they can be easily monitored by measuring the gaseous and highly volatile materials which are produced therefrom.

The present study was undertaken in order to gain an insight into the oxidation and weathering processes taking place in the Alberta oil sand.

EXPERIMENTAL

The high vacuum apparatus employed in this study was similar to that used previously (1-2). The experimental details for the collection and analysis of gases and the volatile materials have also been described (1-2). About 130 g Athabasca oil sand was placed in a 500 cm³ Pyrex vessel fitted with a breakseal and several 1 cm³ ampoules. The vessel was attached to the vacuum apparatus and degassed at room temperature for one hour. Oxygen was then introduced into the vessel at about 150 torr, the vessel was sealed off and heated to the desired temperature in a silicone oil bath. The vessel was shaken intermittently and the ampoules were sealed at desired time intervals and analyzed for oxygen on a 2.4 m molecular sieve column. The samples heated at 130°C in the absence and presence of oxygen were analyzed for both non-condensable and condensable materials at -196°C. Standard extraction procedures for bitumen and for the separation of asphaltene and maltene from the oil sand samples were followed (8). Elemental analyses for C, H, N, O and S were performed in the Microanalytical Laboratory of the Chemistry Department.

Between 5 and 10 g bitumen, asphaltene or maltene was introduced into a 250 cm³ Pyrex vessel. The vessel was joined to a Hoke valve fitted with a standard taper joint on the other end through which it was attached to another Hoke valve fixed to the vacuum apparatus. The volume enclosed between the two Hoke valves was used as a sampler. All samples were evacuated uniformly at ambient temperature before introduction of 250 torr oxygen. The oxygen concentration was determined by transferring it from the sampler into the gas burette and injecting it into the *gc*. The silicone oil bath was used to heat samples at 137°C. For higher temperatures, an electric furnace equipped with a 2-mode API Instrument Co. temperature controller and a Hewlett-Packard 3420 A d.c. differential voltmeter was employed. The consumption of oxygen was followed by expanding oxygen from the vessel into the sampler at desired time intervals and measuring the concentration as described above.

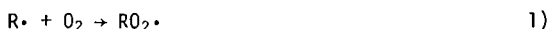
RESULTS AND DISCUSSION

The presence of oxygen has an enhancing effect on the rate of the low temperature thermolysis of the Athabasca oil sand, bitumen, asphaltene and maltene. The product yields obtained from heating oil sands at 130°C for 24 hours in the absence and presence of oxygen are presented in Table I. The products include C₁-C₇ hydrocarbons including *neopentane*, CH₃CHO, CO, CO₂, COS and H₂S. In the presence of oxygen, CH₃COCH₃ and SO₂ are produced in addition to these compounds. Unfortunately, the acetone peak masked the C₅ hydrocarbon peaks and consequently the latter could not be determined accurately. It is evident that in the presence of oxygen, the rates of production of hydrocarbons are increased by factors ranging from 2 to 70, those of the apparent oxidation products by up to 500, and H₂S is probably converted to SO₂.

The thermolysis products obtained from heating bitumen at 137°, 172° and 207°C are given in Table II. The product distribution is similar to that from the whole oil sand (Table I), but the ratios of the product yields in the presence and absence of oxygen at 207° are higher than those at 137°C. The rates of production of hydrocarbons at 207°C in the presence of oxygen are increased by factors up to 100 and those of the apparent oxidation products, by up to 170. Oxidation of asphaltene and maltene at 172°C produced similar results.

Although many details of the complex reaction network involved in the oxidation of hydrocarbons by molecular oxygen have not yet been elucidated, it is commonly accepted that a chain mechanism is operative and that one of the first products formed is a hydroperoxide which may be oxidized further or decompose thermally, thereby initiating new chains (9,10). At 100° and 130°C Kovalev and Denisov (11) reported that peroxides, alcohols and carbonyl compounds are intermediate products whose time profile concentrations pass through a maximum (11). It is also known that these intermediates are responsible for the enhanced yields of hydrocarbons and oxygenated compounds in the thermolysis of hydrocarbons in the presence of oxygen (9-11). The enthalpy changes of the oxidation and combustion reactions leading to the observed end products range between 80 and 105 kcal per mol of oxygen (7).

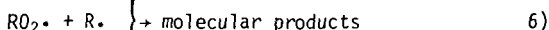
The efficiency of oxygen in the low temperature thermolysis of the oil sand, bitumen, asphaltene and maltene could also be explained by such a general mechanism, where the initial reaction between the organic free radicals formed by thermolysis and molecular oxygen to form a hydroperoxy radical



is followed by the chain propagating steps



Typical chain terminating steps could be



The combustion type reactions in our system will produce additional amounts of hydrocarbons, carbon monoxide, carbon dioxide and water.

A simple mechanism for the oxidation of hydrogen sulfide to sulfur dioxide could be expressed as follows:



The overall heat of oxidation is exothermic by about 124 kcal per mol.

The rates of consumption of oxygen by the oil sand were studied at various temperatures between 24° and 130°C. The data obtained are plotted in Figure 1. The semi-logarithmic plots of the concentration of oxygen in the gas phase as a function of time at each temperature follow first order reaction kinetics. The half-lives, i.e., time required for one-half of oxygen to be used up, vary between 111 days at 24° and 0.6 hours at 130°C. The rate constants, k, were estimated from the slopes of these plots and Equation 10 was used for the Arrhenius plot of $\ln k$ versus $1/T$:

$$\ln k = \ln A - E_a/RT \quad (10)$$

where k is the rate constant, A the preexponential factor, E_a the activation energy, R the gas constant and T is the temperature in °K.

The Arrhenius parameters estimated from the plot are temperature dependent (Table III). Around room temperature, the rate of depletion of oxygen features a lower activation energy and preexponential factor than at the higher temperatures. The temperature dependence of the rate parameters is indicative of changes in the reaction mechanism and suggests a largely surface-catalyzed, i.e., heterogeneous reaction network at the lower temperature, changing over to non-catalytic gas phase reactions at the higher temperatures. It is to be noted that an increase in temperature from 24° to 130°C brings about a 4000-fold rate increase in oxygen uptake. The last column of Table III lists the time required to deplete 99 percent of oxygen added at each temperature and is equivalent to 7 half-lives.

Bousaid and Ramey determined the rates of oxygen disappearance in the 13.9° API Athabasca crude at 23°, 38° and 52°C and found them to follow first order reaction kinetics (5). In this temperature range, they estimated an activation energy of 12.7 kcal per mol which is in agreement with our value of 13 kcal per mol. However, the rate constants and preexponential factor estimated from their data are larger than ours by about two orders of magnitude. We have also estimated the activation energies for the oxidation of hexadecane by molecular oxygen in the temperature ranges 100°-120° and 120°-150°C from the rate data of Kovalev and Denisov to be 17 kcal and 40 kcal per mol, respectively (11). These results show trends similar to ours.

The rates of disappearance of oxygen in bitumen at 137°, 172° and 207°C and in asphaltene and maltene at 137° and 172°C obey first order kinetics (Figure 2). The rate constants estimated from these plots are listed in Table IV. It is apparent that the trend in reactivity is oil sand, asphaltene, bitumen and maltene in decreasing order. It should be pointed out that the rate of oxygen uptake is a measure of the oxidizability of the fractions, which in turn is a function of the chemical composition of the sample.

In the oil sand experiment at 130°C, the 6 mmol oxygen added was completely consumed: 9.3% appeared in the volatile oxygen-containing products and 45% in the bitumen as determined by the elemental analysis (Table V). The rest was presumably converted to water and other oxygenated compounds which were lost during the bitumen extraction. Table V shows that the bitumen contents of non-oxygenated and oxygenated oil sand samples are the same, 13.3%. However, the maltene and asphaltene contents of the former were 83.2 and 16.8 while those of the latter were 76.1 and 23.9%, respectively. It should be noted that in these experiments the oxygen was completely consumed and that the alteration effect of oxygen would have been much larger if the oxygen concentration had been maintained throughout the course of the experiment.

The substantial increase in the asphaltene content of the oxygenated sample, at the expense of maltene, demonstrates that exposure of the oil sand to air has an adverse effect on the quality of the bitumen. The increase in asphaltene content would likely lead to an increase in the yield of coke formation and a lowering in the yield of synthetic crude in the upgrading process. The possibility of aerobic oxidation should therefore be taken into consideration in the storage of the mined oil sands, especially during the summer months when sand temperatures could significantly exceed ambient air temperature. It could also be a factor in affecting bitumen quality during storage of liquid bitumen and in the initial stages of the *in situ* recovery processes of the bitumen.

ACKNOWLEDGEMENTS

The authors thank the Alberta Oil Sands Technology and Research Authority and the Department of Energy, Mines and Resources for financial support, and Dr. P. Neudorfl for helpful suggestions.

REFERENCES

1. Strausz, O.P., Jha, K.N., and Montgomery, D.S., *Fuel*, (1977) 56, 114.
2. Jha, K.N., Montgomery, D.S., and Strausz, O.P., In: "Oil Sand and Oil Shale Chemistry, Eds. O.P. Strausz and E.M. Lown, Verlag Chemie International, New York, 1978, in press.
3. Moschopedis, S.E., and Speight, J.G., *Fuel*, (1975) 54, 210 and references therein.
4. Reed, R.L., and Reed, D.W., *Petro. Trans., AIME*, (1960) 219, 99.
5. Bousaid, I.S., and Ramey, Jr., H.J., *Soc. Petrol. Engg. Jour.*, (1968) 137.
6. Tadema, H.J. and Weijdema, J., *Oil and Gas Jour.*, (1970) 77.
7. Burger, J.G., and Sahuquet, B.C., *Soc. Petrol. Engg. Jour.*, (1972) 410.
8. Selucky, M.L., Chu, Y., Ruo, T., and Strausz, O.P., *Fuel*, (1977) 56, 359.
9. Sieg, L., "Low Temperature Oxidation", ed. Jost, W., Gordon and Breach Science Publishers, New York (1965) 191.
10. Allara, D.L., Mill, T., Hendry, D.G., and Mayo, F.R., "Oxidation of Organic Compounds, Vol. II", *Adv. Chem. Series*, 76, (1968) 40.
11. Kovalev, G.I., and Denisov, Y.T., *Neftekhimiya* (1976) 16, 457.

Table I. Composition of Gases from the Oxidation of the Athabasca Oil Sand at 130°C^a

Product	10 ⁻⁸ mol hr ⁻¹ kg ⁻¹ oil sand				
	Nil		6 mmol		O ₂
	Nil	6 mmol	Nil	6 mmol	
Methane	4.97	81.8	C ₅	34.8	37.0
Ethylene	0.82	57.0	C ₆	2.74	148.0
Ethane	1.14	21.6	C ₇	3.68	11.5
Propylene	1.95	67.9	CH ₃ CHO	5.50	1,640
Propane	0.73	20.1	(CH ₃) ₂ CO	n.o. ^c	459
<i>i</i> -Butane	0.20	1.74	CO	11.1	5,920
<i>i</i> -Butene	0.72	25.7	CO ₂	2,830	56,400
Butane	14.5	29.5	COS	0.41	42.2
Butenes	0.35	7.70 ^b	H ₂ S	35.7	n.o.
<i>Neo</i> -pentane	20.0	n.d. ^b	SO ₂	n.o.	23.4

^aThe oxygen pressure was 150 torr and the sample was heated for 24 hours.

^bNot determined, due to the large interfering peak of acetone.

^cNot observed.

Table II. Composition of Gases from the Oxidation of the Athabasca Bitumen as a Function of Temperature^a

Product	10 ⁻⁸ mol hr ⁻¹ per 100 g bitumen				
	137°C		172°C	207°C	
	Nil	3.3 mmol	3.6 mmol O ₂	Nil	3.9 mmol
		O ₂		O ₂	
Methane	2.6	11.0	36.4	114	1,000
Ethylene	1.2	3.4	52.1	21	171
Ethane	n.o. ^b	2.5	68.5	14	234
Propylene	1.8	6.4	59.0	2.0	209
Propane	n.o.	4.5	49.0	17	202
<i>i</i> -Butane	0.6	3.4	41.8	13	41.0
<i>i</i> -Butene	n.o.	2.1	23.4	n.o.	36.0
<i>n</i> -Butane + Butenes	3.5	4.5	476	20	440
Acetaldehyde	2.4	108	494	18	2,920
Acetone	n.o.	2,760	2,830	n.o.	51,100
Carbon monoxide	44.0	392	421	213	12,400
Carbon dioxide	330	1,320	11,700	2,880	33,800
Carbonyl sulfide	1.0	7.7	129	39.0	556
Sulfur dioxide	n.o.	1.8	314	n.o.	28
Hydrogen sulfide	n.o.	n.o.	n.o.	1,270	270

^aThe samples had 250 torr pressure of oxygen.

^bNot observed.

Table III. Arrhenius Parameters for the Uptake of Oxygen by Athabasca Oil Sand

Temp. °C	k hr ⁻¹ kg ⁻¹ oil sand	E_a kcal/mol	A hr ⁻¹ kg ⁻¹ oil sand	Time required to deplete 99% of O ₂ added
24	2.6×10^{-4}	13	1×10^6	2.0 years
60	2.6×10^{-3}			0.2 year
85	1.1×10^{-2}			17 days
105	9.8×10^{-2}	29	6×10^{15}	47 hours
130	1.1			4.1 hours

Table IV. Rate Constants for Oxygen Depletion

t°C	Oil Sand	Asphaltene	Bitumen	Maltene
	hr ⁻¹ kg ⁻¹ oil sand	hr ⁻¹ per 100 g		
130	1.1	-	-	-
137	-	0.22	0.076	0.055
172	-	0.22	0.20	0.102
207	-	-	0.36	-

Table V. Elemental Composition of Athabasca Oil Sand^a

Fraction	[O ₂] ^b	C	H	N	O	S
		%				
Bitumen						
13.3%	none	82.58	10.26	0.39	1.36	5.22
13.3%	6 mmol	82.21	10.09	0.40	1.99	4.95
Asphaltene						
16.8%	none	79.35	8.14	1.06	1.58	7.39
23.9%	6 mmol	76.68	7.95	0.97	3.30	7.97
Maltene						
83.2%	none	83.74	10.90	0.20	1.03	3.78
76.1%	6 mmol	83.05	11.09	0.09	0.99	3.87

^a130 g of the Athabasca oil sand was heated at 130°C for 24 hours.

^bAn oxygen pressure of 150 torr was used.

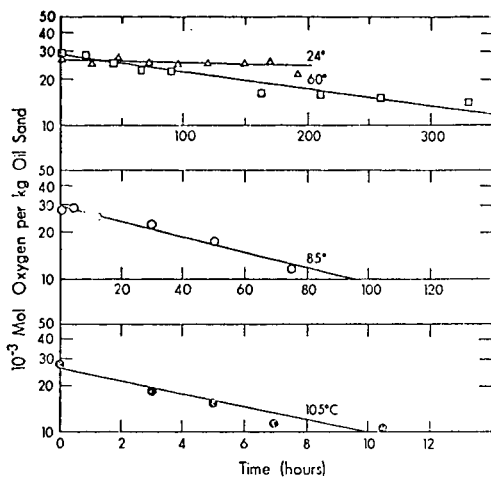


Figure 1. Depletion of oxygen concentration as a function of time in the Athabasca oil sand: Δ , 24°C; \square , 60°C; \circ , 85°C; \bullet , 105°C.

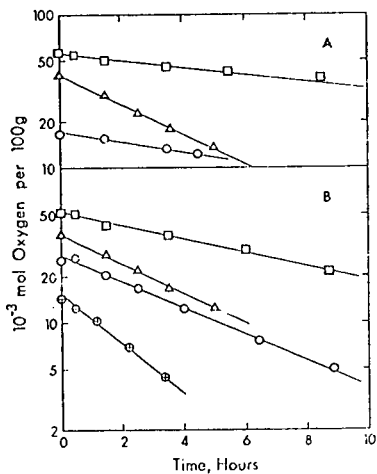


Figure 2. Depletion of oxygen concentration as a function of time in the Athabasca bitumen (\circ), asphaltene (Δ) and maltene (\square): A, 137°C; B, 172°C and \emptyset , bitumen at 207°C, abscissa reduced to half.

INFLUENCE OF CHEMICAL FACTORS ON
PRIMARY PROCESSING OF UTAH TAR SAND BITUMEN

James W. Bunger, Donald E. Cogswell and Alex G. Oblad
Department of Mining and Fuels Engineering
University of Utah
Salt Lake City, Utah 84112

INTRODUCTION

Research of recovery and processing technology applicable to Utah tar sands is currently in progress. Development of this hydrocarbon resource has not yet occurred, principally because of high costs associated with present recovery methods. The processing of bitumens is also expected to be relatively more expensive than conventional petroleum processing because of the heavy nature and high heteroatom content of the bitumen. In processing of bitumen the primary conversion appears to be the most important step because of the possible high cost of hydrogen processing or loss in yields attendant with reducing the high molecular weight bitumen to synthetic crude. Methods and conditions of primary processing have a major effect on the composition of the products subsequently used as feedstocks for secondary processing. Secondary processing for production of fuels and other hydrocarbon products will probably utilize adaptation of processes developed for conventional petroleum.

The primary process most commonly used for upgrading of heavy oils, petroleum residuum or bitumen is some form of coking such as delayed or fluid coking. For these processes the range of operating variables which can be employed is rather limited and the product distribution and quality (composition) generated is primarily a function of the feedstock composition. Because the coking process is relatively inexpensive, industrial processes are often content with optimizing coking yields and then subsequently optimizing some secondary process more specifically aimed at altering the composition to produce a desired product. Such an approach is presently used with the Athabasca deposit where 15 to 20 weight percent of the feed is converted to a high sulfur coke and the liquid products are subjected to an expensive hydrotreating to obtain a synthetic crude oil amenable to conventional refining.

Recent work on the structure of Utah and Athabasca bitumens (1,2) has shown that Uinta Basin (Utah) bitumens possess a significantly different hydrocarbon and non-hydrocarbon structure than Athabasca bitumen. The higher molecular weight, higher viscosity, and lower volatility points toward a heavier material for the Uinta Basin bitumen, but the higher hydrogen content and API gravity, and the lower asphaltene content and carbon residue points toward a less aromatic bitumen. Interpretation of the structural analysis indicates that the Uinta Basin bitumen is comprised of relatively high molecular weight naphthenic hydrocarbons. The Athabasca bitumen is of lower molecular weight, but higher in aromatics. A comparison of compound type analysis suggests that Athabasca bitumen contains roughly twice the amount of aromatic carbon that Uinta Basin bitumen contains.

The differences apparent in the two groups of bitumens suggested that direct adaptation of process conditions used with Athabasca bitumen may not be the most desirable route for development of processes for Utah bitumens. Therefore, several alternatives for the primary conversion of bitumen have been examined, in addition to coking. Examination of alternate processing steps served two useful purposes. First, results of such a study helped identify processes particularly amenable to this unusual feedstock. Second, by paying particular attention to the structure of the feedstock and products more will be learned about conversion mechanisms and pathways influencing residual material processing.

In this paper results from coking, catalytic cracking, and hydrolysis of virgin Asphalt Ridge bitumen are compared. This study includes the effect of variables on yields and product composition. Product distribution and composition are compared

as a function of process variables and the conversion process employed. Detailed structural analysis is used in the evaluation of the respective processes. Implications of the product structure to thermal and catalytic conversion pathways are discussed.

EXPERIMENTAL

Analytical Methods

Physical properties and elemental analysis were obtained by conventional analytical techniques. All average molecular weights reported are those obtained by VPO in benzene. Average molecular weights determined in this fashion are expected to give values somewhat higher than the true average molecular weight because of solute-solute molecular associations (3). Liquid and gas densities were obtained by an electronic densitometer accurate to better than three significant figures.

Separation of products into compound type classes was accomplished by the dual silica-alumina column chromatographic technique (4) without prior separation of acids, bases, and neutral nitrogen compounds. Simulated distillation was accomplished by previously published procedures (1) utilizing as an internal standard a series of alkyl benzenes.

Coking

Batch coking experiments were conducted in a stainless steel reactor fitted with a Vycor glass liner. The reaction was brought to temperature by a preheated fluidized sand batch heater. Charge to the reactor was approximately 10 g. (See also references 5, 6). Pressure, when applied, was with helium, without sweep.

Catalytic Cracking

Two reactor configurations were used in order to assess various factors influencing catalytic cracking. (See also reference 8). One configuration was a semi-batch downflow reactor patterned after the CAT-A (7) test in which bitumen and catalyst are preheated before mixing. The other configuration was a batch type reactor in which feed and catalyst were intimately mixed prior to heating. This configuration minimized the diffusion limitations but required volatilization of products in a static atmosphere.

Hydropyrolysis

Reactor design for hydropyrolysis has been published by Ramakrishnan *et. al.* (9). The reactor tube was coiled 3/16 x 236 inch stainless steel tube which was held isothermally within $\pm 10^{\circ}\text{C}$ of the desired temperature. The interior surface was pre-sulfided to minimize catalytic effects.

RESULTS AND DISCUSSION

The approach taken in this work was to subject virgin bitumen to various processing steps and to then evaluate the results in terms of product yield and composition. Because the cost of recovery is expected to be high, it is critical that the processing steps maximize both yield and product quality. The ever increasing cost of hydrogen processing places an additional constraint on economics so optimum utilization of hydrogen is also a prime consideration.

The major primary processes which have been preliminarily examined are coking, catalytic cracking, hydropyrolysis, visbreaking and deasphalting. Catalytic hydrocracking and hydrotreating of virgin bitumen have not been examined in enough detail to make comment at this point. Visbreaking or deasphalting may play a role as pretreatment to the primary conversion process.

Characteristics of Asphalt Ridge bitumen are given in Table 1 and have been previously discussed in the literature (2,3,5,6).

Coking

Results of the coking (destructive distillation) of various deposits have been previously reported (5). These results showed that heteroatom content of the liquids followed the trends exhibited in the virgin bitumen. Total yields of liquids and gases were a function of hydrogen content; conversely the higher the aromatic content, the greater the coke yield. A secondary correlation was observed between increasing molecular weight and decreasing liquid and gas yield for a given hydrogen content.

Table 1

	C	H	N	S	O
Elemental Analysis	86.2	11.3	1.1	0.4	0.9
Average molecular weight (VPO-benzene)			713		
Viscosity (Poise @ 77°F, cone-plate, .05 sec ⁻¹)			69,300		
API gravity			12.5		
Heating value (Btu/lb)			19,305		
Asphaltenes (n-pentane)			11.8		
Carbon residue (Rammbottom)			9.1		
% distillable below 535°C			40		

The effect of temperature on process yields is given in Figure 1. The data represent ultimate yields from a series of isothermal runs. Note that near asymptotic values are reached by a temperature of 460°C. Elemental analysis and physical properties of liquids obtained at selected temperatures are given in Table 2.

Table 2

Characteristics of Pyrolysis Condensates
from Isothermal Cracking of Asphalt Ridge Bitumen (6)

Property	Temperature of Pyrolysis		
	380°C	415°C	460°C
Carbon	86.7	86.7	86.7
Hydrogen	12.1	12.3	12.2
Nitrogen	0.25	0.39	0.48
Sulfur	0.33	0.29	0.29
Oxygen	0.50	0.30	0.31
C/H Ratio	0.603	0.591	0.599
Density (20°C) g/cc	0.897	0.893	0.892
API gravity	25.9	26.7	26.9
Refractive index	1.4970	1.5010	1.4998
Molecular weight	261	296	321

The results shown in Table 2 reveal remarkably little difference in the average properties considering that the total condensate yields varied from 11% to 82% of the bitumen between 380°C and 460°C. Some difference is noted in the average molecular weight due to higher temperature of distillation of cracked products. Simulated distillation reveals that about 12% of the virgin bitumen would exhibit a TBP below 380°C; thus, a significant percentage of the 380°C products might be expected to be virgin material. For the 460°C condensate, no more than 27% of the condensate can be attributable to virgin compounds and to the extent that virgin material of this boiling range undergoes cracking the percentage contribution of virgin distillate would be reduced.

Although the properties of the condensates varied little over the temperature range examined, visual inspection of the residue/coke revealed that drastic chemical changes

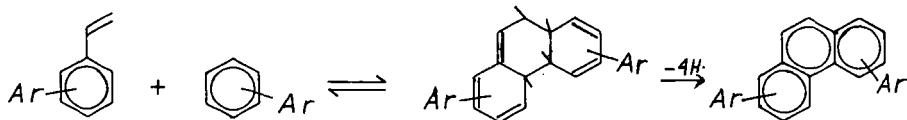
were being affected over the temperature range studied. At lower temperatures the residue was a viscous, soluble fluid, while at higher temperatures the residual material resembled a glassy char or coke. In an attempt to determine the temperature effect on the formation of this coke, presumably condensed aromatic species, the solubility of the residue in pyridine was measured. For this test to be meaningful, it was reasoned that dealkylation, dehydrogenation, or cyclization reactions would not likely result in the production of pyridine insoluble material, but that condensation or polymerization reactions producing higher ring aromatics would. The mechanisms leading to production of higher condensed aromatics are not well understood and will be referred to in this discussion simply as condensation reactions.

Results of pyridine solubility of residues are shown by the dotted line in Figure 3 and reveal that a dramatic change in pyridine solubility occurs between 425° and 435°C. Also plotted in Figure 3 is the percent yield of residue. This curve exhibits an inflection point some 22°C lower than the inflection point in the pyridine solubility curve. Scales on the vertical axis have been arbitrarily adjusted to allow some visual comparison of the various parameters measured. The data shows that volatiles formation and char formation are not simultaneous events and that the major reactions leading to volatiles and char formation occur at substantially different temperatures. Aromatics condensation apparently does not occur appreciably below 422°C even though over 70% of the bitumen has been produced as cracked products at this temperature. (See Table 8 for maximum possible contribution of virgin distillate).

In order to help confirm that pyridine solubility of the residue was a significant index for measuring aromatics condensation, a second parameter, H/C ratio, was measured. The results of this examination are also plotted in Figure 3 and reveal an inflection point quite near to the inflection point for pyridine solubility. This data showed that a linear correlation between H/C ratio and depth of cracking did not exist but that the reactions giving rise to the reduction in H/C ratio may possibly be the same as those resulting in pyridine insolubility. A correlation of pyridine solubility with H/C ratio reveals a linear relationship between 380° and 423°C, another linear relationship of different slope, between 433° and 460°C, with a non-linear transition region between 423° and 433°C. This correlation is shown in Figure 4 along with the corresponding temperature of cracking. The entire transition region actually occurs over a narrow temperature range of about 10°C.

Based on this information one can speculate about the general mechanism giving rise to the results. From 380° to 423°C primary cracking is limited to rupture of relatively weak σ bonds. The free radicals thus formed can participate in transfer or propagation reactions with aliphatic or naphthenic hydrocarbon systems. The decrease in pyridine solubility of the residue, which is accompanied by a dramatic decrease in H/C ratio, may be attributable to dehydrogenation of naphthenic ring systems, dealkylation reactions and volatilization of saturated hydrocarbons. Naphthenic ring systems may or may not be associated with aromatics but the inductive effects of aromatic rings, as exemplified by the compound tetralin, are known to promote hydrogen transfer.

Above 423°C additional reactions are introduced. These reaction mechanisms are not identified but they are characterized by several features observed in the results presented above. If fractional reduction in H/C ratio is used as a measure of the progress of reaction, an activation energy of about 70 Kcal/mole is calculated for the reaction occurring between 423° and 433°C. The calculations assumed zero order dependence on reactant concentration as assumptions of higher order produced an unreasonably high activation energy. The calculated activation energy is consistent with several possible polymerization and/or condensation reaction mechanisms. One possibility is that aromatic or benzyl hydrogens are abstracted in a free radical propagation step. The resulting phenyl or benzyl free radicals subsequently attack other aromatic rings to form biphenyl or diphenyl methane type linkages. The resulting molecules subsequently undergo further addition or ring closure depending on the alkyl substituents which might be present. An alternative reaction mechanism which might be considered is that of Diels-Alder type condensation of α -olefin aromatics acting as the diene and aromatics as the dienophile:



The reaction involves a partially hydrogenated intermediate which donates hydrogen in the process of volatiles formation.

In the region between 433° and 460°C the reduction in hydrogen content is attributable to several factors. One factor is the loss of aromatic C-H resulting from condensation of aromatics as discussed. Another factor is the significant increase in primary decomposition reactions such as dealkylation of aromatics. Analysis of products produced between 430° and 460°C show a definite trend toward increased paraffinic carbon compared to lower temperature products which were more naphthenic. Whereas transfer and free radical propagation reactions can occur at moderate temperatures, primary decomposition requires higher temperatures. Whichever the dominant mechanism, Figure 4 shows that the loss of hydrogen at higher temperatures has a much greater influence on decreasing the solubility of the residue than occurred at the low temperature end where considerable loss of hydrogen content had little effect on pyridine solubility.

There are several important implications of the proposed gross mechanism to thermal processing of bitumen. First, production of refractory molecules can be inhibited by maintaining temperatures below 425°C. The residue obtained at these conditions should remain amenable to further processing. Second, inhibition of condensed aromatics formation above 425°C can be accomplished only by shortening the residence time (reducing the relative importance of second order reactions) or by dilution of the aromatics such as with hydrogen or hydrogen rich molecules. This interpretation appears to be consistent with the vast body of processing literature which has empirically determined that processes operating below 425°C are significantly different from those operating above this temperature where residence time becomes highly important.

Industrial coking processes typically operate at pressures higher than atmospheric. Correspondingly, the effect of pressure (P) on yields and yield structure was determined, holding the temperature constant at 460°C. Results are given in Figure 2. The results show that the amount of coke formed increases steadily with increasing pressure. These results and those acquired for visbreaking of bitumen at elevated pressures suggest that pressure exerts an influence on chemical reactions over and above the effects pressure has on volatility and diffusion of products.

The products from this set of experiments were evaluated in terms of elemental analysis and physical properties. Results are shown in Table 3. Elemental analysis are not shown because variations from the atmospheric pressure results (Table 2) were minor. The API gravity results show interesting curvature at about 80-100 psig. The yield data in Figure 2 suggested that the liquids curve may not be a smoothly decreasing function of pressure, as drawn. Should these deviations in API gravity and yields as a function of pressure prove to be real, it may have interesting implications regarding the effect of pressure on thermal cracking mechanisms.

Catalytic Cracking

Analysis of Uinta Basin bitumen revealed a material that was high in naphthenic character (2). The results are exemplified by the group type analysis of P. R. Spring saturated hydrocarbons where over 60% of the saturates are comprised of substituted decalins and perhydroanthracenes and perhydrophenanthrenes (1). Only 7% of the saturates which represented 27% of the bitumen contained no alicyclic rings. The

highly naphthenic character of aromatic containing molecules is thought to persist in the remaining 73% of the bitumen.

Table 3
Properties of Condensates Derived at Elevated Pressures

Property	Pressure (psig)				
	0	40	80	120	250
API gravity	26.9	33.4	34.1	37.1	39.2
n_{D}^{20}	1.4998	1.4891	1.4914	1.4830	1.4801
Avg. molecular weight	321		263		265

Naphthenic gas oils are highly responsive to catalytic cracking and give high yields of branched alkanes. Based on this rationale, direct catalytic cracking was attempted. The presence of significant quantities of basic nitrogen, metals, or particulates would be expected to have an appreciable impact on a commercial operation and utilization of catalytic cracking may require some form of feed pretreatment. However, at the present stage of research it is important to assess the chemical responsiveness to catalytic cracking. Preliminary results of this study and a description of catalysts have been previously reported (8).

Gravimetric results for cat cracking under selected conditions are given in Table 4. Results of Bt(1) reveal that significant catalytic activity was present at 412°C; purely thermal cracking (Figure 1) produced only 47% liquids plus gases at this temperature. Results of Bt(2) show that significant cracking occurred with the powdered molecular sieve catalyst. Further, the catalyst exhibited a strong selectivity toward production of liquids rather than gases and the slightly higher API gravity reflects the increased amount of hydrogen retained in the liquids. These trends are expected from molecular sieve catalysts when zeolite catalyzed cracking is operative.

Table 4
Catalytic Cracking Results

Feed (Run)	Catalyst	Mode	Cat/Oil	T°C	Gas	Liquid	Residue (Coke)	API (Liquid)
Bt(1)	S/A	SB	1.3	412	6	67	26	27.9
Bt(2)	M.S.(f)	SB	1.8	412	1	79	20	29.5
Bt(3)	S/A	SB	1.3	470	11	76	13	25.1
Bt(4)	S/A	B	2.0	460	10	74	16	30.8
M(5)	S/A	B	2.0	460	10	78	12	32.0
Bt(6)	M.S.	B	3.0	460	7	80	13	27.1
VB(7)	M.S.	B	3.0	460	4	83	13	28.8

Symbol Designation: Bt (virgin bitumen); M (pentane soluble maltenes from virgin bitumen); VB (visbroken bitumen, 425°C, 150 psig, ~11 min.); S/A (Houdry 159CP silica-alumina catalyst); M.S. (Mobil Durabead-8 molecular sieve catalyst); SB (semi-batch Cat A mode); B (batch mode); f (powdered catalyst).

When temperatures were raised to 460-470°C additional yields were experienced. Results of Bt(3) and Bt(4) show good agreement between the two reactor configurations. The batch operation, requiring volatilization of products, exhibited a tendency to retain heavier materials with the coke. The results of runs Bt(3) and Bt(4) are quite encouraging because they exhibit yield and product quality equal to or better than experienced with thermal cracking.

An attempt was made to remove coke precursors by prior deasphalting. Results of cat cracking of the maltenes, which represented 90% of the virgin bitumen, are given in Run M(5). Removal of 10% asphaltenes resulted in a coke reduction of only 4%. In retrospect, this is not too surprising because the asphaltenes from Uinta Basin bitumen, although consisting of the highest molecular weight species present, also contain significant quantities of hydrogen (H/C = 1.2) and contribute to the volatiles product yield. Conversely, not all of the coke precursor aromatics are precipitated due to the effects that the naphthenic and alkyl substituents have on increasing the solubility of the aromatics. Thus, a one-to-one correlation between molecules comprising the asphaltene fraction and coke precursors does not exist.

Results of run Bt(6) suggested that substantial thermal reactions were taking place. Property data of liquids and gas analysis have strong resemblance to the thermally derived products. The thermal vs. catalytic effects are illustrated in the gas analysis for selected runs in Table 5. Compared to the thermal gases the cat cracking gases, Bt(4), exhibited a strong selectivity for production of C₃ and C₄ and gave very high yields of isobutane. Results for the run Bt(6) show some characteristics of cat cracked products but also show many similarities to the thermal products. The results of Bt(6) are presented to illustrate the difficulty which may be encountered through competitive reactions and is not intended to represent optimum results for this catalyst.

Table 5
C₁ to C₄ Gas Analysis

	<u>Thermal</u> <u>(460°C)</u>	<u>Mol-Sieve</u> <u>Run Bt(6)</u>	<u>Sl/Al</u> <u>Run Bt(4)</u>	<u>Hydropyrolysis</u> <u>(525°C)</u>
Methane	41.0	32.3	18.9	27.5
Ethane	16.5	16.1	10.3	18.3
Ethylene	15.1	5.0	4.2	5.5
Propane	10.0	15.4	12.2	23.4
Propylene	11.6	10.2	15.4	2.8
n-butane	1.3	5.4	3.3	10.6
i-butane	1.4	4.0	18.0	7.3
Butylenes	3.1	11.6	17.7	4.6

When the average molecular weight of the feed was reduced from about 700 to about 500 by visbreaking, significantly greater catalytic activity was observed (Run-VB(7)). These results are consistent with the general observation that catalytic activity was strongly enhanced if some reduction of molecular size preceded the contact with the catalyst.

The results of catalytic cracking have shown that the bitumen is highly responsive to catalytic cracking if the molecular size can be reduced to minimize diffusional limitations. It thus appears that a good catalytic cracking feedstock should be derivable from the Uinta Basin bitumen. It is quite possible, that by a more systematic and thorough search for optimum catalysts, process configurations, and process conditions considerable improvements on the results given in Table 4 can be realized.

Hydropyrolysis

The Asphalt Ridge bitumen was subjected to hydropyrolysis in a tubular flow reactor. Yields and process conditions are given in Table 6. Results show that the virgin bitumen can be converted to liquids and gases with little or no coke formation.

Virtually no change in pressure drop across the reactor was observed over the course of the 15 to 20 minute runs. These yield results suggest that molecular hydrogen has successfully inhibited the condensation reactions discussed in the section on coking.

Table 6
Hydropyrolysis Yields and Process Conditions

Reaction Conditions			Yields		
Temp. °C	Pressure psig	Residence Time (Seconds)	Weight Percent		
			Gas	Liquids	Coke
500	1500	18	17	83	0
525	1500	18	27	73	0

Elemental analysis and physical property data for the liquids are given in Table 7. Results show that little change was affected in the elemental composition and hydrogen to carbon ratio. However, physical property data reveals a dramatic increase in API gravity and a large reduction in molecular weight. The percentage hydrogen added was calculated from a material balance on hydrogen and included the amount added to the gases. The amount of hydrogen added to the system appears to be closely related to the amount of gas produced. On the average, the liquid products are slightly more condensed than the starting bitumen. The gases formed derive largely from the paraffins and alkyl substituents present. Pentane asphaltenes amounted to 3.5% of the liquids, were quite hydrogen deficient ($H/C = 0.97$), and contained a 5% nitrogen concentration.

Table 7
Hydropyrolysis Product Characteristics

	Feed	Temperature of Run	
		500°C	525°C
Carbon	86.2	86.7	86.8
Hydrogen	11.3	11.6	11.4
Nitrogen	1.1	0.8	0.8
Sulfur	0.4	0.3	0.3
Oxygen	0.9	0.3	0.3
C/H ratio	.640	.627	.639
API gravity	12.7	22.1	25.2
Average molecular weight	713	336	321
Refractive index		1.52	1.52
Wt. % H ₂ added to total products		0.8	1.2
SCF H ₂ /bbl feed		600	900

The preliminary results of the hydropyrolysis are particularly interesting because hydropyrolysis promises to be a simple process which can produce a drastic reduction in molecular weight without a high consumption of hydrogen.

Simulated Distillation

Simulated distillation results are given in Table 8 for virgin bitumen and the various liquid products. These results show significant changes in volatility were affected, even in the case of mild visbreaking. The lightest products were those from thermal cracking at 80 psig and catalytic cracking. In both cases, yields were about 74% of the charge material; however, the cat cracking run produced 4% more gases.

The catalytic cracking produced 23% gasoline. This gasoline was found to exhibit a calculated 50% point at 128°C and a calculated research octane of 78. Analytical results showed that the octane number was reduced by the presence of some low octane thermal products in the heavy gasoline range.

Table 8
Simulated Distillation
Cumulative Weight Percent

Corresponding, BMCOA Fraction(1)		Cumulative Weight Percent					
No.	Cut Pt. °C	Bt	TC(0)	TC(80)	CC	HP	VB
1	50			1.2	0.9	1.0	
2	76			2.7	2.4	2.2	
3	100		1.2	5.0	8.3	4.5	0.5
4	125		2.3	7.7	11.2	7.3	1.1
5	150		4.2	11.9	14.9	10.6	1.7
6	175		6.3	16.5	18.9	13.5	2.7
7	200	0.1	8.7	21.6	22.8	17.2	4.0
8	225	0.4	11.0	26.5	27.3	20.9	5.5
9	250	1.1	14.7	33.4	32.5	25.6	7.4
10	275	2.4	19.4	40.9	38.2	30.5	10.3
11	305	5.0	25.2	50.3	46.0	37.6	13.9
12	335	7.4	32.5	60.4	54.9	44.5	18.6
13	365	10.4	40.3	69.7	62.9	51.2	24.2
14	395	13.8	49.5	78.6	71.0	58.0	29.7
15	425	17.3	58.8	86.2	78.6	64.5	35.8
16	455	21.7	68.8	91.9	85.2	71.6	41.6
17	485	27.4	80.4	96.2	92.1	77.7	48.0
18	515	32.7	90.6	98.8	96.6	82.1	55.6
19	538	39.8	96.6	100.0	99.1	84.6	62.0
Residue	>538	100	100		100	100	67.1
10% Point °C		362	211	146	115	145	100
50% Point °C		>538	397	303	321	359	247
90% Point °C			511	444	449	>538	463
							>538

Symbol Designation: Bt (virgin bitumen); TC (thermally cracked @ 0 psig and 80 psig, respectively); CC (cat cracked Bt(4), Table 4); HP (hydropyrolysis, 525°C liquids); VB (Visbreaking, 475°C, 80 psig, ~8 min.).

The simulated distillation results for the hydropyrolysis liquids reveal a broad boiling point distribution. Although substantial amounts of light material are produced, certain heavier aromatics remain virtually unchanged. These aromatics are present in the hydropyrolysis liquids but went to form coke in the coking and cat cracking conversion processes. The distillation data presented here suggest that the hydro-pyrolysis liquids, with their relatively low olefin content, would make a good feed-stock for refining.

Separation into Compound Types

Separation of total liquid products into saturated, mono-aromatic, di-aromatic, and poly-polar aromatic compound types gives important information regarding the distribution of structural features. Results of the separation are given in Table 9.

Perhaps the most striking feature of these results is the high percentage of purely saturated hydrocarbons. All samples have high concentrations of higher aromatics as well, indicating a very broad distribution of compound types. The

comparatively low percentage of saturates in the hydropyrolysis liquids can be explained on the basis that nearly twice the gases were formed and 12% heavy material is present that was removed with the coke in the other two processes. Elemental analysis revealed that the vast majority of nitrogen and sulfur compounds were retained with the poly-polar aromatics. The high percentage of monoaromatics in the hydro-pyrolysis liquids seems to indicate that some hydrogenation of higher aromatics has occurred.

Table 9
Compound Type Classification of Products

<u>Fraction</u>	<u>Thermal 460°C, 0 psig</u>	<u>Catalytic Bt(4)</u>	<u>Hydropyrolysis 500°C</u>
Saturates	55.1	62.0	48.5
Monoaromatics	11.7	9.1	15.3
Diaromatics	8.4	5.5	5.6
Poly-polar aromatics	24.8	23.4	30.6
	<u>100</u>	<u>100</u>	<u>100</u>
Percent Recovery	89.6	85.3	94.8

CONCLUSIONS

The unusual chemical nature of Uinta Basin bitumen requires that examination of various primary processes and a search for optimum conversion conditions be made. The principal chemical objective in primary processing is to reduce the molecular weight with a minimum cost in light product yields and a minimum requirement for hydrogen. Coking was shown to produce high yields of liquids and gases with a low sulfur coke as a potentially valuable by-product. Temperature was shown to have a significant effect on total yields in coking but had little effect on volatiles composition. Pressure was shown to have a significant effect both on composition and yields. Catalytic cracking produced high yields of liquids and gaseous products. Further research to find optimum conditions and the most appropriate role for catalytic cracking in bitumen processing is indicated. Hydropyrolysis was shown to convert bitumen in virtually 100% yields to gases and medium volatility liquids with low consumptions of hydrogen. This process shows good potential as a viable primary processing step. Analysis revealed that the structure of products can be significantly affected by various processing sequences studied. Analytical results are highly instructive as to what must be accomplished chemically during the conversion of virgin bitumen. The structure of the products also gives important clues as to the gross mechanisms of conversion. The results of this study provide a basis for further evaluation of the most desirable approach to processing of Uinta Basin bitumen.

ACKNOWLEDGEMENTS

Appreciation is extended to Dr. Robert Beishline and students of Weber State College for the distillation of products to produce the gasoline cuts and for the dual silica-alumina column separations of the catalytically and thermally cracked products.

This work was sponsored by the U.S. Department of Energy and the State of Utah.

REFERENCES

- (1) Bunger, J. W., "Shale Oil, Tar Sands and Related Materials", T. F. Yen, ed., Amer. Chem. Soc., Washington, D.C., 121-136 (1976).
- (2) Bunger, J. W., K. P. Thomas and S. M. Dorrence, "Analysis of Compound Types and Properties of Utah and Athabasca Tar Sand Bitumens", Fuel, submitted for publication.
- (3) Bunger, J. W., Preprints, Division of Petroleum Chemistry, Amer. Chem. Soc. 22, 2, 716-727 (1977).
- (4) D. E. Hirsch, et. al., Anal. Chem. 44, 6, 915 (1972).
- (5) Bunger, J. W., S. Mori and A. G. Oblad, Preprints, Division of Fuel Chemistry, Amer. Chem. Soc. 21, 6, 147 (1976).
- (6) Bunger, J. W., D. E. Cogswell and A. G. Oblad, The Oil Sands of Canada-Venezuela, 1977. D. A. Redford and A. G. Winestock, eds., CIM Special Volume 17, 178-182 (1977).
- (7) Alexander, J. and H. G. Shimp, National Petroleum News 36, p. 537 (1944).
- (8) Bunger, J. W., D. E. Cogswell and A. G. Oblad, Preprints, Div. of Petr. Chem., Amer. Chem. Soc. 22, 3, 1008 (1977).
- (9) R. Ramakrishnan, J. Shabtai and A. G. Oblad, Preprints, Div. of Petr. Chem., Amer. Chem. Soc. 23, 1, 159 (1978).
- (10) Eastwood, S. C., C. J. Plank and P. B. Weisz, Proceedings of the 8th World Petroleum Congress, 245 (June, 1971).
- (11) Rim, J. J., "Chemical Characterization of Molecular Sieve Catalysts", Ph.D. Thesis, Department of Fuels Engineering, University of Utah, 113, (1974).

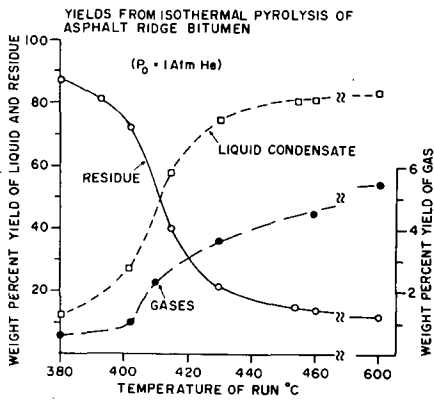


Fig. 1

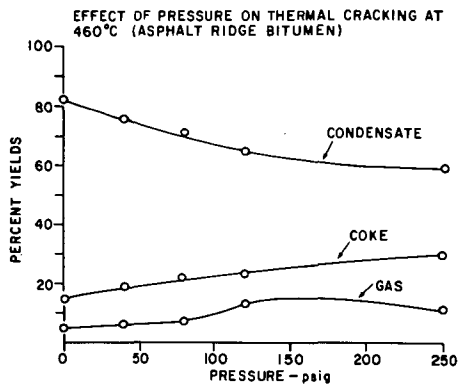


Fig. 2

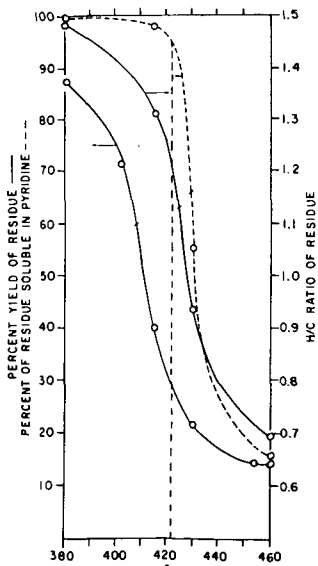


Fig. 3

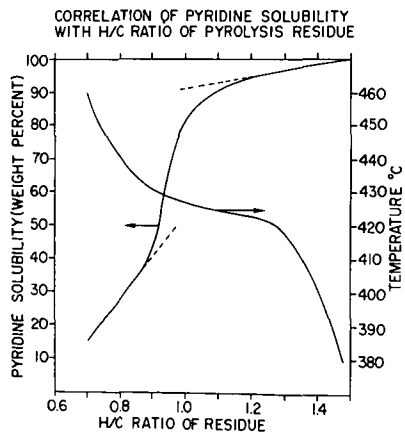


Fig. 4

A REVIEW OF A TECHNICAL AND STATUS OF POTENTIAL ROUTES TO LIQUID FUELS FROM
COAL IN THE U. S., Dr. Joseph A. Klinepeter, Manager, Liquefaction and
Technical Services, Conoco Coal Development Company, Library, PA. 15129

Many concepts for the conversion of coal to liquid products are being studied in the U. S. For direct liquefaction processes, SRC II, H-Coal, and the CSF and Exxon Donor Solvent processes, are in various stages of development, and the $ZnCl_2$ process, which is capable of producing gasoline directly from coal, is under test in a 1/TPD unit. Mobil Oil Company is making significant strides towards improving the Sasol Fischer-Tropsch indirect conversion process. The technology and present status of each of these processes will be reviewed.

OIL SHALE, Dr. Harry McCarthy, Vice President, Science Applications Inc.,
9485 Colfax Avenue, Lakewood, Colorado 80215

Energy supply/demand projections show a serious shortfall in liquid petroleum by 1985. The vast reserves of oil shale represent the best alternate source of liquid petroleum to help fill this shortfall. The economic/technical analysis of the various process options will be given to present the effect on supply of the various technical options. A timetable will be presented to show that to effect the shortfall by the mid-1980's, work must be initiated now.

ANALYSIS OF A DREAM: BIOMASS, Dr. Paul Weisz, Manager of Research, Mobil Research and Development Company, P. O. Box 1025, Princeton, N. J. 08540

An analysis will be presented of the basic parameters, problems, constraints, and challenges of the Biomass concept for fuels or basic chemicals. The "gasohol" concept provides a starting model for study, from which a generalized model is developed to provide insights for the future.

U. S. NATIONAL ENERGY POLICY-EFFECTIVENESS IS A VERY PRESSING ISSUE,
Dr. William C. Peters, Acting Manager, Pittsburgh Energy Research Center,
U. S. Department of Energy, Pittsburgh, PA 15213

The "cornerstone" of the proposed National Energy Plan and probably future Energy Policy is energy Conservation (efficiency). Energy Conservation seems to have no opponents; however, a consensus on just what can, should, and will be done with it is clearly lacking. Part of the problem stems from the way we have traditionally measured how efficiently our energy resources are consumed. Obviously, when high-grade energy is converted to a low-grade energy for societal benefits, something is lost. The usual yardstick "energy efficiency", which arises from the first law of thermodynamics, does not and cannot in the strictest sense reflect this loss, since energy is always conserved.

If engineering, administrative, executive and political decisions have been made under impressions, or for that matter misimpressions, stemming from traditional energy concepts and analysis, then why has the cry of knowledgeable prominent people not been taken up enthusiastically? This question along with an examination of the proper role of sound technical concepts in energy conservation and the insuing National Energy Plan implications will be presented. In addition, the attitude toward "effectiveness" in 1978 will be assessed and second law analysis issue discussed in the hope of stimulating an early resolution.

ENERGY MYTH AND REALITY; CHANGING AMERICAN PERCEPTIONS. Thomas Craven,
Tom Craven Film Productions, 316 East 53rd Street, New York, N. Y. 10022

The way we conceive of and use energy in the United States is very slow to change. Why have we been unsuccessful in rethinking of the way we live, the way we conceive of and use energy in the west? What is the role of the scientist, engineer, economist in preparing the nation for the inevitable changes which are coming in the ways we obtain and use energy?

U.S. ENERGY AND CAPITAL, Herbert W. Krupp, Vice President & Energy Economist, Energy Group Bankers Trust Co., 280 Park Avenue, New York, N.Y. 10017.

This topic will contain an estimate of the financing requirements of the Energy Industries (oil gas, coal, electrical and gas facilities). These financial requirements will be compared with the capital market. Moreover, the obstacles to energy industries in attracting these types of financial requirements will be covered.

SOME NEW EVIDENCE PERTAINING TO THE CHEMISTRY AND MECHANISMS OF COAL LIQUEFACTION.
Wendell H. Wisler, Department of Mining and Fuels Engineering, University of Utah,
Salt Lake City, UT 84112.

Experimental observations have indicated that in solvent extraction and/or catalytic hydrogenation of bituminous coal in the range 400-500°C as much as 20-30% of the radical stabilization to produce liquid products involves hydrogen from the coal (i.e. coal pyrolysis reactions). Pyrolysis of a high volatile bituminous coal in this temperature range in a TGA apparatus with small samples (e.g. 10 mg), rapid heat-up (1-2 minutes) and continuously recorded weight change follows second order kinetics during 60-90% of the product evolution. A model compound with structure such that its pyrolysis is intended to simulate coal pyrolysis has been synthesized and pyrolyzed. The products of pyrolysis of this compound have been analyzed by MS and GC. Reaction kinetics are examined. Implications relative to coal pyrolysis kinetics and reaction paths are discussed. Reaction paths in the catalytic hydrogenation of linear (anthracene) and non-linear (phenanthrene) condensed aromatics are considered as indicated by GC analysis of the products of these reactions.

CARBON-13 NUCLEAR MAGNETIC RESONANCE: A POWERFUL TOOL IN THE ASSESSMENT OF THE STRUCTURE OF SOLID COALS by Ronald J. Pugmire, Kurt W. Zilm, David M. Grant, Wendell H. Wiser, and Ralph E. Wood, Departments of Chemistry and Mining and Fuels Engineering, University of Utah, Salt Lake City, Utah 84112.

A number of western coals of varying rank have been studied in the solid state by means of carbon-13 NMR employing cross-polarization and magic angle spinning techniques. The solids spectra have been compared to the coal derived liquids. By means of artificially broadening the high resolution spectra of the coal derived liquids, a striking similarity in line shape and position is observed, particularly in the case of bituminous coal, when compared to the solid coal. It is noted however, that certain bands visible in the solids are no longer present in the liquid state. The significance of these results are discussed in terms of the carbon skeletal structure and changes therein associated with liquefaction reactions.

KINETICS AND MECHANISM OF SOLVENT EXTRACTION OF COAL - RELATIONS TO CHEMICAL STRUCTURE. Larry L. Anderson, Doohee Kang, Department of Mining and Fuels Engineering, University of Utah, Salt Lake City, UT 84112.

High volatile bituminous coals were extracted with tetralin in a batch-recycle reaction system. The reactions which produce benzene, hexane and pyridine soluble fractions show definite regimes which are significantly different in the way hydrogen is required from the donor solvent. Analysis of the liquid products as to chemical type and molecular weight reveal structures not present in long term reactions typical of SRC production. Oxygen structures in the primary products and the kinetics of the reaction to produce these species give information which may be related to the size of structural units in the coal and the connecting linkages.

HYDROLYSIS OF COAL-DERIVED LIQUIDS AND OTHER HEAVY OILS AND SOLIDS. J. Shabtai,
A. G. Oblad, Department of Mining and Fuels Engineering, University of Utah, Salt
Lake City, UT 84112.

A new thermal hydrocracking process for upgrading of heavy hydrocarbon oils and solids, e.g. coal liquids, tar sand bitumens, and petroleum residues, has been developed. In a typical example, a heavy coal liquid, which contained about 45% by weight of components boiling $>500^{\circ}\text{C}$, was hydrolyzed at 525°C and a hydrogen pressure of 1500 psig to yield 74% by weight of a light liquid product distilling between $60 - 380^{\circ}\text{C}$. The mechanism of some of the important hydrolytic reactions involved in the process was elucidated by parallel studies with model compounds, e.g. $\text{C}_{10} - \text{C}_{16}$ n-paraffins, condensed arenes, and polycyclic naphthenes.

Aromatic And Aliphatic Carbon Contents
of Coals and Oil Shales by ^{13}C NMR

Gary E. Maciel and Victor J. Bartuska
Department of Chemistry, Colorado State University
Fort Collins, Colorado U.S.A. 80523

and

Francis P. Miknis, Laramie Energy Research Center
U.S. Department of Energy
Laramie, Wyoming 82070

For many types of samples in the field of fossil fuels, e.g., oil shales and typical coals, only a small fraction of the organic substances can be extracted from a solid under mild conditions that would be expected to retain the primary structural integrity of the organic compounds. Hence, the constraint of analytical techniques to liquid samples has been very restrictive. This constraint has been shared by nuclear magnetic resonance (nmr), for which high-resolution analytical applications have been limited to liquid samples until very recently. The "standard" ^{13}C nmr techniques, including pulse Fourier transform (FT) approaches¹ have not been generally useful for solid samples because of (a) the excessive line broadening due to dipole-dipole interactions between ^{13}C and ^1H magnetic dipoles, (b) chemical shift anisotropies (different shielding values for the many different orientations of the molecules in an amorphous state with respect to the magnetic field direction), and (c) long ^{13}C spin-lattice relaxation times (T_1).² All of these problems are eliminated in liquids (or in the case of long T_1 values, at least greatly reduced) by the normal tumbling motions occurring randomly in the liquid state.

This paper is concerned with the refinement and application of recently introduced ^{13}C nmr techniques for obtaining high resolution spectra of solid samples. Dipolar line broadening in the ^{13}C spectra, due to protons, is eliminated by high-power proton decoupling; when this is carried out under the Hartmann-Hahn condition, ^{13}C - ^1H cross polarization occurs, which enhances the ^{13}C signal intensity and largely overcomes the problem of long ^{13}C relaxation times.³ The primary line-broadening effect that would remain, chemical shift anisotropy, is eliminated by rapid spinning (2.2 to 2.6 kHz) of the solid sample about an axis tilted at $54^\circ 44'$ (the magic angle) relative to the direction of the static magnetic field of the instrument.⁴⁻⁷ Under rapid magic-angle-spinning conditions, the ^{13}C resonance lines that are obtained are essentially what one would expect of a corresponding nonviscous liquid sample. Examples of the type of spectra one might expect for a pure (chemically homogeneous) sample are shown in Figures 1 and 2. For a complex chemical mixture, such as coal or oil shale, one may still expect to obtain broad resonance peaks, as is usually found to be the case in experimental results (Figures 3 and 4). The reason for the broad peaks is the presence of a large number of chemically similar species present in the sample, for which the (isotropic) chemical shifts and resonance positions are close together and cannot be resolved even under conditions of reasonably high resolution. The typical result for a coal or oil shale sample is a broad peak due to aromatic and olefinic carbons and another broad peak due to aliphatic carbons (Figures 3 and 4).

The specific experimental approach that we have employed in this work is a single-contact technique based on the more general experiment originally described by Pines, Gibby and Waugh.³ A 90° ^1H pulse is applied, followed by a 90° phase shift, after which the ^1H rf power is maintained during the ^1H - ^{13}C cross polarization and for ^1H decoupling during ^{13}C data acquisition. Radiofrequency power at the ^{13}C resonance frequency (at a level determined by the Hartmann-Hahn condition) is applied during the contact period (1-8msec), then turned off during the period in which the ^{13}C free induction decay (FID) is observed.

Our experiments were carried out at 15.1 MHz on a home-built spectrometer, based upon a 14-kgauss Varian 12-in magnet and a JEOL EC-100 Fourier transform data system. The Hartmann-Hahn condition was achieved with a 40 gauss H_1 field for ^{13}C and a 10-gauss H_1 field for ^1H . The spinning rates of 2.2-~~to~~-2.6 kHz were achieved with a spinner of the general Andrew-type,³ using 14 lb/in² pressure from a "house" air supply. Higher spinning speeds could be achieved with higher pressures and/or helium. The spinner contained about 1.1 cm³ of sample.

As can be seen in Figures 1-4, a great deal of structural detail is available in the spectra of solid pure substance, while for coal and oil shale, only broad bands are obtained. In some cases these bands contain "hints" of fine structure (e.g., bumps and shoulders), which should become more distinct in a high-field spectrometer. Even in the 14-kgauss spectra of the type shown in Figures 3 and 4, clear separations between the aromatic/olefinic and aliphatic resonances are achieved. This is in contrast with the overlapping resonance bands of spectra obtained without magic-angle spinning, in which chemical shift anisotropies cause overlapping of the resonances from these different structural classes of carbons.^{7,9,11}

From ^{13}C nmr spectra of the type shown in Figures 3 and 4, one can hope to make quantitative determinations of aromatic/olefinic and aliphatic carbon contents. However, many questions must be raised to determine the reliability of the above-mentioned approach for quantitative analytical purposes. These questions revolve largely about the dynamics of the experiment, i.e., the characteristic relaxation times of the pertinent processes (^1H and ^{13}C relaxation in the rotating frame, ^{13}C - ^1H cross polarization, ^1H and ^{13}C spin-lattice relaxation). The essential question is: can experimental conditions and corrections be found so that all organic carbon types are "counted" equally in the ^{13}C experiment? Many experiments have been carried out to characterize the conditions for typical coals and oil shales, so that optimized experiments could be designed. Comparisons with experiments carried out with high-power ^1H decoupling, but without ^{13}C - ^1H cross polarization, are essential for assessing the efficiency and deviations from uniformity of the cross polarization process. Success in optimizing the experimental conditions for determining aromatic/olefinic and aliphatic carbon contents determines the scope and accuracy of the approach. One key feature of calibrating the ^{13}C approach so that absolute aromatic/olefinic or aliphatic carbon contents can be determined is an external ^{13}C standard. The requirements for an external standard involve both the chemical shift (to avoid critical peak overlaps) and relaxation times (to avoid intensity distortions).

With a method capable of determining aromatic/olefinic and aliphatic carbon contents, various comparisons and correlations are possible. These include comparisons among related samples (e.g., oil shale and shale oil; coal and solvent-refined coal or hydrogenated coal), and correlations with pertinent fuel parameters, e.g., gal/ton obtained from oil shale or BTu/ton for coal or oil shale.

Acknowledgement

The authors gratefully acknowledge support of this research by the U.S. Energy Research and Development Administration, Laramie Energy Research Center.

References

1. T.C. Farrar and E.D. Becker, "Pulse and Fourier Transform NMR," Academic Press, New York, 1971.
2. J.A. Pople, W. G. Schneider and H.J. Bernstein, "High-resolution Nuclear Magnetic Resonance," Ch. 3, McGraw-Hill, New York, 1959.
- 3a. A. Pines, M.G. Gibby and J.S. Waugh, 1972, *J. Chem. Phys.*, 56, 1776.
b. A. Pines, M.G. Gibby and J.S. Waugh, 1973, *ibid.*, 59, 569.
4. I.J. Lowe, 1959, *Phys. Rev. Letters*, 2, 285.
5. H. Kessemeier and R.E. Norberg, 1967, *Phys. Rev.*, 155, 321.
6. E.R. Andrew, 1971, *Progr. Nucl. Magn. Reson. Spectrosc.*, 8, 1.
7. V.J. Bartuska, G.E. Maciel, J. Schaefer and E.O. Stejskal, 1977, *Fuel*, 56, 354.
- 8a. J. Schaefer, S.H. Chin and S.I. Weissman, 1972, *Macromol.*, 5, 798.
b. E.O. Stejskal, J. Schaefer, J.M.S. Hemis and M.K. Tripodi, 1975, *J. Chem. Phys.*, 61, 2352.
9. D.L. VanderHart, H.L. Retcofsky, *Fuel*, 1976, 55, 202.
- 10a. F.P. Miknis, A.W. Decora, and G.L. Cook, Pulsed Nuclear Magnetic Resonance Studies of Oil Shales - Estimation of Potential Oil Yields, *U.S. Bureau of Mines*, RI 7984 (1974).
b. E.W. Cook, *Fuel*, 1974, 53, 16.
11. G.E. Maciel, V.J. Bartuska and F.P. Miknis, 1978, *Fuel*, 57, in press.

Figure Captions

- Figure 1. ^{13}C nmr spectrum of catechin, obtained at 15.1 MHz under conditions of high-power ^1H decoupling, ^1H - ^{13}C cross polarization and magic-angle spinning. Spectral width 530 ppm, higher shielding to the right.
- Figure 2. ^{13}C nmr spectrum of polymethylmethacrylate, obtained at 15.1 MHz under conditions of high-power ^1H decoupling, ^1H - ^{13}C cross-polarization and Magic-angle spinning. Spectral width 530 ppm, higher shielding to the right.
- Figure 3. ^{13}C nmr spectrum of coal (Indiana), obtained at 15.1 MHz under conditions of high-power ^1H decoupling, ^1H - ^{13}C cross polarization and magic-angle spinning. Spectral width 530 ppm, higher shielding to the right. Spinning sidebands are marked with arrows.
- Figure 4. ^{13}C nmr spectrum of New Zealand shale, obtained at 15.1 MHz under conditions of high-power ^1H decoupling, ^1H - ^{13}C cross polarization and magic-angle spinning. Spectral width 530 ppm, higher shielding to the right.



Figure 1

D-GATECHIN
500 scans

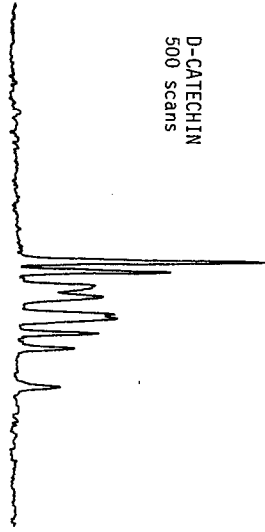


Figure 3

INDIANA BITUMINOUS
COAL
3000 scans

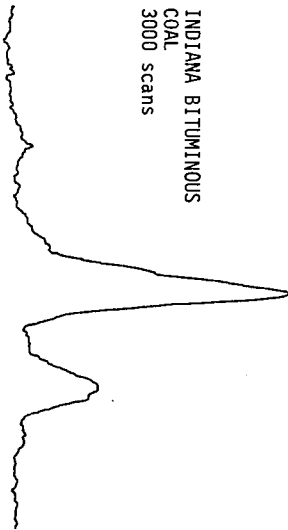


Figure 2
POLY(METHYL METHACRYLATE)
500 scans

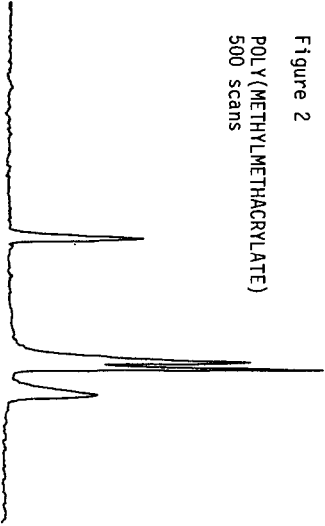
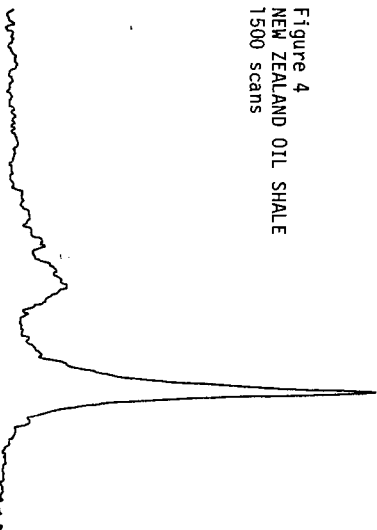


Figure 4
NEW ZEALAND OIL SHALE
1500 scans



8KHz (530 ppm)

A Re-evaluation of Carbon Ring Structure in Coal

A.W. Scaroni and R.H. Essenhigh

Combustion Laboratory, The Pennsylvania State University, University Park, Pa. 16802

INTRODUCTION

Working models of coal constitution are important because of their potential predictive capacity. A basic approach is to develop a qualitative structure of coal which can be given subsequent quantitative expression. Without a model we are faced, as at present, with the prospect of endless repeat of experiments on all coals of interest. With a working model, however, experimental results on certain coals under certain conditions can in principle be generalized to allow prediction of properties, both physical and chemical, of other coals or the same coals under untested conditions. This is an ultimate objective of developing a working model of coal constitution.

Traditional coal tests provide relatively little insight into structural configuration. Ultimate analysis will yield the elements and their proportions but nothing of their arrangement. The volatiles expelled during carbonization may not have been present as such in the raw coal. They can be formed *in situ* by primary or secondary reactions. The use of results from such methods for structural analysis, therefore, has always been indirect and inferential.

Direct information on structure, however, is obtainable from X-ray scattering from coals. During such experiments Hirsch (1), for example, found that up to 80% of the carbon is ordered and evidently exists as flat plates or lamellae made up of condensed aromatic rings. By measuring the diameters of the lamellae Hirsch estimated that the number of rings in each lamella was rank dependent varying from 4 or 5 in bituminous coals to 30 or more in anthracite. The remainder of the coal was amorphous to X-rays.

Van Krevelen and co-workers (2) predicted physical and chemical properties from the ultimate analysis. The equations were based on the general equation for alkanes. Ayre and Essenhigh (3) criticize this approach on two grounds: it gives no insight into the structure in coal and prediction of the number of rings in each of Hirsch's lamellae showed considerable discrepancy with experimental values. They, in turn proposed a qualitative model of the coal molecule based on the Hirsch structure and derived an equation relating the number of rings per lamella to the total carbon percentage in the coal. The quantitative expression was based on a relationship previously proposed by Essenhigh (4) between the weight percent oxygen and carbon in coal.

In this present paper the essential features of the Ayre and Essenhigh analysis are used but incorporating an improved relationship between the hydrogen/carbon and oxygen/carbon atomic ratios in coal.

QUALITATIVE MODEL

The structure of coal proposed by Ayre and Essenhigh is an elaboration of that described by Hirsch. The basic unit is considered to be the crystallite which contains all the ordered carbon as condensed aromatic lamellae plus a fixed quantity of amorphous material situated around the edges of the lamellae. The lamella carbon is loosely identified as fixed carbon, and the amorphous material as volatile matter as measured by proximate analysis. Each crystallite may contain a single lamella or groups of two, three, or more lamellae stacked parallel with each other. The amorphous material which is weakly

bonded to the edges of the lamellae, possibly by double or triple bonds, provides for some cross linking between lamellae. A fraction of the amorphous material, however, is considered to be more closely associated with the lamellae than the rest and can be thought of as an integral part thereof, so each lamella contains some hydrogen, oxygen and nitrogen (and possibly sulfur). The coal molecule is thus based on the single lamella with a fixed quantity of associated volatile matter.

According to the X-ray results the percentage of ordered carbon, the number of rings per lamella and the degree of parallel stacking of the lamellae increase with rank. At low carbon percentages the coal is highly porous, the number of rings per lamella is low, and the lamellae are randomly ordered. As the carbon percentage rises the parallel packing of the lamellae improves and both the number of rings per lamella and the fraction of carbon in rings increase. At 89% C what Hirsch described as a perfect "liquid" structure is reached where the crystallite packing is an optimum but a large fraction of the internal pore volume is isolated. A further increase in rank leads to a more rapid increase in the number of rings per lamella and a greater fraction of ordered carbon. At 94% C the structure is almost perfectly graphitic. The changes with rank are illustrated in Figure 1. Coalification is the process of transforming the open structure into the anthracitic structure.

TWO-COMPONENT HYPOTHESIS

Clark and Wheeler (5) identify two main stages of volatile evolution when coal is heated: the constituents easily evolved on heating to 650°C (hydrocarbons, gases, vapors, tars); and, the volatiles less easily evolved on heating above this critical temperature (mainly hydrogen with reduced quantities of carbon bearing materials). The easily evolved volatiles can be considered as being generated from the weakly bonded amorphous material around the edges of the lamellae. The hydrogen rich fraction is evolved as a result of ring coalescence. The two components are thus identified as: the loosely associated amorphous material; and the lamellae of condensed rings and related O and H atoms.

QUANTITATIVE EXPRESSION

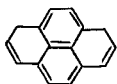
Ayre and Essenhig (3) established first a general equation for the condensed aromatic ring structure. The number of carbon atoms, C_L , in a condensed aromatic structure containing R rings was shown (3) to be given by

$$C_L = 4 + 3R \quad 1)$$

and the number of hydrogen atoms H_L for a structure with N double bonds is

$$H_L = 10 + 4R - 2N \quad 2)$$

Equations (1) and (2) are based on naphthalene, and assume ring addition so as to minimize carbon atom addition. As an example



$$\begin{aligned} R &= 4, N = 7 \\ C_L &= 16 \\ H_L &= 12 \end{aligned}$$

Some of the double bonds may be saturated by hydrogen atoms. If n is the fraction that remain unsaturated

$$\begin{aligned} H_L &= 10 + 4R - 2nN \\ &\approx 10 + 4R - 4n(R - 1) \end{aligned} \quad 3)$$

Equation (3) is an approximate expression rarely in error by more than 2. The hydrogen/carbon ratio in the lamellae is therefore

$$H_L/C_L = [10 + 4n + 4(1-n)R]/(4 + 3R) \quad 4)$$

Oxygen and nitrogen have been omitted from the analysis since their proportions of atoms are small.

WHOLE COAL ANALYSIS

The next step is to express the hydrogen/carbon ratio in the lamellae in terms of measurable quantities. Identifying the lamella carbon as fixed carbon, Ayre and Essenhigh showed that

$$m_H H_L / m_C C_L = (100/C^*) - 1 - (O^*/C^*) \quad 5)$$

where C^* and O^* are weight percent carbon and oxygen; and m_H and m_C are molecular weights of hydrogen and carbon. It is not possible to neglect the percentage of oxygen on a weight basis.

To proceed it is necessary to establish relationships between C^* , H^* , and O^* . Since N^* and S^* are usually relatively small we have

$$C^* + H^* + O^* \approx 100 \quad 6)$$

In addition, an empirical linear relationship between $(O/H) [= (O/C)/(H/C)]$ and (O/C) was established by Essenhigh and Howard (6) that was recently reconfirmed by Yarzab (7) using the Penn State Coal Analysis Data bank. This is illustrated in Fig. 2, noting that the correlation coefficient for the plot was 0.9889. The further relationship that follows is

$$H^*/C^* = A(O^*/C^*)/[1 + B(O^*/C^*)] \quad 7)$$

where A and B are empirical constants with: $A = 1/(\text{intercept of Fig. 2})$; and $B = (\text{slope of Fig. 2}/\text{intercept of Fig. 2})$.

In using such data there is often concern expressed that these are whole coal analyses which ignores maceral constituents. As illustrated in Fig. 3, however, Kessler (8) has shown recently, on a somewhat similar plot, that maceral analyses lie on an essentially common band, thus justifying the use of whole coal analyses as in Eq. (7).

It is now possible to solve for O^*/C^* as a function of C^* . The relationship between the number of rings per lamella, R and the total carbon percentage, C^* is obtained by combining equations (4) and (5)

$$[10 + 4n + 4(1-n)R]/[12(4 + 3R)] = (100/C^*) - 1 - (O^*/C^*) \quad 8)$$

Using equations (6), (7) and (8), the value of R as a function of C^* is illustrated in Figure 4 for various values of n. The best fit line to Hirsch's experimental data is for $n = 0.6$, suggesting that between half and three quarters of the double bonds remain unbroken.

The molecular weight of the lamellae, M_L is then given by

$$M_L = [100 m_C (4 + 3R)]/C^* \quad 9)$$

and is shown in Figure 5 for the case $n = 0.6$. Also, the molecular weight of the coal "molecule", M is given by

$$M = M_L C^*/C_L^* \quad (10)$$

and is shown in Figure 5, using for values of C_L^* the fixed carbon percentages from Hirsch's original data. The minimum in the whole coal molecular weight is a little unexpected. Walker (9) has suggested it represents the increasing contributions of the greater oxygen percentage in the lignites.

DISCUSSION

Figure 4 shows that the predicted behavior parallels the experimental trends. In particular, choosing $n = 0.6$, agreement between prediction and experiment is respectable good. Below about 80% carbon the value of R is constant, and tends to infinity at 100% carbon. This can be explained by considering the process of coalification. The rise in the carbon percentage as coalification proceeds can only occur if a fraction of the primary coal material is eliminated (by coalification as a long term chemical reaction). It is reasonable to assume that the fraction that remains is reorganized so that, as proposed by Ayre and Essenhigh (3)

primary coal material \rightarrow lamella + material eliminated.

If this is so, raw coal will consist of the lamella with its closely associated fraction of hydrogen, carbon, and nitrogen plus some unchanged parent material. If the unchanged parent material is identified as the amorphous material surrounding the lamellae, then this material contains all the volatile carbon. A plot of fixed carbon versus volatile carbon (Figure 6) is indicative of the growth of lamellae at the expense of the parent material. At about 90% fixed carbon the parent material has run out so that coalification can only continue at the expense of the lamellae, which coalesce. This is consistent with Horton's (10) two stage theory of coalification.

As the number of lamellae increases, the proportion of associated parent material will drop so the molecular weight of the coal molecule will drop slightly as the carbon percentage increases. At about 90% carbon, however, ring coalescence occurs and the molecular weight will rise rapidly. These trends are illustrated in Figure 5.

The model is intended, of course, as a first step in a full model of coal structure. It is clearly lacking in that nitrogen and sulfur are missing. It is also not yet able to predict the degree of detail on pyrolysis described, for example, by Suuberg *et al* (11). The initial agreement between theory and the X-ray results of experiment, however, is encouraging and suggests that the model is probably adequate as a framework or skeleton for further developments.

SUMMARY

1. X-ray data suggest that the coal molecule may be viewed in terms of a lamella of condensed aromatic rings of carbon plus a fraction of loosely associated volatile matter.
2. The model described is in agreement with the X-ray data, showing that the number of rings per lamella is constant at 4 or 5 up to about 90% carbon above which it rapidly rises with rank.
3. The model shows that the molecular weight of the coal molecule drops slightly as the carbon percentage rises to 90% above which it rises rapidly with rank.

4. The lamella carbon is identified as the fixed carbon and the amorphous material as the volatile matter as determined by the proximate analysis.
5. The model is consistent with the Two-Component Hypothesis of coal constitution (5) and the Two-Stage Theory of coalification (10).

REFERENCES

1. Hirsch, P.B., Proc. Royal Society, 226A, 143 (1955).
2. Van Krevelen, D.W., et al, Fuel, 33, 79 (1954)
Fuel, 36, 85 (1957).
3. Ayre, J.L. and Essenhigh, R.H., Sheffield Univ. Fuel Soc. Journal, 8, 44, (1957).
4. Essenhigh, R.H., Fuel, 34, 497 (1955).
5. Clark, A.H. and Wheeler, R.V., Trans, Chem. Soc., 103, 1754 (1913).
6. Essenhigh, R.H. and Howard, J.B., The Pennsylvania State University Studies, 31 (1971).
7. Yarzab, R.F., Coal Research Section, The Pennsylvania State University, Private Communication (1976).
8. Kessler, M.F., Fuel, 52, 191 (1973).
9. Walker, P.L. Jr., Department of Material Sciences, The Pennsylvania State University Private Communication (1978).
10. Horton, L., Fuel, 31, 341 (1952).
11. Suuberg, E.M., Peters, W.A. and Howard, J.B., American Chemical Society Fuels Division Preprints, 22 (1), 112 (1977).

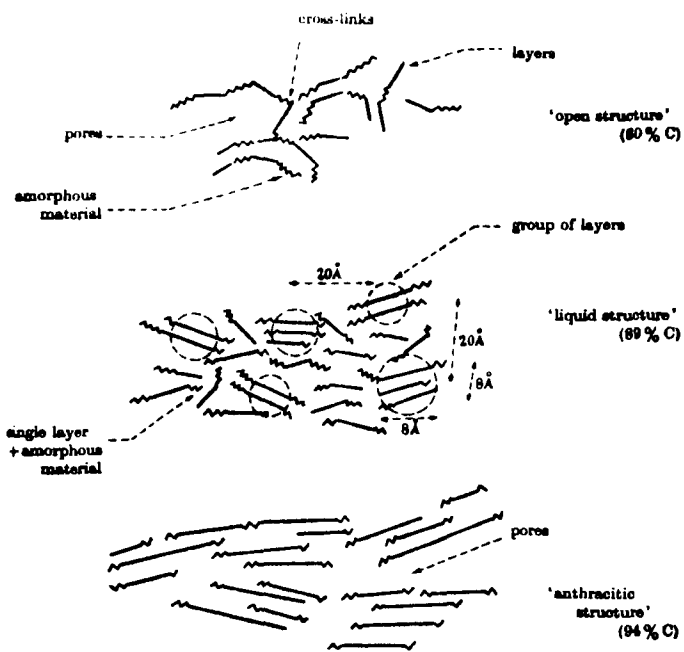


Figure 1 - Coal Structure as a Function of Rank
(source: Hirsch (1))

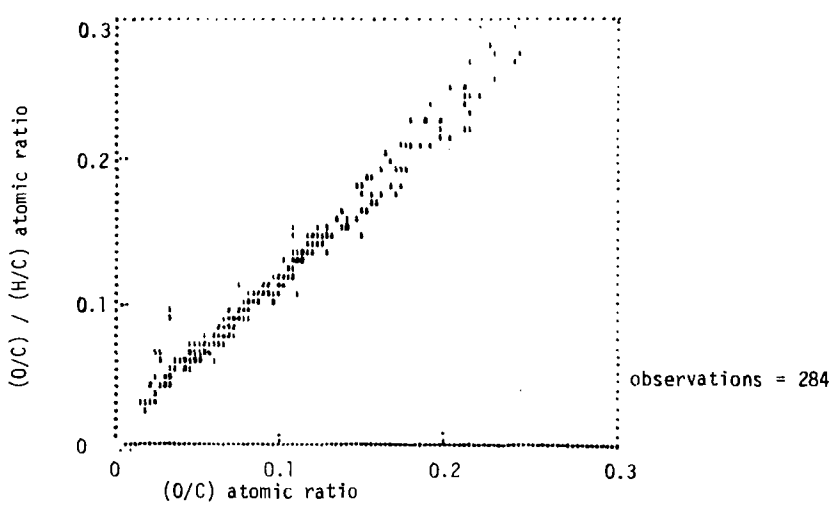


Figure 2 - Variation of $(O/C) / (H/C)$ with (O/C) atomic ratios for various coals. (Source: Yarab, (7)).

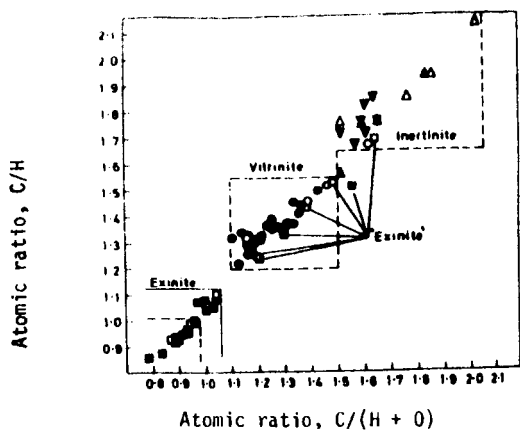


Figure 3 - Variation of C/H ratio with C/(H + O) ratio for various macerals. (Source: Kessler, (8))

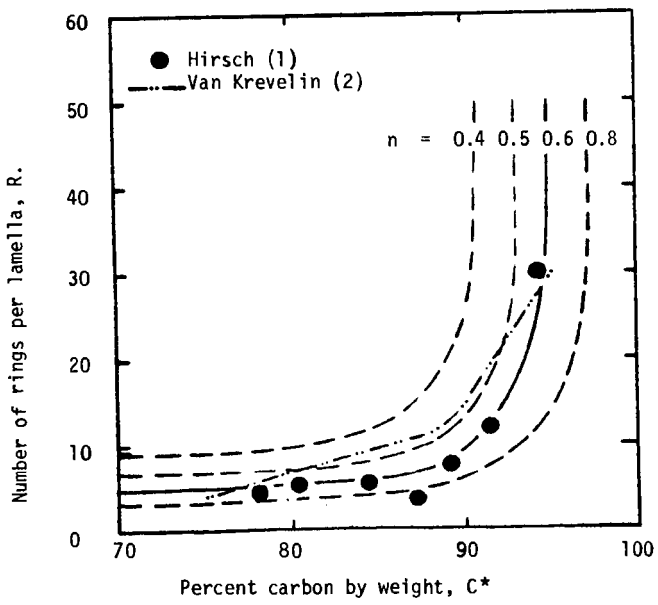


Figure 4 - Variation of number of rings per lamella with carbon percentage by weight.

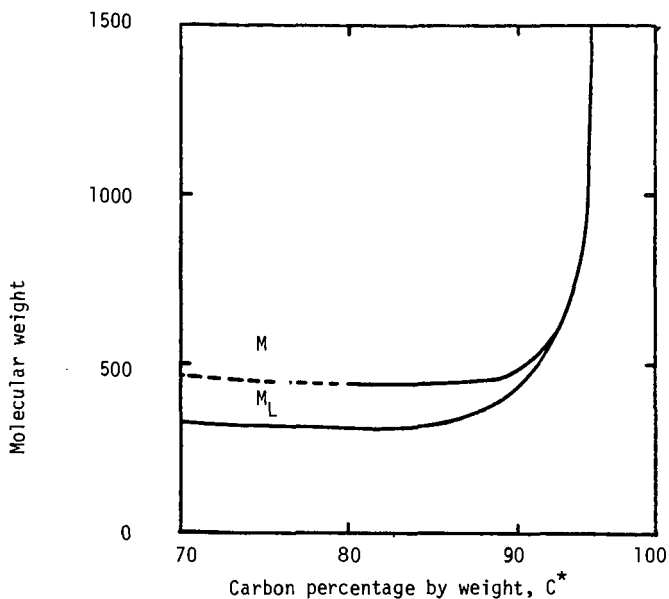


Figure 5 - Variation of molecular weight of lamella and coal molecule with weight percent carbon.

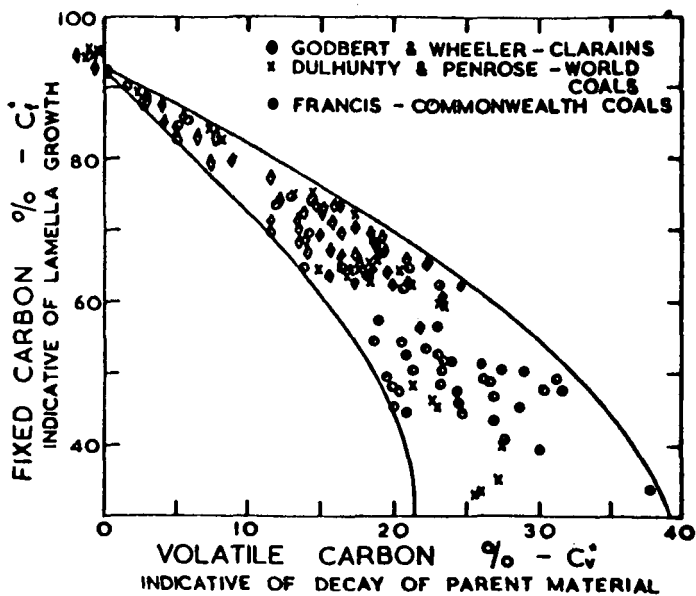


Figure 6 - Relation between lamella growth and decay of parent material. (Source: Ayre and Essenhigh, (3))

Organic Structure Studies of Fossil Fuels
by Nuclear Magnetic Resonance

Victor J. Bartuska and Gary E. Maciel
Department of Chemistry, Colorado State University
Fort Collins, Colorado 80523

and

Francis P. Miknis and Daniel A. Netzel
Laramie Energy Research Center, U.S. Department
of Energy, Laramie, Wyoming 82070

Nuclear magnetic resonance (nmr) is playing an increasingly important role in the characterization of the organic constituents of fossil fuels.¹⁻¹⁷ The nmr techniques that are currently being applied to fossil fuel characterizations utilize both the ^1H and ^{13}C nuclides and can conveniently be divided into those that apply to liquid samples and those that apply to solids. For solids one has to contend with line-broadening influences of dipole-dipole interactions and chemical shift anisotropies (especially for carbon) and with long spin-lattice relaxation times; some recent advances have largely circumvented these problems for ^{13}C .¹⁴⁻²⁰ For liquids, rapid isotropic molecular tumbling averages dipolar splittings to zero and the chemical shift tensor to its isotropic average, and gives rise to relatively efficient spin-lattice relaxation (permitting one to reduce the wait time between pulse repetitions).

For solid fossil fuels, a considerable amount of structural information can be obtained by modern ^{13}C techniques.¹⁴⁻¹⁷ Proton experiments on solids determine the amplitude of the free induction decay (FID) following a 90° pulse; this amplitude is a measure of the organic proton content of the sample for oil shales and has been related empirically to the oil yield one can obtain by retorting (Figures 1 and 2).^{8,9}

For ^{13}C studies on solids, rapid spinning of the intact or powdered sample about an axis making an angle of $54^\circ 44'$, the "magic angle", relative to the field axis eliminates broadening due to chemical shift anisotropy.^{17,19,20} High-power ^1H decoupling eliminates broadening due to ^{13}C - ^1H dipole-dipole interactions.¹⁸ If the high-power ^1H decoupling and ^{13}C resonance are carried out under conditions obeying the Hartmann-Hahn condition,¹⁸ then the problem of long ^{13}C spin-lattice relaxation times can also largely be overcome. The net result of applying these techniques to homogeneous, pure organic solids is sharp-line spectra, reminiscent of spectra obtained on analogous liquid samples. For solid fossil fuels, however, the great complexity of mixtures of closely related chemical structures gives rise to resonance "bands", rather broad lines, encompassing the ^{13}C resonances of a given structural type, e.g., aliphatic carbons. While greater structural detail may sometime be available, (especially from spectra obtained at high field strength), at present the greatest current capability of this approach is a clear distinction between the resonances of aromatic or olefinic carbons and the aliphatic carbon resonances. Typical spectra are shown in Figures 3 and 4.

For liquid samples, standard pulse Fourier transform methods¹⁻⁷ are applicable to both ^{13}C and ^1H . Because of the great chemical complexity typical of samples, very complex spectra are usually obtained. Nevertheless, considerable information can usually be extracted regarding the occurrence of specific structural types.

By combining the various techniques described above, a great deal can be learned about a fossil fuel system and the processes involved in typical characterization procedures and, more importantly, in its conversion into a useable fuel source. We have applied the various nmr techniques described above to solid and liquid samples derived from oil shale of the Green River Formation. The purpose was to explore the potential applicability of nmr methods to answer such questions as: Do procedures for concentrating the kerogen in oil shale alter the distribution of organics in kerogen significantly? How similar are the kerogen, shale oil and bitumen derived from a specific oil shale? What, if any, types of organic structural features are present in the spent shale after retorting?

Using solid-sample techniques one can determine the total organic proton content and the aromatic/olefinic and aliphatic carbon contents of the raw shale, of the solid remaining after bitumens are extracted, of the solid kerogen concentrate obtained from the shale and of the residue from retorted shale. Using standard FT techniques for liquids, analogous information and considerably greater structural detail can be obtained on the bitumens extracted from the shale and on the shale oil retorted from the shale. Examples of relevant spectra are shown in Figures 5-8. In interpreting the intensities of the resonances of such carbon spectra, one has to pay close attention to intensity distortions associated with nuclear Overhauser effects and the dynamics of the cross polarization experiment.²⁰

References

1. Shooley, J.N. and Budde, W.L., Anal. Chem., 48, 1458, (1976).
2. Dorn, H.C. and Wooten, D.L., Anal. Chem., 48, 2146, (1976).
3. Pugmire, R.J., Grant, D.M., Zilm, K.W., Anderson, L.L., Oblad, A.G. and Ward, R.E., Fuel, 56, 295, (1977).
4. Wooten, D.L., Coleman, W.M., Taylor, L.T., and Dorn, H.C., Fuel, 57, 17, (1978).
5. Schweighardt, F.K., Retcofsky, H.L. and Friedel, R.A., Fuel, 55, 313, (1976).
6. Retcofsky, H.L., Schweighardt, F.K. and Hough, M., Anal. Chem., 49, 585, (1977).
7. Retcofsky, H.L. and Friedel, R.A., Fuel, 55, 363(1976).
8. Miknis, F.P., Decora, A.W. and Cook, G.L., U.S. BuMine Rept. Invest. 7984, (1974), 47 pp.
9. Miknis, F.P., Decora, A.W. and Cook, G.L., Science and Technology of Oil Shale (Ed. T. F. Yen), Ann Arbor Science Publishers, 1976, pp. 35-45.
10. Sydansk, R.D., Fuel, 57, 66 (1978).
11. Halla, A. and Craft, B.D., paper No. 75, 1978, Pittsburgh Cleveland Conference on Analytical Chemistry and Spectroscopy.
12. Gerstein, B.C. and Pembleton, R.G., Anal. Chem., 49, 75, (1977).
13. Gerstein, B.C., Chow, C., Pembleton, R.G. and Wilson, R.C., J. Phys. Chem., 81, 565, (1977).
14. VanderHart, D.L. and Retcofsky, H.L., Fuel, 55, 202 (1976).

15. Bartuska, V.J., Maciel, G.E. and Miknis, F.P., Am. Chem. Soc. Div. of Fuel Chem. preprints, 23, No. 2, 19, (1978).
16. Maciel, G.E., Bartuska, V.J. and Miknis, F.P., Fuel, in press.
17. Bartuska, V.J., Maciel, G.E., Schaefer, J. and Stejskal, E.O., Fuel, 56, 354, (1977).
18. Pines, A., Gibby, M.G. and Waugh, J.S., J. Chem. Phys., 59, 569, (1973).
19. Schaefer, J. and Stejskal, E.O., J. Amer. Chem. Soc., 98, 1031, (1976).
20. Schaefer, J., Stejskal, E.O. and Buchdahl, R., Macromolecules, 10, 384, (1977).

Figures

- Figure 1. Proton free induction decay (at 20 MHz) for oil shale before and after heating to remove free water (From Miknis et al, BuMines Rep. Invest. No., 7984 (1974).
- Figure 2. Correlation between proton free induction decay amplitude and average Fischer assay oil yields (From Miknis and Netzel, Magnetic Resonance in Colloid and Interface Science, H.A. Resing and C.G. Wade, Eds., ACS Symposium Series, 34, 182 (1976).
- Figure 3. ^{13}C nmr spectrum of Hanna (Wyoming) coal, with high-power ^1H decoupling, cross polarization and magic-angle spinning, obtained at 15.1 MHz. 530 ppm range. Higher shielding on the right.
- Figure 4. ^{13}C nmr spectrum of Australian oil shale, same conditions as for Figure 3.
- Figure 5. ^{13}C Fourier transform nmr spectrum of shale oil retorted from Colorado oil shale of Fig. 7. 530 ppm range. Higher shielding on the right.
- Figure 6. ^{13}C Fourier transform nmr spectrum of bitumen (in CDCl_3) extracted with benzene from Colorado oil shale of Fig. 7. Same conditions as for Fig. 5.
- Figure 7. ^{13}C nmr spectrum of raw Colorado oil shale. Same conditions as for Fig. 3.
- Figure 8. ^{13}C nmr spectrum of kerogen concentrate obtained from Colorado oil shale of Fig. 7. Same conditions as for Fig. 3.

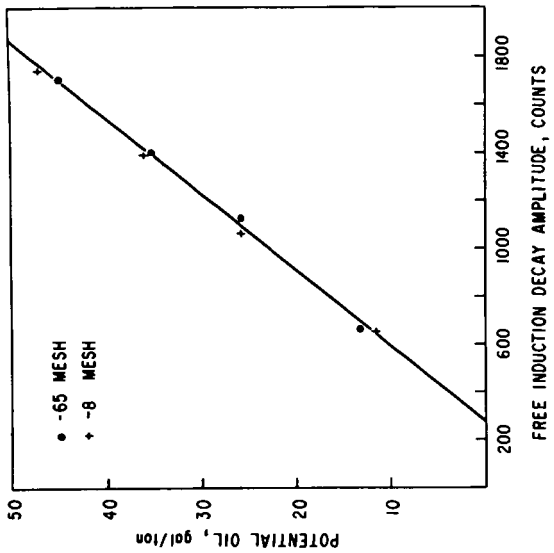


FIG. 2
CORRELATION BETWEEN FID
AMPLITUDE AND OIL YIELD

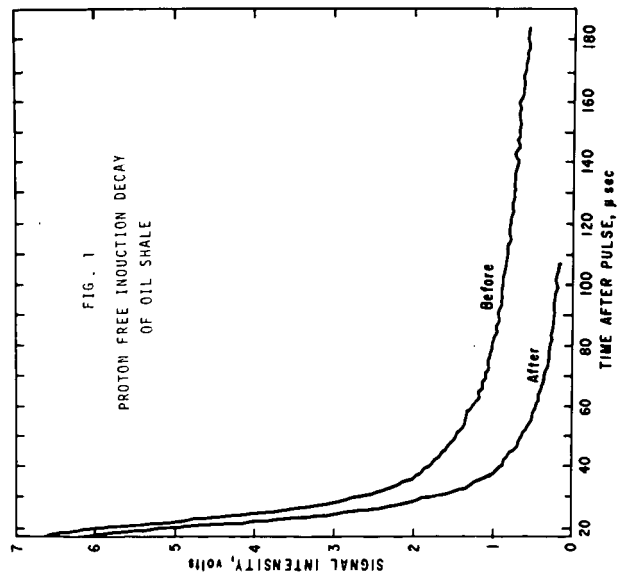


FIG. 3
 ^{13}C SPECTRUM OF
HANNA COAL

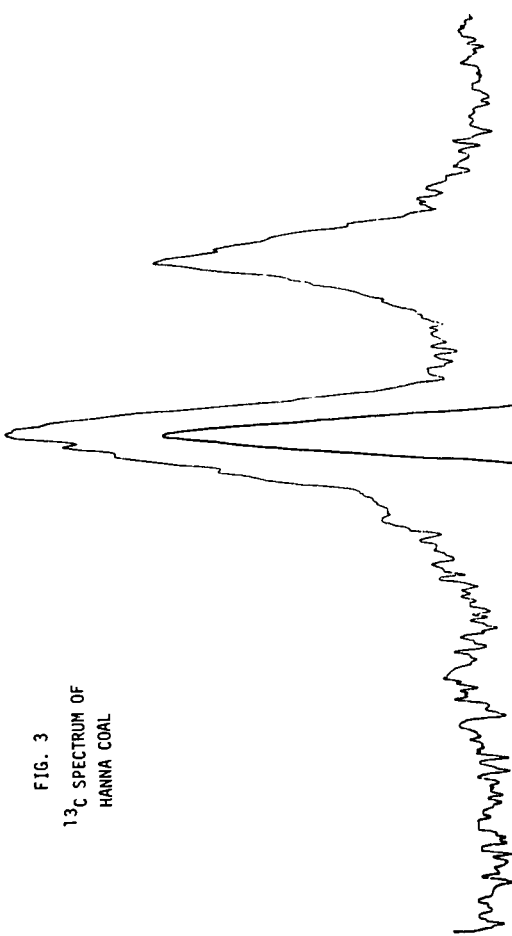


FIG. 4
 ^{13}C SPECTRUM OF AUSTRALIAN
OIL SHALE

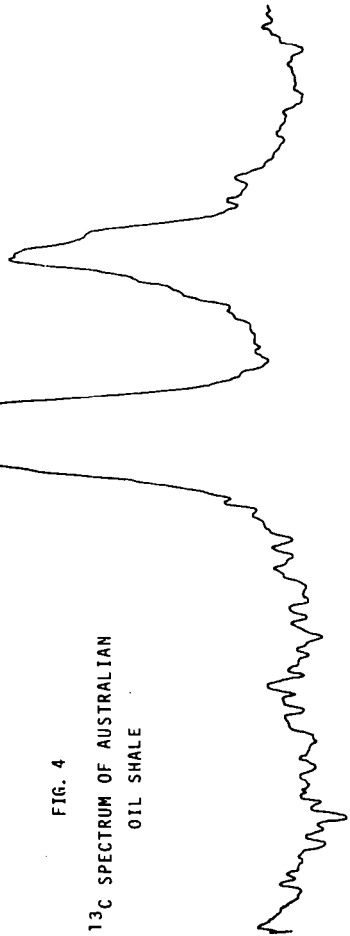


FIG. 5
 ^{13}C FT SPECTRUM OF SHALE OIL

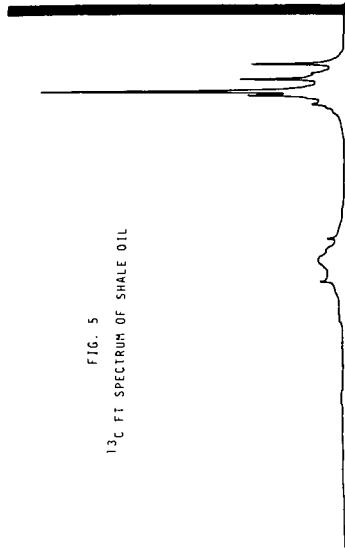


FIG. 7
 ^{13}C SPECTRUM OF RAW OIL SHALE

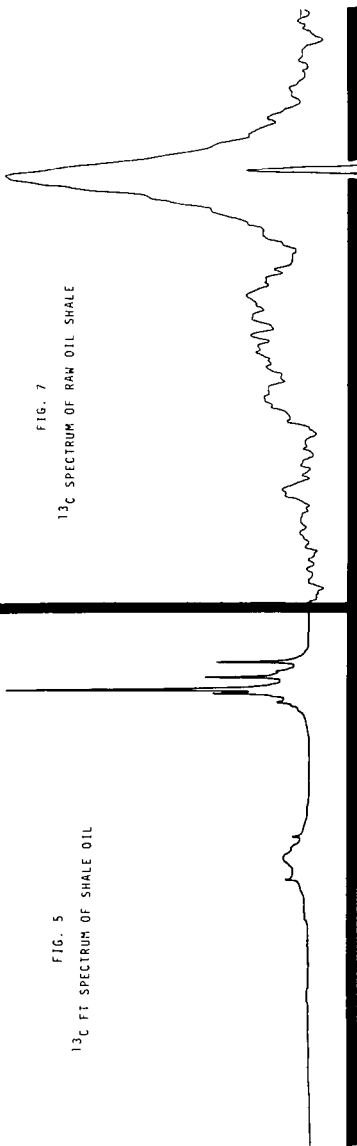


FIG. 6
 ^{13}C FT SPECTRUM OF
OIL SHALE BITUMEN

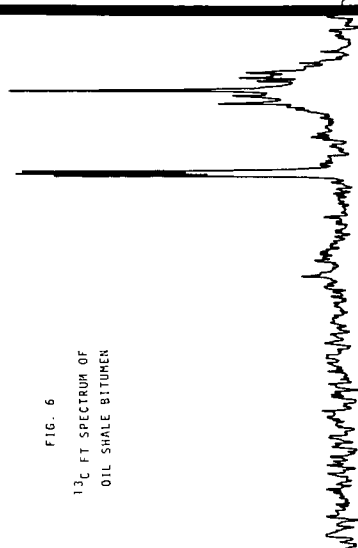
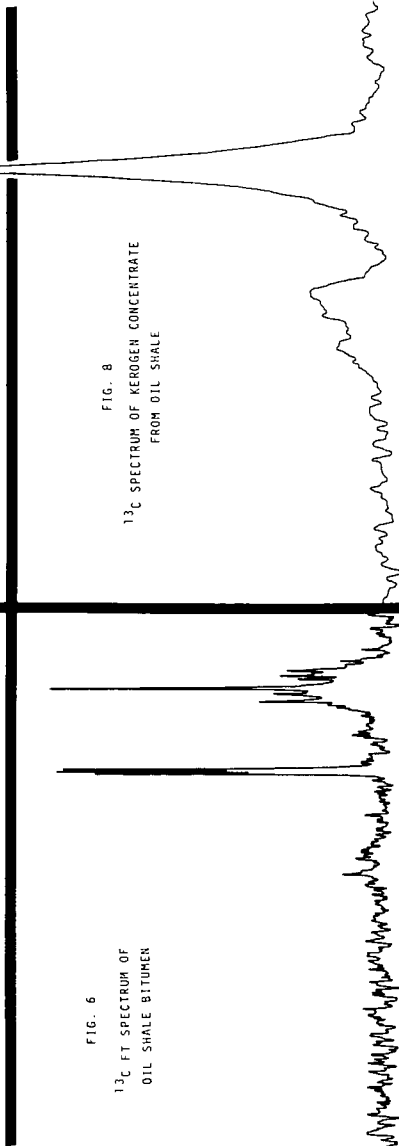


FIG. 8
 ^{13}C SPECTRUM OF KEROGEN CONCENTRATE
FROM OIL SHALE



CHEMICAL CHANGES PRODUCED IN COAL THROUGH
THE ACTION OF LEWIS ACID CATALYSTS

D. P. Mobley, S. Salim, K. I. Tanner, N. D. Taylor and A. T. Bell

Materials and Molecular Research Division
Lawrence Berkeley Laboratory
and
Department of Chemical Engineering
University of California, Berkeley, CA 94720

INTRODUCTION

Molten Lewis acids and in particular $ZnCl_2$ and $SnCl_2$ are known to catalyze the conversion of coal to liquid products (1-15). While the degree of liquefaction attainable with different catalysts is known, the manner in which Lewis acids promote liquefaction is not well understood. The present work was undertaken in an effort to establish more clearly the effects of Lewis acids on coal and to identify the specific chemical reactions which these catalysts affect. The results reported here concern experiments conducted with both solvent refined coal (SRC) and a variety of model compounds. The latter were selected to represent the aliphatic, ether, and sulfide linkages which connect the aromatic and hydro-aromatic groups in coal. Several models of fused ring aromatic clusters were also examined.

EXPERIMENTAL

Apparatus

All reactions were conducted in a 300 cm³ stirred autoclave (Autoclave Engineers, Inc. Model ABP-300). To facilitate the introduction of reactants and the removal of products a snugly fitted glass liner was used to contain the reaction mixture. The temperature and pressure within the autoclave were recorded continuously.

Materials

The SRC used here was produced from a bituminous West Kentucky coal by the Pittsburg and Midway Coal Mining Company in Tacoma, Washington. The SRC was dried overnight in an N_2 -purged oven at 105°C and then ground to pass through an 80 Tyler mesh sieve. The sieved SRC was then stored in a vacuum dessicator until needed for a run.

Model compounds were obtained from a variety of standard commercial sources. These materials were kept dry but were not purified before use.

Lewis acid catalysts were also obtained from several sources. Since several of these materials are hygroscopic (viz. AlCl_3 , FeCl_3 , SbCl_3) the catalysts were first dried in a vacuum oven overnight at 105°C and then stored in an N_2 -purged dry box. Weighing of the catalyst and transfer into the glass liner were also carried in the dry box.

Product Analysis

The liquid products obtained from reactions of SRC were disengaged from the reaction solvent and dried. The dried material was then weighed to establish the fraction of the SRC submitted to reaction which had been converted to liquid products. The stoichiometry of the dissolved products was determined by elemental analysis and the ratio of aliphatic to aromatic hydrogens, $\text{H}_{\text{Al}}/\text{H}_{\text{Ar}}$, by $^1\text{H-NMR}$.

The products obtained from model compound studies were analyzed by gas chromatography. Product identification was established with the aid of a gas chromatograph/mass spectrometer. Where possible product assignments were confirmed by injecting pure compounds into the gas chromatograph/mass spectrometer and comparing their retention times and mass spectra with those of the postulated reaction product.

RESULTS AND DISCUSSION

SRC Studies

Table 1 summarizes the results of screening experiments designed to compare the influence of selected Lewis acid catalysts on the dissolution of SRC in benzene at 300°C . It is apparent that the stronger acids, AlCl_3 , FeCl_3 , SbCl_3 , and HgCl_2 , cause a decrease in SRC solubility over that obtained without a catalyst. The use of ZnCl_2 does not alter the benzene solubility of SRC but contributes significantly to raising the H/C and $\text{H}_{\text{Al}}/\text{H}_{\text{Ar}}$ ratios of the soluble product. Similar results were obtained with SnCl_2 but in this instance a greater fraction of the SRC was dissolved. These results suggest that the acidity of the catalyst should be high enough to promote bond cleavage but not so high as to catalyze rapid retrograde reactions which lead to a diminished solubility of SRC.

The effectiveness of a given catalyst on the solubilization of SRC also depends upon the solvent as shown in Table 2. Here, it is seen that while cyclohexane is a less effective solvent for SRC than benzene, the introduction of either ZnCl_2 or SnCl_2 into cyclohexane has a very pronounced effect on the yield of soluble products.

Model Compound Studies

The cleavage of aliphatic linkages between aromatic nuclei was studied using the model compounds listed in Table 3. To facilitate product identification, cyclohexane was used as the solvent. Reactions were typically carried out for 90 min. at 325°C and 1000 psig of H₂. The ratio of substrate to catalyst was usually 14.3 mole/mole.

Screening studies performed on the unsubstituted diphenyl alkanes showed that the cleavage of the aliphatic bridge in these compounds required the use of a strong Lewis acid such as AlCl₃. In the presence of this catalyst diphenyl methane, ethane, propane, and butane reacted readily at temperatures as low as 250°C. The initial products were always benzene and a phenyl alkane, indicating that cleavage had occurred between a benzene ring and the first carbon of the aliphatic bridge. The phenyl alkane product was not stable, however, and was observed to isomerize or crack to shorter chained products. In the cases of diphenyl propane and diphenyl butane, indan and tetralin were observed respectively as major reaction products. While 70 to 80% of the diphenyl alkanes were converted to products under the conditions noted earlier, diphenyl was less reactive and was only 32% converted. The only product obtained from diphenyl was benzene.

A mechanism which summarizes our observations on the cleavage of diphenyl and the diphenyl alkanes is shown below. The lower reactivity of diphenyl is explained by the fact that the phenyl carbonium ion, formed in the first step of the reaction, is less stable than a phenyl alkane carbonium ion.

The addition of a hydroxyl group to one of the phenyl rings of diphenyl methane was found to contribute an inductive effect, facilitating cleavage of the aliphatic linkage. Since phenol was a major reaction product it was concluded that cleavage had occurred preferentially at the ring containing the hydroxyl group. Experiments were also performed to determine whether the inductive effect of the hydroxyl group would now permit ZnCl₂, a weaker Lewis acid, to cleave the aliphatic bridge. These experiments gave positive results. However, under identical reaction conditions ZnCl₂ provided only half of the substrate conversion obtained with AlCl₃.

To determine the effects of fused ring nuclei upon the cleavage of aliphatic bridges, experiments were conducted with phenyl naphthalene and benzyl naphthalene. By analogy with diphenyl, phenyl naphthalene was relatively unreactive and could be cleaved only to the extent of 10%. Benzyl naphthalene, on the other hand, was completely converted to naphthalene, benzene, and other aromatic products. The reaction of benzyl naphthalene in the presence of ZnCl₂ was also examined. It was found that while ZnCl₂ is not as effective a catalyst as AlCl₃, it would bring about a 40% conversion of the substrate to products.

The cleavage of ether and sulfide linkages occurred more readily than the cleavage of aliphatic linkages and could be catalyzed by $ZnCl_2$. Reaction of diphenyl ether at $325^\circ C$ yielded phenol and benzene. Under similar conditions diphenyl sulfide yielded thiophenol and benzene. Dibenzyl ether and dibenzyl sulfide followed similar reaction paths. Both of these substrates apparently form benzyl carbonium ions which rapidly alkylate the solvent, benzene, to produce diphenyl methane.

The reactions of benzyl naphthyl ether were also explored. In benzene this substrate yielded 2-hydroxynaphthalene and diphenyl methane. These products again illustrate the preferential cleavage of the linkage to produce a benzyl carbonium ion.

The effects of Lewis acid catalysts on fused ring aromatic clusters was also examined, using naphthalene and phenanthrene as models. In the presence of $AlCl_3$, naphthalene was converted to tetralin which in turn cracked to produce benzene. Phenanthrene reacted to produce 9,10-dihydrophenanthrene and smaller quantities of naphthene and tetralin. Thus both naphthalene and phenanthrene appear to react by first hydrogenating and then cracking to produce products of lower molecular weight. It is interesting to note that for temperatures up to $325^\circ C$ no evidence was obtained that $ZnCl_2$ could promote reactions similar to those observed with $AlCl_3$.

CONCLUSIONS

The following conclusions can be drawn from this work.

- $ZnCl_2$ and $SnCl_2$ are particularly suitable catalysts for the dissolution of ^{238}Pu in benzene and cyclohexane.
- The strength of acid required to catalyze the cleavage of aliphatic linkages between aromatic nuclei depends upon the nature of the nuclei, naphthyl and hydroxyphenyl groups being more readily separated from aliphatic linkages than phenyl groups.
- Ether and sulfide linkages are easily cleaved by mild Lewis acids such as $ZnCl_2$.
- The products obtained from the cleavage of aliphatic, ether, and sulfide linkages can be explained by carbonium ion mechanisms.
- Hydrogenation and cracking of fused ring aromatic clusters requires strong Lewis acids such as $AlCl_3$.

ACKNOWLEDGMENT

This work was supported by the Division of Chemical Sciences, Office of Basic Energy Sciences, U.S. Department of Energy.

REFERENCES

- (1) C. O. Hawk and R. W. Hiteshue, U.S. Bureau of Mines Bulletin No. 622(3), 1965.
- (2) C. W. Zielke, R. T. Struck, J. M. Evans, C.P.. Costanza, and E. Gorin, Ind. Eng. Chem. Process Des. Dev., 5(2), 151 (1966).
- (3) C. W. Zielke, R. T. Struck, J. M. Evans, C. P. Costanza, and E. Gorin, Ind. Eng. Chem. Process Des. Dev., 5(2), 158 (1966).
- (4) W. Kawa, S. Friedman, L. V. Frank; and R. W. Hiteshue, Preprints, ACS Fuel Chem., Am. Chem. Soc., 12(3) 4347 (1968).
- (5) Research on Zinc Chloride Catalyst for Converting Coal to Gasoline, Research and Development Report No. 39, Vol. III, Books 1,2, prepared by the Consolidation Coal Company for the Office of Coal Research, 1968.
- (6) R. T. Struck, W. F. Clark, P. J. Dudd, W. A. Rosenhoover, C. W. Zielke, and E. Gorin, Ind. Eng. Chem. Process Des. Dev., 8(4), 546 (1969).
- (7) C. W. Zielke, R. T. Struck, and E. Gorin, Ind. Eng. Chem. Process Des. Dev., 8(4), 552 (1969).
- (8) W. Kawa, H. F. Feldmann, and R. W. Hiteshue, Preprints, ACS Fuel Chem., Am. Chem. Soc., 14(4), Part I, 19 (1970).
- (9) Project Western Coal: Conversion of Coal Into Liquids - Final Report, Research and Development Report No. 18, prepared by the University of Utah for the Office of Coal Research, May 1970.
- (10) S. A. Qader, K. Duraiswamy, R. E. Wood, and G. R. Hill, AIChE Symposium Series, 69(127), 102 (1973).
- (11) Coal Processing - Gasification, Liquefaction, Desulfurization: A Bibliography 1930-1974, Atomic Energy Commission, October 1974.
- (12) H. Katzman, A Research and Development Program for Catalysis in Coal Conversion Processes, Electric Power Research Institute Report No. 207-0-0, Palo Alto, Calif., 1974.
- (13) C. W. Zielke, W. A. Rosenhoover, and E. Gorin, Preprints, Div. of Fuel Chem., Am. Chem. Soc., 19(2) 306 (1974).
- (14) D. S. Ross and J. Y. Low, "Homogeneous Catalysis - Acid Catalysis", in Homogeneous Catalytic Hydrocracking Processes for Conversion of Coal to Liquid Fuels, Stanford Research Institute, Menlo Park, Calif., Quarterly Report Nos. 2,3, 1976.

- (15) R. E. Wood and W. H. Wiser, Ind. Eng. Chem. Process Des. Dev., 15(1), 144 (1976).

Table 1

Effects of Lewis Acid Catalysts on
the Liquefaction of SRC in Benzene

Reaction Conditions: T = 300°C Catalyst mass = 5 gm
 P = 2000 psig H₂ SRC mass = 5 gm
 t = 90 min Solvent volume = 70 ml
 ω = 1250 rpm

Catalyst	Sol. (%)	Charac. of Sol. Prod. H/C	H _{Al} /H _{Ar}
None	46.7	0.85	1.33
AlCl ₃ ^a	20.3	0.89	1.32
ZnCl ₂	46.8	1.01	2.54
SnCl ₂	57.9	0.97	2.22
SbCl ₃	38.2	0.95	2.18
HgCl ₂	37.8	0.93	1.79

^a 1.0 gm AlCl₃ charged

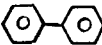
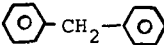
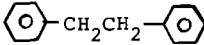
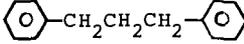
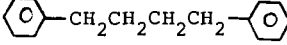
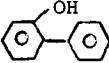
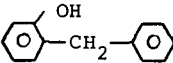
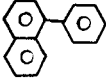
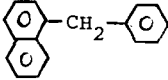
Table 2

Effects of Solvents on the Liquefaction of SRC

Reaction Conditions: T = 300°C Catalyst mass = 5 gm
 P = 2000 psig H₂ SRC mass = 5 gm
 t = 90 min Solvent volume = 70 ml
 ω = 1250 rpm

Catalyst	Solvent	Sol. (%)	Charac. of Sol. Prod.	
			H/C	H _{Al} /H _{Ar}
None	Benzene	46.7	0.85	1.33
None	Cyclohexane	15.1	0.91	1.50
ZnCl ₂	Benzene	46.8	1.01	2.54
ZnCl ₂	Cyclohexane	35.4	1.06	3.38
SnCl ₂	Benzene	57.9	0.97	2.22
SnCl ₂	Cyclohexane	29.8	1.00	2.68

Table 3
Model Compounds Containing Aliphatic Linkages

Compound	Structural Formula
Diphenyl	
Diphenyl methane	
1,2-Diphenyl ethane	
1,3-Diphenyl propane	
1,4-Diphenyl butane	
2-Phenyl phenol	
2-Benzyl phenol	
1-Phenyl naphthalene	
1-Benzyl naphthalene	

AN ESR INVESTIGATION OF FREE RADICALS IN COALS AND IN COAL CONVERSIONS

L. Petrakis and D. W. Grandy

Gulf Research & Development Company
P. O. Drawer 2038
Pittsburgh, PA 15230

I. Introduction

Free radicals in coal are not well understood or characterized despite their apparent great significance in liquefaction (1). The fate of these thermally generated free radicals is believed to determine the type of product obtained and may be associated with problems in coal conversion such as reactor coking and poor yields. This study of free radicals in coals was initiated to gain some insight as to the number and types of free radicals under a number of conditions that might be significant in coal conversion processes. Since the discovery of free radicals in coals by Uebersfeld (2) and Ingram (3), electron spin resonance (ESR) spectroscopy has been used in the study of coal and coal-derived materials by many workers (2-8).

As a technique, ESR is attractive, since radical concentration and chemical information can be obtained with relative ease in a minimal period of time. The spectral parameters of interest are the g-value of the radicals, radical concentration, peak-to-peak linewidth of the first derivative signal, and in some cases, the spectral lineshape.

II. Experimental

Six coals, ranging in rank from lignite to low volatile bituminous, were examined by ESR after a variety of treatments. The analytical data for these coals are summarized in Table I. Several sample treatments were used. Four coals were treated by evacuation to $\sim 10^{-4}$ torr with heating for 2 hours in 2 mm I.D. ESR tubes with subsequent sealing under vacuum. Several coals were treated under liquefaction conditions by mixing them with approximately equal weights of either naphthalene or tetralin in ESR tubes and heating them under 1800 psi of H_2 or N_2 . Some samples were prepared without solvent. The effects of different heating rates, solvents, gases, and residence times on the ESR parameters will be discussed. Duplicate samples were prepared in many cases to check reproducibility. All spectra were recorded at room temperature with Varian V-4500 single- and dual-cavity x-band spectrometers. Details of the measurements and peripheral equipment used are described in Ref. 8. The possible effect of many different factors, such as solid state effects, "skin" effects, sample inhomogeneity, and coal particle fractionation, on these measurements was considered and is discussed elsewhere (8).

III. "Room Temperature" Experiments

The results obtained in the ESR experiments on coals evacuated at $\sim 100^\circ C$ and at room temperature are essentially in agreement with the results obtained by earlier workers (4). The g-values show a large difference between the lignite and subbituminous coal and the four higher rank coals. (See Table II.) In the case of the higher rank coals, their g-values are typical of π -type aromatic hydrocarbon radicals (9,10). The subbituminous coal and the lignite have higher g-values indicating that atoms other than carbon and hydrogen are important in the electronic structure of the radical.

The spectral linewidth of all samples was measured as run in vacuum. Several samples yielded spectra which consist of a sharp line (~ 1 gauss) superimposed on a broader signal. As noted by Retcofsky et. al., a small amount of fusain ($\sim 1\%$) in coal can account for the sharp component seen in spectra of evacuated samples (4).

The radical concentrations for the six coals follow the expected increase with rank with two exceptions. The Kentucky #11 coal has an extremely high free radical concentration for its rank. The Lower Dekoven coal is somewhat lower than expected, probably due in part to its extremely high ash content.

The lineshapes of the spectra were estimated in some cases. The lineshape functions considered were the Lorentzian and Gaussian functions. The samples yielded spectra which range from some nearly equal linear combination of the two functions, as is the case with the Wyodak coal, to the very broadly sloping, multi-component spectra sometimes found for the higher rank coals. The lineshapes of coal spectra are probably affected by unresolved hyperfine, anisotropic effects or the large number of somewhat chemically different radicals found in coals.

IV. Heat-Treated Coals

Four of the coals, Wyodak, Pocahontas #3, Illinois #6, and Lower Dekoven, were evacuated and heated to temperatures up to 600°C. Radical concentrations, g-values, and linewidths were measured for each sample. The radical concentration of the coals is seen to change dramatically over the temperature range studied. Up to 400°C, only moderate changes in radical concentration occur. Radical concentration increases sharply between 400°C and 500°C and drops substantially on going to 600°C (8). This behavior is qualitatively in agreement with the work of Smidt and Van-Krevelen, among others (6).

Figure 1 shows the change in g-values of the radicals in the coals as a function of temperature. Two of the coals, the Pocahontas #3 coking coal and the Illinois #6 high-volatile bituminous coal, show a minor decrease in g-values from 2.0029 to 2.0027. Such a change in g-value shows a minor change in radical structure, the radical tending to become more hydrocarbon in nature. The Wyodak sub-bituminous coal shows a very large decrease in g-value, from 2.0037 to 2.0027, which occurs below 500°C. One of the bituminous coals, Lower Dekoven, Illinois, shows some interesting changes in g-value when heated. Between 250° and 500°C the g-value decreases to an abnormally low value of 2.0023. There are several possible explanations for this behavior, among these is the appearance of σ -type radicals. Many σ radicals have g-values around 2.0024 and some are known have g-values as low as 2.0008 (11). From the increase in the g-value of the radicals in the Lower Dekoven coal on heating to 600°C and the decline in radical concentration, it is likely that the σ -radicals are involved in recombination reactions.

V. Liquefaction Experiments

Several coals were treated using various temperatures, heating rates, solvents, reagent gases, and residence times to determine their effect on the ESR spectral parameters. The Wyodak subbituminous coal was selected to determine experimental conditions to be used on a series of coals. In our initial experiments, this coal was heated at $\sim 13^\circ\text{C}/\text{min}$ to 440°C in 1800 psig of N_2 or H_2 gas and held at that temperature for 2 hours. Examination of these samples at room temperature by ESR showed essentially no difference in g-values (2.0028), or linewidth (5.1 vs 5.5). Some difference in radical concentration between the samples treated with the two gases does occur, the samples treated in H_2 having somewhat fewer radicals, $25 \pm 13 \times 10^{18}/\text{g}$ vs $45 \pm 3 \times 10^{18}/\text{g}$. The same coal was reacted with tetralin or naphthalene in 1800 psi of H_2 or N_2 at the same temperature, heating rate, and for the same length of time. Linewidths and g-values were the same for all combinations, within experimental error, being about 5 gauss and 2.0027 to 2.0028, respectively. Free radical concentration of tetralin-treated Wyodak coal appears to be the same, around $25\text{-}30 \times 10^{18}$, whether H_2 or N_2 gas is used. Naphthalene-treated coals do show some slight dependence (less than a factor of 2) of the free radical concentration on the gas used, the concentration being lower when H_2 is used. The difference in radical concentration in this coal in what should be the best donor, tetralin and H_2 , compared

to the worst donor system, naphthalene and N_2 , is only slightly more than a factor of 2. Using tetralin with H_2 and naphthalene with N_2 as the treatments for the coal samples, the effects of heating rate and residence time were investigated. The radical concentration in samples was reduced in samples heated at a faster rate ($32^\circ\text{C}/\text{min}$) and held at the maximum temperature for a shorter time (10 min). The tetralin- H_2 -treated samples showed a reduction in radical concentration that was much larger. The difference in radical concentration between the treatment schemes is about 5 to 1 for the Wyodak coal, again with the naphthalene- N_2 -treated samples having more free radicals remaining. Doubling the residence time from 10 minutes to 20 minutes had no apparent effect on tetralin- H_2 -treated samples. Some of the radical concentration data collected for different heating rate-residence time treatments for the two solvent-gas treatment schemes are shown in Figures 2 and 3 for the temperature range 400° to 500°C .

Two other coals, Kentucky #11 and Hagel lignite, were studied by ESR after treatment with the tetralin- H_2 and naphthalene- N_2 systems. All samples were heated at $\sim 32^\circ\text{C}/\text{min}$ under 1800 psig and after they were kept at the desired temperature for 10 minutes, the reactor was cooled rapidly (~ 3 minutes to RT) by high-pressure air. A plot of the g-values of the Kentucky #11 coal radicals as a function of temperature is shown in Fig. 4. Around 420°C there is a considerable difference in g-values for the samples treated by the donor and non-donor systems. As the temperature is raised to $\sim 475^\circ\text{C}$, these differences disappear. The differences in g-values cannot be easily interpreted since all of these fall in the range of hydrocarbon radicals, and differences as large as these seen here are found between the anion and cation of the same radical species (9,10). The Hagel lignite runs show no such temperature dependence of g-values in the 400° - 500°C range, with most of the samples having very similar g-values, between 2.0027 and 2.0028. Spectral linewidths for these two coals show no dependence upon temperature between 400 and 500°C or the solvent-gas treatment system used. The lignite samples had spectral linewidths generally between 5 and 6 gauss. There was more scatter in the linewidths found for the Kentucky #11 samples, ranging from 4 to 6 gauss. The free radical concentration of the Kentucky #11 samples is shown in Figure 5. Here the differences between the donor and non-donor treatments are apparent, as it was in Fig. 2 for the Wyodak coal. The Hagel lignite shows similar effects due to donor capabilities of the sample treatment; however, there is a generally higher concentration in all cases, the tetralin- H_2 -treated samples having radical concentration $\sim 20 \times 10^{18}$ compared with $\sim 40 \times 10^{18}$ for the naphthalene- H_2 -treated samples. It is believed that the lower radical concentration found for the tetralin- H_2 -treated samples is due to hydrogen transfer to the radical sites. A few extraction experiments were attempted on the Wyodak coal samples after the liquefaction treatments to see if a correlation between radical concentration and toluene-insolubles could be made. No significant differences were found, although this may be due to large experimental scatter. Conversions on a toluene soluble, daf basis are from 64 to 77%. Further effort in this area is planned.

VI. Solvent-Refined Coal

SRC filter feed, process solvent, and filter wash solvent were obtained from the Pittsburg & Midway Coal Mining Co. SRC pilot plant near Tacoma, Washington. The samples used in most of this work are the dried filter solids, process solvent, filter wash solvent, the filtrate, which is about 50% process solvent and 50% filter-feed with solids removed, and the filter feed as received. A sample of the solid SRC product from the Catalytic, Inc., SRC pilot plant in Wilsonville, Alabama, was also examined. The results of the ESR measurements are shown in Table III. All values are for the organic paramagnetic species present.

VII. Conclusions

In general, concentrations of naturally occurring free radicals are of the order of $5\text{-}15 \times 10^{18}/\text{g}$. In coals heated in vacuum, the concentration of radicals is

quite high, $100-200 \times 10^{18}/g$, and reaches a maximum between 400 to 500°C, dependent on rank and maceral content. Coals heated to similar temperatures in the presence of a high-pressure (2000 psig) gas have somewhat lower concentrations ($<100 \times 10^{18}/g$). This could result from small molecules or radicals escaping less readily in a high-pressure gas than in vacuum. The gas acts as a solvent. Naphthalene affects free radical concentration in a manner similar to that of the gases by acting as a solvent. Tetralin, as a hydrogen donor solvent, is the most effective treatment among those tried for consuming free radicals. Hydrogen transfer is presumed to occur and in some cases this hydrogen transfer quenches some of the naturally occurring free radicals in coal. The free radical concentration of SRC is similar to that found for other solvent-treated systems.

VIII. References

- (1.) R. C. Neavel, Fuel **56**, 237 (1976).
- (2.) J. Uebersfeld, A. Etienne, and J. Combrisson, Nature **174**, 614 (1954).
- (3.) D.J.E. Ingram, J. G. Tapley, R. Jackson, R. L. Bond, and A. R. Murnaghan, Nature **174**, 797 (1954).
- (4.) H. L. Retcofsky, J. M. Stark, and R. A. Friedel, Anal. Chem. **40**, 1699 (1968).
- (5.) D.E.G. Austin, D.J.E. Ingram, P. H. Given, C. R. Binder, and L. W. Hill, p. 344, "Coal Science," Advances in Chemistry, Series #55 ACS, (1965).
- (6.) J. Smidt and D. W. VanKrevelen, Fuel **38**, 355 (1959); COAL, pp. 393-399, Elsevier, Amsterdam (1961).
- (7.) B. C. Gerstein, C. Chow, R. G. Pembleton, and R. C. Wilson, J. Phys. Chem. **81**, 565 (1977).
- (8.) L. Petrakis and D. W. Grandy, Anal. Chem. **50**, 303 (1978).
- (9.) M. S. Blois, Jr., H. W. Brown, and J. E. Maling, FREE RADICALS IN BIOLOGICAL SYSTEM, p. 130, Academic Press, Inc., New York (1961).
- (10.) B. G. Segal, M. Kaplan, and G. K. Fraenkel, J. Chem. Phys. **43**, 4191 (1965).
- (11.) P. Smith, R. A. Kaba, L. M. Dominguez, and S. M. Denning, J. Phys. Chem. **81**, 162 (1977).

Table I

CHEMICAL ANALYSIS (DAF)

	C	H	O	S	N	ASH(dry)	RANK
Wyodak Gilllete, WY	72.2	5.5	21.0	0.3	1.0	9.2	Subbit C
Hagel-ND*	71.0	4.9	21.8	.72 (total)	1.6	9.7	Lignite
Kentucky #11*	76.4	5.4	10.0	5.7 (total)	2.2	16.0	HVB
Illinois #6	82.0	5.4	9.5	1.0	1.7	6.5	HVB
Lower Dekoven-IL*	80.6	5.8	4.8	7.7	1.8	21.9	HVA
Pocahontas #3-WV	86.4	3.9	6.8	0.9 (total)	1.2	3.3	LV

*Data supplied by P. Given, Pennsylvania State University.

Table II

ESR PARAMETERS OF COALS
All samples evacuated 2 hr at 105°C

	<u>g-Value</u>	<u>Linewidth</u>	<u>Raical Concentration per g x 10⁻¹⁸</u>
Hagel Lignite	2.0040	6.7	4.7
Wyodak Subbit C	2.0037	7.43	5.8
Kentucky #11 HUB	2.0029	1.9	14.1
Illinois #6 HUB	2.0029	1.34 & 6.02	6.8
Lower Dekoven HVA	2.0028	0.86 & 4.14	4.1
Pocahontas #3 LV	2.0029	0.97 & 6.03	15.8

Table III

SRC ESR DATA*

<u>Sample</u>	<u>g-Value</u>	<u>Linewidth (gauss)</u>	<u>Concentration (spins/g)</u>
SRC Filter Cake Solids	2.0026	2.9	18 x 10 ¹⁸
Filtrate	2.0031	6.4	0.7 x 10 ¹⁸
Filter Feed	2.0027	1.4	3.5 x 10 ¹⁸
Recycle or Process Solvent	2.0029	9.4	0.2 x 10 ¹⁸
Wash Solvent	2.0037	6.8	6 x 10 ¹⁵
Wilsonville SRC Solid Product	2.0028	1.0	15 x 10 ¹⁸

*All materials are from the P&M SRC pilot plant at Tacoma, Washington, except as noted.

Figure 1. g-Value Vs Temperature

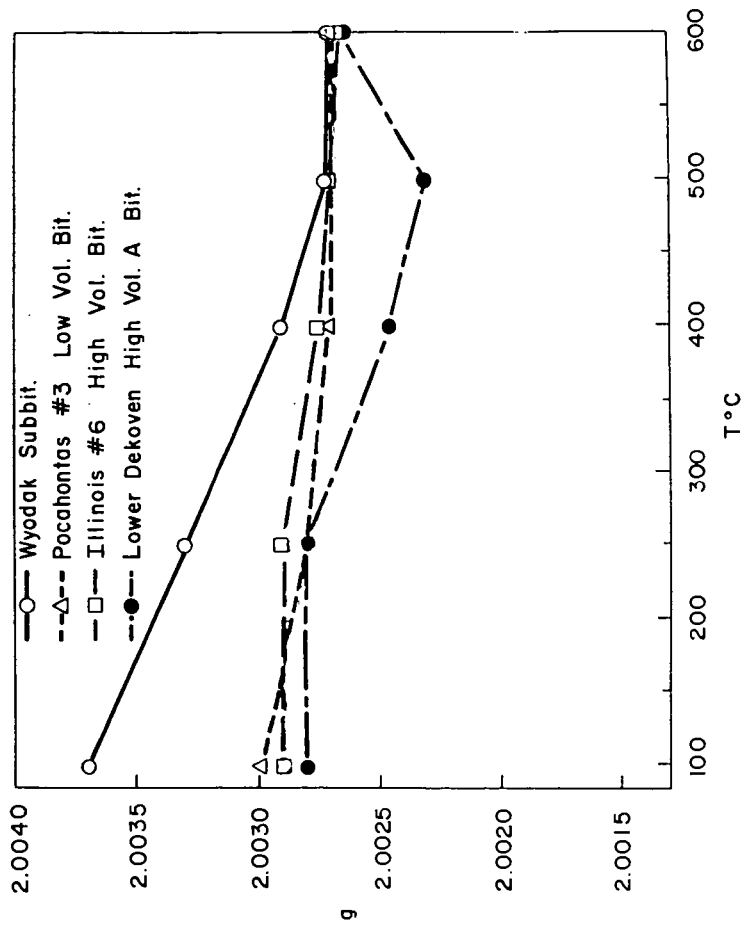


Figure 2. Radical Concentration Vs Temperature

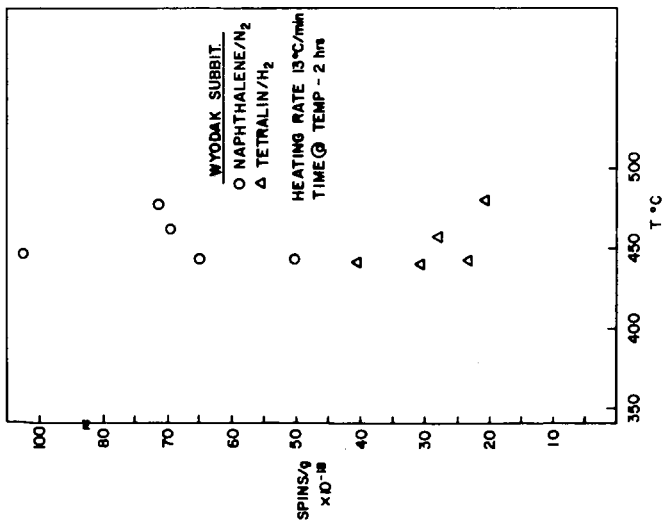


Figure 3. Radical Concentration Vs Temperature

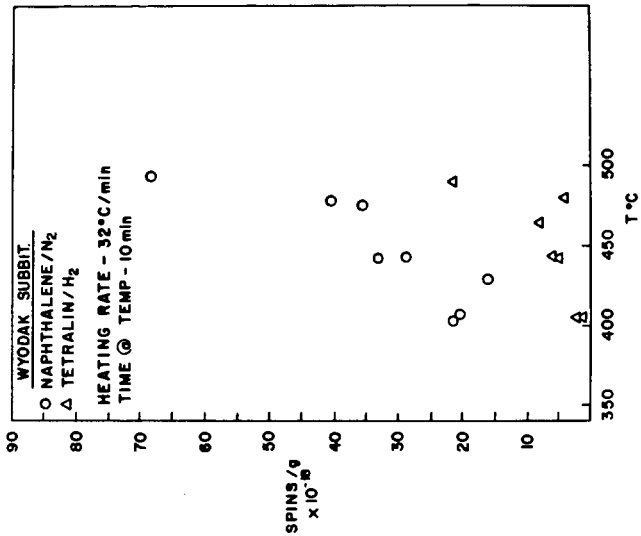


Figure 4. g-Value Vs Temperature

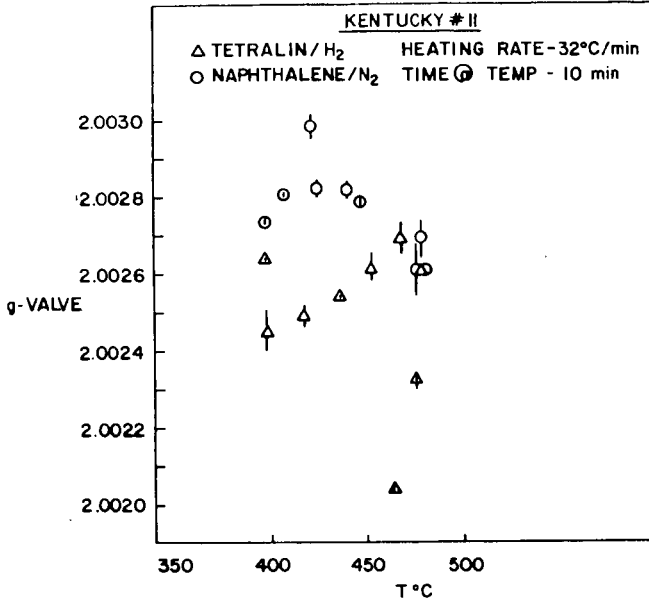
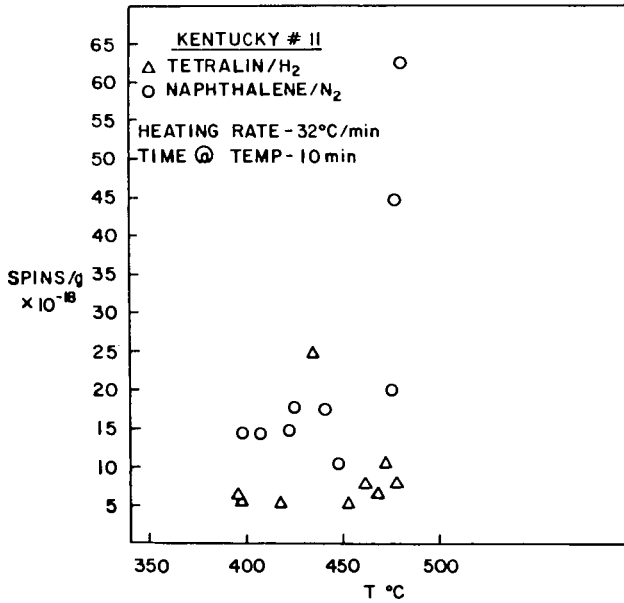


Figure 5. Radical Concentration Vs Temperature



DEUTERIUM TRACER METHOD FOR INVESTIGATING THE CHEMISTRY OF COAL LIQUEFACTION

Raymund P. Skowronski, Laszlo A. Hередy
Rockwell International, Atomic International Division
8900 De Soto Avenue, Canoga Park, California 91304

Joseph J. Ratto
Rockwell International, Corporate Science Center
1049 Camino Dos Rios, Thousand Oaks, California 91360

INTRODUCTION

Conversion of coal to liquids by hydrogenation involves an increase of the hydrogen content of the coal. The effective use of this costly gas is, therefore, of significant importance to commercial hydrogenation processes. An intensive research effort has been under way to obtain a better understanding of the hydrogenation reaction mechanisms and thereby to improve hydrogen utilization and the efficiency of the process. This paper describes the development of a deuterium tracer method for the investigation of the mechanism of coal hydrogenation.

The deuterium tracer method consists of conducting coal hydrogenation experiments with deuterium, or deuterium and a deuterated donor solvent, separating the products by solvent-fractionation and analyzing the fractions for protium and deuterium structural types by proton and deuterium NMR spectrometry. In an alternative application of the method, which has been investigated, pairs of hydrogenation experiments are conducted, one with protium and one with deuterium, under identical experimental conditions. The hydrogenated products are separated by solvent-fractionation and the fractions are analyzed for hydrogen structural types by proton NMR spectrometry. The difference between the two spectra gives a quantitative measure of the hydrogen which is incorporated into different structural positions in the coal.

In the past, relatively little use has been made of deuterium as an isotopic tracer for investigating coal chemistry.^(1,2) Very recently, however, renewed interest in the applications of deuterium to coal science has been evident.⁽³⁻⁵⁾

EXPERIMENTAL

A high volatile A bituminous coal (81.8% C, dmmf basis) from the Loveridge Mine, Pittsburgh Seam, was used. The coal was ground to -200 mesh and stored under dry nitrogen until used. It then was dried at 115°C for 4 h before use.

High-purity (99.95% according to the supplier's specifications) protium and technical grade (>98.8 atom % deuterium and total hydrocarbons <1 ppm according to the supplier's specifications) deuterium were used. The benzene, hexane isomer mixture, and methanol utilized for the solvent-fractionation analyses were all Baker reagent grade. Chloroform-d was used as the solvent for the NMR spectrometric analyses.

The experiments were performed in a 1-liter stirred autoclave (Autoclave Engineers). The combined solid and liquid products from each of the hydrogenation experiments were solvent-fractionated into oil, asphaltene, benzene-methanol soluble, and residue fractions. Samples of fractions from those experiments in

which deuterium was used were combusted, and the resulting water was collected. The water samples then were analyzed by mass spectrometry (MS) to determine the protium and deuterium contents of each.

The product gases were analyzed by gas-solid chromatography coupled with mass spectrometry (GC-MS) to determine both the amount of each component in the gas phase and its isotopic composition. Both the MS and GC-MS were performed by Shrader Analytical and Consulting Laboratories, Inc.

The NMR spectra of the soluble fractions were obtained using a JEOL FX60Q Fourier Transform NMR Spectrometer. Elemental analyses were conducted with a standard combustion train.

RESULTS AND DISCUSSION

Exploratory hydrogenation experiments were conducted to establish baseline conditions for the systematic investigation of deuterium incorporation. The criterion that was established for baseline conditions was that the benzene-soluble portion of the products be 25-50 wt % of the total products. Moderate conversion to benzene solubles was desired because it was expected that isotopic scrambling and nonspecific deuterium incorporation could be kept to a minimum under such reaction conditions.

The results of the exploratory experiments indicated that an experiment performed at 400°C, 3200 psig, for 1 h, with a 100 rpm stirring rate, should give the desired quantity of soluble products. Accordingly, the first pair of protium/deuterium experiments (4 and 5) was conducted under these conditions. The second pair of hydrogenation experiments (6 and 7) was performed at a lower temperature and for a shorter reaction time in order to investigate deuterium incorporation at a very low conversion. The parameters for each experiment were 380°C, approximately 3000 psig, and 15 minutes reaction time. The yield of soluble products and the degree of deuterium incorporation were considerably lower than in the first pair of experiments.

The results of both pairs of experiments are summarized in Table 1. In both experiments, the atom percent deuterium content of the fractions increased from the oil (hexane soluble) to the less soluble fractions and it was highest in the insoluble residue.

Table 2 lists the deuterium/protium ratios for the structural positions of the various fractions from Experiment 4. These numbers indicate the relative deuterium content in each position. The higher the number, the greater the deuterium incorporation in this position relative to other structural positions. The term ${}^2\text{H}_x$ refers to the quantity of deuterium that is in a specific structural position and, therefore, $({}^2\text{H}_x/{}^2\text{H})$ refers to the fraction of the total deuterium that is in a given structural position. Similarly, $({}^1\text{H}_x/{}^1\text{H})$ refers to the fraction of the total protium that is in a given structural position.

Significant specific deuterium incorporation is noted in the α -alkyl (benzylic) positions in all the fractions and in the γ -alkyl positions of the asphaltene fraction. Large specific incorporation of deuterium in α -alkyl positions is illustrated in Figure 1, where the proton and deuterium NMR spectra of the oil fraction from Experiment No. 4 are compared. The deuterium incorporation in the γ -alkyl position of the asphaltenes is quite interesting because protium-deuterium exchange is expected to be relatively low in such a structural position. Further research will be conducted to establish whether this finding is related to the mechanism of asphaltene production.

The value for the β -alkyl region of the benzene-methanol fraction is equivalent to the γ -alkyl value for the asphaltene fraction. Data from a number of other experiments, however, indicate that the β -alkyl value is atypical, while the γ -alkyl value is typical.

A coal hydrogenation experiment was conducted with $^2\text{H}_2$ and tetralin- d_{12} at 400°C and 3000 psig. Significant specific deuterium incorporation was observed in the α -alkyl position in all fractions. Similarly, most of the protium in the recovered tetralin- d_{12} was concentrated in the α -alkyl position.

Another set of experiments was designed to test the reactions of coal with deuterium under 3000 psig pressure at different temperatures and under different degrees of contact opportunity. The gaseous products from each of these experiments were analyzed by GC-MS to determine their isotopic composition. Together with data on the composition of the solvent-fractionated liquid and solid products, this information is being used to develop a tentative mechanism for the coal hydrogenation reaction.

The two techniques used to determine into which structural positions in the coal deuterium is incorporated during hydrogenation were discussed in the introduction. The measured values of deuterium incorporation, obtained from deuterium NMR spectrometry, were compared with the calculated values obtained from proton NMR spectrometry. In those cases where the ^2H content of the sample was over 10-15 atom % there was good agreement between the calculated and measured values for deuterium incorporation.

ACKNOWLEDGMENT

This research was supported by the U.S. Department of Energy under Contract EF-77-C-01-2781.

REFERENCES

1. Y. C. Fu and B. D. Blaustein, *Chem. Ind.*, 1257 (1967)
2. T. Kessler and A. G. Sharkey, Jr., *Spectrosc Lett.*, 1, 1977 (1968)
3. F. K. Schweighardt, B. C. Bockrath, R. A. Friedel, and H. L. Retcofsky, *Anal. Chem.*, 48, 1254 (1976)
4. A. F. Gaines and Y. Yürüm, *Fuel*, 55, 129 (1976)
5. J. R. Kershaw and G. Barrass, *Fuel*, 56, 455 (1977)

TABLE 1
SUMMARY OF RESULTS FOR EXPERIMENTS 4-7

Parameter	Expt. 4	Expt. 5	Expt. 6	Expt. 7
Reactant Gas	$^2\text{H}_2$	$^1\text{H}_2$	$^1\text{H}_2$	$^2\text{H}_2$
Reaction Time (h)	1.0	1.0	0.25	0.25
Temperature ($^{\circ}\text{C}$)	400	400	380	380
Pressure (psig)	3200	3200	2700	3000
Reactor	1 Liter 250 Milliliters			
Products (%)	Atom % ^2H (Expt. 4)		Atom % ^2H (Expt. 7)	
Oil	22	22	5	5
Asphaltene	25	25	<1	*
Benzene-Methanol Soluble Fraction	6	6	7	7
Insoluble Residue	47	47	87	87
				19.5

*Insufficient sample for analysis

TABLE 2
 COMPARISON OF PROTIUM AND DEUTERIUM
 DISTRIBUTIONS IN COAL HYDROGENATION PRODUCTS
 (EXPERIMENT 4)

Functional Region	$(^2\text{H}_x/^2\text{H})/(^1\text{H}_x/^1\text{H})$ Ratio		
	Oil	Asphaltene	BMS
	Experiment 4		
γ - Alkyl	0.6	1.2	0.9
β - Alkyl	0.5	0.6	1.2
α - Alkyl*	2.2	1.9	1.5
Aromatic**	0.9	0.8	0.8

*Includes α^2 - Alkyl Region
 **Includes Phenolic Region

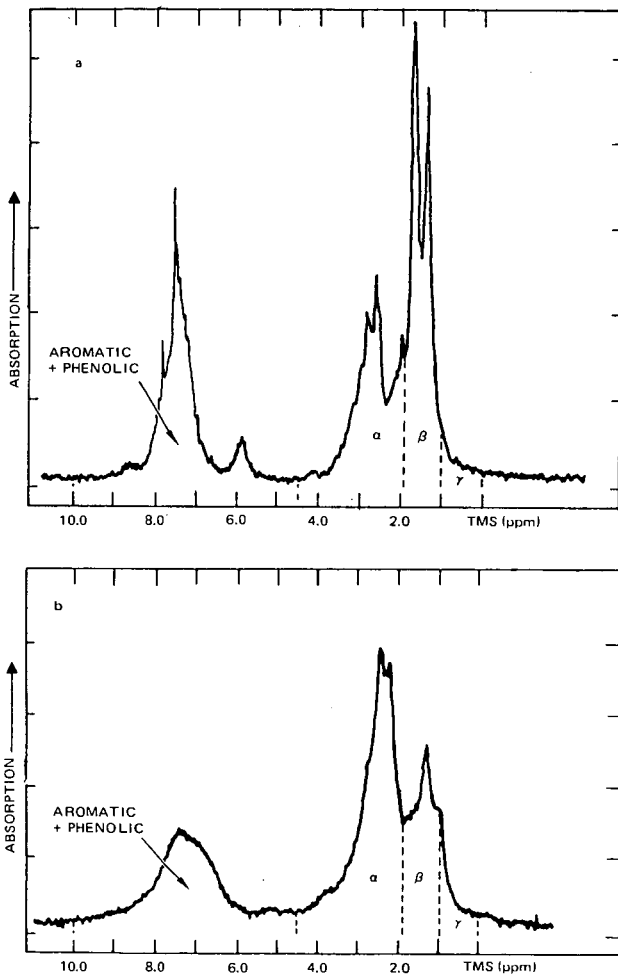


FIGURE 1. PROTON^(a) AND DEUTERON^(b) NMR SPECTRA OF THE OIL FRACTION FROM EXPERIMENT No. 4

THE ROLE OF OXYGEN FUNCTIONAL GROUPS IN THE MECHANISMS OF COAL LIQUEFACTION

A. J. Szladow and P. H. Given

Department of Materials Science and Engineering,
The Pennsylvania State University, University Park, Pa. 16802

The hypothesis that the generation of soluble products in coal liquefaction is related to the cleavage of ether bridges or cross-links was proposed by Fisher et al. (1) and reiterated 20 years later by Takegami et al. (2). Recently, several workers have reported investigations on related topics, which include reductive alkylation (3,4), behavior of model compounds (5), and the distribution of oxygen-containing functional groups in liquefaction products (6). Nevertheless, the role of oxygen functionalities in coal liquefaction seems to us still to be obscure, and we therefore report here some attempts to clarify the matter. We have restricted our study to coal-tetralin interactions and relatively short contact times, in order to study phenomena in the early stages of the process.

EXPERIMENTAL

A high volatile bituminous coal having a low mineral matter content was chosen for the study (Table 1). Liquefaction runs were simulated in microreactors (~45 cc stainless steel tubes, with Swagelok fittings) charged with 5g of dried coal and 10 cc tetralin. Reactions were carried out at temperatures of 340 to 400°C and at contact times up to 30 minutes. Rapid heating of the contents was achieved by immersion of the vessels in a preheated fluidized sand bath; cooling was achieved by plunging the vessels into cold water. To ensure good mixing microreactors were vertically oscillated 450 times per minute with an amplitude of 1.25 cm. A more detailed description of the reactor assembly was given in (7). After reaction was completed, the contents were transferred to a 500 cc flask, diluted with hexane to a total volume of 500 cc, stirred and left for 24 hours to allow the precipitate (asphaltenes, preasphaltenes and residue) to be formed. To ensure that no change of sample properties occur during handling, such as oxidation or condensation of oxygen functional groups, a procedure was designed to avoid exposure to air, elevated temperatures or vacuum. The precipitate was filtered, washed with hexane and dried at room temperature in a stream of nitrogen for 24 hours. To correct analysis and extraction yields for adsorbed solvent, a portion of precipitate was dried in a vacuum ($<10^{-1}$ torr) at 100°C and the weight loss noted.

The following determinations were carried out on the hexane-insoluble precipitate. Figure 1 presents the procedure in block diagram.

1. Hydroxyl groups were determined by acetylation (8). The procedure was modified by using a larger excess of acetic anhydride.
2. Carbonyl groups were determined from the nitrogen uptake during reaction with hydroxylamine hydrochloride (9). We are aware that the amounts reported may not strictly correspond to carbonyl groups, but may include other functionalities. However, since carbonyl groups probably constitute the major part of the functionalities determined we will refer to all of them as carbonyls. This problem does not affect the conclusions expressed in a later part of this paper.
3. Benzene and pyridine solubilities were determined by exhaustive extraction under a nitrogen atmosphere in a Soxhlet apparatus.
4. High temperature ash was determined according to ASTM procedure D 271.

This value was used to calculate coal conversion to gases and hexane-solubles using the following equation derived from material balance considerations:

$$\% \left[\begin{array}{l} \text{hexane-solubles} \\ + \text{gases} \end{array} \right] = \frac{A_i - A_o}{A_o} \frac{10^4}{M_o} \quad 1)$$

where A_i = ash content of precipitate
 A_o = ash content of coal
 M_o = mineral matter in coal.

5. Elementary analyses including direct oxygen were determined using a Perkin-Elmer Model 240 microanalyzer.

The loss of total oxygen was calculated from the difference between direct oxygen determinations and is reported per total initial oxygen in coal. The values will include a portion of the inorganic oxygen, estimated to be no more than 5-10% of the total oxygen; this error will presumably be the same for coal and insoluble reaction products.

A special sample of liquefied coal was prepared to investigate the effect of hydrogen bonding on benzene solubilities. Samples were prepared by reacting coal with tetralin at 400°C for 10 minutes, and then following the above described procedure to obtain the hexane-insoluble precipitate.

We were able to introduce different quantities of trimethylsilyl groups on to the hydroxyl groups by varying the reflux time of 2g of sample in 40 cc tetrahydrofuran and 10 cc hexamethyldisilazane. After reaction, the contents were diluted with hexane, filtered and the residue was washed with hexane. Because some hexane-soluble materials were generated by the above procedure, the filtrate was collected and solvent plus unreacted hexamethyldisilazane removed by distillation, after which the undistilled material was weighed. The number of hydroxyl groups blocked was estimated from the change in H/C atomic ratios between a blank run (sample + THF), and the products of silylation (residue + dry solid from filtrate).

Differences in solubilities between blank and blocked samples are reported as the increase of benzene solubilities.

RESULTS AND DISCUSSION

Yields of pyridine-solubles, benzene-solubles and hexane-solubles plus gases are plotted *versus* the loss of oxygen for various contact times and temperatures in Figures 2a-d. There appear to be correlations between the various sets of data, from which it is tempting to draw mechanistic conclusions. Thus, as already noted, Fisher et al. (1) used a similar correlation to that in Figure 2a, between conversion to benzene-soluble products and loss of total oxygen content, to infer that splitting of ethers was a rate-determining step. But other correlations found here (Figures 2b and 2c) could support alternative hypotheses, such as that the elimination of hydrogen-bonding between hydroxyl groups is crucial to liquefaction. In any case, there is a correlation between loss of total oxygen and oxygen as OH (Figure 3). Thus we believe that in coal liquefaction, where a number of processes are undoubtedly occurring concurrently, unambiguous conclusions about mechanisms cannot be drawn directly from correlations such as those illustrated in Figures 2a-d. Nevertheless, we believe that useful conclusions can be drawn from the data, though in a less direct way.

In examining the magnitude of changes of the oxygen functionalities during generation of pyridine-soluble materials, we have observed that the major loss of

oxygen occurred with the so-called unaccounted oxygen (unaccounted = total - hydroxyl - carbonyl) and very little change was detected in the contents of hydroxyl and carbonyl groups at these stages of liquefaction (Figure 4). If we presume that the unaccounted oxygen is comprised primarily of the ether oxygen, then Figure 4 strongly suggests an important contribution of these functionalities to generation of pyridine-soluble materials. Although we cannot estimate an exact amount of the ether oxygen being cleaved, we can, however, estimate the maximum amount of the ether oxygen linkages being cleaved per 100 initial carbon atoms in coal. From a material balance we can show that:

$$\left[\begin{array}{c} \text{amount of ether} \\ \text{oxygen cleaved} \end{array} \right] \leq \left[\begin{array}{c} \text{total oxygen} \\ \text{loss} \end{array} \right] - \left[\begin{array}{c} \text{hydroxyl + carbonyl} \\ \text{oxygen loss} \end{array} \right] \quad 2)$$

making the reasonable assumption that the amount of oxygen in the hexane-solubles is insignificant. Figure 5 shows the right side of the above inequality *versus* generation of pyridine-soluble materials plus gases (conversion of coal). The regression equation for the line is:

$$y = - 0.230 + 0.0336x \quad 3)$$

The second coefficient (slope) has a standard deviation $\sigma = 0.0030$. The amount of ether oxygen linkages, ϕ , being cleaved per 100 initial carbon atoms was calculated from the slope using the equation:

$$\phi = \left(\frac{12}{16} \right) \times \left(\frac{10^4}{\% C} \right) \times (\text{slope}) \quad 4)$$

where % C = percent carbon in coal, dmmf.

Substituting % C = 83.47, slope = 0.0336

gives $\phi = 3.0 \pm 0.3$

This number is slightly larger than the amount estimated by Ignasiak et al. (4) in their study of products from reductive alkylation of a high-rank vitrinite, i.e., two ether linkages cleaved per 100 original C atoms. The difference in rank of vitrinites could explain the discrepancy. The question arises, is ether cleavage, in the amount indicated, sufficient to generate the observed yields of pyridine-soluble materials, or does the ether cleavage have only a contributing role, like that discussed below for the effect of hydrogenolysis of hydroxyl groups on generation of benzene-soluble materials.

It should be noted that the plot in Figure 5 is purely empirical. The points represent data obtained in runs at different temperatures and reaction times, so it is somewhat surprising that they lead to a linear regression of high significance. One possible inference from the finding is that the coal behaves in a manner characteristic of a uniformly cross-linked polymer.

We have conjectured from Figure 2c that since hydrogenolysis of hydroxyl groups cannot result in substantial lowering of the molecular weight, the effects observed are due to elimination of hydrogen bonding by removal of the hydroxyl groups. If this is true, then by replacing the hydroxyl hydrogen with a substituent like trimethylsilyl, we should decrease the number of hydrogen bonds and increase the benzene solubility. The results of the treatment with hexamethyldisilazane are shown in Figure 6. A marked increase of benzene solubility suggests that, during liquefaction, hydrogenolysis of hydroxyl groups can play an important role in the generation of benzene-soluble materials. (By extrapolation, the results indicate that over 80% of the total pyridine-soluble material could become benzene-soluble). However, if

we compare the rate (slope) of generation of benzene solubles when hydroxyl groups are blocked to the rate (slope) when hydroxyl groups are removed during liquefaction (dashed line, predicted from Figure 2c by correcting for yield of gases), we must concede that hydrogenolysis of hydroxyl groups during liquefaction cannot account for more than 40% of the benzene-soluble materials generated. The remainder, presumably, is generated via different mechanistic routes.

Suppose it should prove possible to make hydrogenolysis of hydroxyl groups more competitive by introducing selective catalysts. Would we gain anything from such a modification of the liquefaction process? In terms of hydrogen consumption the answer seems to be, yes. To produce more benzene solubles merely by hydrogenolysis of OH groups, we would have to add about 0.8% of hydrogen (w/w of pyridine-soluble materials). On the other hand, Whitehurst et al. (5) give 2.2% for the actual hydrogen consumption in the hydrogenolysis of asphaltols from a similar coal to benzene solubles under SRC liquefaction conditions.

In view of the large amount of experimental work involved, we have only studied one coal. One principal finding is that "unaccounted" oxygen, mostly ether, is removed much more rapidly in the early stages of liquefaction than other oxygen-containing groups, and a maximum amount of ether groups split has been estimated. It has been shown that hydrogenolysis of OH groups has an important effect on the solubility of liquefaction products. The quantitative, or semi-quantitative, aspects of these conclusions probably will not apply to other coals, but it seems likely that the qualitative identification of important phenomena will be relevant generally.

SUMMARY

A number of processes taking place during liquefaction are concurrent and, therefore, no mechanistic inferences can be made from simple relationships between generation of different classes of soluble materials and loss of coal functionalities, such as oxygen functional groups.

The amounts of ether oxygen being cleaved during the process are not larger than 3.0 ± 0.3 ether oxygen linkages per 100 initial carbon atoms in the coal studied, and loss of "unaccounted" oxygen, assumed to be principally ether, increases linearly with conversion, as measured by pyridine solubility.

Blocking of hydroxyl oxygen with trimethylsilyl groups results in an increase in the benzene solubilities of pyridine-soluble materials. However, comparison of the rates of increase when hydroxyl groups are blocked with the rates when hydroxyl groups are removed during liquefaction leads to the inference that during liquefaction no more than 40% of benzene-soluble materials are generated from benzene-insoluble, pyridine-soluble materials by the mechanism of hydrogenolysis of oxygen functional groups.

ACKNOWLEDGEMENT

This work was supported by U.S. D.O.E. under Contract No. EX-76-C-01-2494, for which the authors wish to express their appreciation.

REFERENCES

1. C. H. Fisher and A. Eisner, *Ind. Engng. Chem.*, 29, 1371 (1937). H. H. Storch, C. H. Fisher, C. O. Hawk and A. Eisner, *Bureau of Mines TP 654* (1943).
2. Y. Takegami, S. Kajiyama and C. Tokokawa, *FUEL (Lond.)*, 42, 291 (1963).

3. H. W. Sternberg, 172nd ACS Meeting, San Francisco, Aug. 1976, Fuel Chem. Div. Preprints Vol. 21, No. 7, 11.
4. B. S. Ignasiak and M. Gawlak, FUEL (Lond.), 56, 216 (1977).
5. D. D. Whitehurst, M. Farcasiu, T. O. Mitchell and J. S. Dickert, Jr., EPRI Report AF-480, July, 1977, "The Nature and Origin of Asphaltenes in Processed Coals".
6. D. C. Cronauer and R. G. Ruberto, EPRI Report AF-422, January, 1977, "Investigation of Mechanism of Reactions Involving Oxygen-Containing Compounds in Coal".
7. P. H. Given et al., Quarterly Progress Report to ERDA, FE-2494-2, "The Relation of Coal Characteristics to Coal Liquefaction Behavior", 1977.
8. J. Knotnerus, J. Inst. of Petrol., 42, 355 (1956).
9. L. Blom, L. Edelhausen and D. W. van Krevelen, FUEL (Lond.), 36, 135 (1957).

TABLE 1

Elemental Analysis, PSOC-330, Middle Kittanning Seam, Pa.
all data on dry mineral-containing basis

Mineral Matter	7.96%	Oxygen (direct)	9.03%*
Carbon	76.83%	Hydroxyl oxygen	3.8%
Hydrogen	4.97%	Carbonyl oxygen	1.2%
Nitrogen	1.71%	Vitrinite content	71.4%
Sulphur (organic)	0.67%	Pyridine solubility	13.2%
Oxygen (by difference)	7.86%	Pyritic sulphur	2.08%

*not corrected for interferences by mineral matter.

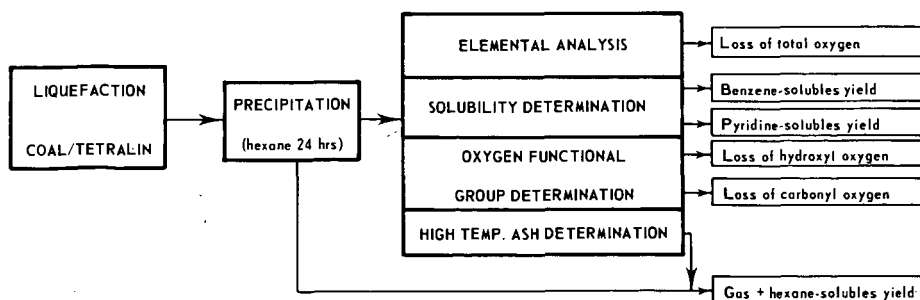


Fig. 1 PROCEDURE BLOCK DIAGRAM

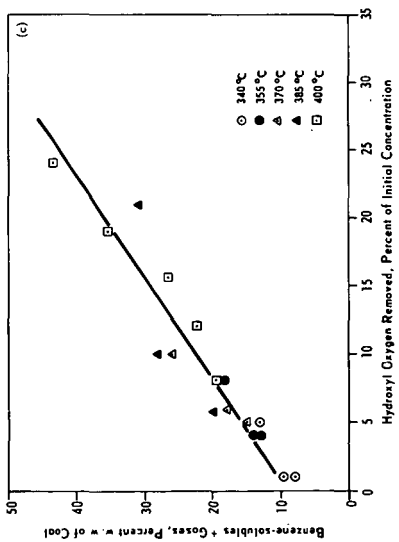
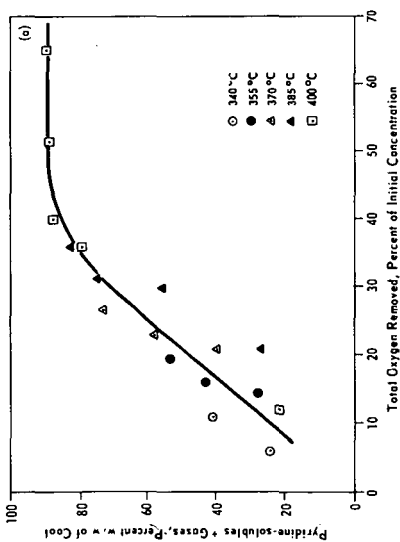
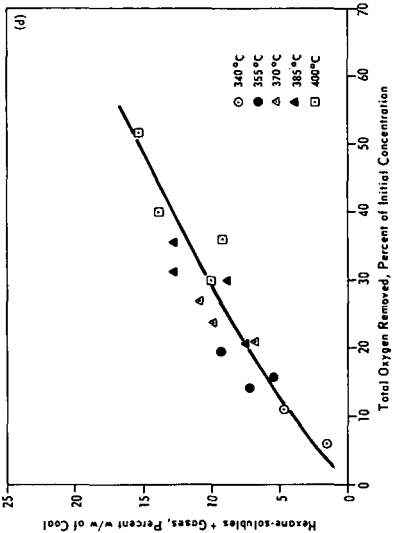
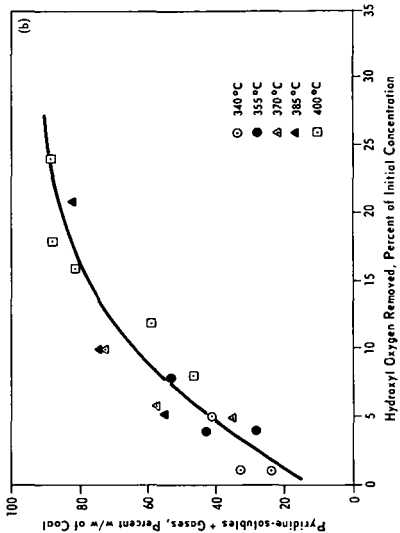


Fig. 2 RELATIONSHIPS BETWEEN GENERATION OF (a) PYRIDINE-SOLUBLE MATTER AND LOSS OF TOTAL OXYGEN, (b) PYRIDINE-SOLUBLE MATTER AND LOSS OF HYDROXYL OXYGEN, (c) BENZENE-SOLUBLE MATTER AND LOSS OF TOTAL OXYGEN, (d) HEXANE-SOLUBLE MATTER + GASES AND LOSS OF TOTAL OXYGEN, ALL ON DRY COAL BASIS

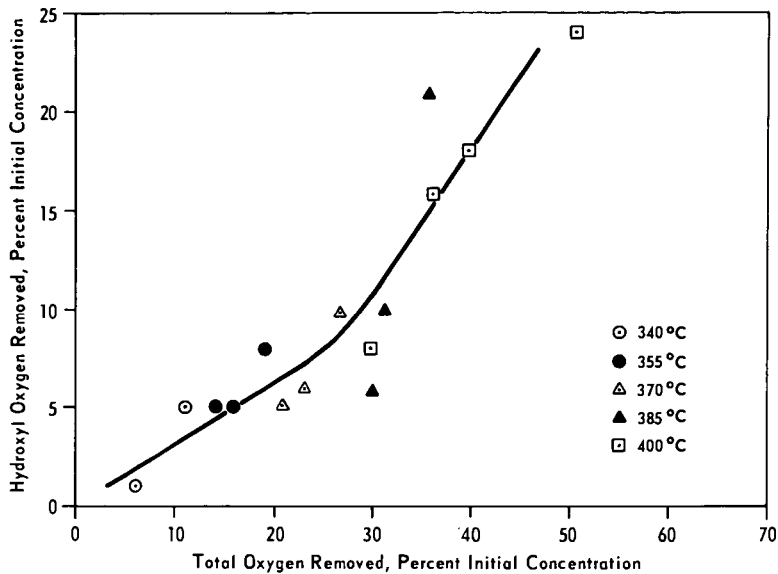


Fig. 3 RELATIONSHIP BETWEEN LOSS OF HYDROXYL OXYGEN AND TOTAL OXYGEN

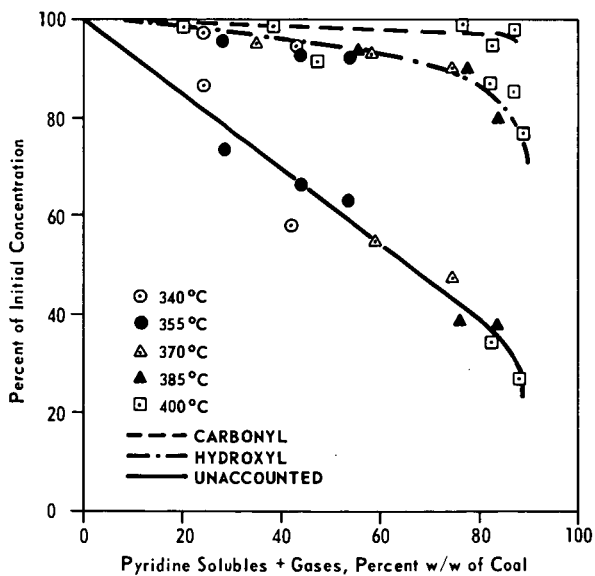


Fig. 4 LOSS OF OXYGEN FUNCTIONAL GROUPS VS GENERATION OF PYRIDINE SOLUBLE MATTER, DRY COAL BASIS

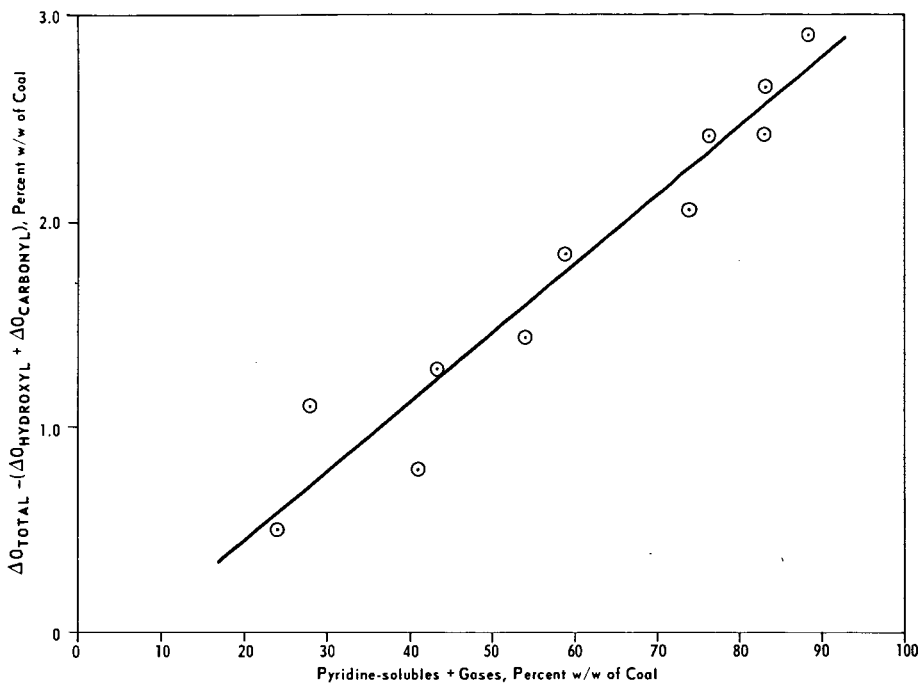


Fig. 5 RELATIONSHIP BETWEEN MAXIMUM ETHER OXYGEN CLEAVED AND GENERATION OF PYRIDINE SOLUBLES + GASES, PERCENT W/W OF COAL

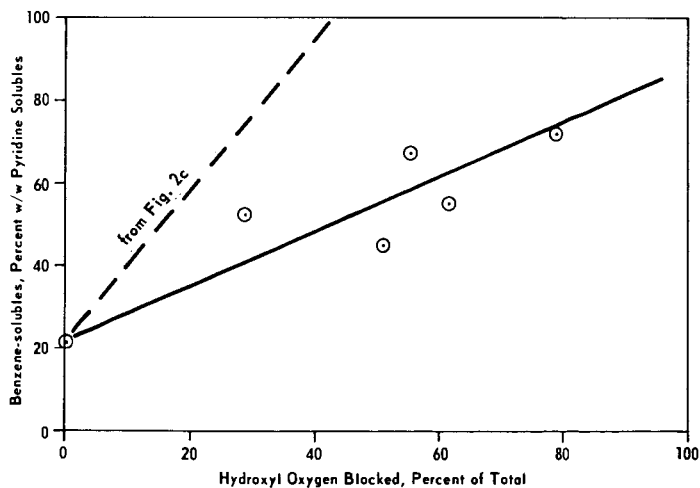


Fig. 6 EFFECT OF HYDROXYL HYDROGEN SUBSTITUTION ON BENZENE SOLUBILITIES

THE KINETICS OF COAL LIQUEFACTION IN A HYDROGEN DONOR SOLVENT

BY: A. ATTAR

Department of Chemical Engineering
University of Houston, Houston, Texas 77004

1. Introduction

One of the most important liquefaction processes involves the treatment of coal with hydrogen donors (HD). HD solvents are materials that can donate hydrogen at the reaction conditions. The industrially important HD's are those which can be regenerated with molecular hydrogen.

Quantitative data on liquefaction was published by Orchin (1944), Orchin and Storch (1948), Oele *et al.*, (1951), Curran *et al.*, (1966), Hill (1966) and Neavel (1976).

In hydrogen donor, liquefaction is believed to proceed by a free-radicals mechanism (Hill (1966), Curran *et al.*, (1966).) However, because of the complexity of the system coal-HD-ASH and catalyst, (when added), little quantitative work if any has been published on modeling coal liquefaction as a free radical depolymerization process. Several empirical models were published however, e.g., Curran *et al.* (1966), Hill (1966), Oele *et al.* (1951), Wen and Han (1975) and Yoshida *et al.* (1976).

The main objective of the present work is to present a fundamental approach to the modeling of coal liquefaction in hydrogen donors, which will permit predictions relevant to the processing of coals at different conditions. The discussion concentrates on liquefaction to heavy boiler fuel although it could be extended to modeling of liquefaction to gasoline.

2.1 Arguments of Material Balance

Conversion of coal to oils requires production of material with a smaller molecular weight and with a larger ratio of hydrogen to carbon. One hydrogen have to be added per each 3-6 carbon atoms in order to obtain the desired H/C ratio for boiler fuels.

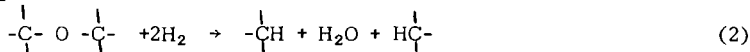
If it is assumed that on the average, each time a bond is broken, two fragments will be formed with approximately equal molecular weights, then each coal molecule will have to be broken 2-4 times to form heavy oil, or 3-6 times to form gasoline.

As an example, consider a "molecule" of bituminous coal with molecular weight of 3000 and ultimate composition of $\text{CH}_{0.88} \text{O}_{0.132} \text{N}_{0.016} \text{S}_{0.0174}$ (MWU= 15.77). Each such coal molecule will have an average of 190 carbon atoms. Typical hydrogenation products may have ultimate composition of $\text{CH}_{1.0} \text{O}_{0.09} \text{N}_{0.016} \text{S}_{0.016}$ (MWU= 14.34) and molecular weight of about 400, and will contain an average of 28 carbon atoms. Such product can be obtained if the original molecule is broken on the average 2.75 times and if 0.32-0.51 hydrogen atoms are added per each carbon atom in the original molecule.

Reduction in the molecular weight can be achieved by elimination of certain "side chained" functional groups, e.g. OH, C=O, SH etc., or by breaking the HC structure of the main molecule, e.g., by reactions like:



or by



Elimination of side chains can result in a reduction in the molecular weight of the order of 16-32 units/group. Breaking of the main chain could result in a much more significant reduction in the molecular weight. The products of the latter reaction could have half the molecular weight of the original molecules. Opening of rings with or without the elimination of a heteroatom does not change significantly the molecular weight.

Most of the oxygen is present in coal in the form of hydroxylic (-OH) ketonic (C = O), and to a lesser extent heterocyclic or etheric (C-O-C) groups (Dryden (1963), (p. 267)). However, products with significantly reduced molecular weight result only when etheric oxygens or sulfidic sulfur are eliminated. Elimination of an OH group requires two hydrogen atoms but elimination of other groups requires four hydrogen atoms.

Data on the concentrations of etheric and sulfidic sulfur indicate that elimination of the etheric oxygen and the sulfidic sulfur could in some cases be sufficient to produce products with sufficiently low molecular weight. However, some saturation of π and c-c bonds is also required in order to bring the H/C ratio to the desired range. If each coal molecule has to be broken 2-6 times to produce heavy oil, then breaking of 1-3 etheric oxygen (if present) bonds and 2-3 sulfur-carbon or carbon-carbon bonds will result in product with M.W. in the range required for boiler fuel. When low volatile bituminous coal is processed breaking of c-c bonds may occur more than 2-3/ coal molecule.

2.2 Fundamental Assumptions

The most important assumptions of the present model are:

1. each coal consists of an assembly of functional groups or bonds with a given initial distribution which is specific to the particular coal.
2. the kinetic parameters, the activation energy and the frequency factor, for the reaction of each functional group with a given reagent, are function only of the reagent and the group, and are independent of the specific coal involved. Once such parameters are evaluated they can be used to model the kinetics of the reactions of similar groups in every coal.
3. the coal "molecules" are large and therefore have a small translational motion. The donor molecules and radicals are much smaller and much more mobile in the solution.
4. the bonds of each coal molecule break according to the hierarchy of the bond energies in each molecule, the weakest bonds first.
5. the depolymerization proceeds by a free radicals mechanism for which the steady state approximation can be applied.
6. the rate of the chemical reaction controls and not the rate of mass transport.
7. the solvent is present in a large excess.

Several additional assumptions are introduced latter which apply to specific cases.

3. Development of the Kinetic Model

A model is developed which describes the depolymerization in solution of a single high molecular weight compound. Classical chemistry of free radicals reactions is built into the model, and that permits to attribute physical significance to some of the reaction parameters. The rate of change of the average molecular weight of the solution is then discussed, and the model is extended to include the kinetics of the redistribution of the molecular weight of a system which initially contains compounds with different molecular weights.

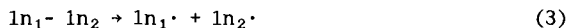
3.1 Chemistry of Free Radicals Depolymerization in a Hydrogen Donor

A free radicals reaction mechanism consists of three types of processes:

1. initiation reactions - which form more radicals than they consume.
2. propagation reactions - which do not affect the number of free radicals in the system.
3. termination reactions - which consume free radicals.

In the system coal-hydrogen-donor, initiation can proceed by various mechanisms, the most plausible ones are:

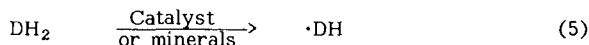
1. decomposition of very weak bonds in the coal macromolecule.



The radicals $1n_1\cdot$ react with the hydrogen donor, DH_2 , and form the donor radical $DH\cdot$.

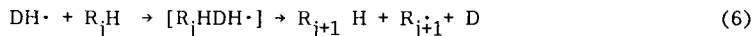


2. interaction between the hydrogen donor molecules, DH_2 , and the mineral matter or catalysts.



The number of weak bonds that can initiate a chain of radicals per unit mass of coal is finite and probably small. Therefore, the rate of initiation, by the decomposition of bonds decreases during the course of an isothermal decomposition. However, since the solvent is usually in a large excess, the rate of initiation by the interaction of the solvent and heterogeneous inorganic minerals is approximately constant.

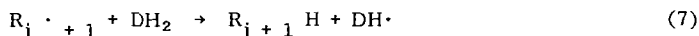
The radical $\cdot DH$ can break carbon-carbon and carbon-oxygen bonds. In the process, the donor molecules are converted into dehydrogenated donor molecules, D. The coal molecules break into smaller molecular fragments; i.e:



This is a propagation reaction.

The index j is used to denote the number of times that the macromolecule has been broken prior to that reaction. All the molecules $R_j H$ and the radicals $R_j\cdot$ are large (M.W. 300-3000) and contain several aromatic rings. It is therefore plausible to assume that they are not very mobile in the solution. Moreover, it is reasonable to assume that the activated complex that is formed in reaction (6), $[R_j HDH\cdot]$ dissociate at the weakest carbon-carbon or carbon-oxygen bond of the macromolecule. Therefore, the weakest bond in the $R_{j+1} H$ product is stronger than that in the parent molecule, $R_j H$. In other words,

the decomposition of the original coal macromolecule, R_0H , proceeds by the hierarchy of the strength of the bonds. The propagation step is completed by the fast reaction:



which replenishes the concentration of the radicals $DH \cdot$.

Since the radicals $R_j \cdot$ are much more bulky than $DH \cdot$, they are less mobile. Therefore, it is reasonable to assume that the dominant termination reaction is:



We were not able to detect the dimer di-tetralin in studies on model compounds. Therefore, reaction (8) describes the dominant mode of termination.

3.2 Modeling of The Depolymerization of a Single Component Macromolecule

Let the initiation reactions proceed at a rate $I = I(t)$, and assume that the steady-state approximation can be applied. Then, the rate of initiation has to be equal to the rate of termination, since the propagation reactions do not change the total concentration of free radicals and because termination is assumed to occur predominantly by binary collisions of $DH \cdot$, then:

$$2k_t [DH \cdot]^2 = I \quad (9)$$

$$[DH \cdot] = \sqrt{\frac{I}{2k_t}} \quad (10)$$

The rate of change of the component R_jH is described by the equation:

$$\begin{aligned} \frac{d[R_jH]}{dt} &= k_{pj-1} [DH \cdot] [R_{j-1}H] - k_{pj} [DH \cdot] [R_jH] = \\ &= \sqrt{\frac{I}{2k_t}} (k_{pj-1} [R_{j-1}H] - k_{pj} [R_jH]) \end{aligned} \quad (11)$$

Denote:

$$\Pi_j = \frac{[R_jH]}{[R_0H]_0} \quad (12)$$

$$d\theta = k_{po} \sqrt{\frac{I}{2k_t}} dt \quad (13)$$

Thus:

$$\frac{d\Pi_j}{d\theta} = \frac{k_{pj-1}}{k_{po}} \Pi_{j-1} - \frac{k_{pj}}{k_{po}} \Pi_j \quad \Pi_j = \beta_{j-1} \Pi_{j-1} - \beta_j \Pi_j \quad (14)$$

where:

$$\beta_j = \frac{k_{pj}}{k_{po}} \quad (15)$$

$$\text{Also: } \frac{d[R_0H]}{dt} = -k_{po} \frac{1}{2k_t} [R_0H] \quad (16)$$

$$\text{or: } \frac{d\bar{\Pi}_0}{d\theta} = -\bar{\Pi}_0 \quad (17)$$

$$\beta_0 = 1 \quad (18)$$

$$\text{Initially, } \bar{\Pi}_j = 0 \quad j > 0 \quad (19)$$

$$\bar{\Pi}_0 = 1 \quad j = 0 \quad (20)$$

Let us assume that an integration constant is chosen so that $\theta(t=0) = 0$. If the process is isothermal, then all the k 's are constant. Thus, it is possible to solve equation (15) by Laplace transform with respect to θ :

$$m \bar{\Pi}_j = \beta_{j-1} \bar{\Pi}_{j-1} - \beta_j \bar{\Pi}_j \frac{\beta_{j-1}}{m+\beta_j} \quad (21)$$

$$\bar{\Pi}_j = \frac{\beta_{j-1} \bar{\Pi}_{j-1}}{m + \beta_j} = \bar{\Pi}_0 \prod_{j=1}^j \frac{\beta_{j-1}}{(m+\beta_j)} \quad (22)$$

$$\text{But: } \bar{\Pi}_0 = \frac{1}{1+m} \quad (23)$$

$$\text{Therefore: } \bar{\Pi}_j = \frac{1}{1+m} \prod_{j=1}^j \frac{\beta_{j-1}}{m+\beta_j} \quad (24)$$

The last equation has poles at every $m = -\beta_j$, and will therefore have slightly different solutions when all the β_j are distinct and different or when some of them are identical. The solutions for the case where all the β_j 's are different and for the case where all the β_j 's $j \geq 1$ are the same as listed in tables 1 and 2.

Table 1: The Kinetics of Isothermal Coal Liquefaction by Successive Depolymerization in Hydrogen Donor Distinct and Different Rates for each Step*

j	$\bar{\Pi}_j$
0	$\bar{\Pi}_0 = e^{-\theta}$
1	$\bar{\Pi}_1 = \frac{1}{1-\beta_1} (e^{-\beta_1\theta} - e^{-\theta})$
2	$\bar{\Pi}_2 = \beta_1 \left[\frac{e^{-\theta}}{(\beta_1-1)(\beta_2-1)} + \frac{e^{-\beta_1\theta}}{(1-\beta_1)(\beta_2-\beta_1)} + \frac{e^{-\beta_2\theta}}{(1-\beta_2)(\beta_1-\beta_2)} \right]$
3	$\bar{\Pi}_3 = \beta_1\beta_2 \left[\frac{e^{-\theta}}{(\beta_1-1)(\beta_2-1)(\beta_3-1)} + \frac{e^{-\beta_1\theta}}{(1-\beta_1)(\beta_2-\beta_1)(\beta_3-\beta_1)} + \frac{e^{-\beta_2\theta}}{(1-\beta_2)(\beta_1-\beta_2)(\beta_3-\beta_2)} + \right]$

$$\left. + \frac{e^{-\beta_3\theta}}{(1-\beta_3)(\beta_1-\beta_3)(\beta_2-\beta_3)} \right\}$$

$$4 \quad \Pi_4 = \beta_1\beta_2\beta_3 \left\{ \frac{e^{-\theta}}{(\beta_1-1)(\beta_2-1)(\beta_3-1)(\beta_4-1)} + \frac{e^{-\beta_1\theta}}{(1-\beta_1)(\beta_2-\beta_1)(\beta_3-\beta_1)(\beta_4-\beta_1)} + \right.$$

$$\frac{e^{-\beta_2\theta}}{(1-\beta_2)(\beta_1-\beta_2)(\beta_3-\beta_2)(\beta_4-\beta_2)} + \frac{e^{-\beta_3\theta}}{(1-\beta_3)(\beta_1-\beta_3)(\beta_2-\beta_3)(\beta_4-\beta_3)} +$$

$$\left. \frac{e^{-\beta_4\theta}}{(1-\beta_4)(\beta_1-\beta_4)(\beta_2-\beta_4)(\beta_3-\beta_4)} \right\}$$

etc.

* $\beta_0=1, \beta_j \neq \beta_i, i \neq j.$

Table 2: The Kinetics of Isothermal Coal Liquefaction by Successive Depolymerization in Hydrogen Donor -

Initial Unique rate followed by steps with an identical rates*

j Π_j

0 $\Pi_0 = e^{-\theta}$

1 $\Pi_1 = \frac{1}{1-\beta} (e^{-\beta\theta} - e^{-\theta})$

2 $\Pi_2 = \frac{\beta}{(1-\beta)^2} e^{-\theta} + \beta e^{-\beta\theta} \left[\frac{\theta}{(1-\beta)} - \frac{1}{(1-\beta)^2} \right]$

3 $\Pi_3 = \frac{\beta^2}{(1-\beta)^3} e^{-\theta} + \beta^2 e^{-\beta\theta} \left[\frac{\theta^2}{2(1-\beta)} - \frac{\theta}{(1-\beta)^2} + \frac{1}{(1-\beta)^3} \right]$

4 $\Pi_4 = \frac{\beta^3}{(1-\beta)^4} e^{-\theta} + \beta^3 e^{-\beta\theta} \left[\frac{\theta^3}{6(1-\beta)} - \frac{\theta^2}{2(1-\beta)^2} + \frac{\theta}{(1-\beta)^3} - \frac{1}{(1-\beta)^4} \right]$

etc.

* $\beta_0 \neq \beta_j \quad j > 0$

$\beta_j = \beta_1 = \beta \quad i, j > 0$

3.3 Analysis of Models of the Initiation Reaction

Four models are proposed which describe various modes of initiations:

3.3.1 Decompositions of Unstable Bonds in the Coal:

It is assumed that initially a finite number of labile bonds exist per unit mass, and that these bonds decompose in a first order reaction.

$$I = - \frac{d[ln]}{dt} = 2k_i [ln] \quad (25)$$

Then, if the systems is isothermal:

$$[ln] = [ln]_0 e^{-2k_i t} \quad (26)$$

and:

$$d\theta = k_{po} \sqrt{\frac{I}{2k_t}} dt = k_{po} \sqrt{\frac{2[ln]_0 k_i}{2k_t}} e^{-k_i t} dt \quad (27)$$

$$\theta = \frac{k_{po}}{k_i} \sqrt{\frac{2[ln]_0}{2k_t}} (1 - e^{-k_i t}) \quad (28)$$

(Denoted as Model B)

3.3.2 Catalytic Interaction Between the Donor and Inorganic Materials:

When the minerals can catalyze the decomposition of the donor, the initiation rate constant will depend on the type of mineral matter, its surface area, quantity, and its porosity. The rate of initiation, I, will be more or less constant, since the concentration of donor and the mineral matter remains more or less constant. In such a case:

$$d\theta = k_{po} \frac{I_0}{2k_t} d\theta \quad (29)$$

and

$$\theta = k_{po} \frac{I_0}{2k_t} t \quad (30)$$

since $\theta(t=0) = 0$ (Denoted as Model A)

3.3.3 Combination Models of Initiation:

In reality, initiation can occur both by decomposition of unstable bonds and by catalytic reactions. In such a case, the rate of initiation will have the former:

$$I = I_0 + k_i [ln]_0 e^{-k_i t} \quad (31)$$

and:

$$d\theta = k_{po} \sqrt{\frac{I}{2k_t}} dt = k_{po} \sqrt{\frac{I_0 + 2k_i [ln]_0 e^{-2k_i t}}{2k_t}} dt \quad (32)$$

(Denoted as Model C) $\theta(t=0) = 0$

When the coal contains more than one type of bond that can dissociate and initiate a chain, one obtains:

$$I = 2k_{i_1} [1n]_{10} e^{-2k_{i_1} t} + 2[1n]_{20} k_{i_2} e^{-2k_{i_2} t} \quad (33)$$

and:

$$d\theta = \sqrt{\frac{\rho_0}{2k_t}} (2k_{i_1} [1n]_{10} e^{-k_{i_2} t} + 2k_{i_2} [1n]_{20} e^{-k_{i_2} t})^{\frac{1}{2}} dt \quad (34)$$

and

$$\theta(t=0) = 0 \quad (35)$$

(Denoted as Model D)

3.4 Modification of the Liquefaction Model to Real Coals

Extraction of coals with different solvents yield a given amount of the various fraction, e.g. asphaltenes, hexane solubles etc. If, it is assumed that the molecular weight and the functionality of these fractions are similar to that of the same fractions which are produced by the liquefaction of coal, then they will contribute to the rate of accumulation of the various fractions. To include these effects in the model, the dimensionless initial concentration of each group, Π_i^0 , have to be taken into account. The equations that result are listed in table 3. Note should be made that it has been assumed that each fraction depolymerize with a specific set of parameters which is a function only of the particular fraction. It could be shown (Attar, 1978) that fractions which are isolated by the "solvent soluble/insoluble" method should have molecular volume or weight and functionality in a given range. "Functionality" is defined in this context as the sum $\sum F_i N_i$, where N_i are the number of atoms of the i-th kind and F, the energy parameter as described by Small (1953): Whithurst et. al., (1976) examined SRC fractions and noted that the molecular weight and composition of the various fractions is independent of the conversion, in accord with the semi-theoretical prediction of Attar (1978). Therefore, in the following text it will be assumed that each j group could be identified with a given "solvent soluble/insoluble" fraction.

Table 3: Kinetics of the Depolymerization of Coal

$$\Pi_j^0 \neq 0 \quad \beta_j \neq \beta_i, \quad i \neq j$$

$$\begin{aligned}
 j & \quad \Pi_j \\
 0 & \quad \Pi_0 = \Pi_0 e^{-\theta} \\
 1 & \quad \Pi_1 = \frac{\Pi_1^0}{1-\beta_1} (e^{-\beta_1 \theta} - e^{-\theta}) + \Pi_1^0 e^{-\beta_1 \theta} \\
 2 & \quad \Pi_2 = \beta_1 \Pi_1^0 \left\{ \frac{e^{-\theta}}{(\beta_1 - 1)(\beta_2 - 1)} + \frac{e^{-\beta_1 \theta}}{(1 - \beta_1)(\beta_2 - \beta_1)} + \frac{e^{-\beta_2 \theta}}{(1 - \beta_2)(\beta_1 - \beta_2)} \right\} + \\
 & \quad + \frac{\Pi_1^0 \beta_1}{\beta_1 - \beta_2} (e^{-\beta_2 \theta} - e^{-\beta_1 \theta}) + \Pi_2^0 e^{-\beta_2 \theta}
 \end{aligned}$$

$$\begin{aligned}
 3 \quad \Pi_3 = & \beta_1 \beta_2 \Pi_0^0 \left\{ \frac{e^{-\theta}}{(\beta_1-1)(\beta_2-1)(\beta_3-1)} + \frac{e^{-\beta_1\theta}}{(1-\beta_1)(\beta_2-\beta_1)(\beta_3-\beta_1)} + \right. \\
 & \left. \frac{e^{-\beta_2\theta}}{(1-\beta_2)(\beta_1-\beta_2)(\beta_3-\beta_2)} + \frac{e^{-\beta_3\theta}}{(1-\beta_3)(\beta_1-\beta_3)(\beta_2-\beta_3)} \right\} + \\
 & \Pi_1^0 \beta_2 \beta_1 \left\{ \frac{e^{-\beta_1\theta}}{(\beta_2-\beta_1)(\beta_3-\beta_1)} + \frac{e^{-\beta_2\theta}}{(\beta_1-\beta_2)(\beta_3-\beta_2)} + \frac{e^{-\beta_3\theta}}{(\beta_1-\beta_3)(\beta_2-\beta_3)} \right\} + \\
 & \frac{\Pi_2^0 \beta_3}{\beta_2-\beta_3} (e^{-\beta_3\theta} - e^{-\beta_2\theta}) + \Pi_3^0 e^{-\beta_3\theta}
 \end{aligned}$$

and so on.

4. Estimation of Parameters

The parameters which are needed are divided into two groups:

1. parameters associated with the propagation - β_j , $j \geq 1$.
2. parameters associated with the initiation and the termination

The kinetics parameters associated with the propagation reaction depend mainly on the structure of the molecules. The kinetic parameters associated with the initiation and the termination depend on the structure of the molecules and will have a different form which depends on which initiation mechanism is assumed.

4.1 Estimation of the Propagation Parameters

The rate limiting step in the propagation is reaction (6)

The corresponding rate parameter is β_j :

$$\beta_j = \frac{k_{pj}}{k_{po}} = \frac{A_{pjo} e^{-\frac{E_{pj}}{RT}}}{A_{po} e^{-\frac{E_{po}}{RT}}} = \frac{A_{pjo}}{A_{po}} e^{-\frac{(E_{pj} - E_{po})}{RT}} \quad (36)$$

It is convenient to evaluate separately the values of A_{pjo}/A_{po} and $E_{pj}-E_{po}$.

4.1.1 Depolymerization of Analogue Bonds.

Application of the polyani relation yield:

$$E_{pj} - E_{po} = \alpha(\Delta H_j - \Delta H_o) \quad (37)$$

If the absolute rate theory is applied to equation (36) and it is assumed that the activated complex is similar to the molecule R_jH , one obtains for the frequency factor

$$A_{po} = A_{pjo} \cong \frac{kT}{hQ_{DH}} \quad (38)$$

The last equation shows that to a first order approximation the frequency factor is independent of j , therefore,:

$$\beta_j = e^{-\frac{\alpha (\Delta H_j - \Delta H_o)}{RT}} \quad (39)$$

4.1.2 Depolymerization by the Hierarchy of the Functional Groups

Following the initial solubilization of the coal, the various functional groups will compete for the hydrogen donors radicals. However, if the heat of reaction of the depolymerization of a particular group is much smaller than that of the other groups it will be eliminated at a much larger rate than the others.

The functional groups which are believed to be present in coal in substantial concentrations can be arranged in the order of increasing stability toward an attack by a hydrogen donor radical. The author calculates that at the initial stages of the liquefaction etheric bonds are broken first and subsequently methelenic bridges are broken at the benzylic position along with sulfidic sulfur. Other groups like -OH, C=O also react, but their elimination will not result in a major decrease in the molecular weight of large coal molecules. If the first bond that is broken is an etheric bond, the second will be either etheric or benzylic and the third, and subsequent bonds that are broken are benzylic bonds. Based on these arguments, the activation energies for breaking the various bonds will probably be $j=0$, 7.8 kcal/mole, $j=1$, 9.0 kcal/mole, $j=2$, 9.9 kcal/mole, $j=3$, 10.5 kcal/mole, $j=4$, 11.1 kcal/mole.

4.2 Estimation of the Initiation and Termination Parameters

The rate of termination was assumed to be diffusion controlled and equal to $2 \cdot 10^9$ lit/mole sec.

The parameters associated with different initiation models are different and can not be estimated by simple assumptions. Two types of parameters are needed: rate constants and initial concentrations. The values of the rate constants for the decomposition of specific bonds is independent of the coal used. However, different values of the initial concentrations are expected to be present in different coals.

The rates of initiation by the decomposition of weak bonds are determined by the thermodynamic bond-dissociation energy and entropy. If initiation occurs by the decomposition of bonds which become unstable around 350°C, for example:



The activation energy of such reactions will be about the same as the bond energy. For reaction (40), $E_a \sim \Delta H \sim 76.4$ kcal/mole. at 400°C. Also, $\Delta S \sim 41.57$ cal/mole°k and by $\log k_o \sim 22.26$. The rate constant for the decomposition at 400°C is $2.87 \cdot 10^{-3}$ sec⁻¹. Since the number of moles of such relatively weak bonds is finite, and depend on the aromaticity of the coal, the number of chains that could be initiated by such a mechanism is finite and depend on the aromaticity of the coal. For coals with an aromaticity of 0.84 and H/C ~ 0.757 the concentration of such groups can not exceed $8 \cdot 10^{-2}$ mole/mole carbon and will probably be no larger than $3 \cdot 10^{-2}$ mole/mole

carbon. The concentration of such groups is in effect smaller since the solvent further dilutes the solution.

The value of the kinetic parameters which determine k_{po} is assumed to be $E_{po} = 7.8$ kcal/mole $A_{po} = 2.2 \cdot 10^7$ (lit./mole sec).

5. Results and Discussion of the Results

In order to apply the model one needs to have data on the initial condition of the coal and on the conditions of the reaction. The data needed on the initial condition of the coal are: 1. the ultimate analysis and the aromaticity. 2. the mineral content and composition; and 3. the distribution of oxygen and sulfur functional groups. Detailed accurate knowledge of the groups distribution is not necessary since the mathematical model lumps many molecules and reduces the sensitivity to the value of β_1 . The data needed on the condition of the reaction are 1. the temperature, 2. the solvent, 3. the pressure and type of gas, and 4. the catalyst.

The concentration of etheric oxygen determine the kinetic parameters chosen for the first and possibly the second propagation step.

The temperature and the solvent determine the values of the rate constants and of the relative rate parameters β_1 . The type of gas and its pressure determine whether solvent regeneration should be included in the model or not. The effect of hydrogen is more important when catalyst is present and/or when deep liquefaction is considered. The catalyst effects mainly the rate of initiation and in a sense, (its effect) is analogous to that of certain components of the mineral matter, e.g. FeS_2 and FeS . Catalysts will permit the liquefaction process to continue after the labile bonds decomposed.

5.1 Case Study: Analysis of the Liquefaction of a Bituminous Coal

The coal is treated in this case study as a single macromolecule so that the relationships among the various fractions will be more clear. The data used are described in table 4. The results of applying the model are described in figures 1 and 2. Figure 1 shows the dimensionless amount of the various fractions in a batch operation, as a function of the dimensionless time parameter θ . To obtain the dependence of θ on the real time t , use Figure 2 which shows the dependence of t on θ for various initiation models. Figure 2 shows also the change in the dimensionless average molecular weight of the SRC as a function of time.

Acknowledgement: The author wishes to thank the U.S. DOE for its support of this work. (Grant No. EF-77-G-01-2735). The author is in debt to Mr. David Agar, to Mr. Steven Shen and to Mr. Glenn Swin for their help in the calculations.

Note: Because of space limitations, several sections of the manuscript, case studies and calculations have been removed. The complete paper will be published soon. The main sections that were omitted include the rate of desulfurization and deoxygenation, the change in the molecular weight, several case studies, and the references.

Table 4: Case Study: Liquefaction of a Medium Volatile Bituminous Coal in Tetralin at 427°C

Approximate initial ultimate analysis:

$C_{1}H_{0.88}O_{0.132}N_{0.0160}S_{0.174}$ Ash: 14.7 wt.% Pyritic Sulfur: 1.3 wt.%

j	Bond Broken	Initial Conc. of Fractions	Epj Kcal/mole	Apo lit/mole sec)
0	-O- very weak	100	7.8	$2.2 \cdot 10^7$
1	-O- weak	-	9.0	
2	$\phi-CH_2CH_2\phi$	-	9.9	
3	$\phi-CH_2-\phi$	-	10.5	
4	$\phi-CH_2-\phi$	-	11.1	

Initiation and Termination Models:

$$I_0 = 8 \cdot 10^{-6} \quad I = I_0 + k_{i1} [lni]_0 e^{-k_{i1} t} \quad k_{i1} = k_{i10} e^{-\frac{E_{i1}}{RT}} =$$

$$[lni]_0 = 0.01 \quad 2k_t = 2 \cdot 10^9 \quad k_{i10} = 2 \cdot 0 \cdot 10^{22} \text{ sec}^{-1} \quad E_{i10} = 76.4 \text{ kcal/mole.}$$

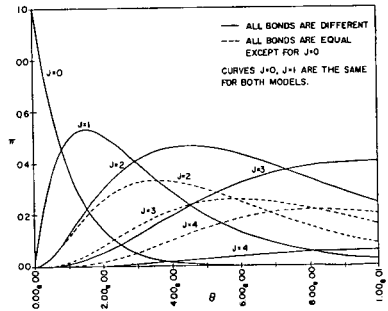
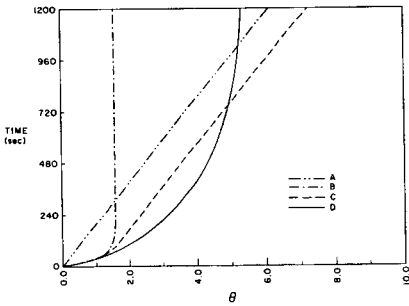


Figure 1: The Kinetics of Coal Liquefaction in Hydrogen Donor

Molecular Weight Distributions of Reductively
Alkylated and Depolymerized Coals

J.W. Larsen, P. Choudhury¹ and L. Urban¹

Department of Chemistry, University of Tennessee
Knoxville, Tennessee 37916
and
Oak Ridge National Laboratory*, P.O. Box X
Oak Ridge, Tennessee 37830

The intellectual starting point for this work is our belief that bituminous coals consist of largely aromatic "clusters" linked together by various bridges to form a three dimensionally cross-linked macromolecular network in which some extractable molecules are dissolved. The simplest way of making the coal soluble is to cleave enough bridges to destroy the network. Soluble fragments should result. By looking at the molecular weight distribution of these fragments produced by selectively cleaving bridges, the relative importance of the various types of bridges can be determined. Two well developed ways for accomplishing such cleavage are the well known Heredy-Neuwirth depolymerization² and the Sternberg reductive alkylation,³ which cleave methylene bridges and primarily ethers respectively. Their chemistry has been reviewed.⁴ We will concentrate here on the Heredy-Neuwirth depolymerization.

Figure 1 shows the results of depolymerizing Bruceton coal. The fraction soluble in benzene ethanol (70/30 v/v) is stable and passes through a 0.5 μ filter. The pyridine "solution" is stable, in that nothing precipitates on standing. However 6.8% of the "dissolved" material is removed by a 2.7 μ filter. The remaining solution will not pass a 0.5 μ filter. Ultracentrifugation of the pyridine "solution" (60,000 rpm; 3 hrs) results in precipitation of 40% of the pyridine solubles. Before centrifugation, the number average molecular weight (M_N) of the pyridine "solubles" was 400, quite comparable with results reported by others.⁵ After centrifugation, M_N was 1,000. The increase is due to the removal of colloidal material and the latter number is the true M_N for the dissolved material. Similar results have been obtained with a vitrinite sample (PSOC 126). As a result of these observations, all M_N values reported for products of Heredy-Neuwirth depolymerization must be regarded as questionable and probably erroneous. We are currently determining whether the colloidal material emerges from the coal unchanged or whether it is a reaction product.

The molecular weight distribution measured for the benzene-ethanol soluble fraction of depolymerized Bruceton coal by gel permeation chromatography (μ -Styragel columns 10⁵, 500, 100 A^o, THF solvent) followed by vapor pressure osmometry of individual fractions is shown in Fig. 2. Several important points emerge. First, there must be association in THF as indicated by the higher M_N for the fraction in that solvent. Separation on the gpc columns is only partly on the basis of size. Finally, silylation of the depolymerized coal does not decrease its M_N in pyridine, apparently there is little association via hydrogen bonds involving CH groups in that solvent.

Acknowledgment. We thank the U.S. Department of Energy for support of this work.

*Operated by Union Carbide Corporation under contract W-7405-eng-26 with the U.S. Department of Energy.

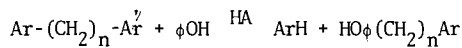


Figure 3. The Depolymerization Reaction

Coal	C (wt %, daf)	Alkylation technique	Solvent	Mol. wt.	Extract- ability (wt %)
W. Va. lvb	90.6	HNO ₃ -φOH/BF ₃ -Ac ₂ O	CHCl ₃	530	14
Clarian hvb	60.0	HNO ₃ -φOH/BF ₃ -Ac ₂ O	CHCl ₃	1725	84
Ohio 8 Hvab	80.9	HNO ₃ -φOH/BF ₃ -Ac ₂ O	CHCl ₃	645	95
McFarlane Hvcb	67.3	HNO ₃ -φOH/BF ₃ -Ac ₂ O	CHCl ₃	375	96
Japanese	75.8	φOH/PTS	Pyridine	320	98
	78.0	φOH/PTS		340	100
	81.7	φOH/PTS		440	90
	81.9	φOH/PTS		450	96
	83.1	φOH/PTS		460	98
	84.6	φOH/PTS		500	92
	86.2	φOH/PTS		480	98
	89.6	φOH/PTS		1100	32
Lignite	71	φOH/BF ₃	φOH	300	21
			φH-MeOH	300	48
Sub-bituminous	77	φOH/BF ₃	φOH	350	2
		φOH/BF ₃	φH-MeOH	290	15
High-volatile vitrain	82	φOH/BF ₃	φOH	920	13.5
		φOH/BF ₃	φH-MeOH	525	25
High-volatile bituminous	85	φOH/BF ₃	φOH	930	7
		φOH/BF ₃	φH-MeOH	730	15
High-volatile bituminous	86	φOH/BF ₃	φOH	750	19
Low-volatile bituminous	91	φOH/BF ₃	φOH	360	5.4

Figure 4. Phenol Free Molecular Weights (Number Average) of Depolymerized Coals (From J.W. Larsen and E.W. Kuemmerle, Fuel, 55, 162 (1976)).

Figure 5. Molecular Weight Distribution of the True Pyridine Solubles After Centrifugation

Fraction No.	Wt. %	Cumulative Wt. %	\bar{M}_N
1	< 0.5		
2	14.7	14.7	> 3000
3	20.3	35.0	> 3000
4	15.2	50.2	> 3000
5	15.5	65.7	2960
6	12.8	78.5	2440
7	7.0	85.5	880
8	5.9	91.4	560
9	4.3	95.7	560
10	2.7	98.4	370
11	1.6	100.0	370

References

1. University of Tennessee.
2. L.A. Heredy and M.B. Neuworth, *Fuel*, 41, 221 (1962).
3. H.W. Sternberg, C.L. Delle Donne, P. Pantages, E.C. Moroni, and R.E. Markby, *Fuel*, 50, 432 (1971).
4. J.W. Larsen and H.W. Kummerle, *Fuel*, 55, 162 (1976).

Characterization of Solvent Refined Coal by High Pressure Liquid Chromatography and other Analytical Techniques

C.D. Hathaway, C.W. Curtis, S. Meng, A.R. Tarrer, and J.A. Guin

Chemical Engineering Department
Auburn University
Auburn, Alabama 36830

Solvent Refined Coal (SRC) has previously been investigated by gel permeation chromatography (GPC)(1-3) and open column liquid chromatography (4,5). These studies have concentrated on comparison among various untreated coals and SRC's along with the determination of classes of chemical compounds present in SRC. In this paper the basic chemical nature of SRC is investigated, both on a molecular size basis and on a component basis.

By determining the basic chemical characteristics of SRC, important ground work can be laid for understanding the structure of SRC and for a fundamental understanding of the parent coal. Through knowledge of the molecular size distribution of SRC it may be possible to determine the process parameters which control the product composition. Knowledge of the chemical entities composing SRC, should make it possible to better structure the process so as to enhance product quality.

To provide a better understanding of the chemical makeup of SRC, this work presents an in-depth study of its chemical characteristics. SRC is analyzed at three different separation levels: 1) initially, the THF soluble portion of SRC is analyzed by GPC and the molecular size distribution is obtained; 2) GPC is used as a preanalysis step in which individual fractions are collected according to their elution time for subsequent detailed analysis; and 3) the SRC fractions are separated into component peaks or chromatographic bands by high pressure liquid chromatography (HPLC) and gas chromatography (GC).

Experimental

Materials Studied

Four SRC's, Amax, Western Kentucky 9/14, Monterey and Illinois #6, and their respective feed coals were obtained from the Wilsonville SRC Pilot Plant. The light recycle oil was obtained from Southern Services, Inc.

Chromatographic Analyses

GPC and HPLC were performed on a Waters ALC/GPC 202 high pressure liquid chromatograph equipped with a differential refractometer and a Schoeffel Spectroflow SF 770 variable wavelength ultraviolet-visible detector. For dual wavelength analyses, an Altex Model 153 Analytical UV Detector was used with a 254 nm filter. All chromatographic solvents were prefiltered through a 0.2 μm Fluoropore filter before use.

GPC was performed using three μ -styragel columns, sizes 500 \AA , 100 \AA , 100 \AA , in series with tetrahydrofuran (UV grade, Burdick and Jackson) as mobile phase. Injection volumes and effective concentrations for analytical separations and for preparative analysis were 10 μl at 10 mg/ml and 100 μl at 50 mg/ml, respectively. Polyethylene glycol standards of molecular weights 285-315, 380-415, 570-670, 950-1050 and 3000-3700 from Union Carbide, and various polynuclear aromatics were used as calibration standards.

HPLC was performed for each of the six fractions obtained from GPC analysis. Reverse phase chromatography was employed for fractions 5 and 6 using two μ -Bondapak C₁₈ columns (30 cm long, 4 mm in diameter) with a mobile phase of equal volume portions of acetonitrile (nanograde, Mallinckrodt), 2-propanol (spectroquality, J.T. Baker) and water (glass-distilled). Ultraviolet detection, set at 254 nm and

0.1 AUFS, monitored the sample.

Fractions 1-4 were separated by normal phase chromatography employing a μ -porasil column (30 cm in length and 4 mm diameter) and a two-component mobile phase of hexane and 2-propanol. Isocratic solvent systems ranging from 100% hexane to 75% hexane/25% 2-propanol were used to effect a separation.

Gas chromatographic analysis of fractions 5 and 6 was performed on a Varian Model 1800 GC equipped with a flame ionization detector (FID) with nitrogen as the carrier gas. A Varian Model 3700 GC equipped with a flame photometric detector (FPD) with helium as the carrier gas was used for sulfur compound analysis. In both analyses, temperature programming and a methyl phenyl silicon column (10 feet by 1/8 inch) were used.

Analytical Methods Used in Fractional Analysis

Elemental analysis was performed on a Perkin Elmer Model 240 Elemental Analyzer equipped with a Microbalance and a Model 31 Tektronix Calculator. Samples were prepared by open-air evaporation of the THF from each fractional residue.

Fluorescence spectroscopy was performed on a Farrand Mark I Fluorescence Spectrometer with a standard quartz sample cell. Sample preparation consisted of dissolving each fraction in THF at concentration levels ranging from 1 to 10 mg/ml.

Infrared spectroscopy for fractions 1-4 was performed on a Digilab FTS 10 System I Fourier Transform infrared spectrometer (FTIR) and fraction 5 on a Perkin-Elmer 621 infrared spectrometer. Fractions 1-4 were run as KBr pellets and fraction 5 as a thin film.

Mass spectral analysis was performed on approximately 100 mg of each fraction with a Dupont Model 21-491 Mass Spectrometer equipped for solid sampling.

Ultraviolet spectroscopy was performed on a Cary 17 UV/Vis Recording Spectrometer using a standard 1 cm path length quartz cell and UV grade THF as solvent.

Results and Discussion

In this study, GPC is used as a method for the characterization of four SRC's and their respective feed coals, as well as a means of preliminary separation for the SRC's. The molecular size distributions of the tetrahydrofuran soluble portion of Amax, Illinois #6, Western Kentucky 9/14 and Monterey SRC's as determined by GPC is shown in Figure 1. The molecular size distributions of Western Kentucky SRC and Monterey SRC have higher molecular weight distributions than those of Illinois #6 and Amax SRC.

A comparison of the molecular size distributions of the THF soluble portion of SRC to the THF soluble portion of the feed coals is also shown in Figure 1. A large difference in the relative solubility of SRC and the feed coal is observed (See Table 1). The differences in the molecular weight distributions of the coals and SRC's are portrayed by their initial and final elution times as shown in Table 2. Two SRC's, Amax and Illinois #6, and one coal, Amax, show substantial differences in elution time. Both SRC's are delayed in initial elution time and continue past the experimental elution time for the smallest aromatic compound, benzene. The final elution time of Amax coal is also delayed - 33.0 minutes - compared to approximately 30.0 minutes for the other coals. These increased elution times can be attributed to partial adsorption of the components on the μ -styragel columns.

GPC Fractional Analysis

To analyze the chemical nature of solvent refined coal, the SRC must first be subdivided into smaller analyzable fractions. To accomplish this, the GPC eluent of Amax SRC was arbitrarily divided into six fractions. These fractions were collected at three minute intervals beginning at approximately 15.5 minutes, where the SRC eluent was first detected by the differential refractometer. The elution times of the Amax SRC fractions are compared in Figure 2 to the elution times of calibration standards and to known SRC asphaltene and oil fractions from Soxhlet extractions. The elution times from an autoclave reaction mixture, which most

closely approximates SRC process conditions, show that asphaltenes elute between 15.5 and 26.6 minutes and that the oil elutes between 23.6 and 32.2 minutes. Therefore, according to their elution times, Amax SRC GPC fractions 1-3 primarily consist of asphaltenes*, fraction 4 is a combination of oil compounds and asphaltenes, and fractions 5 and 6 are primarily composed of the oil fraction consisting of small condensed ring systems. (6)

Mass Spectrometry

Each GPC fraction was analyzed by electron impact mass spectrometry. The largest m/e value obtained for each fraction as shown in Table 3 is essentially limited by the volatility of each fraction at the maximum probe temperature 3000°C. This fact is exemplified by the nearly equivalent m/e values obtained for Amax SRC and GPC fraction 5 - 579 and 580 respectively. Residues remained on the mass spectrometer probe from each fraction and SRC sample indicating that only a portion of each sample was analyzed. Since all of the fractions, including the two oil fractions 5 and 6, have high molecular weight compounds, the GPC fractions of Amax SRC cannot be easily correlated to a molecular weight separation.

The mass spectral fragmentation pattern of fractions 1 and 5 are shown in Figure 3. These fragmentation patterns clearly illustrate the substantial differences in the chemical compositions of the GPC fractions. The fragmentation pattern of fraction 1 has mass peaks covering the entire mass range while fraction 5 has an intense cluster of mass peaks resembling a Gaussian distribution between mass number 150 to 400. The fragmentation pattern of fraction 2 closely resembles that of fraction 1; whereas, the fragmentation pattern 4 is similar to fraction 5. The fragmentation patterns of fractions 3 and 6 are both weak and sparse. These fragmentation patterns give an indication of the compounds composing the fractions. Fractions 1 and 2 contain easily fragmented compounds - such as heteroatom-containing aromatics or substituted aromatics. The concentrated Gaussian distribution of mass peaks in fractions 4 and 5 appears to be a true distribution of the molecular ions of the compounds present in the fractions, suggesting that these fractions contain compounds which give strong parent peaks and which do not easily fragment such as polynuclear condensed ring aromatics.

Fluorescence and Ultraviolet Spectroscopy

The fluorescence emission spectra of fractions 3, 4, and 5 are shown in Figure 4. The apparent fluorescence maxima for the three fractions range from 434 nm to 450 nm and the fluorescence bandwidths at half-height range from 144 to 168 nm. These values correspond to the apparent wavelength maxima and bandwidths of various polynuclear aromatics and coals as described by Retcofsky (7). Retcofsky and co-workers have shown that the apparent fluorescence wavelength maxima for polynuclear aromatic compounds of three or more condensed rings range from 383 to 482 nm. Retcofsky reports that the pyridine extracts from 5 coals have an apparent wavelength maxima ranging from 390 to 455 nm (with four of the coals ranging from 440-455 nm) and have an apparent bandwidth at half-intensity between 120-140 nm. Comparison of the apparent emission maxima and bandwidth of the SRC fractions (see Figure 4) to the fluorescence of the coals and standard polynuclear compounds gives strong evidence that the types of compounds present in fractions 3, 4 and 5 are polynuclear aromatic compounds of three or more condensed rings.

Ultraviolet spectroscopy of the Amax SRC GPC fractions compared to Amax SRC (THF soluble portion) and recycle oil show (Figure 5) considerable variation in the band structure. The UV spectra of fraction 1 shows definite band structure at 217, 243, and 262 nm; fraction 2 has absorption bands at 218, 242 and 264 nm. Fractions 3, 4, 5 and 6 show no band structure. The absorption bands of Amax SRC - 217, 241 and 261 nm - are very similar to fractions 1 and 2. In contrast,

* Preasphaltenes are not considered due to their insolubility in THF.

the numerous absorption bands of light recycle oil are shifted to longer wavelengths - 272, 278, 283, 285, 319 and 336 nm. This shift agrees with the fact that the oil is composed essentially of condensed polynuclear aromatic compounds of 2, 3, and 4 rings (6). The band structure in fractions 1 and 2 and Amax SRC is obviously due to a prominent functional group present in these samples but absent or in much lower concentration in the other GPC fractions and light recycle oil.

Elemental Analysis and Infrared Spectroscopy

Elemental analysis performed on each GPC fraction indicates considerable variation in the carbon and nitrogen percentages (see Table 4). Fractions 1-3 have a significantly lower carbon percentage than do fractions 4 and 5. In contrast, the percentage of nitrogen is definitely higher in fractions 1 and 2 as compared to fractions 4 and 5. The hydrogen values vary among the different fractions but not in any predictable fashion.

Infrared analysis of Amax GPC fractions 1-5 shows distinctive differences in the aliphatic band stretches, CH_2 at 2920 cm^{-1} and CH_3 at 2960 cm^{-1} , and the aromatic CH stretch at $3000\text{--}3100\text{ cm}^{-1}$. Table 5 shows the ratio of the aromatic C-H to the aliphatic CH_2 stretch and the ratio of CH_3 to CH_2 stretch for the Amax GPC fractions. Information concerning the types of compounds present in these fractions can be obtained from the ratios of the band stretches. With increasing elution time, GPC fractions 1-5 show increased aromaticity. A substantial increase in the CH/CH_2 ratio is seen in fraction 5. The CH_3/CH_2 ratio increases in fractions 1-3 and levels off at fraction 4; however, fraction 5 shows a dramatic increase in the CH_3/CH_2 ratio. These ratios along with the elemental analysis (see Table 4) give strong evidence that fractions 1 and 2 have either more heteroatoms or less aromatic compounds than do fractions 3, 4, and 5. Fractions 1 and 2 also have a greater percentage of methylene groups indicating that they have either longer hydrocarbon chains or more saturated cyclic groups in comparison to the other fractions. Fractions 3 and 4 have increased aromatic structure and shorter side-chains or fewer saturated cyclic compounds than 1 and 2. The large change in both the aromatic/ CH_2 and the CH_3/CH_2 ratios show that fraction 5 is totally different from the other fractions. Fraction 5 is largely aromatic with more methyl than methylene groups.

HPLC and GC Chromatographic Analysis of GPC Fractions

The Amax SRC GPC fractions are further separated by HPLC and GC into their component species (fractions 5 and 6) or into chromatographic bands (fractions 1-4). Since the elution times of fractions 5 and 6 correspond to that of oil and since both 5 and 6 are soluble in the reverse phase solvents, reverse phase affinity mode separations are successfully used.

As shown in Figure 6a, fraction 6 is separated into 30 peaks - some only partially resolved - by reverse phase HPLC. Several peaks in fraction 6 have been tentatively identified by spiking; they are: naphthalene, phenanthrene, fluoranthene, and pyrene. GC analysis of fraction 6 shows one major peak, identified by spiking as pyrene. Several other peaks - phenanthrene, fluoranthene and dibenzothiophene - have been identified by spiking as shown in Figure 6b.

Reverse phase HPLC separates fraction 5 into 35 peaks (see Figure 6c). There are more peaks present in fraction 5 than in fraction 6. At the same total concentration level the UV absorption of the chromatographic peaks is much greater in 5 than in 6. The gas chromatogram of fraction 5 shown in Figure 6d shows three major peaks which have been identified by spiking as phenanthrene, fluoranthene and pyrene. Fourteen intermediate and minor peaks are also present. Two of these components - dibenzothiophene and chrysene - have been identified.

The components identified in fractions 5 and 6 are essentially all 2, 3, and 4 condensed ring polynuclear aromatic compounds with one heteroaromatic sulfur species. Many of the compounds present in fractions 5 and 6 are also present in recycle oil (8). The origin of some of these polynuclear aromatic compounds in the final SRC product

can be attributed to one of two sources: 1) these compounds may be residual recycle oil which is not completely distilled or 2) these compounds may be an integral portion of the SRC organic matrix.

Normal phase HPLC separations of fractions 1-4 have been attempted since reverse phase HPLC is totally unsuccessful due to the lack of solubility of fractions 1-4 in reverse phase solvents. Analytical separations of fractions 1-4 are difficult due to their insolubility in many solvents; however, some progress has been made as shown in Table 6. Under normal phase conditions with a mobile phase of hexane (95%) and 2-propanol (5%), no bands in fraction 1 and 2 elute before 20 column volumes. With the same solvent system fractions 3 and 4 show some resolution into peaks and chromatographic bands at $k' < 20$. When a more polar mobile phase is used - hexane(75%)/2-propanol (25%), all the components in fractions 3 and 4 elute as a single band while fractions 1 and 2 elute as two broad bands in less than four column volumes. Under both mobile phases, condensed ring standards - such as phenanthrene, anthracene, dibenzothiophene and rubrene - all elute at the void volume of the column. Considering the mobile phase necessary to effect a separation, fractions 1 and 2 appear to have a composition quite different from fractions 3 and 4. Fractions 1 and 2 appear to be composed of polar compounds or condensed ring systems with high molecular weights; while fractions 3 and 4 appear to be composed of more non-polar but high molecular weight compounds.

Conclusions

GPC clearly shows that the molecular weight distribution of SRC is consistent with SRC being partially composed of oil and asphaltenes. The fractions, collected from the GPC elution of Amax SRC, are fairly well-defined: fractions 1-3 are composed of asphaltenes, fraction 4 is a combination of oil and asphaltenes, and fractions 5 and 6 are oil. The major constituents of fractions 5 and 6 have been identified as mainly three or four condensed ring polynuclear aromatics; fraction 6 contains primarily pyrene and fraction 5 contains three major components - phenanthrene, fluoranthene and pyrene. From the experimental evidence, fractions 1-4 can be characterized by their bonding type and chromatographic behavior. Fractions 1 and 2 appear to be somewhat polar, high molecular weight compounds dominated by chain structure possibly within an aromatic framework, while fractions 3 and 4 seem to be fairly high molecular weight but essentially non-polar compounds with a more prominent aromatic structure. Future HPLC work is planned to effect more complete separations of the components in fractions 1-4 for subsequent compound identification.

References

1. H. M. Coleman, D. L. Wooton, H. C. Dorn, and J. T. Taylor, Anal. Chem., 49 (4), 533 (1977).
2. H. M. Coleman, D. F. Wooton, H. C. Dorn, and J. T. Taylor, J.Chrom., 123, 419 (1976).
3. D. T. Wooton, H. M. Coleman, J. T. Taylor, and H. C. Dorn, Fuel, 57 (1), 17 (1978).
4. M. Farcasiu, Fuel, 56 (1), 9 (1977).
5. M. Farcasiu, T. O. Mitchell, D. D. Whitehurst, Chemtech, 7 (11), 680 (1977).
6. J. W. Prather, A. R. Tarrer, J. A. Guin, D. R. Johnson, and W. C. Neely, Prepr., Div. Fuel Chem., Am. Chem. Soc., 21 (5), 144 (1976).
7. H. L. Retcofsky, T. J. Bendel and R. A. Friedel, Nature Physical Science, 240, 18 (1976).
8. J. A. Guin and A. R. Tarrer, U. S. Department of Energy Report No. FE-2454-1, November, 1977.

TABLE 1. Solubility of Amax SRC and Four Demineralized Feed Coals in Tetrahydrofuran

<u>Material</u>	<u>Percent Soluble in THF*</u>
Amax SRC	86.65
Amax Coal	8.75
Monterey Coal	5.02
Western Kentucky Coal	3.88
Illinois #6 Coal	1.60

*Concentration level: 100 mg/ml

TABLE 2. Comparison of Elution Time for Solvent Refined Coals and their Feed Coals

<u>SRC</u>	<u>Elution Time (minutes)</u>	
	<u>Initial</u>	<u>Final</u>
Amax	24.40	46.75
Monterey	16.25	31.75
Illinois #6	21.90	43.25
Western Kentucky	15.50	29.75
<u>Feed Coals</u>		
Amax	15.75	33.00
Monterey	16.00	30.35
Illinois #6	15.90	30.48
Western Kentucky	15.00	28.75

TABLE 3. Highest Mass Spectral for Amax SRC Fractions and Amax SRC

<u>Fractions</u>	<u>m/e*</u>
1	650
2	640
3	370
4	680
5	580
6	658
Amax SRC	579
Asphaltenes (Amax Coal)	693

Probe temperature: 300°C
 Ionizing voltage: 1400 V

TABLE 4. Elemental Analysis of Amax GPC Fractions and Amax SRC

<u>GPC Fractions</u>	<u>% C</u>	<u>% H</u>	<u>% N</u>
1	81.25	5.24	1.69
2	79.12	5.80	1.38
3	80.30	6.26	1.68
4	82.98	4.40	1.27
5	84.55	6.58	0.75
Amax SRC (THF insoluble portion)	84.18	4.64	1.60
Amax SRC	86.07	5.17	1.52
Recycle Oil	89.22	8.44	0.85

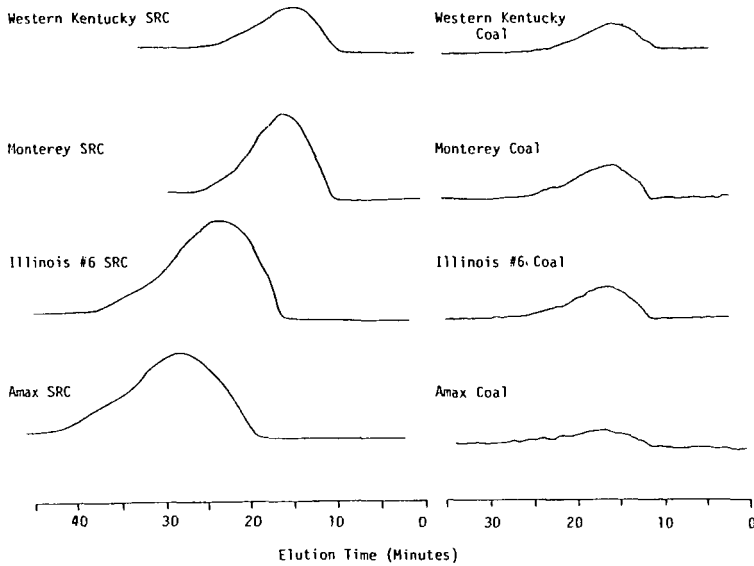
TABLE 5. Infrared Ratios of Amax SRC GPC Fractions

<u>Fractions</u>	<u>Ratios</u>	
	<u>Aromatic/Aliphatic (CH/CH₂)</u>	<u>Methyl/Methylene (CH₃/CH₂)</u>
1	0.077	0.79
2	0.151	0.81
3	0.201	0.92
4	0.298	0.88
5	0.837	1.28

TABLE 6. Normal Phase HPLC Analysis of Fraction 1-4

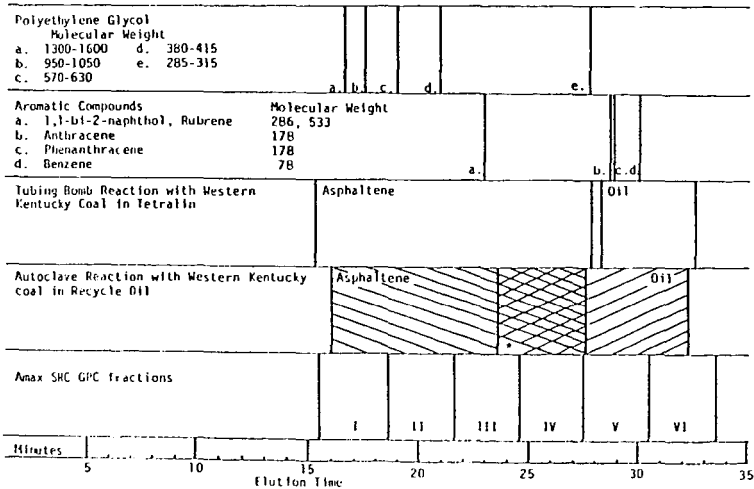
<u>Fraction</u>	<u>Mobile Phase</u>	
	<u>Hexane (95%)/2-Propanol (5%)</u>	<u>Hexane (75%)/2-Propanol (25%)</u>
1	No bands to $k' = 20$	Two broad bands, $1 < k' < 4$
2	No bands to $k' = 20$	Two broad bands, $0 = k' < 1.8$
3	13 peaks (poorly resolved) $k' < 20$	Single broad band, $k' = 0$
4	3 bands, $0 < k' < 1$	Single band, $k' = 0$

Figure 1. GPC^a of the SRC's and the Feed Coals^b



- a. UV detection at 300 nm
- b. Coals demineralized (ASTM)

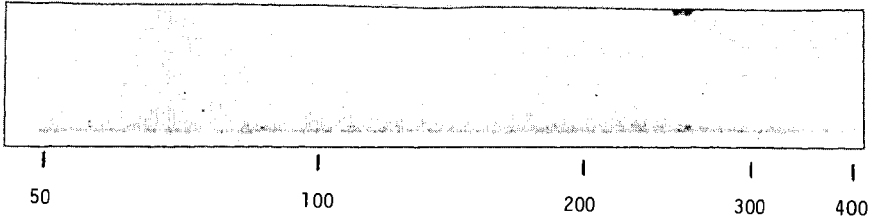
Figure 2. Comparison of the Elution Times of Amax SRC GPC Fractions to Known Standards



*Overlapped peak includes both asphaltene and oil fractions.

Figure 3. Mass Spectra of Two Amax SRC GPC Fractions

Fraction 1



Fraction 5

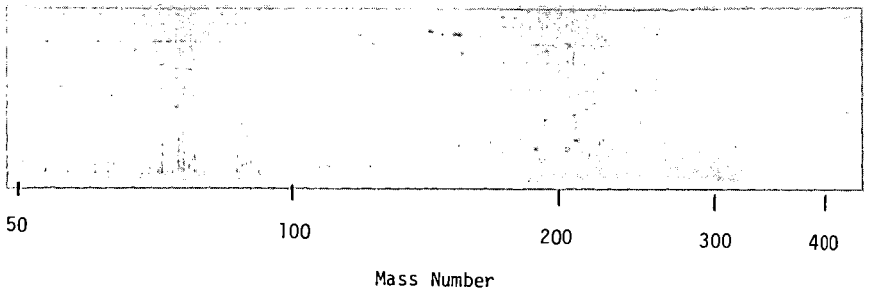
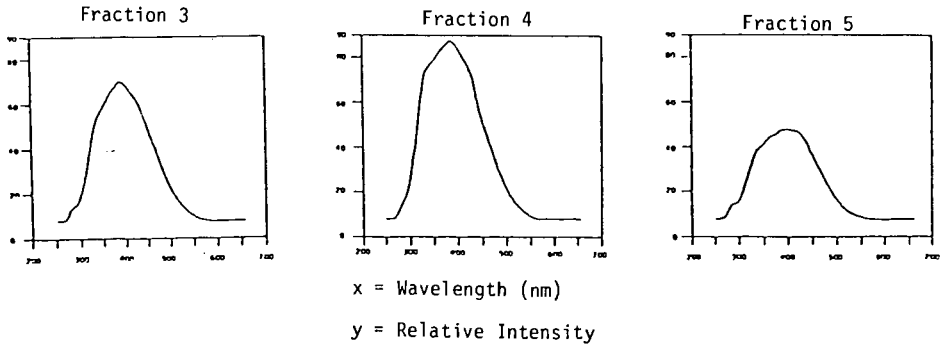


Figure 4. Fluorescence Spectra^a of Three Amax SRC GPC Fractions



a) Uncorrected emission spectra

Figure 5. Ultraviolet Spectra of Amax SRC, Light Recycle Oil and Amax SRC GPC Fractions

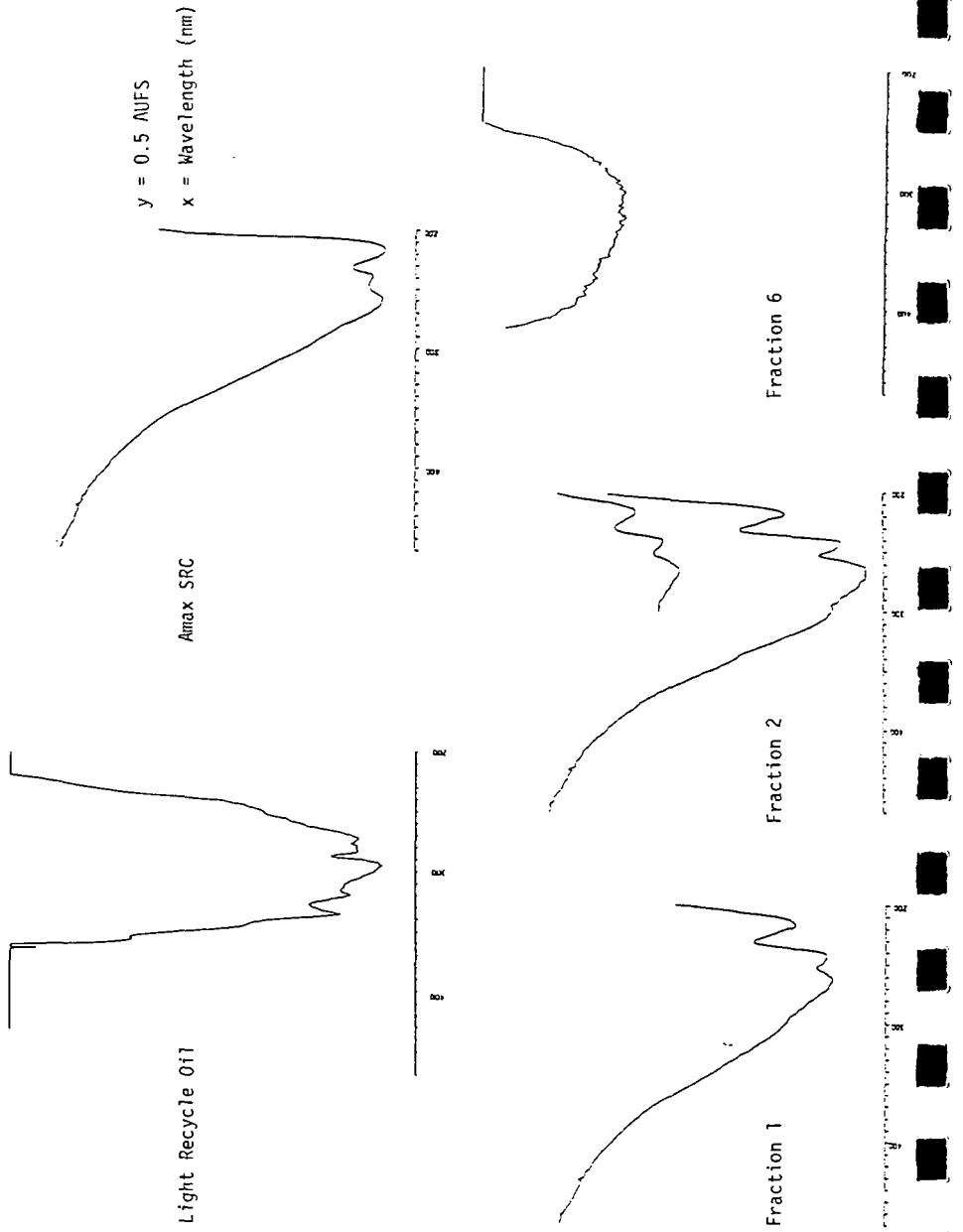
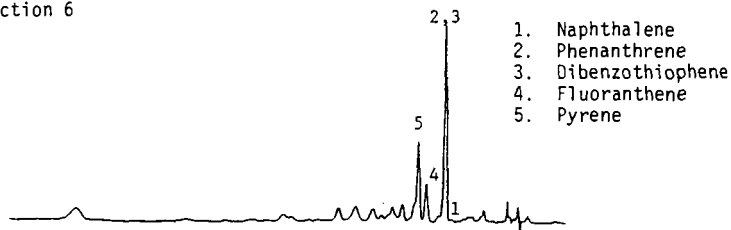
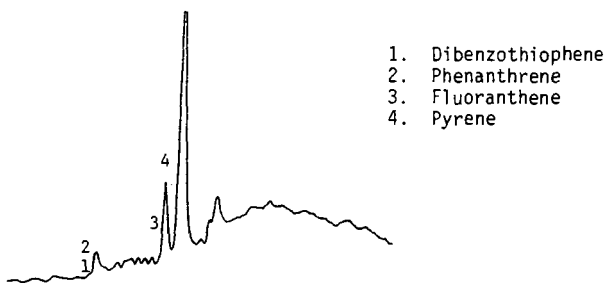


Figure 6. Liquid and Gas Chromatograms of Fractions 5 and 6

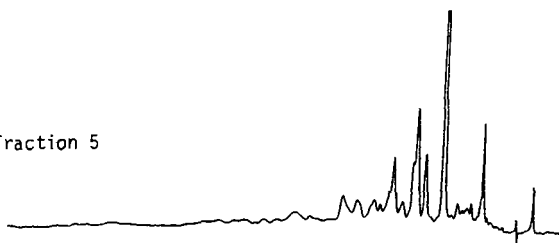
a) HPLC of Fraction 6



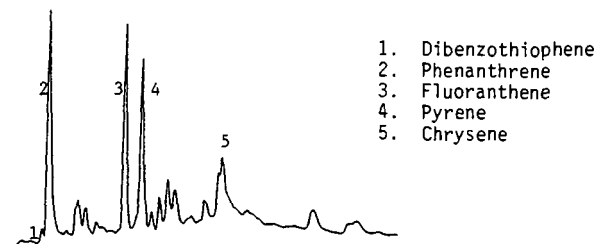
b) GC of Fraction 6



c) HPLC of Fraction 5



d) GC of Fraction 5



Chemistry of Texas Lignite
Liquefaction in a Hydrogen-Donor
Solvent System

C. V. Philip and Rayford G. Anthony

Department of Chemical Engineering
Texas A&M University
College Station, Texas 77843

INTRODUCTION

Lignite can be converted to clean fuels and chemicals by reacting it with hydrogen in the presence or absence of a hydrogen donor solvent. The polymeric organic constituents of the lignite are cleaved pyrolytically to produce gases and liquids. The ratio of gas to liquid which is produced depends on the temperature, pressure, presence and type of solvent, the use of hydrogen and whether dry or wet lignite is used. The complexity of the liquid product is a function of the severity of the degree of processing.

Alkalies and oxidizing agents have been used (1) to study the structure of different types of coals at mild processing conditions. The use of milder reaction conditions minimizes reactions between coal-derived products, which produce a complex mixture whose components have little resemblance to the original lattice structure of the coal (2). While this approach can be used to reveal the structure of certain predominant moieties in coal, these reagents fail to completely depolymerize the coal. The products may also react with each other even though the process conditions are mild.

The reaction of lignite at temperatures less than 750°F in the presence of hydrogen and tetralin produces a liquid mixture containing a substantial fraction of aliphatic compounds. The chemical nature of the products released from the lignite into the tetralin phase, their structural relationship to lignite, and a procedure for characterizing the reaction products are discussed in this paper.

EXPERIMENTAL

Freshly mined lignite is ground, sieved through a 10 mesh net and used immediately to avoid moisture loss and air oxidation. Technical grade tetralin is used as the hydrogen donor solvent. The reaction vessel is a 300 cc autoclave without the stirrer assembly. Eighty grams of lignite slurried in 60 grams of tetralin is the normal charge to the autoclave. The reactor is flushed of any traces of oxygen and finally hydrogen or helium is added at room temperature to a pressure of approximately 1200 psi. It takes about 30 minutes to heat the reactor with the charge to 700°F. Both gas and liquid samples are collected through the sampling valves during the course of the reaction. At the end of the reaction the reactor is cooled and the pressure is released. Reaction conditions are reported in Table 1.

The products consist of a tetralin-rich liquid phase, a residue saturated with the tetralin-rich liquid, and a water-rich phase. The tetralin-rich phase contains liquid components derived from the lignite which are soluble in tetralin and components which result from dehydrogenation of tetralin due to hydrogen transfer. The saturated residue contains components in the tetralin and water phases, components insoluble in tetralin and water, mineral matter and unreacted lignite. The tetralin-rich liquid is analyzed by use of gel permeation chromatography (GPC) and gas chromatography (GC). The saturated residue is extracted with tetrahydrofuran (THF) by use of a Soxhlet extractor. The extract is concentrated in a rotary evaporator to give a solution containing approximately 50% THF and 50% extract. The extract, therefore, contains the same components present in the tetralin-rich phase as well as components

which are insoluble in tetralin. The extract plus THF were then analyzed by use of GPC and GC. The water-rich phase was not analyzed.

The GPC separations were done on a Waters Associate Model ALC/GPC 202 Liquid Chromatograph equipped with a refractometer (Model R 401) and a UV detector. A valve injector is used to load the column with the sample. Generally a 200 μ l of undiluted sample was used. Two 100 Å μ Styragel columns (7.8 mm id X 300mm) were used through out the work. Reagent grade THF which had been distilled after refluxing over sodium wire to ensure that it is completely dry and devoid of any peroxide inhibitor, is used as the GPC solvent. THF was stored under dry nitrogen and all the separations were conducted in an anaerobic atmosphere to prevent the formation of peroxides. The tetralin-rich phase and extract were separated into three fractions as shown in Figure 1. Fraction 1 contains mostly colloidal carbon and some high molecular weight species. Fraction 2 was carefully evaporated to remove THF from the lignite-derived product. The product was then analyzed by GC and by GC-MS (3,4). Fraction 3 contains tetralin, tetralin-derived species and low molecular weight species derived from the lignite. Fraction 3 is collected and analyzed by use of GC which separates the low molecular weight species, tetralin and tetralin-derived products.

The gas samples were analyzed by use of a five column, three valve, automated gas chromatograph which is dedicated for gas analysis. The system is composed of a Carle GC and a Hewlett Packard 3385A automation system.

RESULTS AND DISCUSSION

When tetralin is used as the solvent in the liquefaction of lignite, most of the lignite-derived products are soluble in the tetralin-rich (liquid) phase. GPC can be used to separate the major constituents into three fractions. Figure 1 shows the separation obtained when 200 μ l of the liquid product are injected into the GPC. The first fraction is composed of species with boiling points greater than 500°C as well as colloidal carbon. This fraction can be collected and analyzed by use of NMR. Since most of the high molecular weight species have a limited solubility in the solvent system composed of tetralin and tetralin-derived products, fraction 1 represents only a small portion of the lignite-derived products. For all practical purposes fraction 2 represents the bulk of the lignite-derived products. Figure 3 shows the separation of the second fraction obtained by GC. Most of the components are identified by GC-MS and listed in Table 2 in the order that they appear in the chromatogram shown in Figure 3. The third fraction in Figure 1 is composed of low molecular weight lignite-derived products, tetralin, naphthalene, decalin and dihydronaphthlene. A gas chromatogram of this fraction is shown in Figure 2.

Comparison of the gas chromatograms shown in Figures 2 and 3 of fractions 2 and 3 reveals the success of the GPC separation of the lignite-derived products from the solvent and its reaction products. The amount of tetralin and tetralin-derived products in fraction 2 is insignificant. The lignite-derived products with boiling points close to the boiling point of tetralin, as well as, compounds of molecular size and weight comparable to that of tetralin are concentrated in fraction 2. The lignite-derived products are concentrated in fraction 2 because, (1) aliphatic compounds of comparable molecular weight are larger in molecular size relative to tetralin, and (2) the polar compounds hydrogen bond with the GPC solvent, tetrahydrofuran, which increases their effective molecular size relative to tetralin. Those products which appear in fraction 3 are readily separated by gas chromatography as shown in Figure 2.

Since the lignite-derived products are concentrated in fraction 2, GPC can be used to monitor the rate of liquefaction of lignite. Figure 4a-d illustrate gel permeation chromatograms of reaction samples which were collected at different time intervals during a liquefaction experiment. The GPC area representing fraction 2 increases with the reaction time. As more lignite-derived products are produced the peak resolutions between fractions 1 and 2 are lost due to overloading the column with a 200 μ l undiluted liquid sample. However, the areas due to fractions 1 and 3 do

not change. The formation of peaks in fraction 3 is due to a nonlinearity in the refractivity due to the concentration of tetralin in THF. The linearity of the area due to fraction 2 with an increase in lignite derived concentration is checked by obtaining GPCs of samples diluted with tetralin and with THF. The samples diluted with tetralin yielded chromatograms which show separations similar to Figure 4a. The sample diluted with THF yielded the same pattern for fraction 2 but, also, yielded a single narrow peak for fraction 3. The area due to fraction 1 decreases in direct proportion to the extent of dilution. The product collected in fraction 1, therefore, does not necessarily increase with the reaction time or the extent of liquefaction.

Monitoring the rate and extent of liquefaction by analyzing the tetralin-rich phase by GPC is based on the following assumptions: (1) The tetralin phase has a homogeneous composition throughout the system (i.e. the tetralin-rich phase inside the porous structure of unreacted lignite is the same as that in the bulk phase.) (2) The tetralin does not bind with the lignite lattice to create a solvent system with different solubility functions. (3) The majority of the lignite-derived products are dissolved in the tetralin-rich phase. Some polar compounds will dissolve in the water-rich phase and others may be only partially soluble in the tetralin and water phases. To determine the difference in the composition of the tetralin-rich phase and the components contained in the porous structure of the unreacted lignite, the products collected by extracting the saturated residue with THF were separated by GPC and fraction 2 was analyzed by GC. The products obtained are shown in Figure 5. The components contained in fraction 2 from the tetralin-rich liquid phase are shown in Figure 6. The relative peaks of the two gas chromatograms indicate the difference in concentration of the lignite-derived products in the tetralin-rich phase and the residue phase. The relative peak heights of the nonpolar compounds in the chromatograms are the same, therefore, the analysis of the tetralin phase may be used to estimate the extent of liquefaction with respect to the nonpolar components.

The liquid products produced due to primary reactions between lignite and tetralin may undergo further chemical rearrangement. To determine the extent of secondary reactions, the lignite-derived products were analyzed by GPC and GC after a reaction time of 7 hours. The gas chromatogram of fraction 2 from the GPC is shown in Figure 7.

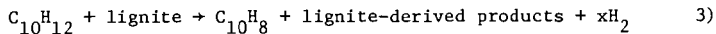
The relative intensity of the alkane peaks in Figures 5, 6, and 7 are similar. Since the product distribution of the lignite-derived liquid does not change for reaction times ranging from a few minutes to several hours, it appears that the alkanes and most of the major components do not rearrange or undergo secondary reactions after they are released from the lignite lattice. Careful examination of the smaller nonalkane peaks reveals that a few of the minor components have had a change in relative peak heights and hence concentrations. These components are undoubtedly participating in secondary reactions.

Some gas production always occurs in the liquefaction of lignite. The composition of the gas phase as a function of reaction time is presented in Table 3. The concentration of carbon dioxide reaches a maximum value after a reaction time of approximately one hour and then slowly decreases. The concentration of hydrogen sulfide follows a similar pattern. The concentration of carbon monoxide is essentially constant during the entire reaction. Production rate of methane decreases after an initial surge and the production rate of hydrogen appears to be constant. Since the hydrogen production rate and CO concentrations are constant it appears that the following reactions are not major pathways for the production of CO₂, CO and H₂.



Tetralin acts as a hydrogen donor and as a solvent for the products released

from lignite i.e.



Pyrolysis and direct hydrogenation can also, cleave the lignite lattice to produce the products listed in Table 2 (3,4,5). The conversion of tetralin to naphthalene as a function of time is illustrated in Figure 8 by plotting the ratio of naphthalene to tetralin as a function of reaction time. The extent of this conversion is directly related to the amount of lignite-derived product obtained in fraction 2 from the GPC.

The dehydrogenation of tetralin to naphthalene appears to be independent of the gaseous atmosphere in the system. Even when hydrogen is initially in the system, the hydrogen required for liquefaction is provided by the tetralin.

CONCLUSIONS

The conditions used in these experiments were mild enough to prevent both excessive gas production due to high temperature pyrolysis and chemical rearrangement of products released during the liquefaction process. Since the possibility of the water gas reaction is excluded, the production of carbon dioxide is due to the carboxylic acid groups present in the lignite lattice and alkanes constitute the bulk of the lignite liquefaction products. The alkanes can be produced from lignite by pyrolysis, by pyrolytic hydrogenation using hydrogen or hydrogen donor solvents at the same temperatures and pressures.

Although pyrolysis gives the smallest yield and the hydrogen donor solvent system gives the largest yield, the relative composition of alkanes is essentially constant. The lignite lattice contains alkane chains in varying lengths and they are released during liquefaction without fragmentation. The other major products listed in Table 2 are alkylated aromatics, alkylated indanes and alkylated phenols. Some of these products undergo secondary chemical rearrangements during prolonged reaction times. Lignite is one of the youngest members of the coal family and still contains intact some of the original plant structural skeleton. Formation of these lignite structural constituents from wood lignin can be easily envisioned.

ACKNOWLEDGMENTS

The financial support of the Texas Engineering Experiment Station, the Texas A&M University Center for Energy and Mineral Resources, and Dow Chemical Co., Freeport, Texas is very much appreciated. The lignite was furnished by Alcoa at Rockdale, Texas and by Dow Chemical Co.

REFERENCES

1. F. R. Mayo, "The Chemistry of Coal Liquefaction" Preprints ACS Fuel Div., 22 No. 5, 103, Chicago (Aug. 1977).
2. R. Hayatsu, R. E. Winans, R. G. Scott, L. P. Moore, and M. Studier, "Oxidative Degradation Studies of Coal and Solvent Refined Coal" Preprints ACS Fuel Div., 22 No. 5, 156, Chicago (Aug. 1977).
3. C. V. Philip and R. G. Anthony, "Characterization of Liquids and Gases Obtained by Hydrogenating Lumps of Texas Lignite" Preprints ACS Fuel Div., 22 No. 5, 31, Chicago, (Aug. 1977).
4. C. V. Philip and R. G. Anthony, "Hydrogenation of Texas Lignite" TEES Publications, Tech Bn., 78-2, 10(1978).
5. C. V. Philip and R. G. Anthony, "Organic Chemistry of Coal," ACS Symposium Series, In Press.

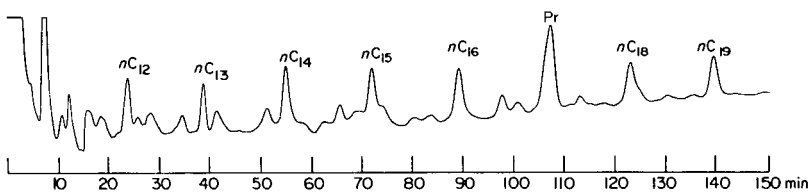
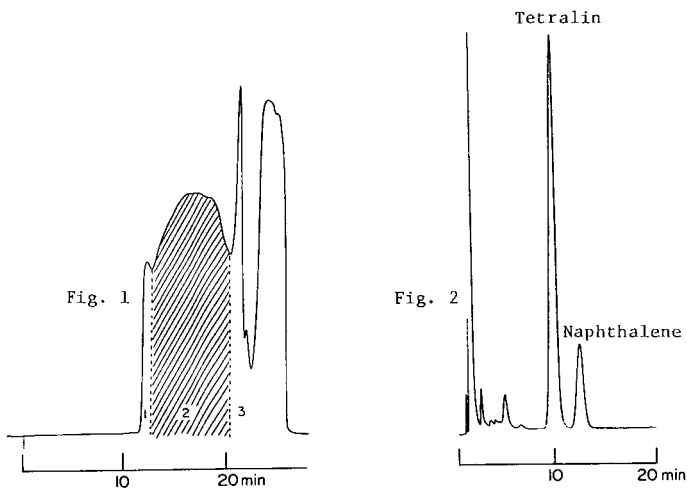


Fig. 3

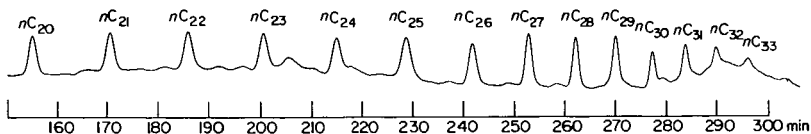


Figure 1. GPC separation of products in the tetralin-rich phase. 1. Colloidal carbon and high molecular weight species; 2. lignite-derived products; 3. tetralin and naphthalene and low molecular weight species.

Figure 2. Gas chromatogram of fraction 3 on a 10% SP2250 on 100/120 supelcoport, 1/4" id x 3'SS; column at 160°C isothermal.

Figure 3. Gas chromatogram of fraction 2 on a 10% SP2100 on 100/120 supelcoport 1/4" x 8'SS; temperature program: 80 - 270°C at 0.5°/min. The peaks were identified by GC-MS and are listed in Table 2.

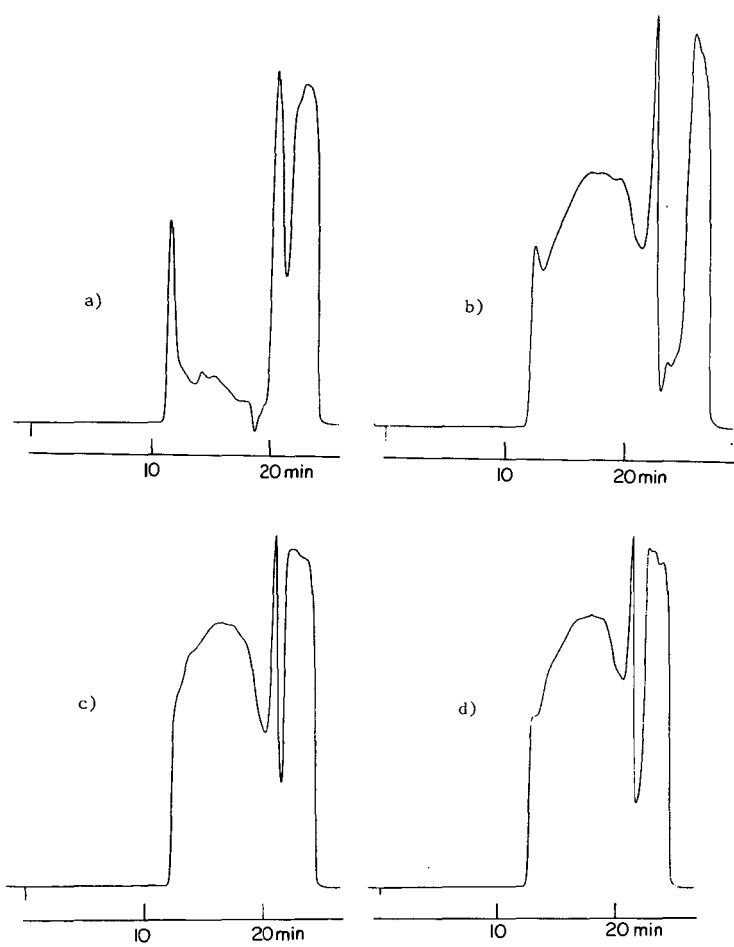


Figure 4. Gel permeation chromatograms of 200 μ l samples of tetralin-rich phase from run #56 (reaction conditions are listed in Table 1) at reaction times of a) 1 hr. b) 1 1/2 hrs. c) 2 hrs. and d) 7 hrs.

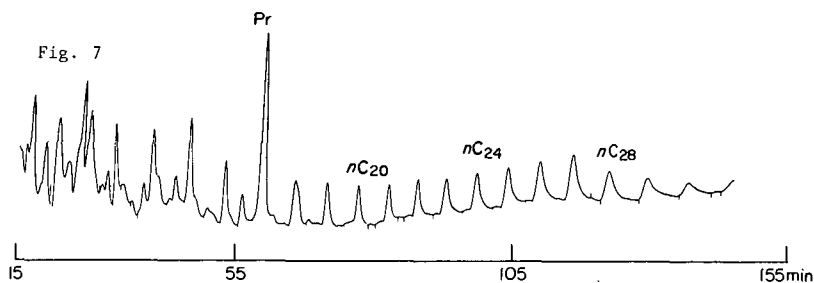
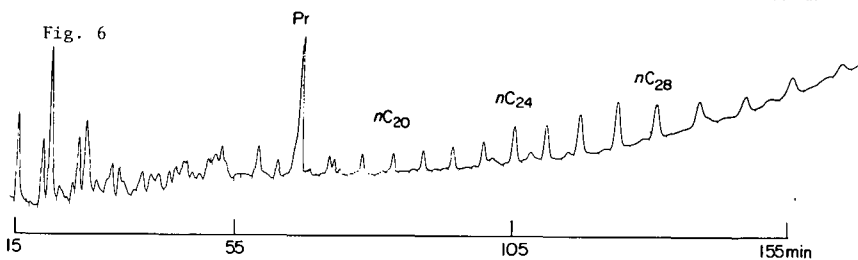
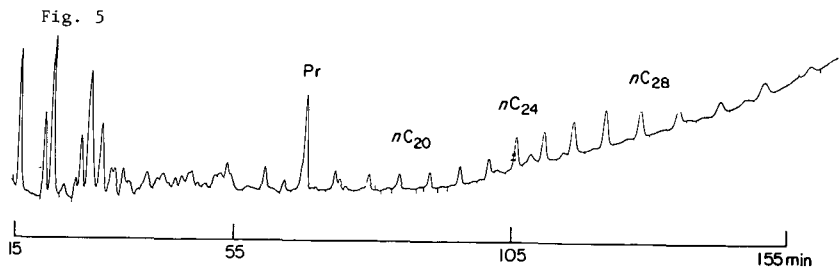


Figure 5. Gas chromatogram of the GPC fraction 2 of the extract of lignite derived products after 2 hrs. of reaction. GC conditions are the same as in Figure 2 except the temperature program of 80 - 250°C was 1.5°C/min. For peak identification, see Table 2.

Figure 6. Gas chromatogram of the GPC fraction 2 of the tetralin-rich phase after 2 hrs. of reaction. Figure 5 GC conditions. For peak identification see Table 2.

Figure 7. Gas chromatogram of the GPC fraction 2 of the tetralin-rich phase after 7 hrs. of reaction. GC conditions are the same as in Figure 5.

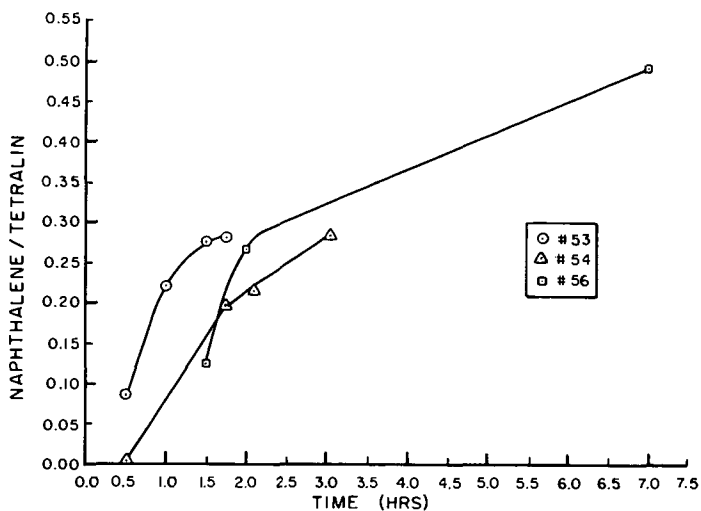


Fig. 8. Naphthalene to tetralin ratio in the tetralin-rich phase during lignite liquefaction process as a function of time.

Table 1. Reaction Conditions of Liquefaction Experiments

No.	Lignite (grams)	Gas	Tetralin (grams)	Initial Pressure (psig)	Max. Pressure (psig)	Reaction Time (Min)	Average Temperature °F
53	80.1	H ₂	60	1250	4400	235	715 ₊₁₅
54	80.0	He	60	1250	5100	130	705 ₊₁₅
56	100.0	H ₂	60	1100	5200	420	718 ₊₁₅

Table 2. Identification of Major Compounds in GPC Fraction 2

Peak No.	Compound	Peak No.	Compound
1	Phenol	26	Trimethylnaphthalene (iso.)
2	1-Ethyl-3-methylbenzene and Decane	27	C ₁₆ H ₃₄ and Trimethylnaphthalene (iso.)
3	<i>o</i> -Cresol	28	<i>n</i> -Hexadecane
4	<i>p</i> -Cresol	29	Diethyl methyl-naphthalene
5	<i>n</i> -Undecane and methylcresol	30	C ₁₇ H ₃₆ and Tetramethylnaphthalene
6	<i>o</i> -Ethylphenol	31	<i>n</i> -Heptadecane
7	2,6-Dimethylphenol	32	Alkylated naphthalene
8	<i>p</i> -Ethylphenol	33	C ₁₈ H ₃₈
9	<i>p</i> -Cymene	34	<i>n</i> -Octadecane
10	C ₁₂ H ₂₆ and 1,3-Dimethylindan	35	C ₁₉ H ₄₀
11	<i>n</i> -Dodecane and 2-Methyl-6-ethylphenol	36	C ₁₉ H ₄₀
12	3-Methyl-6-ethylphenol	37	C ₁₉ H ₄₀
13	C ₁₂ H ₁₆	38	<i>n</i> -Nonadecane
14	3-Methyl-6-ethylphenol	39	<i>n</i> -Eicosane
15	C ₁₃ H ₂₈ and 1,6-Dimethylindan	40	<i>n</i> -Heneicosane
16	1,2-Dimethylindan	41	<i>n</i> -Docosane
17	<i>n</i> -Tridecane	42	<i>n</i> -Tricosane
18	C ₁₁ H ₁₆ (Methylated benzene) and C ₁₄ H ₃₀	43	<i>n</i> -Tetracosane
19	<i>n</i> -Tetradecane	44	<i>n</i> -Pentacosane
20	Dimethylnaphthalene	45	<i>n</i> -Hexacosane
21	2,3-Dimethylnaphthalene	46	<i>n</i> -Hepacosane
22	C ₁₅ H ₃₂	47	<i>n</i> -Octacosane
23	<i>n</i> -Pentadecane	48	<i>n</i> -Nonacosane
24	Pentamethylindan	49	<i>n</i> -Triacontane
25	C ₆ -Alkylindan	50	<i>n</i> -Hentriacontane
		51	<i>n</i> -Dotriacontane
		52	<i>n</i> -Tritriacontane
		53	<i>n</i> -Tetracontane

EFFECTS OF NITROGEN COMPOUNDS ON
DEPOSIT FORMATION DURING SYNFUEL STORAGE*

John W. Frankenfeld and William F. Taylor

Exxon Research and Engineering Company
Linden, New Jersey 07036

INTRODUCTION

Both the U.S. and world petroleum reserves are being depleted at a rate that can no longer be ignored. As a result, the development of alternate fuel sources is a virtual necessity within a few decades. Two of the most promising new sources are shale rock and coal. Although processes are available for the production of synthetic liquids from shale and coal, the investment costs associated are very large and the fuels produced will unquestionably be significantly different in chemical composition from present day petroleum-derived materials. Despite considerable variation from various sources and methods of liquification, some generalizations can be drawn: shale liquids will be higher in oxygen and nitrogen, more aromatic and olefinic than petroleum-based fuels; coal liquids will be higher in oxygen content but lower in nitrogen than shale, extremely rich in aromatics and have a somewhat lower olefin content (1). Some of the differences between synthetic and petroleum fuels can be corrected by known processing techniques. However, these are expensive and may never be completely effective. It is important, therefore, to determine which types of variations from known fuels will be deleterious and which can be tolerated.

One of the substances most difficult to remove is nitrogen. In addition, it is known that nitrogen content can adversely effect fuel stability. This is illustrated by Figure 1, where three jet fuels, prepared by catalytic hydrotreating shale liquids, were subjected to the standard JFTOT thermal stability test (2). Clearly, the higher the nitrogen content of a fuel, the poorer its thermal stability. Some of the samples were severely hydrotreated yet still retained significant amounts of nitrogen and exhibited poor thermal stability (2).

Recent work at Exxon has shown that nitrogen compounds, especially of the pyrrole type, promote sediment or sludge formation in JP-5 jet fuel stored under ambient conditions. The reaction is first noted by an almost immediate darkening of the fuel. This is followed by the appearance of sludge which continues to increase on standing. The reactions to form sediments were strongly influenced by light, acids and oxygen present in the fuel.

As a result of these preliminary observations, the present study was undertaken to investigate this phenomenon further. The major objectives of this program are: (1) to determine whether other nitrogen containing species, likely to occur in synfuels, will have effects similar to pyrroles, (2) to test for interactions between nitrogen compounds and other impurities, (3) to determine the effects of storage parameters such as light, temperature and oxygen content of the fuel on sediment formation and (4) to elucidate the chemical structure and mechanism of formation of the sediments produced.

EXPERIMENTAL

The test compounds were the highest quality commercially available. They were purified by distillation when necessary. High quality n-decane was employed

*Sponsored by NAVAIR 310C, Contract No. N00019-76-C-0675, Dr. Hyman Rosenwasser, technical monitor.

Table 3. Components in Gas Samples Collected at Various Time Intervals and Reaction Conditions Listed in Table 1

Number	Time (min)	H ₂	CO ₂	C ₂ H ₆	CH ₄	CO	C ₃ H ₈	C ₃ H ₆	i-C ₄ H ₁₀	H ₂ S	n-C ₄ H ₁₀
53-1	40	76.8	10.8	0.3	0.8	0.3	0.2	0.05	0.04	0.1	0.07
53-2	70	75.3	16.5	0.7	1.8	0.5	0.4	0.06	0.06	0.2	0.10
53-3	98	66.2	22.9	1.5	3.5	0.7	0.9	0.06	0.10	0.2	0.18
53-4	120	68.3	21.5	1.6	3.7	0.6	0.9	0.04	0.10	0.2	0.19
53-5	235	67.9	18.6	1.7	4.1	0.5	1.0	0.04	0.12	0.2	0.28
54-1	40	0.2	15.0	0.4	1.1	0.3	0.3	0.06	0.03	0.7	0.07
54-2	80	0.3	12.4	0.4	1.5	0.4	0.3	0.04	0.04	0.5	
54-3	110	0.5	14.8	0.8	2.2	0.4			0.06	0.6	
54-4	130	0.7	14.1	0.9	2.4	0.5	0.5	0.04	0.03	0.3	0.13
56-1	120	63.6	24.3	1.9	5.2	0.8	1.0	0.07	0.09	1.2	0.22
56-2	240	53.6	31.2	4.6	10.7	0.7	2.5	0.07	0.22	1.6	0.59
56-3	420	57.6	27.7	4.2	12.6	0.6	1.4	0.02	0.08	0.6	0.17

TABLE 1
Effects of Nitrogen Compounds on Sediment Formation in Purified n-Decane

Compound Added (1)	Storage (2) Conditions	Cumulative Sediment (g/500g Decane)				Comments
		1 Day	5 Days	20 Days	30 Days	
None	Light	-	-	-	-	Clear, Colorless
None	Dark	-	-	-	-	Throughout
2,5-Dimethylpyrrole	Light	.362	.718	1.13	1.30	Dark Brown Solution
2,5-Dimethylpyrrole	Dark	.036	0.100	.353	.524	Dark Brown Solution
Indole	Light	.012	.021	.022	.036	Pink Solution
Indole	Dark	-	-	-	-	Colorless
Carbazole	Light	Trace	Trace	.019	.020	Yellow Solution
Carbazole	Dark	-	-	-	-	Yellow Solution
2,4,6-Trimesitylpyridine	Light	-	-	-	-	Clear, Colorless
2,4,6-Trimesitylpyridine	Dark	-	-	-	-	Clear, Colorless
Quinoline	Light	-	-	Trace	Trace	Light, Yellow Solution
Quinoline	Dark	-	-	-	-	Clear, Colorless
2,6-Dimethylamine	Light	-	.004	.004	.005	Purple Solution
2,6-Dimethylamine	Dark	-	.001	.001	.002	Purple Solution
n-Hexylamine	Light	-	-	-	-	Clear, Colorless
n-Hexylamine	Dark	-	-	-	-	Clear, Colorless
Methylcyclohexylamine	Light	-	-	-	-	Yellow Solution
Methylcyclohexylamine	Dark	-	-	-	-	Light Yellow Solution
2-Methylpiperidine	Light	Trace	Trace	.001	.001	Light Yellow Solution
2-Methylpiperidine	Dark	-	Trace	.001	.001	Light Yellow Solution
n-Caproamide	-	-	-	Trace (3)	Trace (3)	Light Yellow Solution
n-Caproamide	-	-	-	Trace (3)	Trace (3)	Light Yellow Solution

(1) Each compound added to purified n-decane at 2000 ppm N level.

(2) Light = (UV) irradiation (366 nm, 1100 μW/cm²); Dark = stored in darkness.

(3) Trace of liquid appeared after 30 days.

as the diluent. This was further purified by percolation through columns of activated alumina to remove traces of reactive, polar materials. The nitrogen compounds were tested at the 2,000 ppm level (nitrogen basis) which is within the limits expected from fuels derived from shale or coal (1). The compound 2,5-dimethylpyrrole was employed as a standard. The oxygenated compounds were added in amounts equivalent to 500 ppm O.

Duplicate sets of samples were set up using glass bottles. One set was stored in darkness at ambient temperature (24°C). The second set was irradiated with long wave (366 nm) UV light with an intensity of 1100 $\mu\text{W}/\text{cm}^2$ (3). A separate sample of *n*-decane with 4,000 ppm N as 2,5-dimethylpyrrole was exposed to normal sunlight to serve as a control. The bottles were removed from storage at intervals, the precipitate filtered and dried under vacuum at 110°C for 1-1/2 hours before weighing and subsequent analysis.

RESULTS AND DISCUSSION

Effects of Various Nitrogen Compounds

Compound type analyses of various light distillates of shale liquids have been reported (4). They show that pyrroles, quinolines, and pyridines are the dominant species present along with lesser amounts of amides, anilides and alkyl amines. Compounds of these types were, therefore, chosen for this study. The effects of various representative nitrogen-containing compounds on sediment formation in purified *n*-decane are given in Table 1. It is clear from this data that sediment formation is not unique to 2,5-dimethylpyrrole (DMP) although of those compounds tested, DMP easily produced the greatest amount. It is interesting that the three compounds giving the most sediment were all of the pyrrole type, DMP, indole and carbazole. Of the other compounds studied, only 2,6-dimethylaniline and 2-methylpiperidine afforded any measurable sediment. However, several of the primary amines produced colored solutions which intensified with time. Their effects on long term storage stability is unknown.

Importance of Light as a Promoter

The importance of light as a catalyst for sediment formation is illustrated by the plots in Figure 2. The difference between the irradiated and dark-stored samples is quite large early in the period and tends to get much smaller later. Thus, with DMP, sediment in the irradiated sample exceeded that for the dark sample by a factor of ten after one day but was only about 38% greater after 60 days. This suggests that exclusion of light will retard but not prevent sediment formation.

The sample stored in sunlight formed sediment slightly more rapidly than the UV irradiated material (Figure 2). This effect is not of practical significance but may have a bearing on the mechanism of sediment formation.

It should be noted that the build up of sediment in the dark follows a straight time relationship while the light catalyzed reaction does not. The dark reaction appears to be at least "pseudo" zero order while the catalyzed reaction is of a higher order. It should also be emphasized that the shape and general magnitude of the curves obtained in *n*-decane is in excellent agreement with those from actual JP-5 fuel.

Influence of Organic Acids and Phenols

Pyrroles are oxidized more rapidly in acidic than neutral media (5). As a result, it was of interest to determine whether organic acids, likely to be present in synfuels, would catalyze the formation of sediments in hydrocarbon media.

FIGURE 1

VARIATION OF JFTOT BREAKPOINT TEMPERATURE WITH NITROGEN LEVEL AFTER HYDROTREATMENT

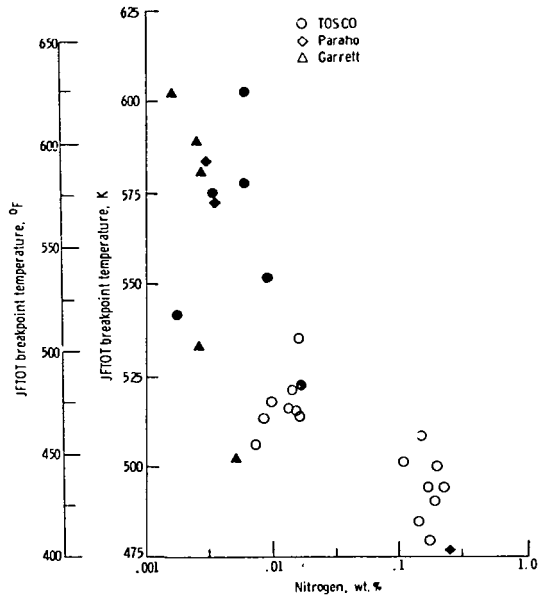
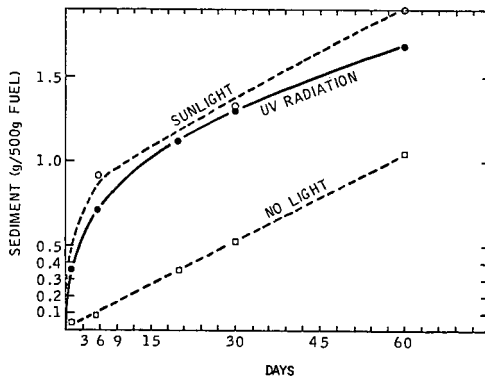


FIGURE 2

EFFECTS OF UV RADIATION ON SEDIMENT FORMATION BY 2,5-DMP IN N-DECANE



Preliminary experiments in JP-5 indicated a significant effect. This was confirmed in experiments using n-decane as the diluent. The results are summarized in Table 2.

TABLE 2
 SEDIMENT FORMATION WITH 2,5-DIMETHYLPYRROLE (DMP)
 UNDER THE INFLUENCE OF ORGANIC ACIDS

Acid (1)	Storage Conditions (2)	Cumulative Sediment (g/500 g Decane)					Appearance
		1 Day	5 Days	15 Days	30 Days	60 Days	
None	Light	.213	.524	.869	1.12	1.52	Dark Red
	Dark	---	.060	.197	.394	.840	Dark Red
<u>n</u> -Decanoic	Light	.390	.821	1.25	1.49	1.84	Dark Red
	Dark	.057	.147	.497	.990	1.50	Dark Red
Cyclohexane Carboxylic	Light	.391	.821	1.26	1.56	1.83	Dark Red
	Dark	.083	.216	.621	1.08	1.84	Dark Red
Benzoic	Light	.259	.476	.858	---	---	Clear,
	Dark	.057	.165	.414	---	---	Colorless
<u>n</u> -Decanoic Alone (3)	Light	---	---	---	---	---	Clear,
	Dark	---	---	---	---	---	Colorless

(1) Nitrogen compounds added at 2,000 ppm N level; acids at 500 ppm O level.

(2) Light = UV radiation (366 nm; 1100 $\mu\text{W}/\text{cm}^2$).

(3) No DMP in these samples.

Both n-decanoic acid and cyclohexanecarboxylic acid significantly increased the rate of sedimentation. This was evident in both light and dark. The acids promoted a 20% increase in sediment in 60 days in the light and by 100% or more in the dark over samples containing DMP alone. Control samples containing the acidic compounds but no DMP gave no sediment nor was any darkening of the fuel observed. Benzoic, a typical aromatic acid, showed no effect under light storage, but did tend to increase deposit formation in the dark.

It would appear that the acid and light catalysts operate independently rather than in any sort of synergistic or antagonistic fashion. This was apparent from a 3x3 factorial analysis of the data from Table 2. In the case of DMP and decanoic acid, the "light effect" accounted for 0.674 g of sediment in 15 days and 0.683 g in 60 days. The corresponding values for the "acid effect" are .303 g and .663 g. The sums of the two acting independently would be .977 g for 15 days and 1.34 g for 60 days. These values are fairly close to the 1.06 g and 1.00 g obtained in the same time periods from the experiment when both light and acid were present. It would appear that the two catalysts do not interact. An analysis was made for cyclohexanecarboxylic acid with similar results.

A number of phenols were examined with respect to promoting sediment formation with DMP in n-decane. All had an inhibitory effect, although considerable variation was observed. Results of these studies are given in Table 3. One of the most effective inhibitors was 2,6-di-t-butylphenol. Plots of sediment formation with DMP both with and without added 2,6-di-t-butylphenol are shown in Figure 3. A 58% reduction in sediment formation was obtained under light storage at 60 days and 80% reduction after 15 days as compared to controls. Under dark storage conditions, the corresponding reductions were 45% and 82%. A 3x3 factorial analysis for these experiments was performed. The "light effect" in this case is .683 g

TABLE 3

EFFECTS OF PHENOLS ON DEPOSIT FORMATION⁽¹⁾ WITH 2,5-DIMETHYLPYRROLE

Phenol Added ⁽²⁾	Cumulative Sediment (g/500 g/Decane)			
	15 Days		60 Days	
	Light	Dark	Light	Dark
None	.869	.197	1.52	.840
2,4,6-Trimethyl-	.681	.123	1.33	1.01
2,6-Di- <u>t</u> -Butyl-	.173	.035	.640	.496
2,4-Dimethyl-	.569	.213		
2,6-Di- <u>t</u> -Butyl-4-Methyl-	.270	.138		
2-Hydroxy-3-Isopropyl- (3-Isopropylpyrocatechol)	.154	.058		

(1) All samples contained 4,000 ppm N as 2,5 dimethylpyrrole.

(2) At levels of 500 ppm O.

(1.52 g - .837 for DMP alone) and the "phenol effect" is -.344 g. The net additive effect would be .339 g (.683 g - .344 g). However, the actual sediment obtained in the presence of both the phenol and light is .640 g, .20 g less than that observed under dark storage alone (60 day results). Apparently, this phenol is effective in combatting the effects of the light catalyzed reaction as well as the sedimentation under dark storage conditions.

The influence of other phenols on sediment formation varied considerably (Table 3). Those with t-butyl or isopropyl groups were most effective in retarding sedimentation. Substitution in position 4 with methyl groups tended to reduce effectiveness although the effect was not large. Work is continuing in this area to elucidate structural effects further.

Similar effects of acids and phenols were observed with indole as the nitrogen compound (Figure 4). Decanoic acid significantly increased sediment formation in the case of indole. A 6-fold increase in sediment was observed in the sample stored under UV light. Insufficient data is available for a factorial design analysis, but, in this case, light and acids may interact in some way to promote especially heavy sediment formation. Di-t-butylphenol appears to have a slight inhibitory effect on sediment formation with indole (Figure 4). The 2,4,6-trimethylphenol showed no detectable influence. These findings suggest that certain phenols may prove useful as sludge-preventing additives for future synfuels of the JP-5 type.

Characteristics and Chemical Structure of the Sediments

Determining the structure of the nitrogenous sediment is useful for elucidating the mechanism of formation and thereby finding methods of preventing it. Although storage conditions and the presence of acid may effect the rate of formation and quantity of sediment, they do not seem to alter the characteristics of the sediment. Elemental analyses of the sediments suggest that the deposits are made up largely of repeating units of the dimethylpyrrole. This is clear since the average C/N ratio in the sediments (6.3/1) is very close to the C/N ratio of dimethylpyrrole (6/1). Thus, no other carbon-containing species have been introduced into the polymer. On the other hand, considerable oxygen (about 1.5 atoms per N) has been incorporated, mostly at the expense of hydrogen. The approximate average molecular composition of 11 sediment samples, obtained under various storage conditions, was:

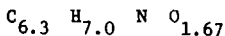


FIGURE 3

EFFECT OF DI-*t*-BUTYLPHENOL ON SEDIMENT FORMATION WITH 2,5-DIMETHYLPYRROLE IN DECANE

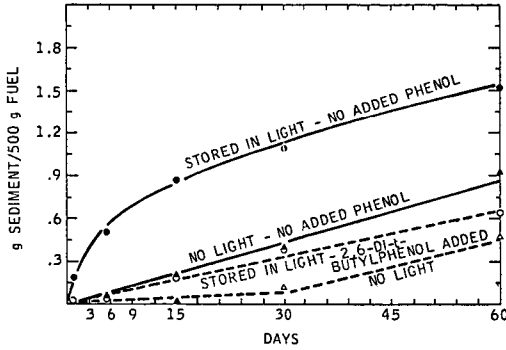
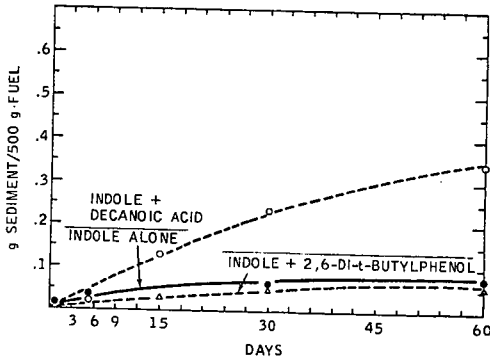
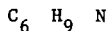


FIGURE 4

EFFECTS OF *n*-DECANOIC ACID AND 2,6-DI-*t*-BUTYLPHENOL ON SEDIMENT FORMATION WITH INDOLE IN *n*-DECANE - STORAGE IN PRESENCE OF UV LIGHT



while that of dimethylpyrrole is:



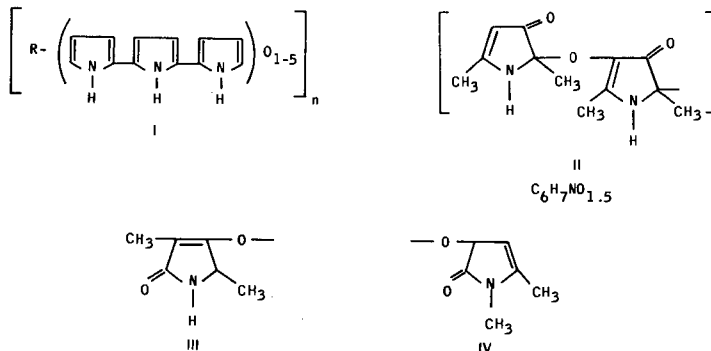
The major infrared bands from the sediments are shown in Table 4. The spectra were obtained as smears or mulls between salt plates since the extreme insolubility of the sediment precludes the measurement of solution spectra. The analysis confirms that the pyrrole ring is intact and suggests that oxygen has been introduced in the form of a carbonyl group. The strong $-CH_3$ absorption relative to $-CH_2$ indicates the methyl groups remain intact and that no long chain $-CH_2-$ units (from other components of the media) have been introduced. Previous reports (5) have proposed structure I, the so-called "pyrrole black" for the sediment obtained from pyrrole added to various fuels. The present results do not support this structure since no "R" group is present and a carbonyl group clearly is. Instead, a structure such as II (7) is more likely. The partial structures, III and IV, cannot be ruled out although an unlikely methyl group migration is required (8).

TABLE 4

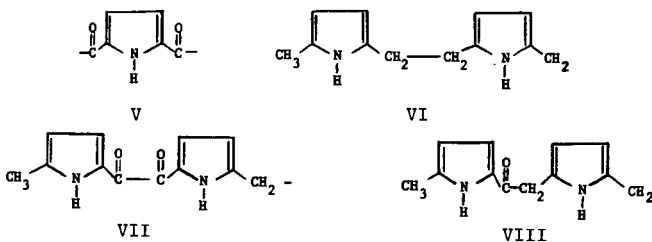
MAJOR IR BANDS IN SEDIMENT FROM 2,5-DIMETHYLPYRROLE (1)

Cm^{-1}	Significance
3300-3500 (s)	-NH or -OH
2970 (s) 1375 (s)	-CH ₃
2925 (w) 1450 (w)	Lack of -CH ₂
1640-1670 (vs)	Conj C=O or Amide

- (1) Smear or mull between salt plates.
 (2) s = strong; vs = very strong; w = weak.



The mass spectra of sediment samples are complicated because of the sediment's polymeric nature. However, some generalizations are possible. If a single structure is present, the representation best fitting all data is II, although partial structures III and IV cannot be ruled out. In addition, the mass spectra of some samples suggests the sediment may consist of several compound types of which four (V-VIII) are prevalent. The average properties of the sediment, as analyzed by elemental and infrared methods, therefore could readily be accounted for by such a mixture.



Surprisingly, the highest parent peaks observed (~400 mass units) correspond to no more than 3-4 pyrrolic units. This is consistent with reports on the autoxidation of 1-methylpyrrole (8). These workers found no more than five repeating pyrrole units in a short chain. Additional work is scheduled in this area to determine the character and mechanism of sediment formation.

CONCLUSIONS

- Nitrogen compounds can be seriously deleterious to the storage stability of synfuels.

- (a) Pyrrolic types and some amines are deleterious; many other nitrogen containing compounds are not.
- (b) The pyrrolic compounds vary in the magnitude of their influence on sediment formation. The rate is very high with 2,5-dimethylpyrrole.

- Storage conditions may play an important role; the effect of light is particularly noteworthy.

- Certain trace impurities are also important in their effects on promoting sediment formation.

- (a) Carboxylic acids accelerate the formation rate; the effect is most pronounced in the dark.
- (b) Some phenols inhibit sediment formation; structural effects are important.

- The sediments appear to have a definitive structure which may be amenable to analysis. With DMP this appears to be low to medium molecular weight oligomers consisting of partially oxidized repeating units of the nitrogen compound.

REFERENCES

1. Taylor, W. F. and Hall, H. J., "Future Synthetic Fuels", Scientific and Technical Application Forecast, Department of the Army, Contract No. DAAD05-73-C-0059 (1975).
2. Reynolds, T. W., "Thermal Stability of Some Aircraft Turbine Fuels Derived from Oil Shale and Coal", NASA TM X-3551 (1977).
3. Compounds of the Pyrrole Type Absorb Strongly in This Region (Friedel, R. A. and Orchin, M., "Ultraviolet Spectra of Aromatic Compounds", Wiley and Sons, Inc., New York, 1951).
4. See, for example, Paulson, R. E., Jensen, H. B., and Cook, G. L., Amer. Chem. Soc., Division of Petroleum Chem. Preprints 16 (1):A49 (1971); Dinneen, G. U. *et al.*, "Composition of Shale-Oil Naphtha", U.S. Bureau of Mines Bulletin 593 (1961).
5. Oswald, A. A. and Noel, F., J. Chem. Eng. Data 6 (2) 294 (1961).
6. Structures such as II have been proposed for pyrrole oxidation products (see Seebach, D., Chem. Ber., 96, 2723, 1963 or Beer, R. J. S. *et al.*, J. Chem. Soc. (1954) 4139).
7. Methyl migrations have been proposed by Seebach (Chem. Ber. 96, 2723, 1963) for certain pyrrols under rather severe oxidative conditions.
8. Smith, E. B. and Jensen, H. B., J. Org. Chem., 32, 3330 (1967).

The Thermodynamics of Coal Chars;
Correlation of Free Energy of Formation with Reactivity

Leslie L. Isaacs

Department of Chemical Engineering
The City College of The City University of New York
New York, New York 10031

INTRODUCTION

A large number of existing and proposed coal conversion technologies yield a char as a by-product or as a process intermediate. These technologies may be classified into the following categories:

1. Coal carbonization procedures, yielding a char by-product.
2. Steam or steam-oxygen gasification. Char is either a gasification intermediate or a by-product.
3. Coal gasification with hydrogen or hydrogen rich gas. The char intermediate is gasified with steam and oxygen or further gasified with hydrogen.
4. Supercritical gas extraction. A char by-product might either be gasified or used as fuel.

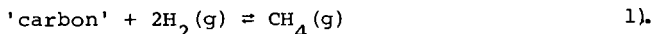
For the proper design of a given process and for the comparison of competing processes, both in the technical and economic sense, an understanding of the gasification reactivity (kinetics) and thermochemistry of the chars is essential.

Broadly speaking, the chemical reactivity of a char (in reference to gasification with steam or carbon dioxide, or hydrogen, or in combustion with oxygen) is its most important property in relation to its subsequent utilization. A traditional test for the measurement of the reactivity of a char is the rate of reaction of the char with carbon dioxide (1). The gasification process can be divided into two distinct stages (2); the first stage due to pyrolysis and the second stage due to the char-gas reaction. The pyrolysis reactivity can be related to volatile matter content of the solid, to the rate of heating and to the pyrolysis temperature. The reactivity of the char in the gasification stage seems to depend on the source of char (nature of the original coal) and the thermal history (heat treatment) of the char (3).

In spite of the efforts of many researchers, kineticists are far from able to make a priori prediction of reaction rates for the gasification of a given coal or char in various devices (processes). Consider the steam gasification process. The situation is highlighted by the fact that an oven coke - resembling blast furnace coke and having intrinsically a low chemical reactivity - gasifies poorly in a steam-oxygen blown gravitating bed gasifier, yet gasifies in a steam fluidized bed with much the same reactivity as an intrinsically reactive char made at low temperatures (4).

In an attempt to correlate the gasification data from steam fluidized beds, Squires (4) proposed that the data be explained by thermodynamic equilibrium considerations. The chemical reaction of

relevance is:



Squires hypothesized that the methane in the effluent stream from a steam fluidized bed stands in a quasi-equilibrium relationship to the hydrogen and carbon material present in the bed. He demonstrated that the calculated "equilibrium" constants for various processes and solid feeds correlated with temperature in the usual manner if the thermal history of the 'carbon' was taken into account. The data for fluidized beds with continuous feed of raw (or lightly pretreated) coals fell on a line indicating higher yields of methane at a given temperature than the data for chars and anthracite coals that had been kept for some time at elevated temperature under nitrogen atmosphere before they were fed to a steam fluidized bed. However, in all cases the methane yields obtained were substantially higher than one would have calculated from thermodynamic equilibrium assuming that the 'carbon' in the feed was graphite. The implications of this observation and hypothesis are that (a) the chars have an excess free energy of formation relative to graphite and (b) the amount of excess energy is a function of the thermal history of the char. Thus, one should be able to correlate the reactivity of a char with its thermodynamic properties. This conjecture is not made to place thermochemical data in competition with structural and kinetic information that has been developed. Indeed, all the information should be regarded as complementary.

To test Squires' hypothesis we may calculate the equilibrium constant, K , for the reaction given by Equation 1 using data for a selected 'carbon', at a given temperature and compare it to the equilibrium constant for the same reaction, at the same conditions, whereas for 'carbon' graphite is assumed to be used. From the standard thermodynamic relationship, the ratio of the equilibrium constants $K^{\text{ch}}/K^{\text{gr}}$ is related to the free energy changes, ΔG , for the reactions by:

$$\ln \frac{K^{\text{ch}}}{K^{\text{gr}}} = \frac{1}{RT} (\Delta G^{\text{gr}} - \Delta G^{\text{ch}}) \quad 2).$$

The symbols have their usual meaning. The superscripts ch and gr indicate that 'carbon' is in the form of char or graphite in the reaction considered (Eq. 1). It is obvious that in the present case

$$\Delta G^{\text{gr}} - \Delta G^{\text{ch}} = G_f^{\text{ch}} - G_f^{\text{gr}} \quad 3).$$

where G_f is the free energy of formation of the species at the reaction temperature. Thus, a test of the hypothesis reduces to the estimation of the free energy of formation of a char relative to that of graphite at a reaction temperature, and comparing the calculated ratio of equilibrium constants to that found experimentally.

The free energy of formation of a substance at a given temperature is usually calculated from the standard heat of formation, the absolute entropy of formation and heat capacity of the substance as a function of temperature. The heat of formation can be calculated

from a measured heat of combustion. Before we proceed to an actual calculation of the free energy formation of a char relative to graphite, a short review of the relevant available data is undertaken.

Standard Heat of Combustion of Chars and Graphite

The API Project 44's value for the heat of combustion of graphite is 7831 calories/gram. Dolch and Rank (5) inferred heats of combustion of chars, prepared from lignite, steam activated charcoal, cellulose and coke from peat as ranging from 8135 to 8277 cal/gram of fixed carbon. The hydrogen content of these materials ranged from 0.5 to 0.8% and carbon contents were above 96.7%. Recently, the heats of combustion of two well characterized chars have been measured (6). These chars were produced in experimental runs on a synthane process test unit and one corresponded to a char heat treated at 400°C and the other to a char heat treated at 900°C. They were produced from an Illinois No. 6 coal feed. The heat of combustion of the 400°C char is 8540 cal/gram carbon and of the 900°C char 8322 cal/gram carbon. The hydrogen-to-carbon ratios as determined from elemental analysis were: 0.73 for the 400°C and 0.20 for the 900°C. Thus the difference in the heats of combustion of chars and graphite ranges from 300 to 700 cal/gram of carbon. The larger heat of combustion of the chars relative to graphite reflects both the energy associated with the residual hydrogen in the chars and the excess heat of formation of the chars. Bronowski (7) reported measurements on the carbonization of bituminous coals. The carbonization process is exothermic and the heat involved is of the order of 500 cal/gram. This is of the same order of magnitude as the excess heat content of the chars as measured by the relative difference between the heats of combustion of chars and graphite on a fixed carbon basis. Thus, in subsequent calculations, the standard heat of formation of a char relative to graphite will be estimated as the difference between the respective heats of combustion on a per gram atom of carbon basis.

The Heat Capacity of Chars and Graphite

The heat capacity of graphite has been measured by numerous investigators. The data available covers the entire temperature range of interest and has been reviewed by Kelly and Taylor (8). It has been noted by many of the investigators that the heat capacity of graphite is dependent on the state of the structural perfection of the graphite specimen. Natural crystalline graphites have the lowest heat capacities at any given temperature. Synthetic graphites prepared by carbonization procedures have excess heat capacities. The amount of excess is mainly a function of the carbonization temperature. Attempts to eliminate the excess heat capacity of the synthetic graphites by heat treatments above 3000°C were unsuccessful. Thus, one should expect that the heat capacity of chars will be in excess of that of graphite.

Heat capacity data on coal chars are extremely scarce. An extensive literature search yielded only three sets of data relevant to the task at hand. The Bartlettville and Albany Laboratories (6) of ERDA measured the heat capacities of the same two synthane process chars for which they measured the heats of combustion. However,

the heat capacities were only measured above 300K. Data in the 50K to 300K region were reported by Kasatochkin, et al., (9) for chars prepared from a fossil carbon, Schungite, and from anthracite coals. These chars were prepared by "heat treatments" (pyrolysis) ranging from 600°C to 2800°C. The third set of data is from the Carbon Research Laboratories, SUNY, Buffalo (10) on chars prepared from resin C pitch by heat treatments ranging from 600°C up. The temperature range for heat capacity measurements was from 1K to 5K.

Some important generalizations can be deduced from the analysis of the above three data sets. First of all, as expected, the chars have an excess heat capacity relative to graphite at all experimental temperatures. The excess heat capacity of the chars is related to the heat treatment temperature. The lower the heat treatment temperatures for a given char the greater is its excess heat capacity relative to graphite.

One may quantify the relation between char heat capacity and heat treatment temperature by noting that the data on the resin-C chars and on Schungite chars can be expressed as:

$$c^{ch}(T) = C_0(T) \exp(a(T)/T_{HT}) \quad 4).$$

Here $c^{ch}(T)$ is the heat capacity of the char at a given temperature (°K) per gram atom of carbon contained in the char, and $C_0(T)$, $a(T)$ are constants and T_{HT} is the heat treatment temperature (°K). We found that this relationship is useful for fitting heat capacity data on all chars as a function of arbitrary heat treatment temperature.

The magnitude of the excess heat capacity is not a function of heat treatment temperature alone. The 900°C synthane process char has more excess heat capacity than the 600°C Schungite char. This difference may be simply due to the structural differences in the coals from which the chars were made. Alternately, it is possible that this difference in excess heat capacities is related to the residual hydrogen content and ash content of the chars. These conjectures should be subjected to experimental verification.

In Table 1 the heat capacity of the 900°C synthane process char is compared to that of graphite as a function of temperature. Entries into this table were obtained as follows: The heat capacity of graphite was taken from literature (11). The heat capacity of the char above 300K is calculated from the Barlettville data (6) directly. Below 300K entries for the char were calculated using the following procedure. We assume that below 300K the synthane char heat capacity has the same kind of functional dependence on temperature as the experimentally determined heat capacities for Schungite (9) and resin-C pitch chars (10). Therefore, if we have the heat capacity of one char as a function of temperature, the values for another may be calculated by assuming that the fractional change in heat capacity between two temperatures is the same. That is, we use a relation of the following form to calculate the heat capacity of the synthane char at a temperature T_2 .

$$\frac{\text{Synthane } C(T_2) - \text{Synthane } C(T_1)}{\text{Synthane } C(T_1)} = \frac{\text{Ref } C(T_2) - \text{Ref } C(T_1)}{\text{Ref } C(T_1)}$$

where C^{Ref} is a reference char of known heat capacity at temperatures T_1 and T_2 , and the C^{Synthane} is known (or has been calculated) at temperature T_1 . For reference char, a char of the same thermal history, i.e., heat treatment temperature is selected. Thus the C^{Ref} versus temperature curve between 50K and 300K was established using Equation 4 to calculate the heat capacities of a Schungite char, hypothetically heat treated at 900°C. The same procedure was used between 1K and 5K using for reference a hypothetical resin-C pitch char.

The reference heat capacity curve was completed between 5K and 50K by smoothly joining the two calculated curves. The accuracy of calculated heat capacities for the Synthane process char is probably of the order of 5 percent.

The Absolute Entropy of Formation of Chars and Graphite

The entropy of formation of carbon in the form of graphite is 1.35 (cal/gram atom-°K) at standard conditions. The entropy of formation of coals at standard conditions have been estimated as 4 to 12 (cal/mole-°K) with the preferred value around 5 (12). Chars are expected to have lower entropies of formation than coals. Since chars are not fully crystalline, structurally ordered materials, they do not follow the third law of thermodynamics. A residual entropy due to structural disorder must be added to the thermal entropy calculable from heat capacity data, in order to have a value of the absolute entropy of formation at a given temperature. Using the data given in Table 1, the standard entropy of formation, S_f^{Std} , for the 900°C synthane process char was calculated as $S_f^{\text{Std}} = S_0 + 2.49$ (cal/gram-atom carbon-°K). Here S_0 is the residual entropy of the char.

The residual entropy for the char could be estimated experimentally. For example, it could be done from the accurate determination of the equilibrium constant for a reaction involving the char. However, due to the lack of data we will arbitrarily assume that S_0 for this char equals one cal/(gram-atom carbon-°K). We feel that this number is of the right order of magnitude.

Test of Squires' Hypothesis

The thermodynamic data assembled in the preceding sections on the 900°C synthane process char are sufficient to test Squires' hypothesis. We expect that the numbers we will get will only be correct to an order of magnitude due to the assumptions we make with regard to the residual entropy of the char, the low temperature heat capacities and heat of formation. The calculation is done considering that the gasification reaction as given by Equation 1 is carried out at 1200K.

As we have indicated, first we must calculate the Gibbs free energy of formation of the char relative to that of graphite at the selected temperature. Then we use Equation 2 to calculate the ratio of the equilibrium constants. The relative free energy of formation at temperature τ may be written in the usual form:

$$G_f^{\text{ch}} - G_f^{\text{gr}} = (H_f - \tau S_f)^{\text{ch}} - (H_f - \tau S_f)^{\text{gr}} = H_f^{\text{ch}} - H_f^{\text{gr}} - \tau (S_f^{\text{ch}} - S_f^{\text{gr}}) \quad 6).$$

Here, all the symbols have their usual meaning, and the superscripts have been defined. All quantities must be evaluated at the reaction temperature τ .

The relative heat of formation at the reaction temperature is given by the expression:

$$H_f^{\text{ch}} - H_f^{\text{gr}} = \Delta H_f^* + \int_{\tau^*}^{\tau} [C^{\text{ch}}(T) - C^{\text{gr}}(T)] dT \quad 7).$$

where τ^* is the standard temperature, and ΔH_f^* equals the difference in the standard heats of formation of the char and graphite. Experimentally determined heats of combustion data can be converted to yield heats of formation. In this case this is not done but ΔH_f^* is estimated as the difference between the measured standard heats of combustion of the char and the graphite. Justification of this procedure has been made in a prior section of this paper. For the 900°C synthane process char ΔH_f^* equals 5.9Kcal/gr atom carbon.

The integral in Equation 7. is evaluated graphically. Data in Table 1 are used to prepare a smooth graph of the heat capacity difference between the char and graphite as a function of temperature. The numerical value of 1.7Kcal/gr atom carbon is obtained by graphical integration for the increase in the relative heat of formation between the standard temperature and the assumed reaction temperature of 1200K. Therefore, $H_f^{\text{ch}} - H_f^{\text{gr}}$ equals 7.6Kcal/gram-atom carbon at 1200K.

The relative entropy of formation can be written as:

$$S_f^{\text{ch}} - S_f^{\text{gr}} = S_0 + \int_0^{\tau} \left[\frac{C^{\text{ch}}(T) - C^{\text{gr}}(T)}{T} \right] dT \quad 8).$$

For S_0 the value of 1 cal/gr-atom carbon-°K is assumed since all the residual entropy is associated with the char. The integral in Equation 8 is again evaluated graphically from a smooth graph of the ratio of the heat capacity difference to the temperature versus temperature. The value of this integral between the indicated limits is 3.82 (cal/gram atom carbon-°K). Thus the relative entropy of formation at 1200K is 4.82 (cal/gram atom carbon-°K).

Substituting the numerical values into Equation 6 we obtain 1.8Kcal/gr atom carbon for the relative Gibbs free energy of formation, $G_f^{\text{ch}} - G_f^{\text{gr}}$, at 1200K. The ratio of the equilibrium constants $K^{\text{ch}}/K^{\text{gr}}$ is calculated with use of Equation 2 and is found to be 2.14 at 1200K. From the experimental data compiled by Squires

(4) for the gasification of pretreated chars in steam fluidized beds the value of 3.5 at 1200K is estimated for K^{ch}/K^{gr} . Considering all the assumptions involved in this calculation the agreement between experimental data and calculation is significant. While this calculation does not provide a clearcut proof of Squires' hypothesis, it does strongly support it.

Conclusions

From the available experimental data one may conclude that coal chars have larger heat capacities and heats of combustion than graphite when these quantities are compared on equivalent amount of carbon content basis. The magnitude of the thermodynamic quantities depends both on the thermal history of the char and on the source of the char. The magnitude of the excess quantities relative to graphite varies with the pyrolysis temperature of the char in an inverse fashion. In case of the heat capacity function a relationship was found (Equation 4) which enables one to estimate the heat capacities of a given char at some assumed pyrolysis (heat treatment) temperature. Chars obtained from a bituminous coal have larger excess heat capacities than chars originating from anthracite coals or fossil carbons. One may speculate that this difference could be related to the amount of residual hydrogen contained in a given char.

Since chars are not fully crystalline ordered solids, they must have some residual entropy of formation. There is no experimental data which allow one to estimate the magnitude of the residual entropy. A value for the residual entropy must be assumed. If one makes the reasonable assumption of one (1) (cal/gram atom carbon-°K) for the value of the residual entropy, then the calculated value of the Gibbs free energy of formation of chars is positive relative to that of graphite. Hence, one concludes that chars should be chemically more reactive than graphite. This conclusion of course is consistent with other experimental data on char reactivity.

In order of magnitude agreement between the numerical values of the equilibrium ratio K^{ch}/K^{gr} as calculated and as inferred from experimental data, tends to support Squires' hypothesis that the observed gasification yield in a steam fluidized bed process depends on equilibrium considerations. For a more quantitative test of the hypothesis more thermodynamic data than presently available are needed.

The available data show the importance of the pyrolysis temperature as a major factor in the thermal history, and consequently in the thermodynamics of the coal chars. However, the thermal history of a char should also depend on the rate of temperature rise to the pyrolysis temperature and on the length of time the char is kept at the pyrolysis temperature (soak time). The effect of these factors on the thermodynamics of the chars should be investigated. For example, one would expect that longer soaking times will reduce the residual entropy.

Acknowledgements

Helpful discussions with Professor Arthur M. Squires of Virginia Polytechnic Institute and State University are gratefully acknowledged. This work was supported by NSF Grant #76-22970 (ENG.)

References

1. S. Okstad and A. Moy, 2nd Conf. on Ind. Carbon and Graphite, Soc. of Chem. Ind., London, 1965; R.G. Jenkins, S.P. Nandi, and P.L. Walker, Jr., Fuel, 52, 288 (1973); T.A. Daly and C.F. Budge, Fuel, 53, 8 (1974); E. Hippo and P.L. Walker, Jr., Fuel, 54, 245 (1975).
2. S. Dutta, C.Y. Wen, and R.J. Bell, Ind. Eng. Chem. Process Des. Dev., 16, 20 (1977); S. Dutta and C.Y. Wen, *ibid* 16, 31 (1977).
3. J.T. Ashu and P.L. Walker, Jr., "Effects of Heat Treatment Conditions on Reactivity of Chars in Air," Technical Report (F.E. 2-30-TR3) to ERDA (Sept. 1977).
4. A.M. Squires, Trans. Inst. Chem. Engrs., 39, 3(1961); Science 191, 689 (1976).
5. M. Dolch and V. Rank, Brennsb. u. Warmew., 19, 72 (1937).
6. Internal Report of the Thermodynamics Research Group, Bartlesville Energy Research Center, ERDA, "Thermal Data on Gasifier Streams from Synthane Test" (1973).
7. J. Bronowski, Chemical Engineering in the Coal Industry, F.W. Sharpely (Ed.), pg. 93 (1956) (Pergamon Press).
8. B.T. Kelly and R. Taylor, Chem. and Phys. of Carbon, ed. by P.L. Walker, Jr. and P.A. Thrower, 10 1(1973) (Marcel Dekker, Inc.).
9. V.I. Kasatochkin, K. Usenbaev, V.M. Zhdanov, K. Sabyraliev, M. Rasalbaev and K. Zhumaliev, Dokl. Akad. Nauk, S.S.S.R. 216, 93 (1974).
10. P. Delhaes and Y. Hishiyama, Carbon 8 31(1970); K. Kamiya, S. Mrozowski, and A.S. Vagh, Carbon 10, 267 (1972).
11. W. DeSorbo, J. Amer. Chem. Soc. 77, 4713 (1955); P.H. Keeson and N. Perlman, Phys. Rev., 99, 1119 (1955); M.M. Spencer, Ind. Eng. Chem., 40, 2152 (1948).
12. O. Krikorian, Lawrence Livermore Laboratory, Internal Document CDTN 72-18 (1972).

Table 1

The Heat Capacities of a 900°C Synthane Process Char and of Graphite

Temperature (°K)	c^{char} (cal/gr-atom carbon-°K)	c^{graphite} (cal/gram atom carbon-°K)
1	0.23×10^{-3}	0.02×10^{-3}
3	1.1×10^{-3}	0.21×10^{-3}
5	4.1×10^{-3}	$.67 \times 10^{-3}$
10	1.4×10^{-2}	3.0×10^{-3}
15	3.2×10^{-2}	1.0×10^{-2}
20	5.4×10^{-2}	1.8×10^{-2}
25	7.7×10^{-2}	2.6×10^{-2}
30	0.103	4.6×10^{-2}
40	0.172	8.3×10^{-2}
50	0.25	0.122
75	0.48	0.253
100	0.73	0.401
125	1.01	0.557
150	1.33	0.730
175	1.65	0.912
200	2.02	1.101
225	2.39	1.291
250	2.73	1.486
275	3.11	1.684
300	3.43	1.96
350	4.03	2.46
400	4.52	2.90
450	4.95	3.24
500	5.33	3.55
600	5.96	4.07
700	6.49	4.49
800	6.90	4.82
900	7.27	5.07
1000	7.57	5.26
1100	7.83	5.41
1200	8.08	5.54

REACTION OF COAL WITH NITRONIUM TETRAFLUOROBORATE

S. K. Chakrabartty, H. O. Kretschmer and D. E. Ungarian

Alberta Research Council, Fuel Sciences Division
11315-87th Avenue, Edmonton, Alberta, Canada, T6G 2C2

If, as is generally supposed, coal is comprised of predominantly aromatic carbon configurations, it should be open to attack by electrophilic agents. However, while sulphonation, halogenation and nitration of coal have been reported (1), interaction of coal with a selective electrophile - for example, interaction with the nitronium ion - have not yet been explored in detail. Some investigations of this reaction have been published by Brown (2) who employed cupric nitrate in acetic anhydride and by Lahiri et al (3) who used mixtures of nitric and sulphuric acids; and in these cases, it was presumed that the active agent was the nitronium ion which formed as an intermediate in the solvent system. With crystalline salts which contain the nitronium ion, e.g. $\text{NO}_2^+\text{BF}_4^-$, $\text{NO}_2^+\text{ClO}_3^-$ now readily available, it should, in principle, now be possible to achieve selective nitration more cleanly in non-aqueous, acid-free systems; and we have in fact used nitronium tetrafluoroborate for "activating" bituminous coal before subjecting it to hypochlorite oxidation (4). But recent studies, notably by Olah et al (5), indicate that such salts can also promote reactions other than nitration. They will, for example, oxidize benzyl alcohols to ketones, induce nitrolysis of alkanes, and cleave ethers. In the case of reactions between nitronium tetrafluoroborate and coal, it must therefore be expected that various oxygen-bearing functions as well as nitro-groups could be established in the coal. The work reported in this paper was undertaken in efforts to determine the validity of these expectations.

EXPERIMENTAL

Reaction with nitronium salt

A mixture of 5 to 90 mmoles of the salt and 25 ml acetonitrile or methylene chloride was stirred at ice-bath temperature to produce a homogeneous suspension, and 1 g of dry coal was added. Reaction was allowed to continue for 16 hours at ice-bath temperature under a blanket of helium. The solvent was then evaporated under reduced pressure, the residue quenched with ice-water, and the product isolated by filtration and washed free of acid.

Similar reactions were performed with model compounds, e.g. polystyrene, adamantane, tetrahydronaphthalene and decahydronaphthalene.

For comparison, one coal sample was nitrated with 1:1 v/v concentrated with nitric-sulphuric acid at ice-bath temperature for 16 hours. The mixture was then poured into crushed ice, diluted to a large volume, the nitro-coal filtered off and finally washed free of acid.

Functional group analysis

The number of nitro groups introduced was estimated by titration with stannous chloride or titanous chloride, using a standard procedure (6).

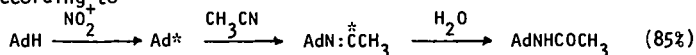
The carboxylic acidity was estimated by ion-exchange with sodium acetate and distilling off the acetic acid, and the hydroxyl-content was determined by acetylation with acetic anhydride in pyridine, following the procedure developed by L. Blom (7).

RESULTS AND DISCUSSION

Tetramethylene sulfone, acetonitrile and various other solvents have been used for nitration with nitronium salts. Initially, acetonitrile was used in this study. The nitration of polystyrene in this system introduced one nitro group per chain-length of four monomer units. The yield of mono-nitrotetralin was 78%. In con-

rust, adamantane and octahydronaphthalene could not be nitrated but varying yields (up to 85%) of some other nitrogen-containing product was obtained. The product derived from adamantane was identified as N-(1-adamantyl)acetamide by comparing melting point, infra-red and ¹H-n.m.r. spectra of the sample with authentic compound. The spectral data indicated the formation of a similar product (in 3% yield) from octahydronaphthalene, whilst tetrahydronaphthalene only furnished the mono-nitro product.

It may be presumed that the nitronium ion, being an oxidant, oxidizes adamantane to the adamantyl radical or ion which, in turn, reacts with the solvent according to



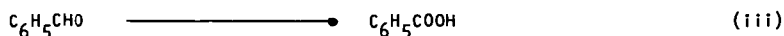
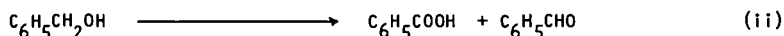
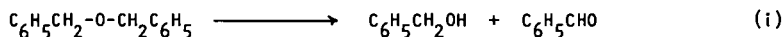
It is interesting to note that of the four model compounds studied, adamantane has the most easily oxidizable C-H bonds. From hypochlorite oxidation (4), it was demonstrated that coal has similar types of C-H bonds, and it is possible that reaction with nitronium salt in acetonitrile may produce an acetamide derivative of coal.

Nitro-coal prepared with nitric-sulfuric acid mixtures gave a titration profile which accounts for all added nitrogen in nitro groups, and similar results were obtained when coal was treated with nitronium salt in methylene chloride. However, in acetonitrile solvent, depending on the amount of nitronium salt used in each reaction, only 48-67% of the added nitrogen could be found in nitro groups (Table 1).

Material balances indicate that little, if any, carbon is lost when the coal is treated with HNO₃/H₂SO₄ mixture or with a nitronium salt in methylene chloride. However, the reaction of coal with nitronium salt in acetonitrile yields products with more carbon and nitrogen content. Since the only extraneous source of carbon was the solvent, the added carbon must come from the reaction of acetonitrile with coal. Moreover, it was also found that for every nitrogen atom added other than as N in nitro groups two carbon atoms were added. And hydrolysis of the products in 1N phosphoric acid gave acetic acid. From these observations it is surmised that a nitronium salt in acetonitrile introduces acetamido as well as nitro groups. The results of reaction between nitronium salts and coal, based on material balances and titration data, are presented in Table 2.

Mazumdar et al (8) have reported that the major reactions during nitration of coal with HNO₃-H₂SO₄ involve introduction of nitro groups and, even under very mild conditions, simultaneous oxidation of the carbon-structure. The oxidation creates carboxyl, hydroxyl and ketonic functions, with formation of carboxyl being the dominant process. But since no loss of carbon was observed, it was concluded that oxidation is limited to methyl groups. Reaction of coal with nitronium salt also induces some oxidation and 7-15% weight increase could be ascribed to newly created oxygen functions. The concentration of oxygen-bearing groups in variously treated coal samples are shown in Table 3.

It is interesting to note that whatever the nitrating system, almost identical oxygen-bearing groups are generated. Since nitronium salts can cleave ethers, the oxidation can be related to such cleavage reactions followed by further degradation depending on the oxidation potentials of the nitrating systems, e.g.



From the nitration studies, some inferences about coal structure can be drawn. Thus, reaction with nitronium salt introduces 3-7 nitro groups per 100 carbon atoms while HNO₃/H₂SO₄ mixtures permit addition of 8-10 nitro groups. If it is assumed that isomerizations of condensed polycyclic aliphatic structures to aromatic structures does not occur during nitration at 0°C, the number of nitro groups per 100

carbon atoms may provide information about aromatic ring size. In Table 4, the average composition of coal sub-units with nitro group are calculated from published data (8). These sub-groups vary from $C_{12}H_9$ to $C_{10}H_6$ and consequently suggest that only benzene or naphthalene nuclei are present in them.

Some support for this deduction is afforded by data relating to reduction of coal with lithium in ethylene diamine. Reduction of aromatic compounds in such or similar systems yields dihydro- or tetrahydro-derivatives, and assuming benzene or naphthalene as the only aromatic structure in the unknown molecule, the hydrogen uptake by the sample can be calculated from the number of such ring per 100 carbon atoms of the samples (Table 5). A comparison of these data with experimental results indicates that the abundance of naphthalene rings increases with rank. It is hardly expected that the reduction of single benzene ring would stop at the tetrahydro-stage. From this discussion we conclude that the smallest hydrocarbon skeletal structure in coal may be in units of $C_{12}H_9$ to $C_{10}H_6$, and that, depending on rank and geographical location, the nucleus of such unit is a benzene or naphthalene ring.

REFERENCES

1. Lowry, H. H. (Editor). Chemistry of Coal Utilization. Vol. I and II. Wiley, London, (1945), Suppl. Vol. p. 1091-92, Wiley, London, (1963).
2. Brown, J. K., Given, P. H., Lupton, V. and Wyss, W. F. Residential Conference on "Science in the Use of Coal", Sheffield, Preprints, A-43, April (1958).
3. Bhattacharyya, A. C., Chatterjee, A. K. and Lahiri, A., Fuel, London 46, 25 (1967).
4. Chakrabartty, S. K. and Kretschmer, H. O., Fuel 51, 160 (1972).
5. (a) Olah, G. A. and Ho-T-L, J. Org. Chem. 42 (18), 3097 (1977);
(b) Olah G. A. and Lin, H. C., J. Amer. Chem. Soc. 93, 1259, (1971);
(c) Olah, G. A. and Ho-T-L, Synthesis 609 (1976).
6. Becker, W. W., Anal. Chem. 22, pp. 185-8 (1950).
7. Blom, L., Analytical Methods in Coal Chemistry, Joh. Luuk C. V., Eindhoven, Netherland, (1960).
8. Mazumdar, B. K., Chatterjee, A. K. and Lahiri, A., Fuel 46 379 (1967).

Table 1. Nitro-groups in Reacted Coal and Model Compounds

Sample	N _{total} mmole/g	N _{NO₂} , mmole/g		N _{NO₂} /N _{total} (added) %
		SnCl ₂	TiCl ₃	
a. 1 g coal reacted with				
(i) HNO ₃ -H ₂ SO ₄ (10°C)	5.1	4.14	4.28	100
(ii) 90 mmole NO ₂ BF ₄ /MeCN	5.6	2.36	2.50	48
(iii) 45 " " " "	3.0	1.28	1.35	57
(iv) 5 " " " "	1.5	0.00	0.49	67
(v) 90 " " CH ₂ Cl ₂	2.9	2.32	2.35	100
b. Model compounds/NO ₂ BF ₄ /MeCN				
(i) Polystyrene	2.0	2.26	2.40	
(ii) Adamantane	7.2	0.00	0.00	
(iii) Aniline	14.5	7.28	6.98	
(iv) Benzoic acid	6.0	6.0	5.98	

Table 2. Reactions with Nitronium-Tetrafluoroborate

Substrate	% Weight Increase	Product	Analysis			
			%C	%H	%N	NO ₂ meq/g
Acetonitrile Solvent						
1. Polystyrene (C ₈ H ₈) FW n x n ¹⁰⁴	10	(C ₈ H ₈) _{3.35} C ₈ H ₇ NO ₂ FW 498	a. 83.39 b. 84.2	6.8 7.0	2.8 2.8	2.0 2.4
2. Coal %C = 85.7	36	C ₁₀₀ H ₆₈ N _{0.93} (NO ₂) _{6.4} (NHCOMe) _{3.9} FW 1904	a. 68.0 b. 69.0	4.4 4.1	8.2 7.9	3.4 3.2
		C ₁₀₀ H _{78.3} N _{0.93} O _{6.76} FW 1401				
3. Coal %C = 88.8	35	C ₁₀₀ H _{59.1} N(NO ₂) ₅ (NHCOMe) _{1.8} FW 1822	a. 68.2 b. 69.0	3.6 3.3	6.0 6.2	2.7 2.6
		C ₁₀₀ H _{65.9} NO _{4.3} FW 1350				
Methylene Chloride Solvent						
4. Coal %C = 88.8	21	C ₁₀₀ H _{55.1} N(NO ₂) _{3.7} FW 1623	a. 74.0 b. 74.0	3.4 3.4	4.1 4.0	2.3 2.3
a. calculated b. found						

Table 3. Oxygen-Bearing Functional Groups in Treated Coal

Sample	-OH meq/g	-COOH, meq/g
1. Coal %C = 88.8	0.9	nil
2. Sample 1/NO ₂ BF ₄ /CH ₃ CN	2.3	3.0
3. Sample 1/NO ₂ BF ₄ /CH ₂ Cl ₂	1.5	0.8
4. Sample 1/HNO ₃ /H ₂ SO ₄	2.2	2.8
5. NO ₂ -Coal* from Coal %C = 89.8	2.8	3.5

*See Reference (8)

Table 4. Nitration of Bituminous Coals*

Coal %C	Nitro gr per 100 C-atoms	Average composition of subunit/NO ₂ gr Number of atoms			
		C	H	N	O
80.8	8.6	11.6	8.9	0.24	1.24
83.6	8.2	12.2	9.6	0.29	0.90
85.5	9.2	10.9	7.9	0.22	0.65
87.1	9.9	10.1	7.7	0.24	0.38
89.8	8.6	11.6	7.3	0.23	0.27
90.2**	9.3	10.8	6.6	0.15	0.31

*Data recalculated from B. K. Mazumdar et al, Fuel 46, 380, 1967.

**From the study by the author.

Table 5. Reduction of Coals by Alkali Metals in Basic Solvent
H-uptake per 100 Carbon Atoms

Coal % C	Calculated value from nitration of Gondwana coal		Experimental value (10) %C	American coal H-uptake
	dihydro	tetrahydro		
80.8	17.2	34.4		
83.6	16.4	32.8	83.1	17
85.5	18.4	36.8	85.1	19
87.1	19.8	39.6	88.7	27
89.8	17.2	34.4	89.3	29
90.2*	18.6	37.2	90.1	45

*Canadian coal